ANALYSIS OF COPPER ISOTOPE RATIOS BY MULTI-COLLECTOR INDUCTIVELY COUPLED PLASMA MASS SPECTROMETRY AND INTERPRETATION OF COPPER ISOTOPE RATIOS FROM COPPER MINERALIZATION

By

KIERRAN C. MAHER

A dissertation submitted in partial fulfillment of
the requirements for the degree of

DOCTOR OF PHILOSOPHY

WASHINGTON STATE UNIVERSITY
Department of Geology

August 2005

To the Faculty of Washington State University:

The members of the Committee appointed to examine the dissertation of KIERRAN C. MAHER find it satisfactory and recommend that it be accepted.

_____
Chair

_____

_____

Acknowledgement

The author of this work wishes to gratefully acknowledge the Department of Geology at Washington State University for financial support (through teaching assistanceships) for 6 semesters. Also appreciation is expressed to Frank Ramos, Charles Knaack, and Garret Hart for assisting in various aspects of elemental and isotopic analyses required for this investigation. Frank Ramos is particularly acknowledged for assistance at the initiation of this project and instruction on chromatographic separation methods.

Gratitude is expressed to Peter Larson for supporting the type of work described herein and for his encouraging words during difficulties encountered during the course of this work. He is also recognized as improving the composition of this dissertation.

The author acknowledges the patience and forebearance by his immediate family, especially Carmen Espirilla Rodriguez, Shemariah and Hadassah, who have supported this investigation in many ways, but especially through love and patience through the moments of stress and fatigue. Finally, my Father is honored for his role in assisting the author in approaching the problems encountered during the course of this investigation.

Despite the assistance provided by others, the interpretations and conclusions put forth in this dissertation are the responsibility of the author.

ANALYSIS OF COPPER ISOTOPE RATIOS BY MULTI-COLLECTOR INDUCTIVELY COUPLED PLASMA MASS SPECTROMETRY AND INTERPRETATION OF COPPER ISOTOPE RATIOS FROM COPPER MINERALIZATION

Abstract

by Kierran C. Maher, Ph.D.

Washington State University

August 2005

Chair: Peter B. Larson

Copper isotope analysis by multi-collector inductively coupled plasma mass spectrometry can routinely determine copper ratios with 2σ precision of ±0.08‰ $\delta^{65}Cu_{NIST\ SRM\ 976}$, correcting machine mass fractionation by the standard-sample bracketing method. The zinc-doping method for machine mass fractionation correction provides similar reproducibility, depending on the zinc isotope pair utilized. Detailed evaluation of possible matrix effects on copper isotope measurements indicates that sample purification through chromatography is unnecessary for reliable analysis of Cu-Fe and Cu sulfide minerals.

Copper isotope ratios measured from high-temperature (>250°C) mineralization from several hydrothermal ore deposits span a larger range than recognized by recent investigations (Zhu et al., 2000). The large range suggests significant isotopic fractionation mechanisms operate at high temperatures and include fractionation during copper remobilization, possible fractionation between predominant metal-transporting complexes in solution, as well as significant equilibrium fluid-mineral fractionation. Mineralization due to high-salinity fluids is expected to have larger ranges in $\delta^{65}Cu$ values than mineralization produced from lower-salinity fluids. Supergene mineralization shows large isotopic fractionations resulting from varied and repetitive isotopic fractionation processes including copper leaching, Cu^{+} to Cu^{2+} oxidation-reduction reactions, and fluid-mineral fractionations. These processes are controlled by changes in the hydrologic system of supergene zones with time.

Hydrothermal chalcopyrite synthesis experiments have successfully precipitated chalcopyrite from elemental nutrient at 225°C and 300°C from fluids of different salinities. Resulting chalcopyrite δ^{65}Cu values indicate that the fluid-mineral fractionation is probably negative, which means that chalcopyrite successively precipitated from the same hydrothermal fluid will be isotopically heavier than the residual fluid. Isotopic data from mineralization at Coroccohuayco, Perú, modeled using this equilibrium fluid-mineral fractionation, indicate that precipitation of chalcopyrite commences distally, likely due to thermal constraints, and advances toward the source of the mineralizing fluid. Zoned isotopic data from chalcopyrite can be successfully modeled as a series of small precipitation steps at fluid-chalcopyrite isotopic equilibrium with large changes in copper isotope ratios, punctuated by larger fractions of copper being precipitated with corresponding minor changes in copper isotope ratios of chalcopyrite.

Table of Contents

Page

Acknowledgement……...…… iii

Abstract……iv

List of Tables…….. viii

List of Figures…….. ix

Section

I. Introduction……..1

Purpose of Investigation..……2

II. Analytical Considerations…….. 4

Effects of Sample Matrix……. 5

Isobaric Interferences……...17

Mass Fractionation Correction……... 17

Sample-Standard Bracketing Correction……. 19

Element Doping Correction……21

Copper Blank……...35

Conclusion……...36

III. Sample Preparation and Analytical Procedure…… 37

Data Reduction……... 39

IV. Analytical Results……... 40

Analysis of NIST SRM 976……40

Day-to-Day Reproducibility: Internal Standards……40

With-in Analysis Reproducibility……...45

Drift on the Neptune® MC-ICPMS……... 47

Copper Isotope Ratios…… 47

Discussion: Ranges in Copper Isotope Ratios……49

Mantle and Bulk Earth Copper Isotope Characteristics…….……..51

Cogenetic Copper Minerals……. 52

V. Variations in Copper Isotope Ratios from Ore Environments…….. 54

Copper Isotope Variations in Hypogene Mineralization…… 56

Source Variations……57

Isotopically Distinct Fluids……..58

Remobilization of Copper……59

Copper Isotope Fractionation Among Complexes in Solution…… 64

Copper Isotope Fractionation in Supergene Ore Zones……. 68

VI. High-Temperature Fractionation of Copper Isotopes Under Experimental Hydrothermal Conditions

……. 73

Procedure…… 73

Chromatography of Fluid……... 76

Results…… 78

Interpretations of Sulfide Synthesis Data……... 81

Implications of Experimental Fluid-Mineral Fractionations…….. 82

VII. Conclusion……. 87

Future Avenues of Research in Copper Isotope Systematics…….....……. 89

References…… 91

Appendix

1. Chromatography of Samples…… 96

2. Results of Copper Isotope Analyses with Geologic Context ……..……..……..... 100

3. Table of Results of Copper Isotope Analyses……..110

4. Manuscript of Maher and Larson (in review)…….. 194

5. Data from Hydrothermal Chalcopyrite Synthesis Experiments……...228

List of Tables

1. Matrix analysis of selected copper minerals……6

2. Comparison of δ^{65}Cu for select samples at different Cu concentrations……22

3. Comparison of corrected δ^{65}Cu using different zinc isotope pairs……..28

4. Comparison of calculated δ^{65}Cu values utilizing nickel doping…… 32

5. Summary of analyses of internal standards over three years…… 42

6. Summary of analytical run reproducibility from various samples…… 46

7. Sulfur and copper isotope analyses for chalcopyrite and bornite samples……53

8. Comparison of ranges in δ^{65}Cu from mineralization from several ore deposits…… 55

9. Isotopic analyses of synthetic chalcopyrite and chromatographically purified fluids……... 79

List of Figures

1. Effect of doping NIST SRM 976 standard (100ppb Cu) with Fe at 1ppm and S at 9ppm…… 8

2. Effect on $^{65}Cu/^{63}Cu$ ratio of samples doped with Pb at different concentrations…… 9

3. The matrix effect on NIST SRM 976 (100ppb Cu) doped with Ni……...10

4. Effect on $^{65}Cu/^{63}Cu$ ratio for NIST SRM 976 doped with a Zn shelf solution……... …..11

5. Effect of a Ni-solution over the $^{68}Zn/^{64}Zn$ ratio of a shelf solution……...12

6. Extreme copper isotopic fractionation induced through chromatography…… 14

7. Elution curves for SUP-1 on MP-1 and MP-1M resins…….15

8. Elution curves for sample BCR-P (basalt standard) on resin MP-1M…….. 16

9. $^{65}Cu/^{63}Cu$ analyses of NIST SRM 976 over three years……18

10. Graphical representation of the time-corrected sample-standard bracketing technique……. 20

11. Irregular machine drift and repeat analysis of samples……...23

12. Graph of $\delta^{65}Cu$ of RAY-1 verses the drift between bracketing standards…….. 24

13. Graph of $\ln(^{68}Zn/^{64}Zn)$ verses $\ln(^{65}Cu/^{63}Cu)$…….. 26

14. Graphs of $\ln(^{65}Cu/^{63}Cu)$ verses ln(zinc isotope ratio) showing differences in correlation factors……. 27

15. The isotopic effect on samples and standards doped with Ni…… 30

16. Graphs of $\ln(^{65}Cu/^{63}Cu)$ verses ln(Ni isotope ratio) for two different Ni isotope pairs…….. 31

17. Significance of data outliers for elemental doping corrections……...33

18. Drift from two analytical sessions in different zinc isotope ratios…… 34

19. Consistent machine drift in $^{65}Cu/^{63}Cu$……41

20. Graph of day-to-day reproducibility of internal standards.....44

21. Results of copper isotope analyses as ranges from different deposits and geologic environments…… 48

22. Graphs of calculated delta values for samples analyzed in this study from different ore deposits.....50

23. Photo of mineralized sample for BEAV-1,2,3,5 analyses……...60

24. Strongly mineralized sample Chab-Este from Tintaya, Perú…….. 61

25. Remobilization of disseminated mineralization (chalcocite-digenite) from vein selvages……63

26. Plan view at sea level and SW-NE cross section of the Resolution porphyry, AZ……65

27. Analytical run from 24 Jun 2005 and from 27 Jun 2005 (chalcopyrite synthesis)……..80

28. Progress of calc-silicate alteration related to porphyry-derived hydrothermal fluid……...83

29. δ^{65}Cu of chalcopyrite verses depth in drill hole 1400 18.9 of Coroccohuayco, Perú……. 85

I. Introduction

Copper is an economically important metal used in many industrial and technological applications. The exploration and exploitation of geologic resources of copper have occurred since before recorded history. With the advent of modern geologic principles, the understanding of deposit genesis and exploitation of copper resources has advanced considerably through improved field methods, increased understanding of the role of the chemistry of hydrothermal fluids, improved metallogenic concepts and models, and the use of both radiogenic and light stable isotopic systems. Recent technological advances in the field of isotopic measurements have added a new dimension to the study of copper in ore deposits, now allowing the routine and precise measurement of the relative abundance of the two isotopes of copper, ^{63}Cu and ^{65}Cu. This analytical tool now allows direct insight into the behavior of copper in the genesis of copper ore deposits.

Analyses of copper isotope ratios of natural samples were published by Walker et al. (1958), and followed by an important overview in ranges of copper isotope ratios in natural materials by Shields et al. (1965). Both of these investigations analyzed copper isotope ratios by thermal ionization mass spectrometry (TIMS). Although demonstrating isotopic variability, these early TIMS measurements of copper isotope ratios were plagued by poor ionization of Cu leading to a precision worse than 1.5 parts per thousand variation from NIST standard reference material 976 (Shields et al., 1965). Advances in multiple-collector inductively coupled mass spectrometer (MC-ICPMS) technology have overcome these early difficulties in measuring copper isotopic ratios. The use of plasma source ionization coupled with multicollector capability (to measure unstable ion signals arising from plasma ionization) now produces analytical precision better than 0.08 parts per thousand in isotopic ratio variations (Maréchal et al., 1999; Zhu et al., 2000; Larson et al., 2003; Maher et al., 2003). With improved analytical reproducibility, slight variations in natural copper isotope ratios can now be routinely measured. Copper isotopes can be used to elucidate ore-forming processes in a way which previously was only implied through the use of often equivocal ore textures, light stable isotope measurements on gangue minerals, fluid inclusion measurements, sulfur isotope measurements, or alteration characteristics. Although these methods are essential in investigating deposit genesis, only by studying copper isotope ratios can genetic processes directly relating to the ore metal in copper mineralization be evaluated.

Shields et al. (1965) published the first reliable paper on isotope measurements of copper utilizing TIMS for copper ore samples. Even though their precision was low (±1.5 parts per thousand deviation from the standard, NIST SRM 976), they measured a significant range in copper isotope ratios from both hypogene (high-temperature, primary) and supergene (low-temperature, secondary) copper minerals, indicating that fractionation mechanisms operated in both of these ore-forming environments. Poor precision of the TIMS analytical method precluded further application of copper isotopes to the study of earth processes. Later, Maréchal et al. (1999) published an investigation outlining the analytical advantages of using MC-ICPMS to measure copper isotope ratios in natural samples with reproducibility of about 0.06 parts per thousand (2σ). Gale et al. (1999) used low-temperature TIMS to improve analytical reproducibility over conventional TIMS in copper isotopic measurements, but found that MC-ICPMS provided even better precision. The significant improvement of MC-ICPMS over either TIMS method has opened up opportunities to reevaluate the utility in studying earth processes using copper isotopes.

Since the introduction of MC-ICPMS in the analysis of transition element isotopes, several investigations have evaluated aspects of copper isotope analysis and applications to earth processes. Maréchal et al. (1999), Zhu et al. (2000), and Larson et al. (2003) have evaluated ranges in copper isotope ratios in copper minerals from a variety of ore deposits. Gale et al. (1999) analyzed copper isotopic variations in copper ingots in hopes of tracing the origin of archeological artifacts. Zhu et al. (2000) and Rouxel et al. (2004) analyzed variations in copper isotope ratios in chalcopyrite mineralization from active sea-floor massive sulfide deposits. Maréchal and Albarède (2002) evaluated fractionation mechanisms of copper on chromatographic ion exchange resin first reported by Maréchal et al. (1999). Several investigations have addressed possible fractionation mechanisms from low-temperature experiments (Zhu et al., 2002; Maréchal and Albarède, 2002; Young and Ruiz, 2003; Erhlich et al., 2004).

Purpose of investigation

The present investigation was designed to address several fundamental questions about the nature of copper isotopes applied to ore deposits. First, what is the range of copper isotope ratios in high-temperature mineralization, and can this range be extended beyond the published data (Shields et al., 1965; Maréchal et al., 1999; Zhu et al., 2000; Larson et al., 2003)? Second, what might control the isotopic variation observed in high temperature ore deposits? Third, do copper minerals from a specific ore deposit show isotopic variations in the same copper mineral

and/or systematic paragenetic trends in mineral isotopic composition? Fourth, what are the possible mechanisms for fractionation of copper isotopes at elevated temperatures (>200ºC)?

Based on theoretical considerations (Urey, 1947) many workers (see Maréchal et al., 1999; Zhu et al., 2002) predict that variations in copper isotope ratios will be greatest in low temperature environments. Consequently, much of the present experimental research has been focused in fractionation mechanisms at low temperature (Maréchal and Albarède, 2002; Zhu et al., 2002; Young and Ruiz, 2003; Erhlich et al. 2004). However, Larson et al. (2003) also observed large variations (>2 parts per thousand) in copper isotopes from high temperature skarn and porphyry copper ores. Graham et al. (2004), utilizing laser ablation sampling in concert with MC-ICPMS, evaluated copper isotope ratios in porphyry-hosted chalcopyrite-bornite ores and discovered variations in copper isotope ratios of over 1 part per thousand from the standard. These recent studies, as well as the TIMS data from Shields et al. (1965), indicate important fractionation mechanisms operate in high-temperature (>200ºC) ore-forming environments. Although the exact fractionation mechanisms in these high-temperature environments have only recently been proposed (Graham et al., 2004; Maher and Larson, in review), these data (and probably ratios of other transition-element isotopic systems) can be used to elucidate processes operating in the hypogene ore-forming environment. This opens up the use of transition-element isotopic systems to understand metallogenesis as well as a practical use in the mineral exploration industry, similar to light stable isotopes (O, C, S).

This presentation outlines the analytical approach, challenges, results, and implications of variations in copper isotope ratios from copper mineralization in ore-forming environments. It emphasizes the analytical technique employed at Washington State University, which satisfies the requirements for reproducibility and general reliability of the analytical method. This dissertation discusses data on various ore-forming environments, but will mostly focus on fractionation mechanisms and their implications for high-temperature hydrothermal systems.

II. Analytical Considerations

Variations in stable isotope ratios are usually on the order of a few parts per thousand, and generally decrease as the temperature increases and as the mass difference between the isotopes becomes smaller. As such, isotopic variations are usually measured relative to a standard reference value, such as VSMOW (Vienna Standard Mean Ocean Water) for oxygen, or PDB (Pee Dee Belemnite) for carbon. As with light stable isotope systems, variations in transition-metal isotope ratios can be described using the δ-notation, or parts per thousand (per mil, ‰) variation from a standard value. With this notation, $\delta^{65}Cu$ is calculated as:

$$\delta^{65}Cu = \left(\frac{^{65}Cu/^{63}Cu_{sample}}{^{65}Cu/^{63}Cu_{standard}} - 1 \right) \times 1000$$

In the case of copper, this is parts per thousand relative to the $^{65}Cu/^{63}Cu$ ratio of NIST SRM 976 (0.4456, Shields et al., 1965). Epsilon-notation (ε) has also been used in other investigations (Zhu et al., 2000; Graham et al., 2004) and differs from δ-notation by a factor of ten. Throughout this investigation reference will be made to the standard delta notation for copper isotopes.

The isotopic analysis of any multi-isotopic element must satisfy several fundamental requirements for the results to be reliable and meaningful. The most important is whether the analysis represents the true isotopic composition of the sample. This question requires the evaluation of factors which may affect the isotopic composition of the samples because the composition of the analyte may potentially exert an influence over ionization of the element of interest ("matrix effect"). These influences must be evaluated for the magnitude of their effect on the true isotopic ratio and removed if there is a significant effect or disregarded if of low significance. Removal of interfering matrix can be accomplished through ion exchange chromatography.

Sample introduction, ion extraction from the plasma, and/or the ion transport process within the mass spectrometer may also change the measured isotopic value and must be evaluated and corrected if significant. This change is known as machine fractionation, mass discrimination, or mass bias. In addition, mass spectrometer drift with time must be corrected for the isotopic results to be meaningful. The overall machine fractionation can be

evaluated by comparison to an isotopic standard and potentially corrected for by bracketing the unknown sample analysis with standard analyses (known as the sample-standard bracketing correction). An alternative correction method is to dope the sample with a different element with known isotopic composition and then correct the unknown sample's isotopic ratio by the doped element isotopic ratio. Finally, isobaric interferences of elements or molecules in the plasma and sample blank must also be evaluated and corrected for if significant.

Effects of Sample Matrix

All elements or molecules other than the target element that are present during an analysis are collectively known as sample matrix. For isotopic analysis of copper minerals in solution, the matrix consists of elements other than Cu derived from the dissolved mineral and from the solutions used in the preparation of the sample. Any of these elements could possibly produce a matrix effect over the true copper isotopic ratio. For Cu-Fe sulfides, the significant matrix is generally only Fe, S, and any other elements associated with acid solutions (e.g., HNO_3). For whole-rock samples, all major elements, and many trace elements, will be present at concentrations much higher than copper.

Relative to copper isotope analysis, some investigators have suggested that copper solution matrices containing Ti and Fe may interfere with analyses corrected for isotopic machine fractionation using Zn-doping (Archer and Vance, 2004). As this is a concern for copper-ratio measurements, the elemental matrix effects on the copper isotope ratio analysis were examined in three ways for this investigation. The first was to determine what other elements were present in the sample solutions and at what concentrations relative to the target element. Several solutions of Cu-minerals at approximately 100ppb Cu were analyzed for the following elements using a quadrupole ICP-MS: Na, Mg, Al, Si, Ca, Sc, Ti, V, Fe, Co, Ni, Zn, Ba, and Pb. The results of some representative analyses are shown in Table 1. The error of the analyses varies, but is related to the true concentration of any specific element in the standard and mass interferences (which may be considerable for common elements such as Si). Analysis of major elements by ICP-MS is not routine, therefore, considerable error could exist in some of the analyses. However, it is apparent that for Cu-Fe sulfides dissolved in solution and diluted to 100ppb Cu concentration (the typical concentration used for isotopic analysis), the concentration of matrix elements is generally individually less than 5ppb, except for Cu, Fe, and possibly S (which cannot be reliably analyzed by this method).

Table 1. Matrix analysis of selected copper minerals.

sample	**Ray-1**	**Ray-2B**	**LS-10**	**LS-48**	**GAC-12 BD**	**18-365I**	**17-389**	**Chalc**	**Tajo**	**T6237E-4**
mineral	Cu[1]	Cu	Cu	Cu	cpy[2]	cpy	cpy	cpy	cpy	cpy
Na	0.00	0.24	0.37	0.42	0.69	0.74	1.00	0.69	0.42	0.57
Mg	0.31	0.32	0.32	0.57	1.08	0.65	0.99	0.59	1.09	1.58
Mg	0.35	0.30	0.35	0.56	1.09	0.65	0.96	0.59	1.11	1.64
Al	0.46	0.94	0.31	1.66	2.64	1.58	1.75	1.53	1.75	1.68
Si	3.01	2.27	2.09	0.00	0.00	0.00	3.03	0.00	0.00	5.37
Ca	0.00	0.00	0.00	0.00	0.00	0.00	0.00	0.00	0.00	3.98
Sc	0.00	0.00	0.00	0.00	0.00	0.00	0.00	0.00	0.00	0.00
Ti	0.03	0.01	0.02	0.02	0.20	0.03	0.04	0.01	0.03	0.08
V	0.00	0.00	0.00	0.00	0.00	0.00	0.00	0.00	0.00	0.00
Fe	2.96	3.05	3.67	2.47	81.95	74.27	171.10	84.11	74.57	79.84
Ni	0.00	0.00	0.01	0.00	0.02	0.17	0.05	0.00	0.15	0.01
Cu	91.50	99.70	90.20	105.80	67.53	82.94	186.10	92.43	75.68	83.35
Zn	0.00	0.00	0.00	0.27	1.52	1.66	1.14	0.61	0.58	0.00
Ba	0.00	0.00	0.01	0.06	0.11	0.06	0.06	0.06	0.04	0.01

Note: Values are ppb.
[1]Native copper.
[2]Chalcopyrite.

The second approach to determining matrix effects is to compare the copper isotopic standard to a solution of the standard doped with matrix elements of interest. This was done by doping NIST SRM 976 with Fe and S at concentrations greater than would be observed in natural Cu-Fe minerals such as chalcopyrite and bornite. Figure 1 presents an analytical run showing the analytically identical Fe- and S-doped standards relative to an undoped standard. This is in agreement with other studies (Rouxel et al., 2004; Graham et al., 2004) which have shown that the presence of Fe and S (among other elements) at concentrations higher than Cu in analytical solution does not affect the measured Cu-ratio outside of analytical reproducibility. For mineral samples where Fe and S are at concentrations up to 9 times higher than Cu, there is no analytically distinguishable effect on the measured isotopic ratio. Doping experiments with Pb at different concentrations found no correlation between Pb concentration up to 100ppb (1:1 Cu to Pb concentration) and copper isotope ratios for two internal standards. Pb concentration of 1ppm (10:1 Pb:Cu) shows δ^{65}Cu slightly outside of 2σ reproducibility for native copper (Ray-1), but no similar correlation exists for an unpurified chalcopyrite internal standard (Sup-1) (Fig. 2; Larson et al., 2003).

Graham et al. (2004) found that doping NIST SRM 976 with Ni and Zn at high concentrations did not significantly influence the standard Cu isotope ratio, although the isotopic values of the undoped standard were not indicated. For the present investigation pure copper solutions (NIST SRM 976) were doped with Ni and Zn at different concentrations. Figure 3 shows that Ni concentrations greater than 10ppb, relative to 100ppb Cu, produce a significant matrix effect on the copper ratio (to 2000ppm). This effect appears to be noticeable even at about 10ppb Ni, although the effect seems to be constant between 30 and 1000ppb Ni. Figure 4 shows that, for a similar experiment where the Cu standard was doped with Zn at different concentrations, the presence of Zn produces an inconsistent and less pronounced matrix effect (to 200ppm) on the copper isotopic ratio. Interestingly, the ^{68}Zn/^{64}Zn ratio of a Zn-only stock solution is affected by Ni in a similar way to the Ni-doped copper standard, with as little as 10ppb Ni matrix significantly affecting the Zn ratio (Fig. 5). The important consideration is that for most copper sulfide and oxide minerals, matrix elements beside Cu and Fe are generally less than one twentieth of the copper concentration (Table 1). In these cases the effect of matrix elements is less than the analytical reproducibility (see below).

Another approach to evaluate the effect of sample matrix on the isotopic composition of a sample is to process the sample through chromatographic separation, thereby removing copper from all other elements except those in the analytical acid solution matrix. This is the established procedure pioneered by Maréchal et al. (1999).

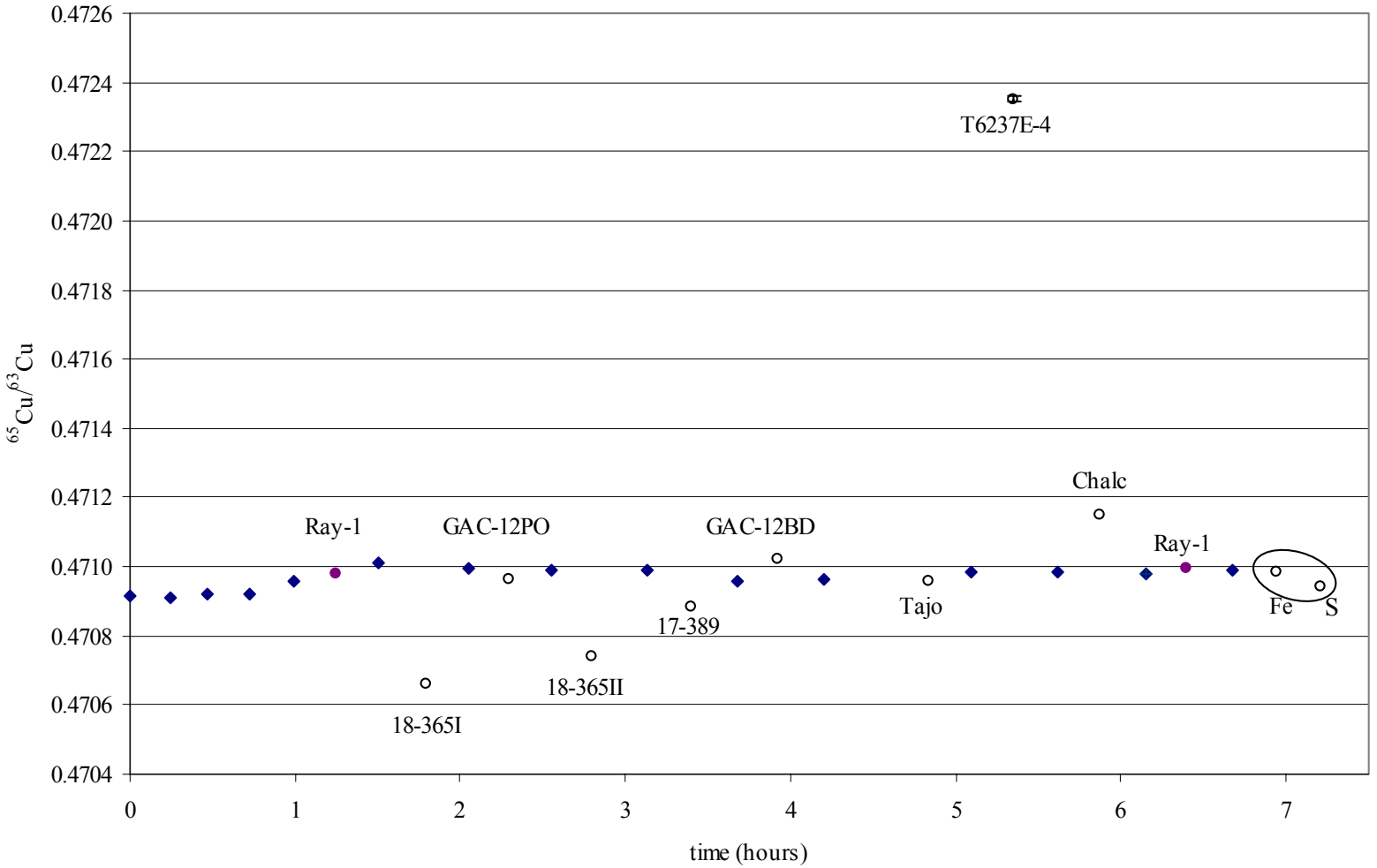

Figure 1. Analytical run (24 Apr 2002) showing effect of doping NIST SRM 976 standard (100ppb Cu) with Fe at 1ppm and S at 9ppm (circled). Analyzed solution at approximately 100ppb Cu. Filled diamonds are analyses of NIST SRM 976 (100ppb) and the error bars are 2σ. Other symbols are sample unknowns as labeled. In this figure the error bars are the size of the symbols.

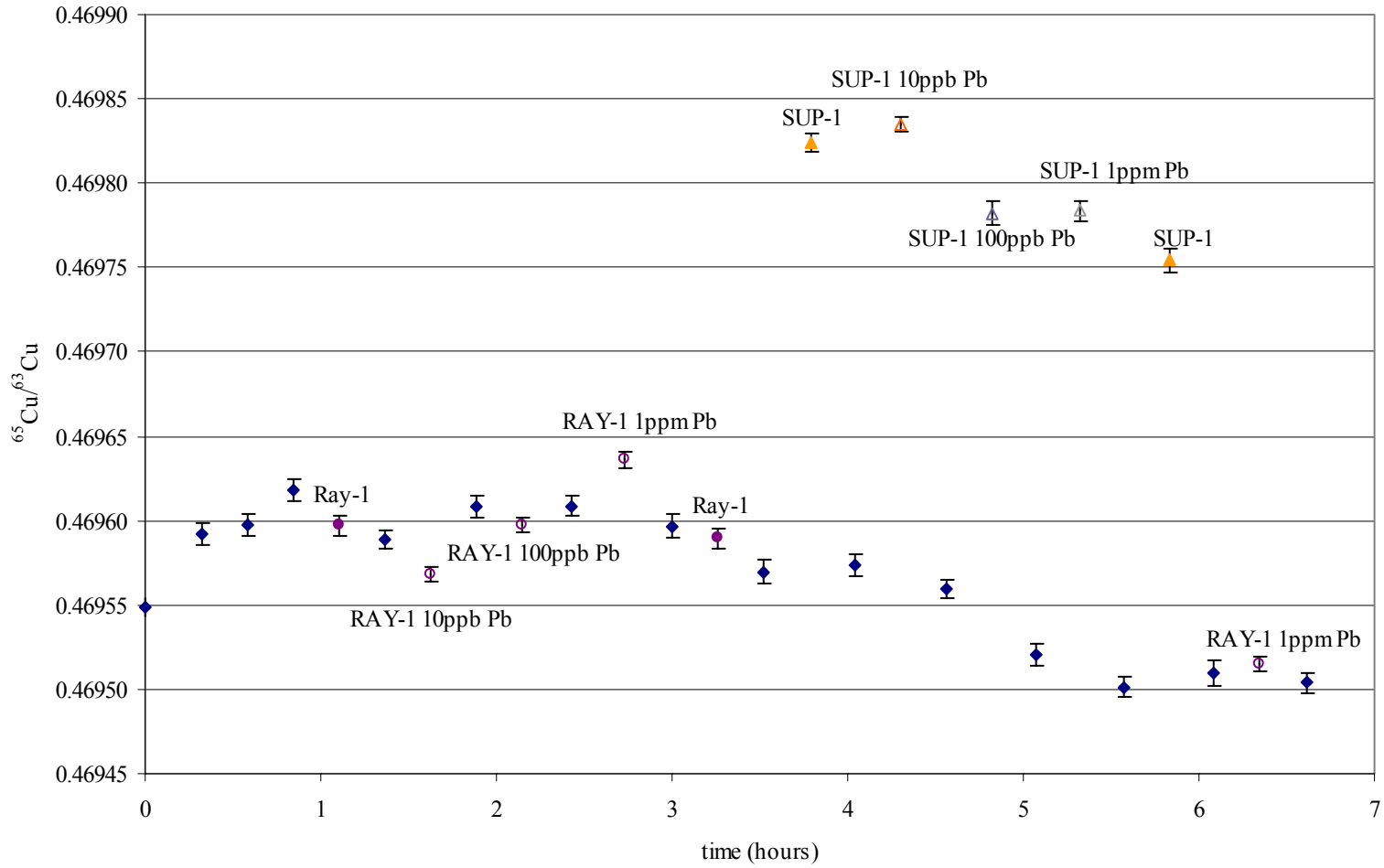

Figure 2. Analytical run (17 Jun 2003) showing effect on $^{65}Cu/^{63}Cu$ ratio of samples doped with Pb at different concentrations. Although the drift is somewhat inconsistent (note axis scale), and analytical reproducibility for this session is relatively poor, the samples are within or close to 2σ reproducibility of their accepted $\delta^{65}Cu$ values. Filled diamonds are analyses of NIST SRM 976 (100ppb) and the error bars are 2σ. Other symbols are sample unknowns.

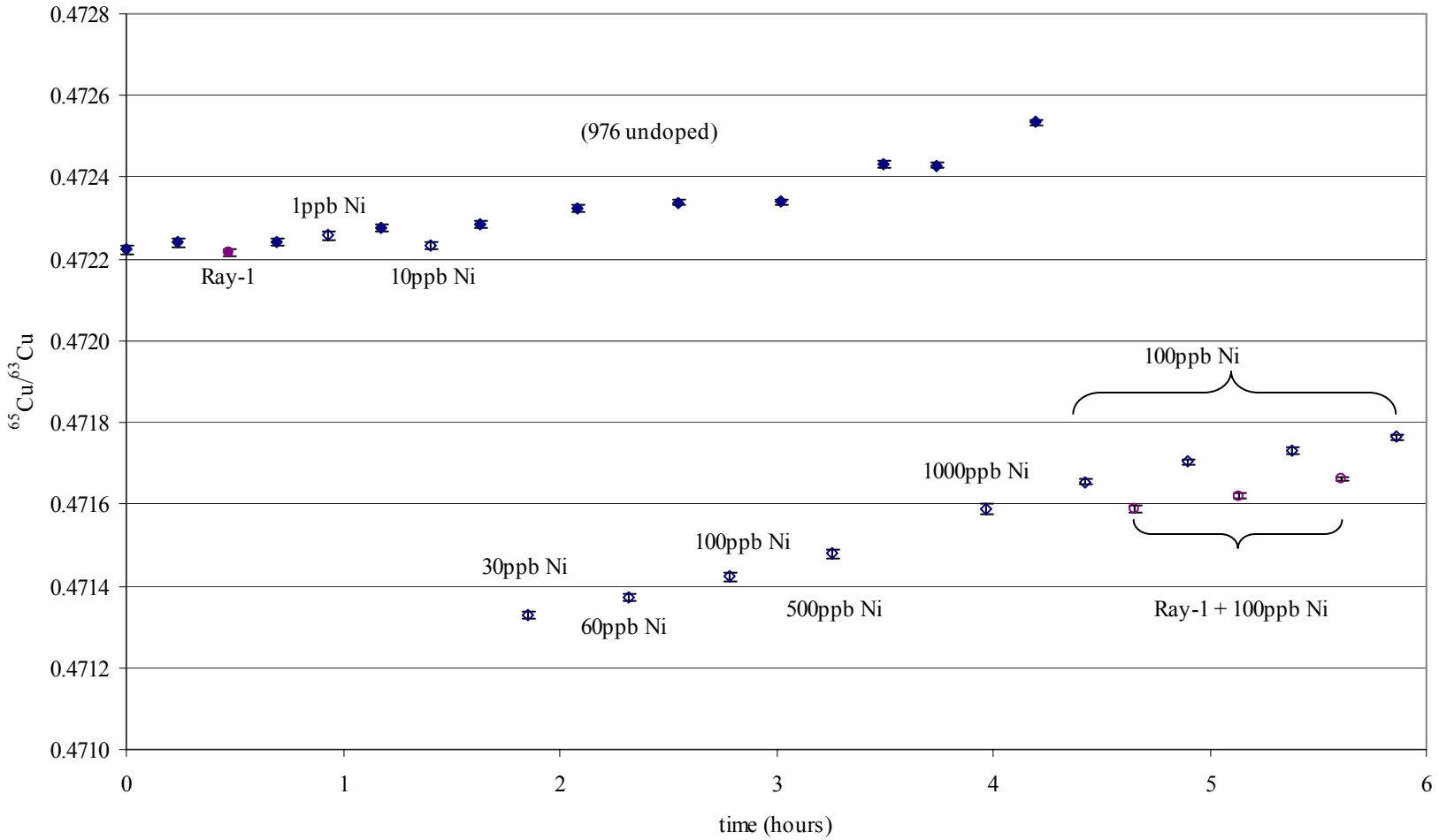

Figure 3. Analytical run showing the matrix effect on NIST SRM 976 (100ppb Cu) doped with Ni at different concentrations (using NIST SRM 986). The effect of Ni matrix over the NIST SRM 976 copper isotope ratio changes little between 30 -1000ppb Ni (20 Jan 2005). Filled diamonds are undoped NIST SRM 976, other samples as labeled.

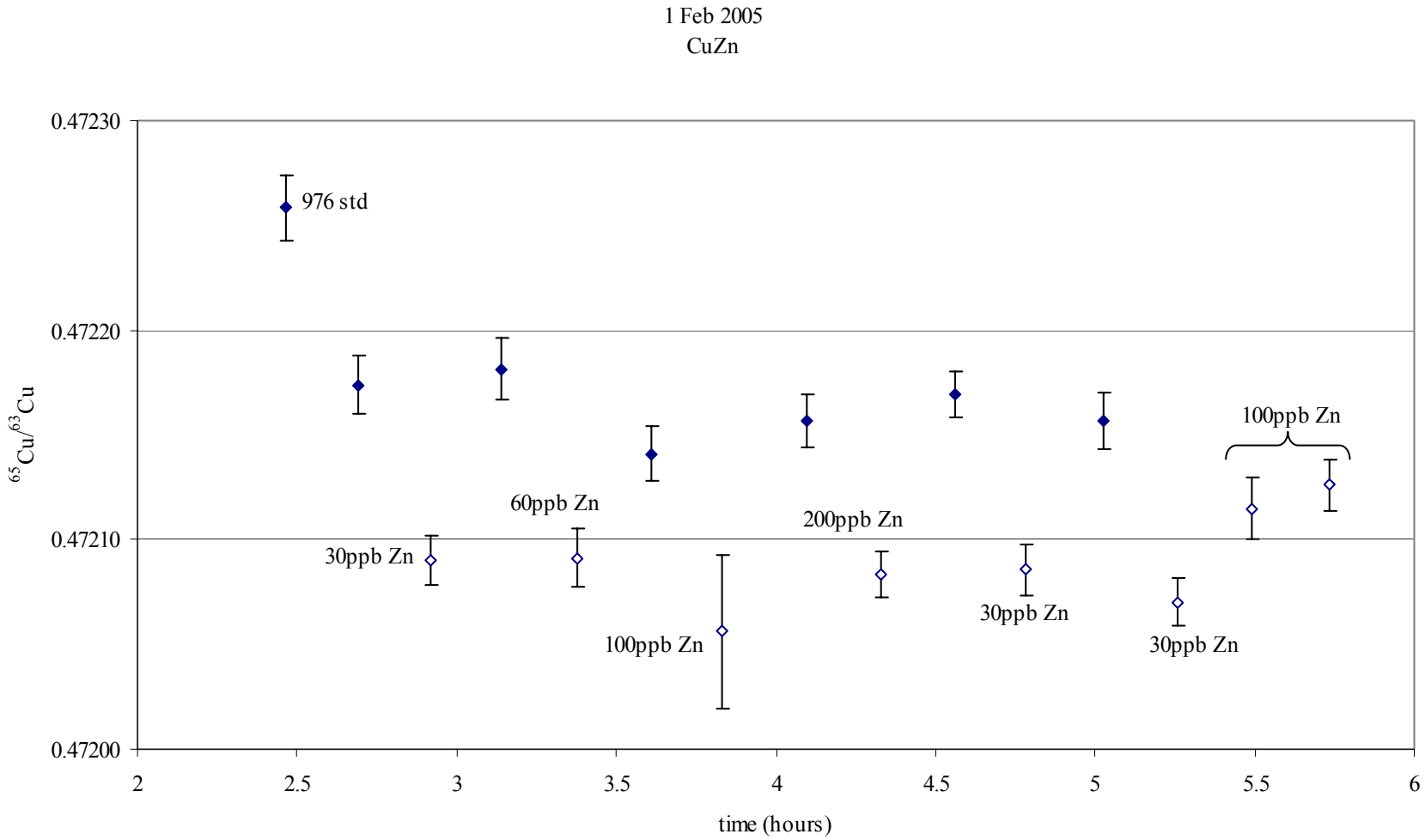

Figure 4. Analytical run (1 Feb 2005) showing the effect on $^{65}Cu/^{63}Cu$ ratio for NIST SRM 976 doped with a shelf solution of different Zn concentrations. Solid diamonds are undoped NIST SRM 976 (100ppb Cu).

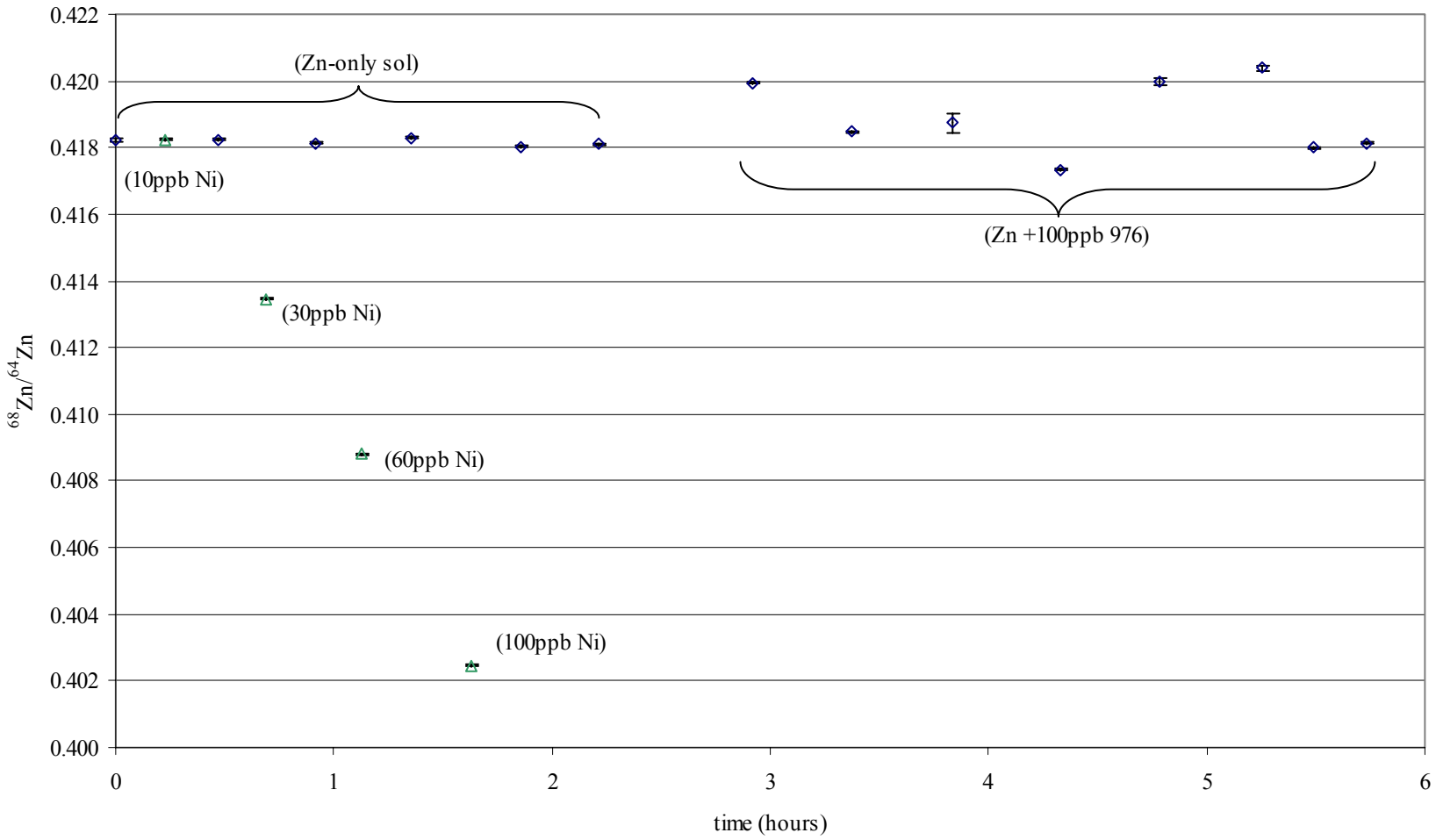

Figure 5. Analytical run (1 Feb 2005) showing the effect of a Ni-solution (NIST SRM 986) of varying concentrations over the $^{68}Zn/^{64}Zn$ ratio of a shelf solution of 100ppb zinc. (Zn-only sol) is the undoped shelf solution of zinc. (Zn +100ppb 976) is the zinc shelf solution doped with 100ppb NIST SRM 976.

This technique depends on complete recovery of copper in the sample during purification, since extreme isotopic fractionation of <10 per mil can occur on the ion exchange resin (Fig. 6) (also, Maréchal et al., 1999; Maréchal and Albarède, 2002).

For purposes of comparison, a purification elution scheme was developed for resins AG MP-1 and AG MP-1M to evaluate the isotopic analyses of a purified relative to unpurified chalcopyrite sample (Sup-1). The procedure for chromatographic separation of copper from sulfide samples is presented in Appendix 1. The elution curves for these resins are presented in Figure 7. Processing procedures on both resins used similar eluant solution (7N HCl + 0.1% H_2O_2) for separation of Cu from the mineral matrix. Fe and Zn are removed from the resin only after changing acid strength or type. The difference in the separation process for these resins is the volume of eluant necessary to remove copper, with the copper eluting from MP-1M earlier than MP-1. Cuprous copper has little interaction with the resin and comes off the resin almost immediately. Thus, copper must be in the cupric form in order for this elution scheme to be successful, and a strongly oxidizing potential (produced by 0.1% H_2O_2) is required of the eluant acid. Processing of the sample Sup-1 by elution on the AG MP-1M resin was performed prior to isotopic analysis. The δ^{65}Cu value of this purified sample (0.52‰) is analytically identical to the average value of unpurified samples (0.54‰, n = 9). These results confirm the interpretations of the doping experiments and indicate that purification of copper sulfide minerals (i.e., chalcopyrite, bornite, chalcocite, etc.) prior to isotopic analysis is probably unnecessary. Other workers investigating hydrothermal ore deposits also suggest that chromatographic separation is not required for obtaining reliable and meaningful copper isotopic results from Cu-Fe sulfides (Rouxel et al., 2004; Graham et al., 2004).

Separation of copper from a bulk rock matrix has also been attempted, although with less successful results. The procedure utilized in this investigation is presented in Appendix 1. A concentrated rock matrix apparently causes copper to be less strongly bound to the resin, with consequent earlier removal than in cases where only a dilute matrix is present. Figure 8 shows elution of copper on MP-1M resin, relative to other selected elements. Copper purification with this resin and the eluant acids utilized requires a multi-step separation technique since a single elution pass produces an incomplete separation of copper from a concentrated matrix. The complex oxidation-reduction reactions which occur on the resin bed also require that strongly oxidized conditions be carefully maintained. Other investigators have used other leaching processes and chromatographic resins to successfully separate Cu from bulk rock (Luck et al., 2003).

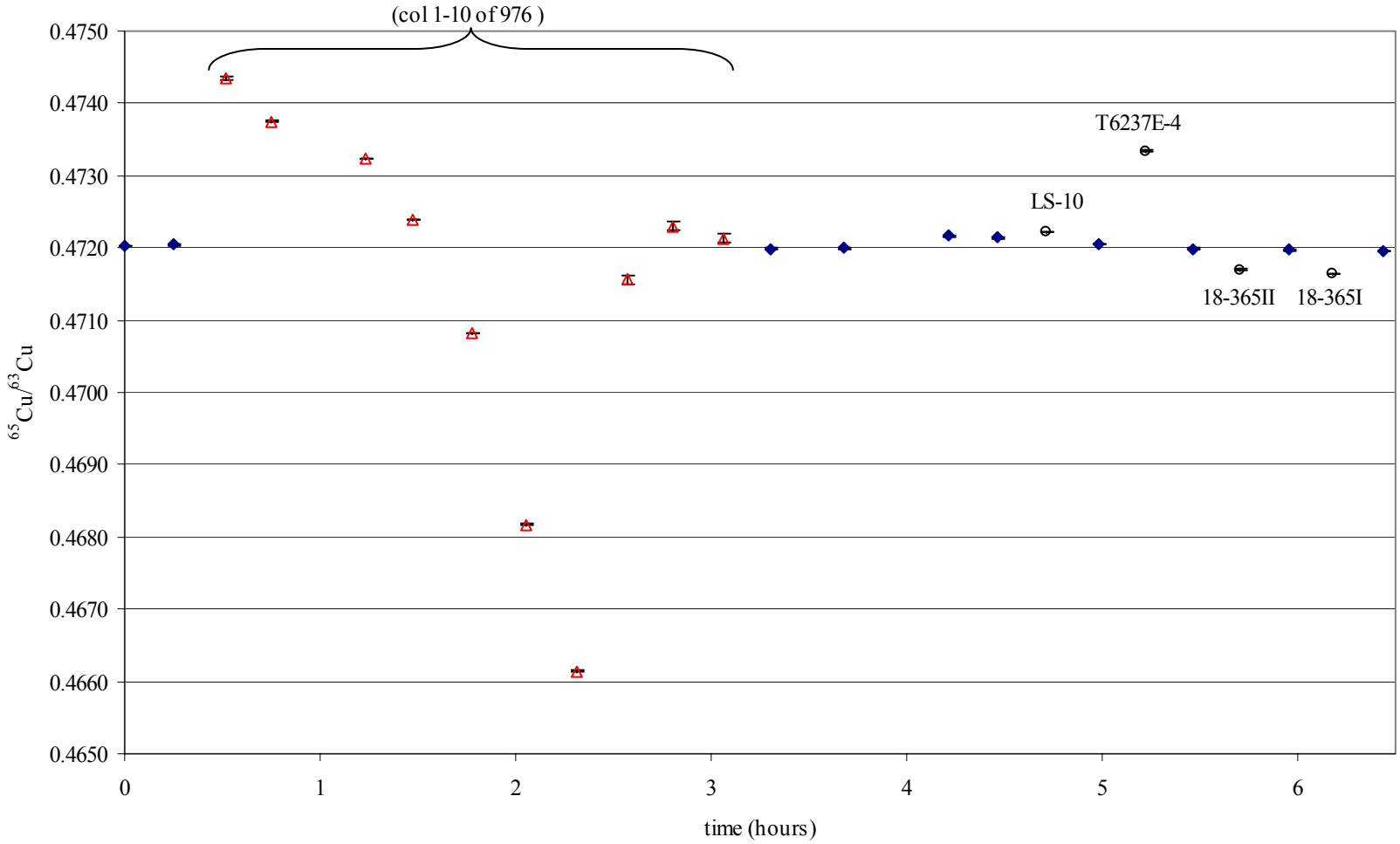

Figure 6. Analytical run (30 Apr 2002) showing the extreme copper isotopic fractionation induced through chromatography. Shown are different collections for NIST SRM 976 processed on MP-1M resin (anion exchange). For comparison, sample T6237E-4 has a δ^{65}Cu value of 2.98 per mil. Closed diamonds are undoped NIST SRM 976 (100ppb Cu), with other symbols as labeled

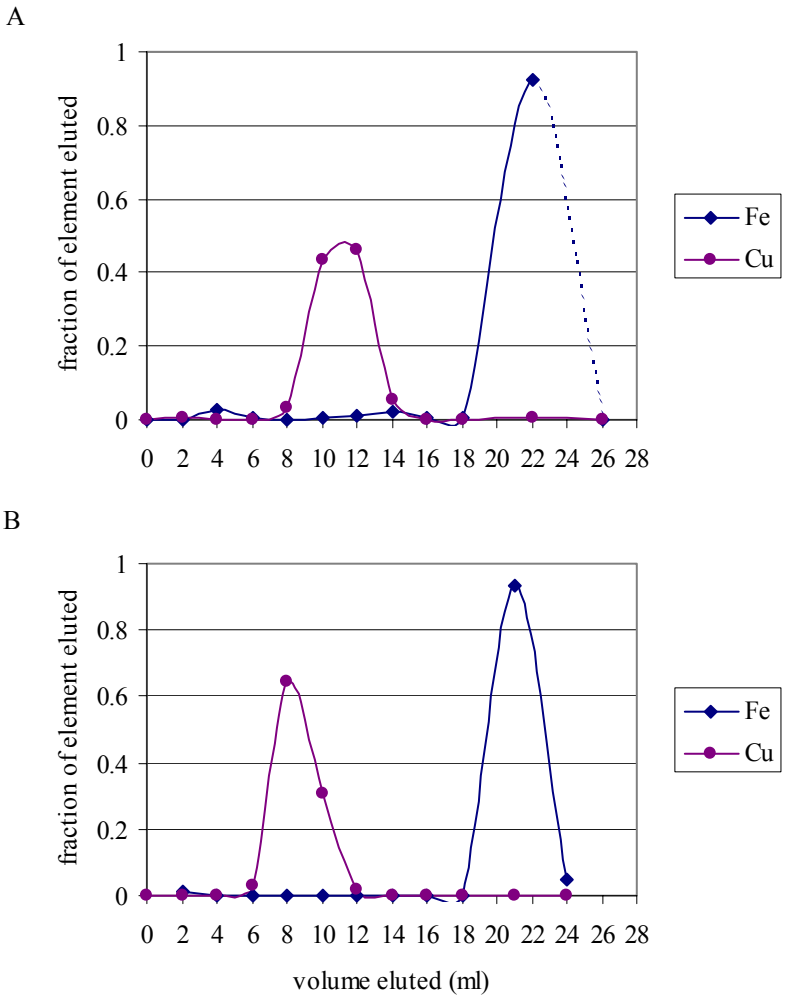

Figure 7. Elution curves for sample SUP-1 on (A) MP-1, and (B) MP-1M resins. Acid is changed at 18ml to remove Fe from the resin (Appendix 1). Dashed curve in (A) is extrapolated. Fraction of element eluted is the fraction of element recovered in that collection relative to total eluted element.

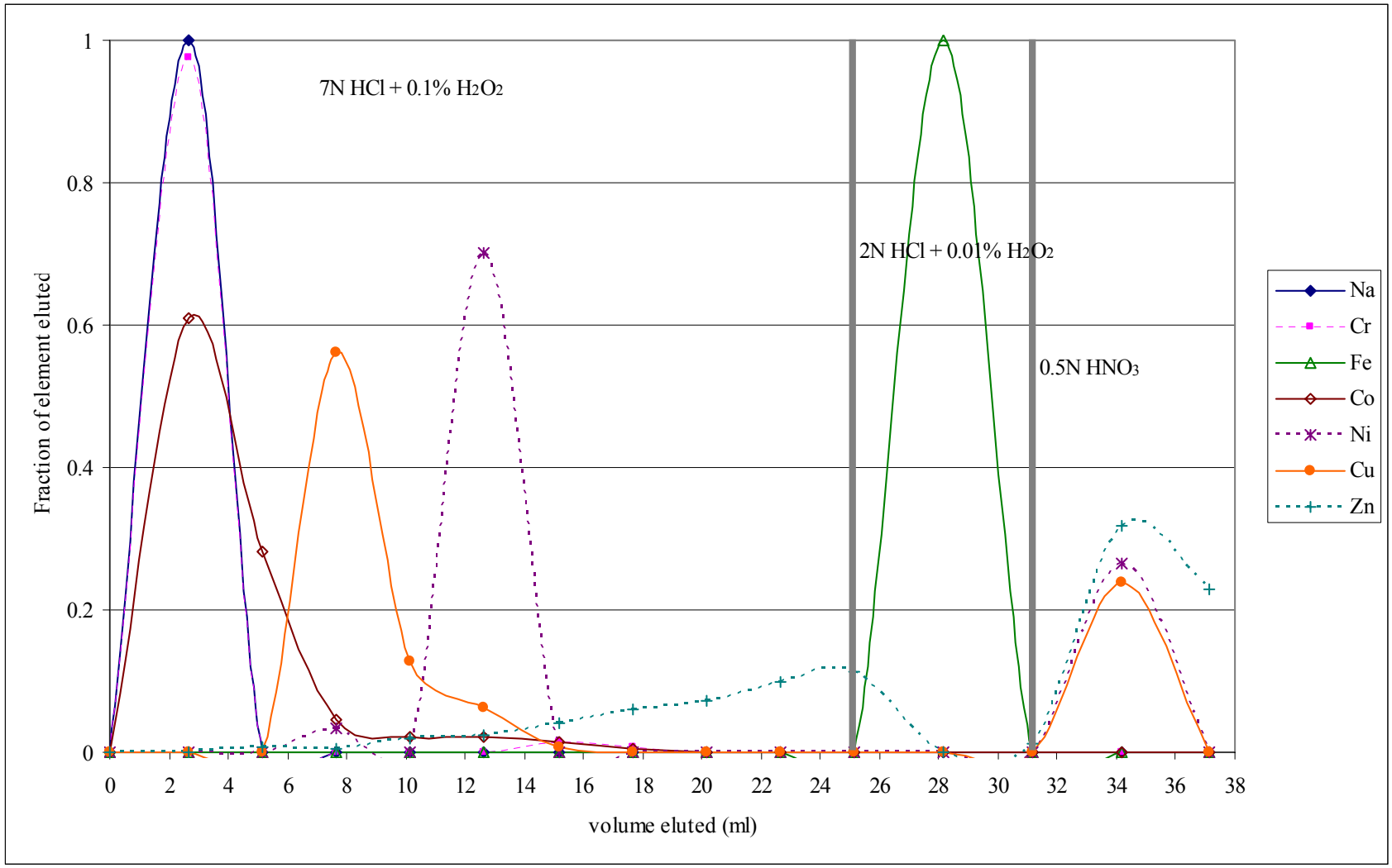

Figure 8. Elution curves for sample BCR-P (basalt standard) on resin MP-1M. Complete separation of copper using a procedure similar to this would require double processing for best copper purification. The reason for the increase in zinc eluted between 12 and 25ml is presently unclear. Heavy vertical lines represent acid change.

Isobaric Interferences

Isotopic mass interference due to isobaric species is a potential problem for any isotopic analysis. Potential isobaric interferences with copper include molecular charged species containing Cl, Ar, Ti, Sc, Ba, Al, Si, Mg, S, and Na (Maréchal et al., 1999; Mason et al., 2004a). Possible interferences can be monitored by examining the mass peaks produced by the individual species or through high resolution mass scans. Of biggest concern from this group is $ArNa^{+}$. However, from elemental analysis of solutions of pure copper minerals, sodium and the other elements are generally very low (Table 1). Samples with high Na would require chromatographic purification. Additional concern in the isotopic analysis of Cu minerals is the presence of molecular S species (i.e., $S^{32}S^{33}$). However, the dissolution procedure employed quantitatively removes sulfur from the samples (see Section III).

Mass Fractionation Correction

Machine fractionation effects, also known as mass bias or mass discrimination, are isotopic fractionation effects produced by processes in the mass spectrometer, such as from the plasma ionization, ion extraction, and/or ion transmission. These effects produce a measurable change from the true isotopic composition of a sample and must be monitored and corrected. The Neptune MC-ICPMS employed at Washington State University produces a considerable machine fractionation of copper isotopes (approximately 3%/amu), whereby the heavier isotope is preferentially extracted and/or transmitted in the ion beam. This fractionation is inconsistent from day to day (Fig. 9), but may be very consistent during a single analytical run (Fig.1). The magnitude of this change during an individual analysis is generally less than that related to a similar TIMS measurement, although it is presently unclear why there is a variation in machine fractionation during a single measurement, since sample is continuously supplied to the plasma by the nebulizing system.

Mass fractionation by the Neptune® drifts slightly during an analytical session so it can be monitored and corrected. The mass fractionation can be described in terms of the β factor, which is calculated as follows:

$$\beta = \frac{\left(\frac{(^{65}Cu/^{63}Cu)_{true}}{(^{65}Cu/^{63}Cu)_{measured}}\right)}{\left(\frac{Mass65_{Cu}}{Mass63_{Cu}}\right)}$$

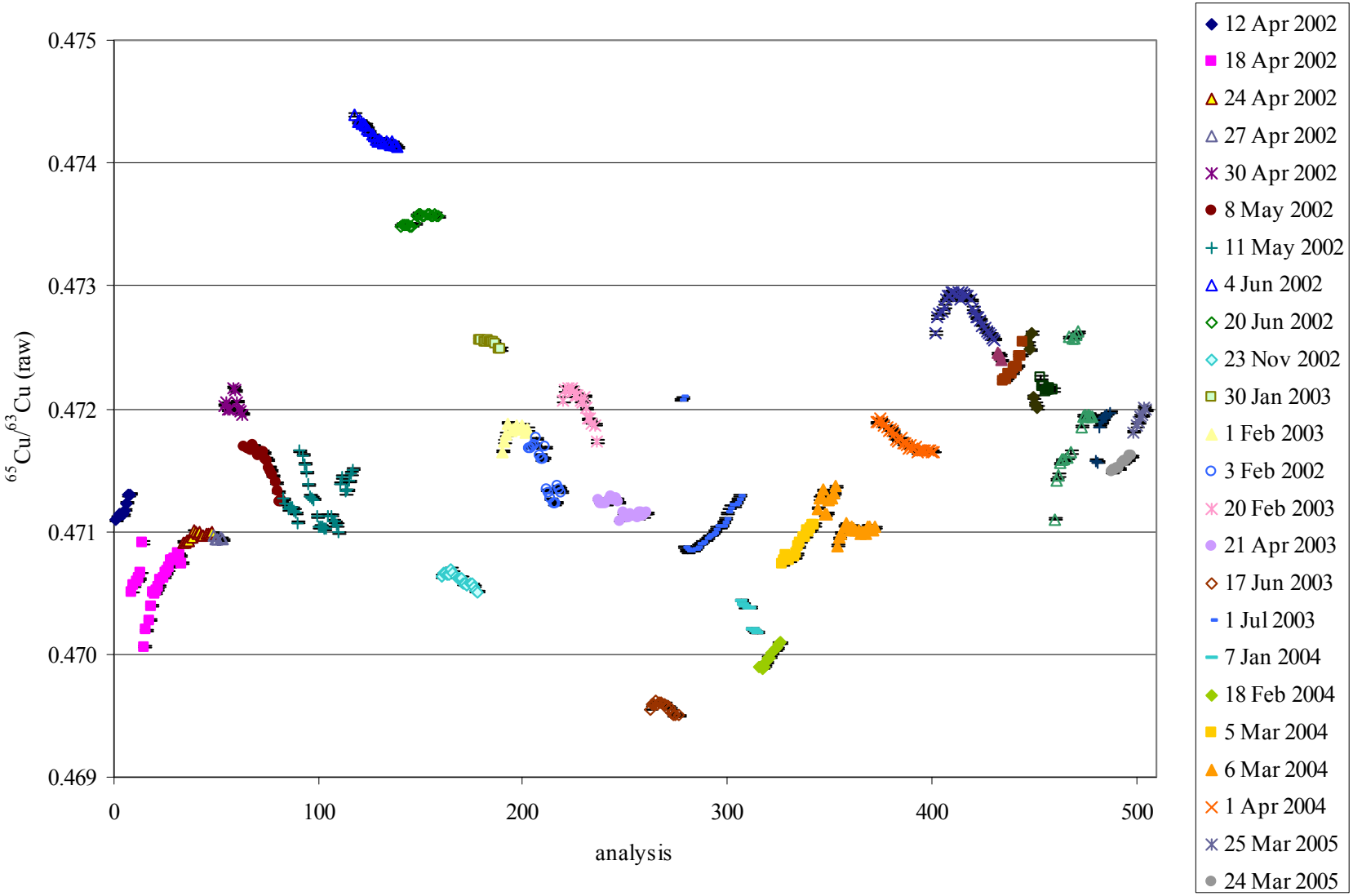

Figure 9. $^{65}Cu/^{63}Cu$ analyses of NIST SRM 976 over three years (505 analyses). Average isotopic ratio of the standard is 0.471606.

The average fractionation coefficient (β) for NIST SRM 976 on the Neptune is -1.82. The machine fractionation factor (mff) based on the exponential law is calculated as:

$$mff = (Mass_{65Cu}/Mass_{63Cu})^{\beta}$$

Using the mean β-factor gives a mean fractionation factor of 0.944861 (n = 505) using an exponential correction, although this value can not be used for individual analytical sessions. Machine drift during the analytical session requires that a slightly different correction be applied to each measurement. The methods utilized to correct machine mass fractionation are by either of two methods. The sample-standard bracketing method corrects machine fractionation by normalizing the sample unknown analysis with a normalizing value determined from bracketing analyses of a standard of known isotopic composition. The external normilization method requires doping the sample with another element of known isotopic composition from which a normalization factor is determined and applied to the isotopes of interest. Since both of these methods can be employed each will be presented in the following discussion.

Sample-Standard Bracketing Correction

The sample-standard bracketing correction technique is commonly used in light stable element isotopic analyses and was first utilized for copper isotopes unassisted by external normalization (element doping) by Zhu et al. (2000). This method consists of running standards alternating with unknown samples and then correcting machine fractionation and machine drift at the same time. A linear extrapolation is made between the measured isotopic ratio of the standards and the value along that extrapolation at the time of the sample analysis is normalized to the standard's true isotopic value. This same normalizing correction is then applied to the unknown sample ratio (Fig 10).

For this correction method to be reliable, the mass fractionation response must be the same for the standard and the sample unknown. Isotopic results from doping experiments and chromatographic purification of chalcopyrite indicate that this is very likely the case for the types of samples analyzed in this investigation. Albarède et al. (2004) have indicated that both unknown sample and standard solutions should have the same target element

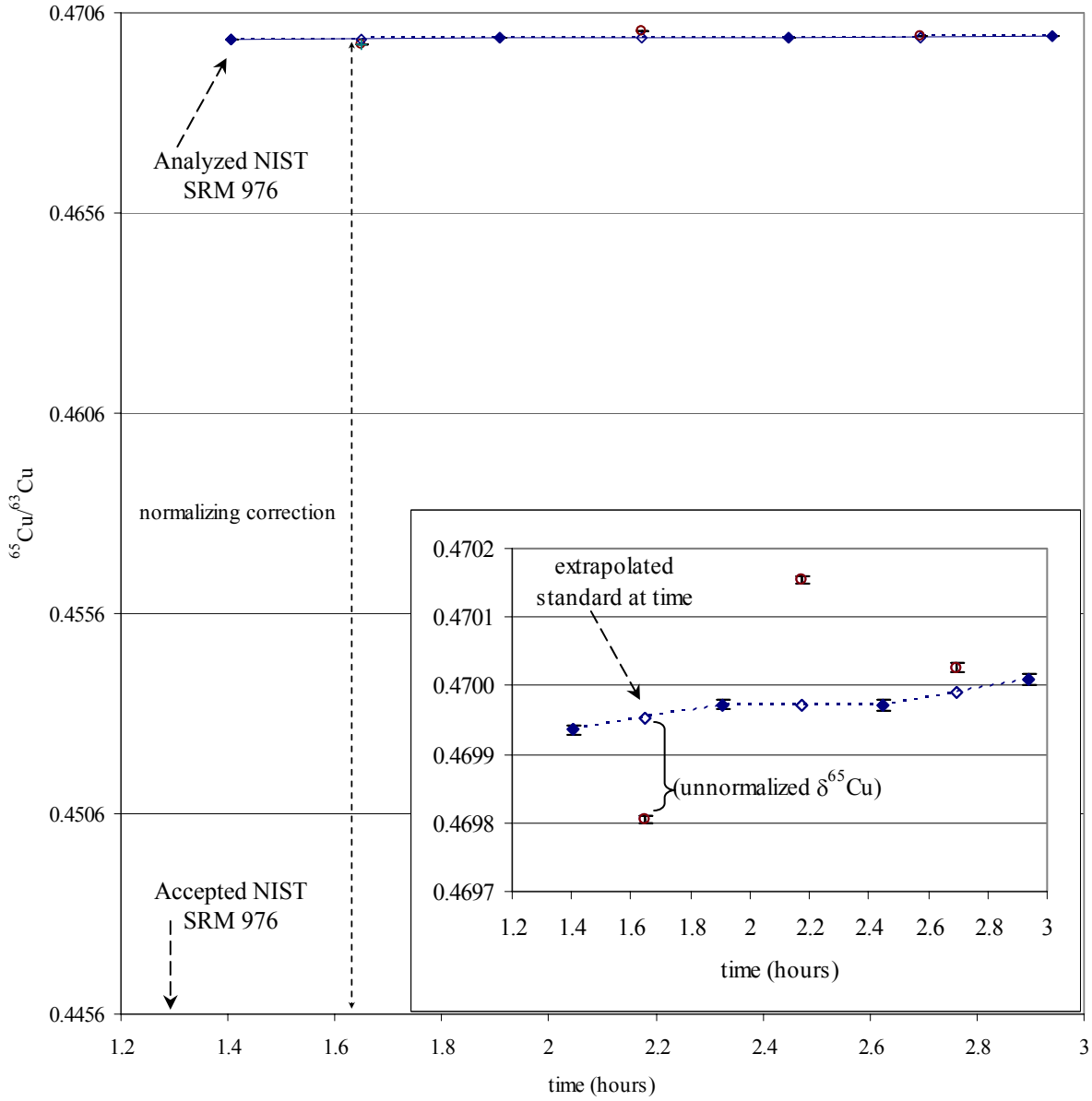

Figure 10. Graphical representation of the time-corrected sample-standard bracketing technique for drift and machine fractionation correction (18 Feb 2004). The inset shows the extrapolation (assumed to be linear) of the standard at time of sample analysis on a different vertical scale.

concentrations and similar solution matrix in order for the sample-standard bracketing correction procedure to be reliable. However, from this investigation it is observed that samples analyzed at copper concentrations significantly different than bracketing samples give analytically identical results as the same sample run at nearly the same concentrations to the bracketing standards (Table 2). It is presently unclear why there is so little difference between the results of samples of very different concentrations, and indicates that the Neptune® at Washington State University is less dependent on this concentration requirement than suggested by Albarède et al. (2004).

The sample-standard bracketing method also requires that standard-to-standard machine drift be constant and machine drift during the analytical session be generally uniform. The Finnigan Neptune at WSU is commonly characterized by stable drift in copper ratios over the course of an analytical session (Fig. 1). Stable machine drift gives more reliable results. Any standards which show large drift during the course of analysis usually require repeat analysis of the unknown sample until the bracketing standards are separated by less drift (Fig. 11). Evaluation of the internal copper isotope standards indicates that there is little correlation in a large drift between bracketing standards and the calculated δ^{65}Cu values, apart from the values commonly, but not always, being outside of 2σ standard deviation reproducibility from the mean value (Fig 12).

The long-term reproducibility of the sample-standard bracketing technique is ±0.08 per mil (2σ, standard deviation) (Appendix 2) determined from repeat analyses of Ray-1 (native copper sample) over three years.

Element Doping Correction

External normalization through element doping has been a popular method for performing machine fractionation corrections. In this procedure a sample is doped with an element with isotopes similar in masses to those of the target element (Maréchal et al., 1999; White et al., 2000; Mason et al., 2004b). The mass fractionation correction is determined from normalizing the external standard isotope ratio to its true value, which is then applied to correct the mass fractionation of the target isotope, in this case, copper. Zinc and nickel both have isotopes with masses near those of copper so standards of these elements have been used for the external correction (Maréchal et al. 1999; Graham et al., 2004; Erhlich et al., 2004). A nickel NIST SRM standard exists for this purpose (986) but no accepted zinc isotopic standard presently exists. Other investigators have developed laboratory zinc isotopic standards by correcting machine fractionation of zinc with the NIST SRM 976 Cu standard. This investigation evaluated zinc doping using the same zinc standard as in Maréchal et al. (1999), kindly provided by J. Vervoort.

Table 2. Comparison of $\delta^{65}Cu$ for select samples at different Cu concentrations relative to bracketing NIST SRM 976 standards.

sample	$\delta^{65}Cu$ (‰)	% of standard[1] concentration	sample	$\delta^{65}Cu$ (‰)	% of standard[1] concentration
LS-10	0.30	108.95	S27-A 1847	0.40	100.69
LS-10	0.27	90.87	S27-A 1847	0.45	248.64
LS-10	0.22	101.44	S27-A 1847	0.45	114.58
LS-10	0.23	112.48	SUP-3A(1)	0.14	30.09
LS-10	0.29	89.49	SUP-3A(1)	0.12	104.91
LS-10	0.22	86.89	SUP-3A(2)[2]	0.06	73.83
LS-10	0.34	91.01	SUP-3A(2)	0.06	82.73
OKM-2	0.00	66.5	SUP-3A(3)	0.04	91.01
OKM-2	0.09	101.25	SUP-3A(4)	0.02	47.45
RAY-1	0.02	98.72	SUP-3B(1)	0.09	119.52
RAY-1	-0.08	102.2	SUP-3B(1)	0.04	136.79
RAY-1	-0.06	131.29	SUP-3C(1)	0.06	106.35
RAY-1	-0.08	106.79	SUP-3C(1)	0.03	120.67
RAY-1	-0.14	100.02	SUP-3C(2)	0.03	99.19
RAY-1 #1	-0.01	115.81	SUP-3C(2)	0.05	98.79
RAY-1(b)	0.02	94.44	SUP-3C(2)	0.01	112.83

[1]% of standard concentration is determined from relative voltages of the ion beams of the samples to the standards.

[2]SUP-3A, SUP-3B, and SUP-3C are dissolutions of the same sample of massive chalcopyrite.

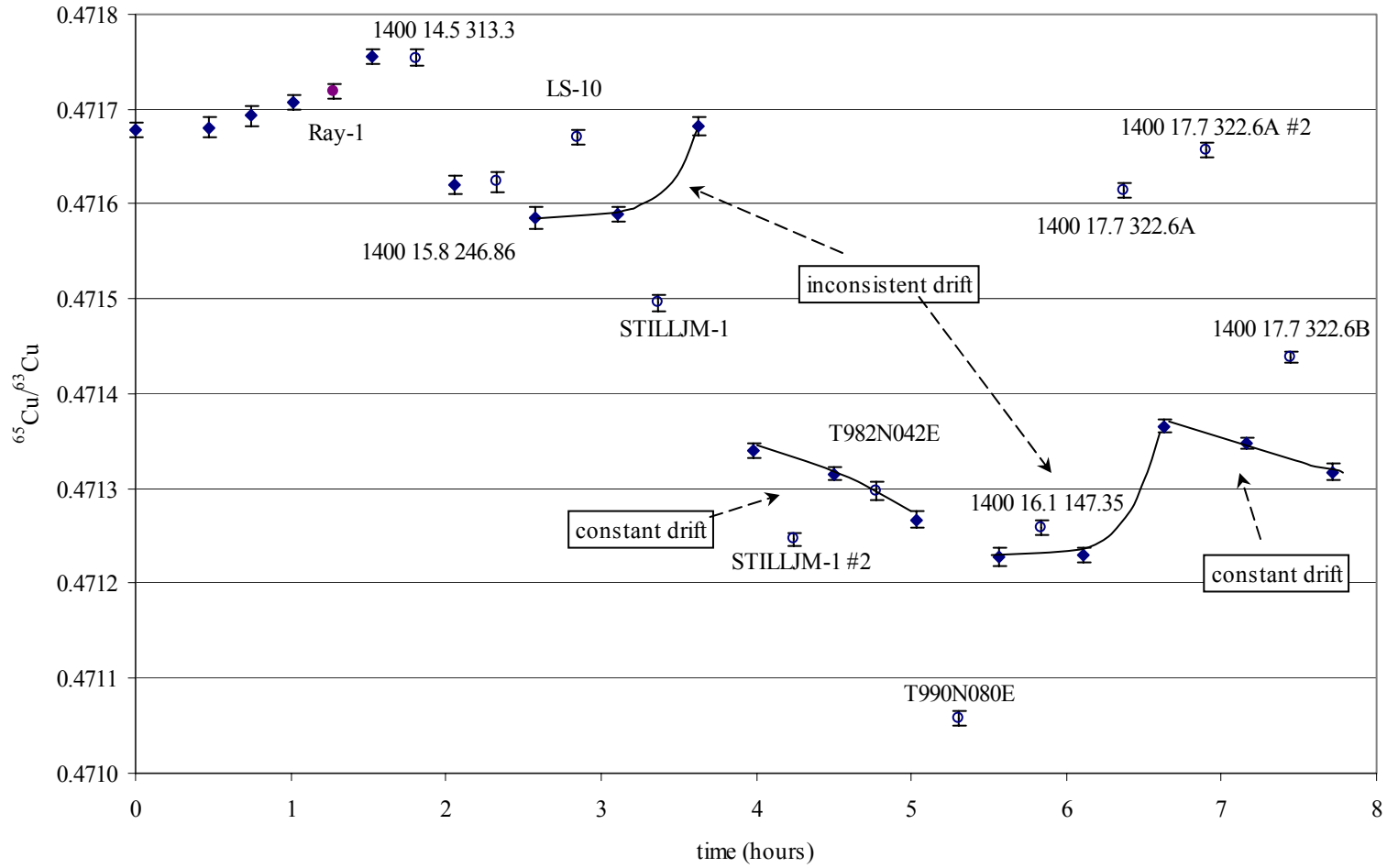

Figure 11. Analytical run (3 Feb 2003) showing irregular machine drift and repeat analysis of samples STILLJM-1 and 1400 17.7 322.6A. Even a linear extrapolation off of the constant drift lines would still give unreliable results in some cases, so these samples must be reanalyzed.

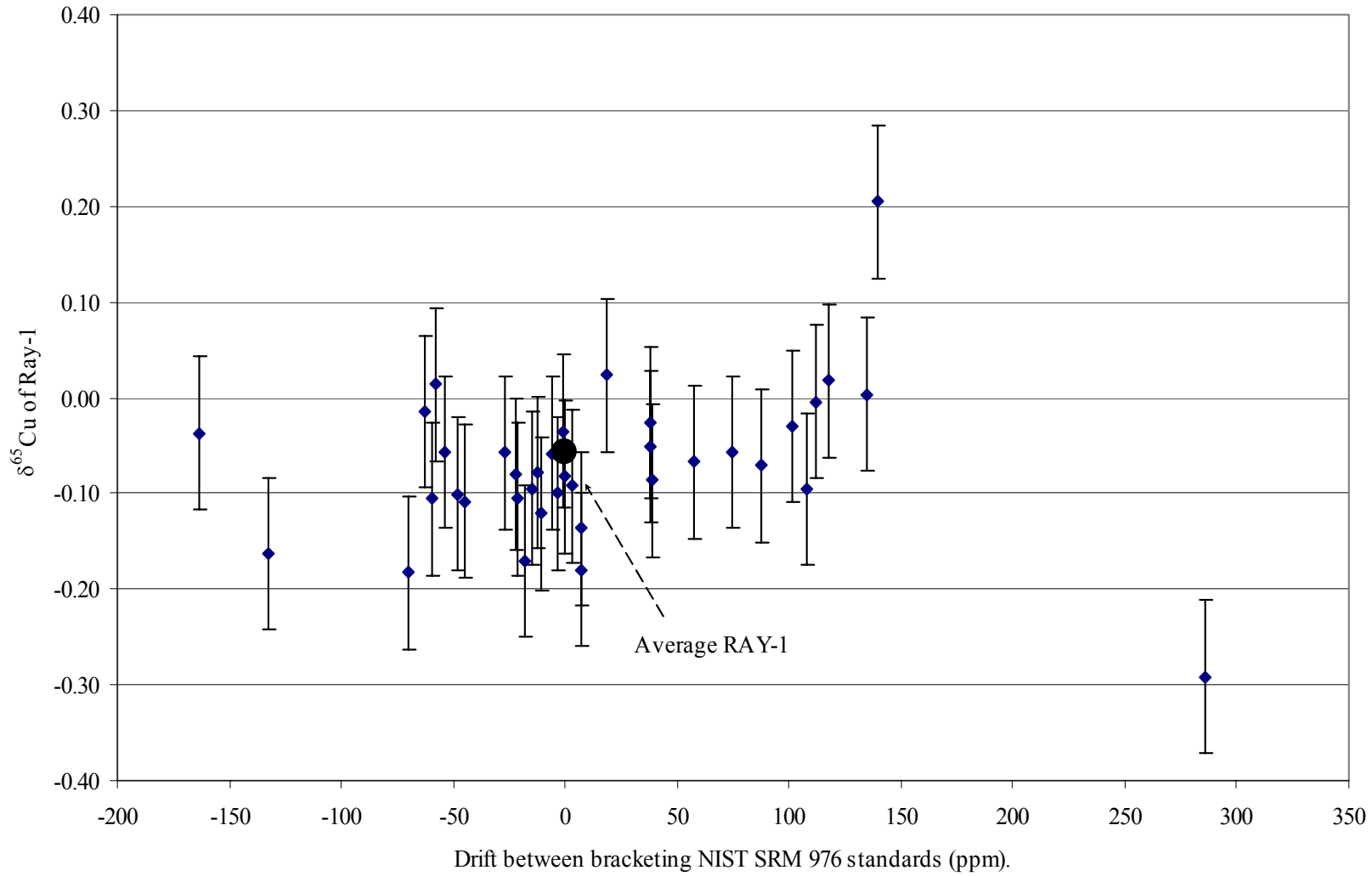

Figure 12. Graph of δ^{65}Cu of RAY-1 vs. the drift between bracketing standards. Error bars are long term 2σ standard deviation reproducibility of standard. Average RAY-1 (large black circle) assumes no drift between standards.

Zinc isotopes are fractionated by ICP-MS somewhat similarly to copper isotopes, although the difference is sufficient to prevent the application of the zinc fractionation factor directly to correct for the machine fractionation of copper (Maréchal et al., 1999). However, if the ratio of the fractionation coefficients (β) of zinc isotopes and copper isotopes in the doped sample are constant, then a correction factor based on zinc isotopes can be determined and applied to copper isotope ratios to account for the difference in machine fractionation between zinc and copper. Maréchal et al. (1999) and White et al. (2000) present the mathematical basis for this correction. The ratio β^{Zn}/β^{Cu} must be constant during the analytical run for this method to be successful. The constancy of β^{Zn}/β^{Cu} is usually graphically determined by plotting the natural logarithm of the measured ratio of a pair of zinc isotopes verses the natural logarithm of the measured copper isotope ratio (Fig. 13). If the data lie on a straight line with good correlation in least squares line fitting, then the requirement that β^{Zn}/β^{Cu} is constant is satisfied. β^{Cu} is then corrected relative to the deviation of the measured relationship (i.e., line) from the theoretical fractionation behavior (which assumes no machine fractionation occurs for any isotopes). This in effect corrects the copper fractionation coefficient by the constant of proportionality between zinc and copper fractionation behavior.

Figure 14 shows how the β^{Zn}/β^{Cu} correlation varies depending on the zinc isotope pair utilized (as seen by the linear array of the natural logarithms of the isotope ratios). $^{68}Zn/^{64}Zn$ and $^{68}Zn/^{66}Zn$ ratios have been employed in published investigations (Maréchal et al., 1999; Maréchal and Albarède, 2002). However, no specific isotope pair has been accepted as the best correcting isotope pair (Maréchal et al., 1999). Table 3 shows the variations in corrected $\delta^{65}Cu$ values for three samples, RAY-1, SUP-1 and BEAV-2, relative to the different zinc isotope pairs utilized. The standard deviation in corrected $\delta^{65}Cu$ is greater for some zinc isotope pairs than the 2σ sample-standard bracketing correction, but less for others. The $^{68}Zn/^{64}Zn$-corrected mean RAY-1 value is generally closest to the mean value from sample-standard bracketing (both -0.06‰), and farthest with $^{67}Zn/^{66}Zn$ (-0.14‰). The standard deviation is also greatest for $^{67}Zn/^{66}Zn$, although this does not necessarily appear to be related to the agreement between the zinc corrected mean $\delta^{65}Cu$ and the accepted mean value from sample-standard bracketing. The sample BEAV-2 shows much poorer reproducibility for all zinc isotope pairs, although in this case the correction using $^{67}Zn/^{66}Zn$ gives the same mean value (1.04‰) as the sample-standard bracketing correction (1.04‰). The variation in corrected values between different isotope pairs has been noted and investigated by Mason et al. (2004b). They argued that the $^{66}Zn/^{64}Zn$ ratio produced the highest precision data with their analytical setup.

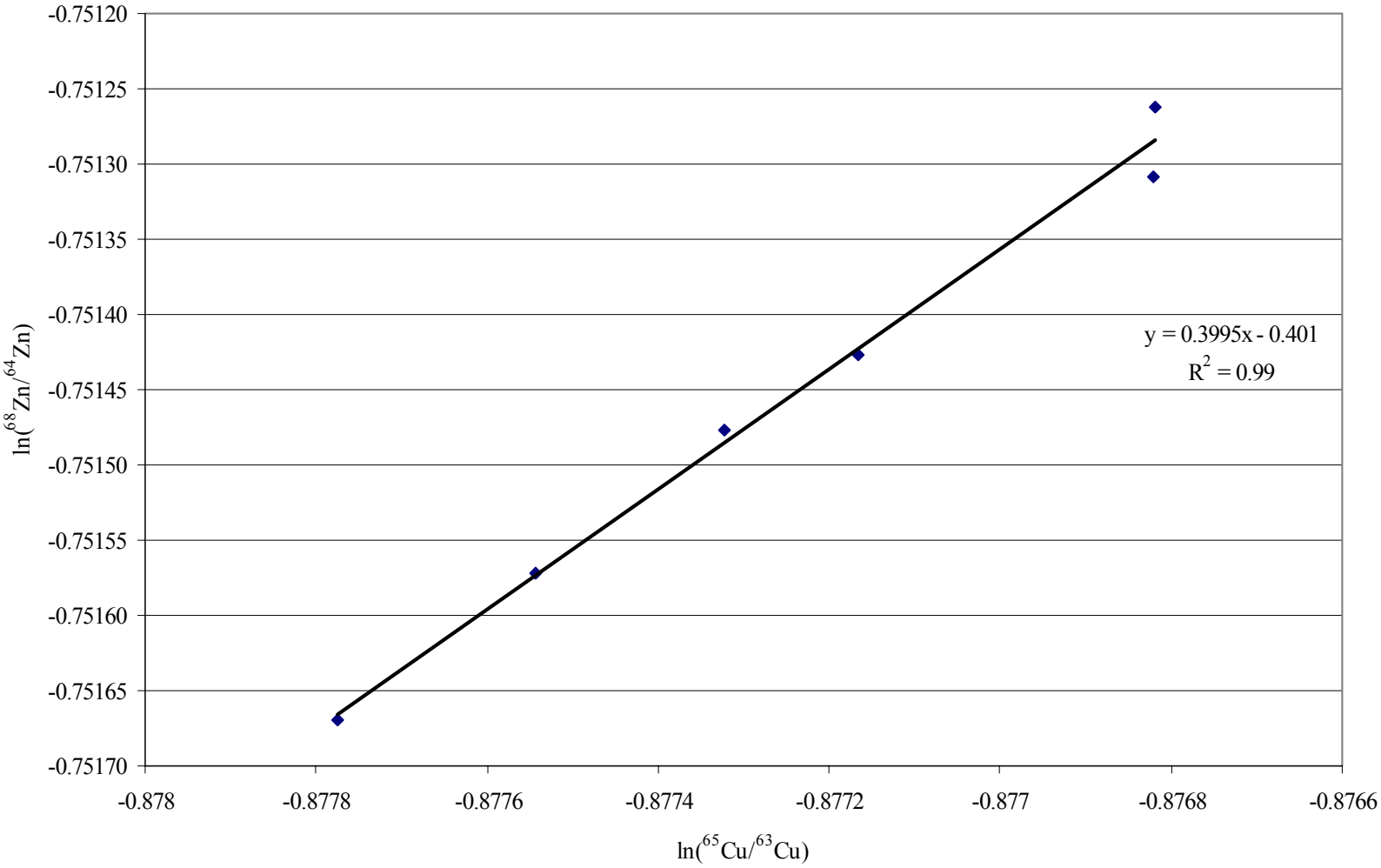

Figure 13. Graph of $\ln(^{68}Zn/^{64}Zn)$ verses $\ln(^{65}Cu/^{63}Cu)$, showing similarity of machine fractionation of both elements by the Neptune® (15 Mar 2005). The good correlation coefficient of the best fit line to the data indicates that during this analytical run β^{Zn}/β^{Cu} was effectively constant for these isotopes

.

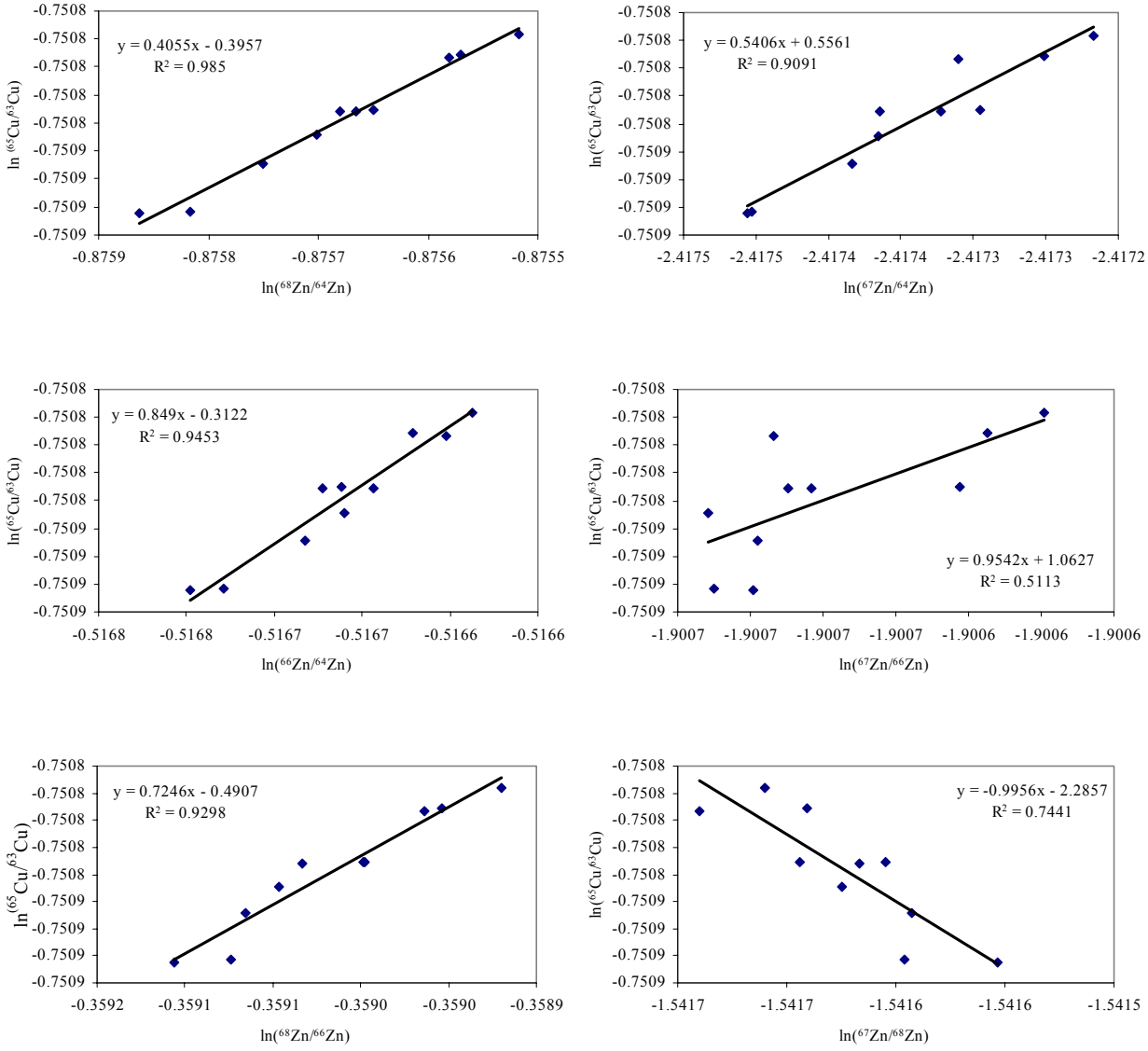

Figure 14. Graphs of ln(^{65}Cu/^{63}Cu) verses ln(zinc isotope ratio) showing differences in correlation factors for different zinc isotope pairs (analyses of 25 Mar 2005). Correlation of the isotope ratios ^{67}Zn/^{68}Zn and ^{67}Zn/^{66}Zn are consistently the poorest.

Table 3. Comparison of corrected $\delta^{65}Cu$ using different zinc isotope pairs.

		corrected $\delta^{65}Cu$ (‰) using the zinc ratio:											
date	sample	$^{68}Zn/^{64}Zn$	$R^{2(1)}$	$^{66}Zn/^{64}Zn$	R^2	$^{68}Zn/^{66}Zn$	R^2	$^{67}Zn/^{68}Zn$	R^2	$^{67}Zn/^{66}Zn$	R^2	$^{67}Zn/^{64}Zn$	R^2
15-Mar-05	RAY-1	-0.037	0.989	0.058	0.987	-0.129	0.991	0.060	0.883	-0.281	0.906	-0.070	0.971
24-Mar-05	RAY-1	0.105	0.688	1.459	0.715	0.619	0.493	0.683	0.016	0.529	0.663	0.960	0.861
25-Mar-05	RAY-1 #1	-0.062	0.985	-0.032	0.945	-0.091	0.928	0.010	0.744	-0.187	0.511	-0.107	0.909
	RAY-1 #2	-0.071	0.985	-0.051	0.945	-0.100	0.928	-0.147	0.744	-0.069	0.511	-0.040	0.909
	RAY-1 #3	-0.060	0.985	-0.078	0.945	-0.056	0.928	-0.081	0.744	-0.083	0.511	-0.064	0.909
	RAY-1 #4	-0.065	0.985	-0.073	0.945	-0.055	0.928	-0.044	0.744	-0.081	0.511	-0.080	0.909
	mean[2]	-0.059		-0.035		-0.086		-0.040		-0.140		-0.072	
	2σ	0.023		0.099		0.056		0.143		0.165		0.044	
15-Mar-05	BEAV-2	0.931	0.989	0.949	0.987	0.914	0.991	0.997	0.883	0.807	0.906	0.898	0.971
24-Mar-05	BEAV-2	1.073	0.688	1.719	0.715	1.619	0.493	1.622	0.016	1.578	0.663	1.639	0.861
25-Mar-05	BEAV-2 #1	0.921	0.985	0.938	0.945	0.899	0.928	0.908	0.744	0.887	0.511	0.923	0.909
	BEAV-2 #2	0.919	0.985	0.934	0.945	0.902	0.928	0.885	0.744	0.877	0.511	0.921	0.909
	mean	0.961		1.135		1.084		1.103		1.037		1.095	
	2σ	0.130		0.675		0.618		0.605		0.628		0.628	
15-Mar-05	Sup-1 +Zn	0.523	0.989	0.543	0.9865	0.503	0.991	0.672	0.883	0.337	0.906	0.467	0.971

[1]R^2 is the correlation of linearity for the data points plotted on ln(Zn isotope ratio) vs. ln($^{65}Cu/^{63}Cu$). It is shown to give an indication of constancy in β^{Zn}/β^{Cu} for the isotopes of zinc indicated.

[2]Data from 24 Mar 2005 not calculated in the mean as β^{Zn}/β^{Cu} was not constant during the analytical run.

NIST SRM 976 Cu standard has also been doped with the nickel isotopic standard (NIST SRM 986) to test the feasibility of using nickel as an isotopic standard to correct for mass fractionation. Both Ni and Cu have similar first ionization potentials so, in theory, nickel should have a more similar plasma ionization behavior to copper than does zinc. Ehrlich et al. (2004) and Graham et al. (2004) have used nickel-doping to correct for copper machine fractionation. However, observations from this investigation indicate that nickel tends to exert a considerable matrix effect over copper on the Finnigan Neptune® (Fig 15). Analyses of SRM 976 doped with SRM 986 (Ni) show more extreme variations in β^{Cu}/β^{Ni} (Fig. 16) relative to β^{Cu}/β^{Zn}, with variation in the correlation of the fractionation coefficient ratio between Ni and Cu depending on which isotope ratios are used (i.e., $^{62}Ni/^{60}Ni$ verses $^{61}Ni/^{62}Ni$). A comparison of Ni-corrected $\delta^{65}Cu$ values for several samples is shown in Table 4. It is difficult to reconcile Ni-doping results from this investigation to those cited above since they do not indicate the specifics of their results, or whether the constancy of β^{Ni}/β^{Cu} in their correction was satisfied.

Elemental doping for correction of machine fractionation of copper requires two important aspects to be satisfied. First, it is clear that if β^{Zn}/β^{Cu} (or β^{Ni}/β^{Cu}) is to be constant then the isotopes of the dopant element must be fractionated in a consistent manner by the ICP-MS system during an analytical run. From the discussion above, it is evident that this may or may not occur, and is not presently predictable on the Neptune®. The second aspect is that in using the method of mass fractionation correction by element doping there must be drift during the course of the analytical session, and in fact the greater the drift the better constrained the relationship of $\ln(^{65}Cu/^{63}Cu)$ vs. ln(dopant isotope ratio), as long as $\beta^{element}/\beta^{Cu}$ is constant. The machine drift must affect all isotopes used in sample measurement and the correction procedure in a consistent manner. Figure 17 shows the significance of machine drift relative to determining the measured slope of the line that is used to correct the copper fractionation factor. The Neptune® MC-ICPMS in the Department of Geology at Washington State University often shows relatively limited and consistent machine drift, and what drift is present may affect certain isotope ratios of the same element differently (Fig. 18). Other first generation MC-ICPMS machines (e.g., Plasma 54) likely have a more erratic drift, making the Zn doping method preferable to the sample-standard method for the machine isotope fractionation correction of copper for these instruments.

Even though precision may be improved by this method over the sample-standard bracketing method, there are disadvantages to using elemental doping in making machine fractionation corrections. This method generally requires chromatographic purification of copper to remove natural Zn or Ni (both of which tend to be low in

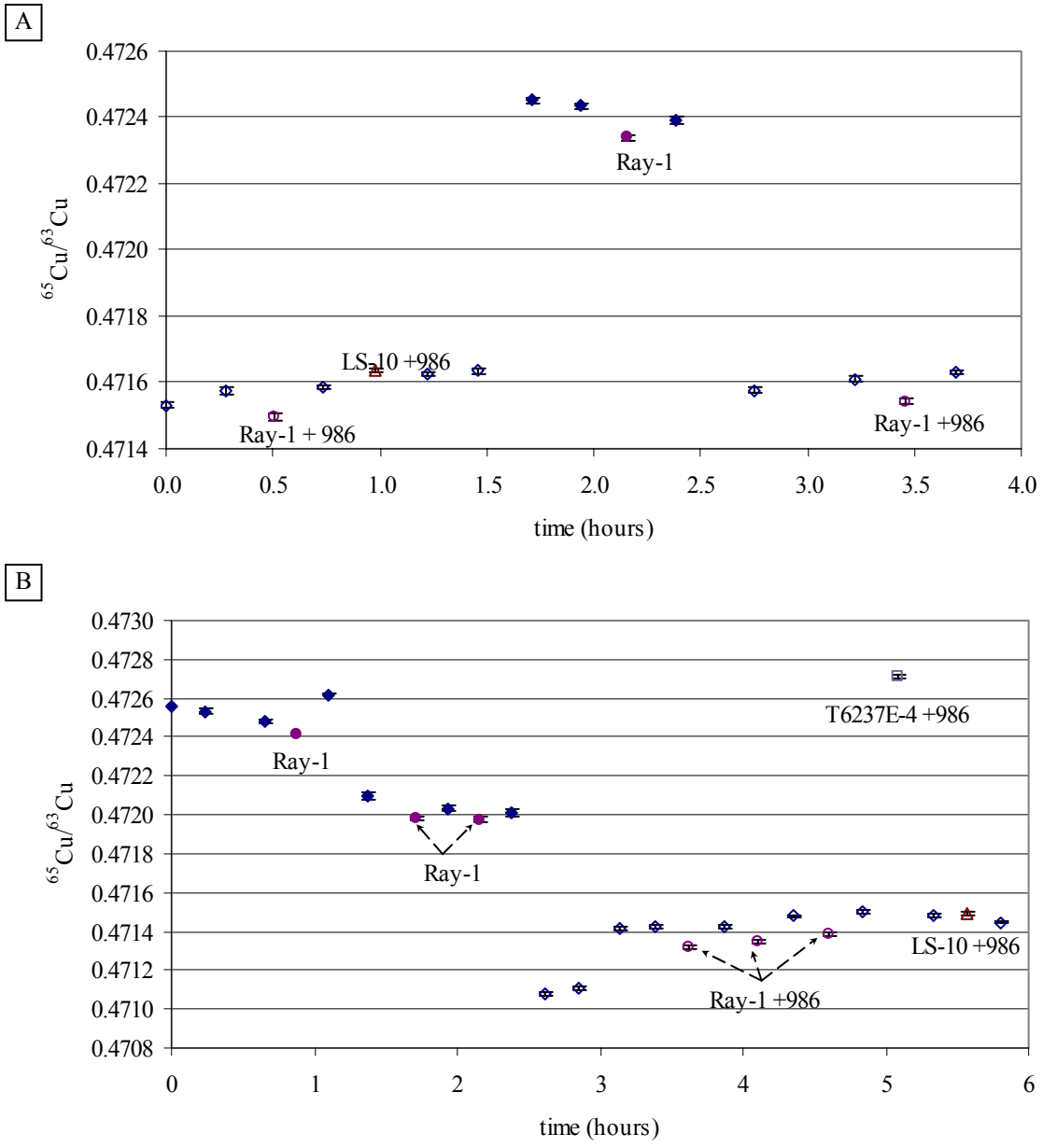

Figure 15. Graph showing the isotopic effect on samples and standards doped with Ni (NIST SRM 986 standard). (A) from 10 Jan 2005. (B) from 27 Jan 2005. See also Fig. 3. Solid diamonds are undoped NIST SRM 976, open diamonds are NIST SRM 976 doped with Ni (100ppb Cu and Ni). Other symbols are samples as labeled.

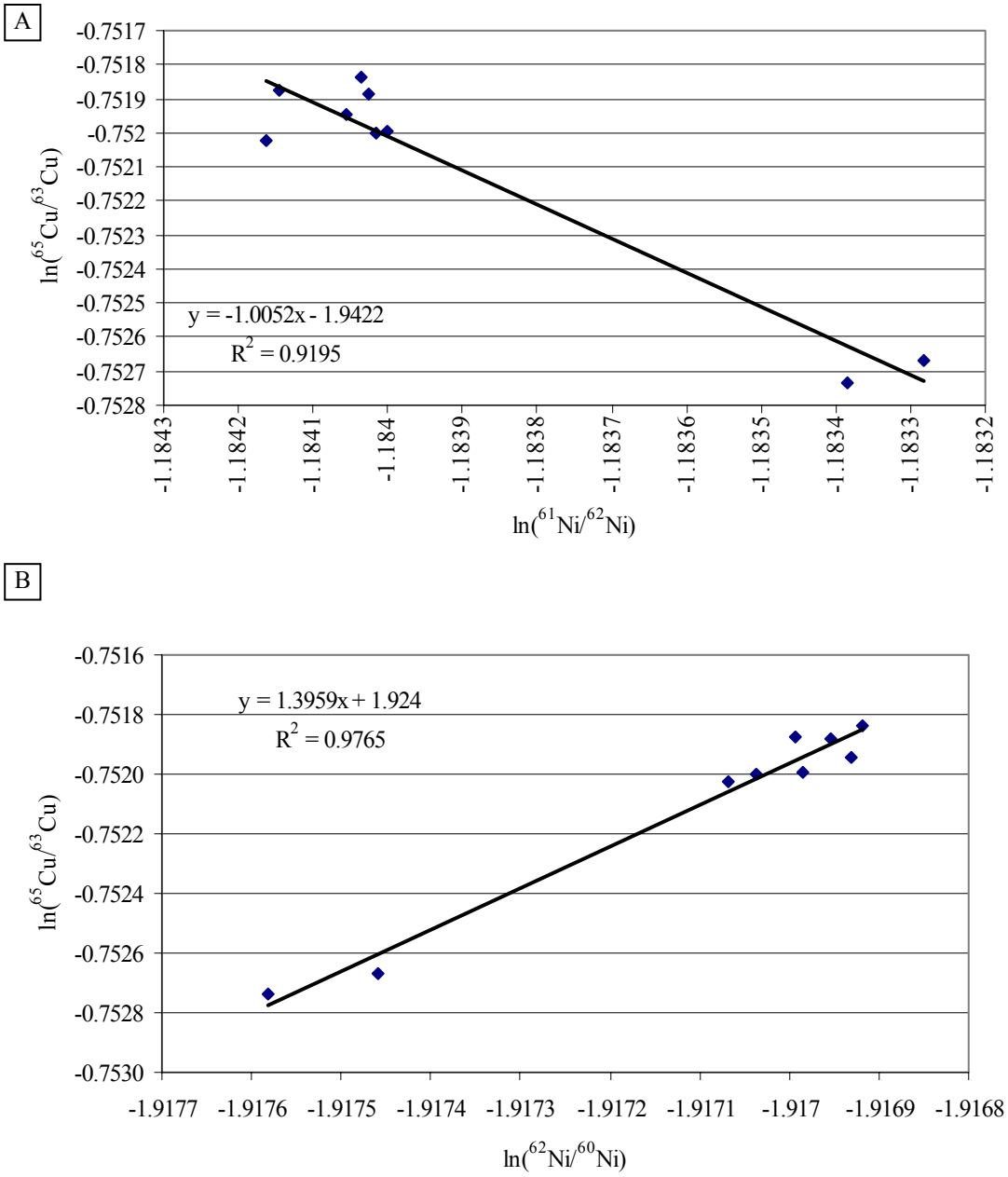

Figure 16. Graphs of ln(^{65}Cu/^{63}Cu) verses different ln(Ni isotope ratio) for two different Ni isotope pairs. (A) using ^{61}Ni/^{62}Ni, and (B) using ^{62}Ni/^{60}Ni (from 27 Jan 2005). The correlation coefficient is significantly different depending on the isotope pair used.

Table 4. Comparison of calculated $\delta^{65}Cu$ values for selected samples utilizing nickel doping for mass fractionation correction.

date	sample	$\delta^{65}Cu$[1] $^{61}Ni/^{62}Ni$	R^2 value[2]	$\delta^{65}Cu$[1] $^{62}Ni/^{60}Ni$	R^2 value[2]
10-Jan-05	Ray-1	-0.179	-	-	-
	Ray-1	-0.133	-	-	-
20-Jan-05	Ray-1	0.005	0.61	-	-
	Ray-1	-0.162	0.61	-	-
	Ray-1	0.034	0.61	-	-
27-Jan-05	Ray-1	-0.083	0.920	-0.051	0.977
	Ray-1	-0.158	0.920	0.032	0.977
	Ray-1	0.065	0.920	-0.064	0.977
	mean	**-0.076**		**-0.028**	
	2σ	0.182		0.042	
10-Jan-05	LS-10	0.012	-	-	-
27-Jan-05	LS-10	0.390	0.920	0.262	0.977
	mean	**0.201**			
27-Jan-05	T6237E-4	2.979	0.920	2.741	0.977
	sample-standard bracketing				
	Ray-1	-0.056	n = 29		
	LS-10	0.267	n = 17		
	T6237E-4	2.983	n = 4		

[1]Calculated $\delta^{65}Cu$ using the nickel isotope pair shown for making the Cu-mass fractionation correction.

[2]Correlation of best-fit line to data as explained in the text.

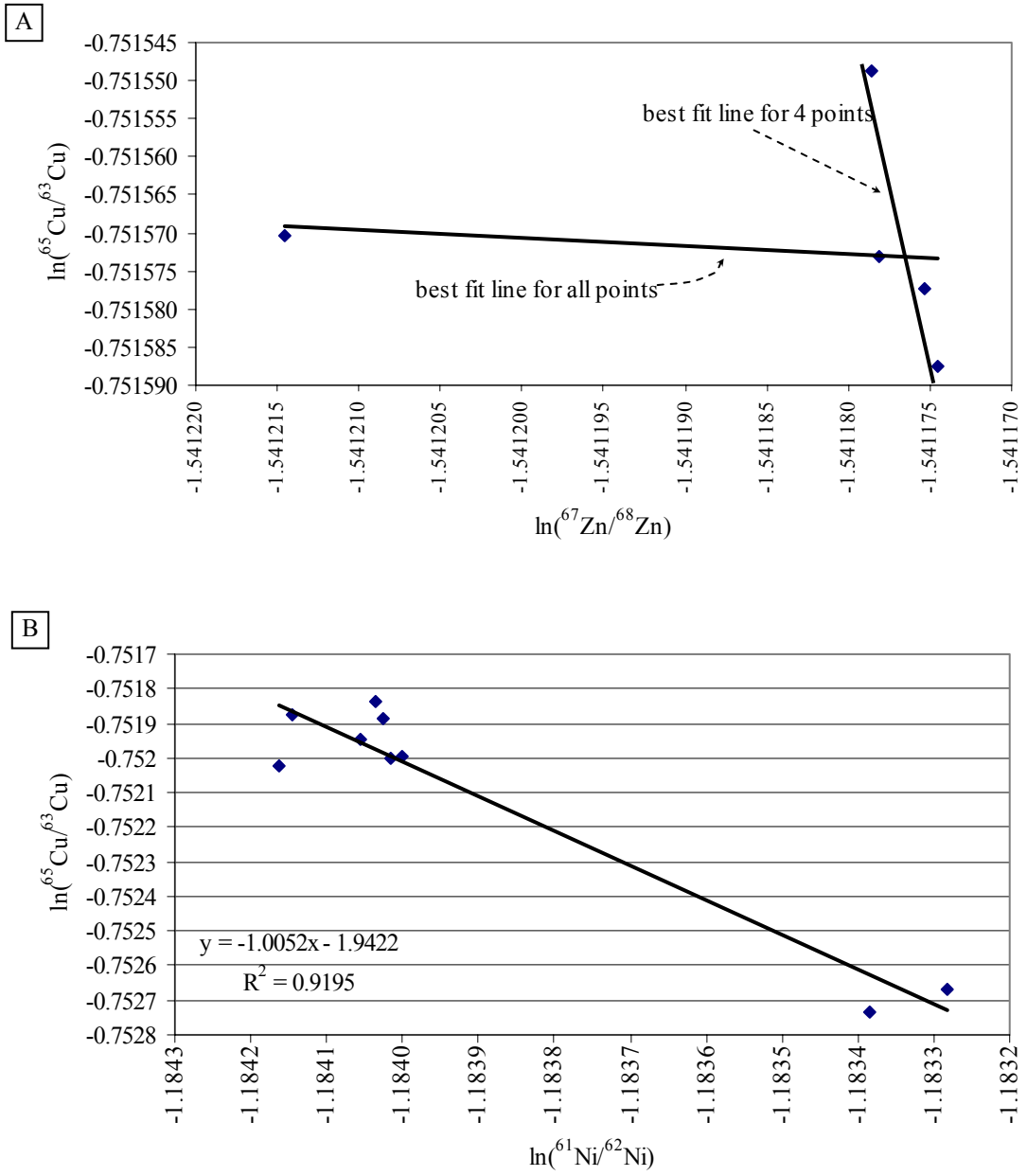

Figure 17. Graphs showing the significance of data outliers in determining the slope of the best fit line for elemental doping corrections for machine fractionation. (A) shows the significant influence over a trend by one data point (24 Mar 2005). The other points by themselves would form a better linear correlation than with the outlier. However, there is effectively very little variation in $\ln(^{65}Cu/^{63}Cu)$ among the points on the graph. (B) shows a similar feature with nickel isotopes (27 Jan 2005). The cluster of points in the upper left corner of (B) would not form a line of good correlation, but the two outliers constrain the line.

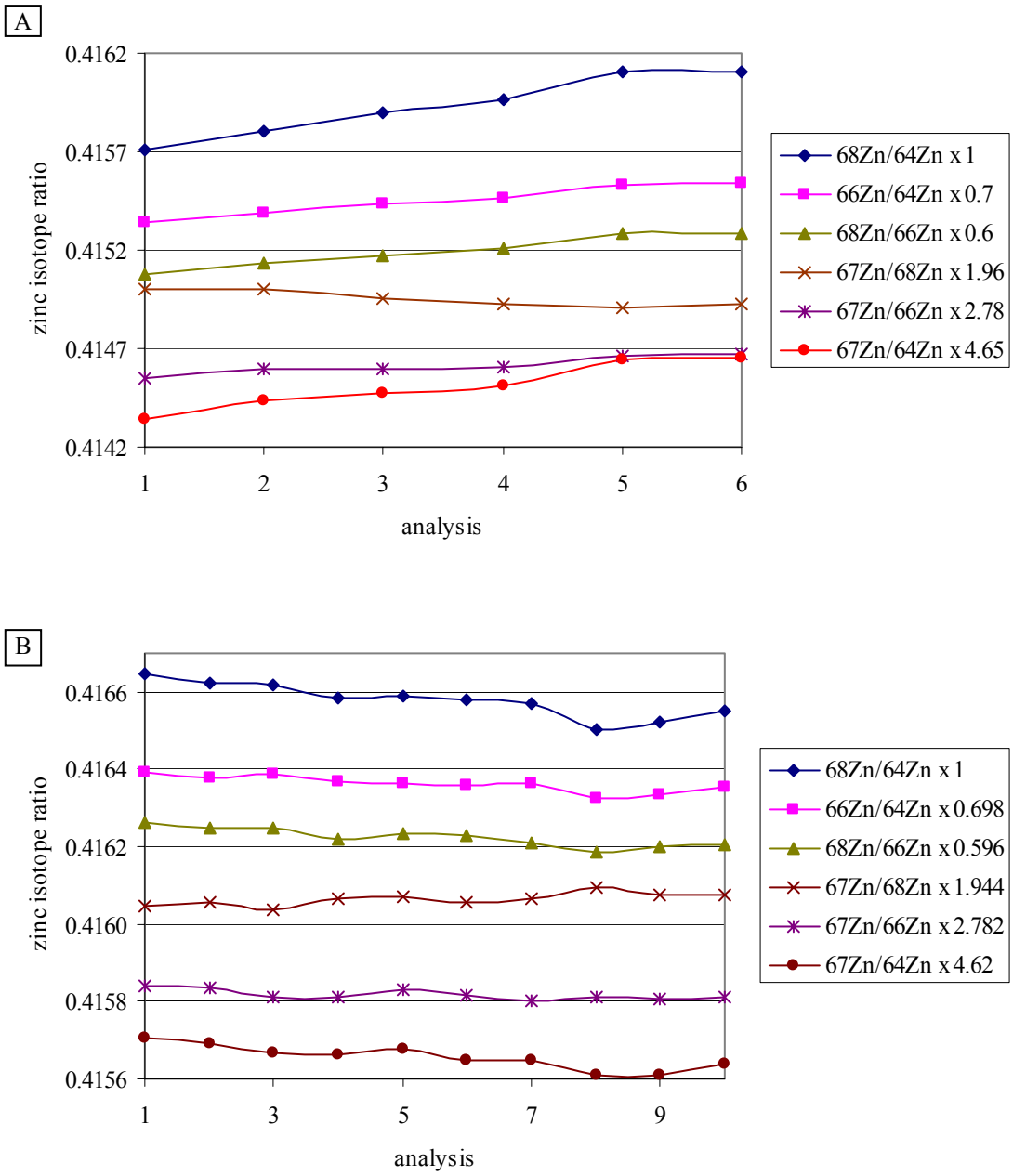

Figure 18. Graphs showing the drift from two analytical sessions in different zinc isotope ratios, normalized as shown in the legends. (A) Analytical run from 15 Mar 2005. (B) Analytical run from 25 Mar 2005. In both days the behavior of $^{68}Zn/^{64}Zn$, $^{66}Zn/^{64}Zn$, $^{68}Zn/^{66}Zn$, and to a certain degree $^{67}Zn/^{64}Zn$, appear to behave similarly in drift. The ratios $^{67}Zn/^{68}Zn$ and $^{67}Zn/^{66}Zn$ are less similar to the others in drift and in some groups of analyses their drift is opposite that of the other ratios.

Cu-Fe sulfides), and minimization of the Zn and Ni blank in the samples and standards. Any Ni or Zn in the solution unrelated to the dopant may affect the measured normalizing element isotopic composition, thereby producing an erroneous correcting factor for copper. The disadvantage of chromatography is that it is time intensive, and more significantly, can produce extreme isotopic fractionation, so that complete recovery of Cu is required. As mentioned above, there is also no generally accepted Zn isotopic reference material with accepted zinc isotope abundances. The elemental doping method requires a similar drift behavior in the target and dopant element isotopes, which apparently is not predictable with the Neptune®. Even when using the elemental doping method, almost all investigators improve analytical precision by analyzing standards interspersed with unknowns during the course of the run (i.e., sample-standard bracketing: Maréchal et al., 1999; Rouxel et al., 2004; Graham et al., 2004; Ehrlich et al., 2004).

Copper Blank

Copper blank, if significant, can cause the measured copper isotope ratio to be different from the true isotopic ratio of the sample. Possible contributions from blank include copper in purified water and acids used in solutions for mineral digestion and dilutions, copper leached from Teflon or plastic containers, as well as environmental contributions from air, dust, etc. Copper blank may also be contributed from the mass spectrometer ("memory"), such as copper on the skimmer cones from previous analyses. The "blank" from the carrier gas, carrier solution and machine memory is determined prior to each analysis and subtracted from the measured ratios by the Neptune® software. The process blank has been determined for sample dissolution and gives a ^{65}Cu signal of 0.0065 volts, and represents approximately 13.2ng of copper with a $\delta^{65}Cu$ value of -0.11 (±0.69) ‰. The large error is due to the uncertainty in the measured ratio on such a small copper signal, which is nearly 200 times less than a 100ppb Cu signal. It is important to note that part of the blank may be produced from copper "memory" on the skimmer cones.

Copper blank determined from the chromatographic process represents approximately 11.6ng of copper. Total copper blank from a dissolved and chromatographically purified copper mineral would represent approximately 24.8ng of copper. Thus, avoiding chromatography eliminates approximately 50% of the copper

blank, although even at 25ng of copper, this is 100 times less copper than in a 100ppb Cu solution and would not likely produce a significant influence over the isotopic analysis. Even if the blank were larger, it is unlikely to exert a significant effect on the measured isotopic ratio of copper, since the measured blank does not have an extreme $^{65}Cu/^{63}Cu$ ratio.

Conclusion

The Finnigan Neptune® MC-ICPMS at Washington State University is a stable instrument with generally constant drift during an analytical run. Sample-standard bracketing has been shown to be an acceptable method for correcting for drift and machine fractionation. Zinc doping may be an effective correction method but the day-to-day reproducibility by this approach to date has not yet been shown to improve that achieved by the sample-standard bracketing technique. In addition, care must be made in choosing the zinc isotope pair best suited for satisfying the constancy of β^{Zn}/β^{Cu}. This investigation suggests that the $^{68}Zn/^{64}Zn$ isotope pair may be best suited for correction purposes on the Neptune®, although this conclusion has not been exhaustively tested. Further work utilizing Zn as a dopant element may produce a better day-to-day reproducibility than is presently recognized for this method. Using Ni as a dopant in correcting machine fractionation has shown to be less reliable than Zn, mostly because of non-constancy in β^{Ni}/β^{Cu}.

III. Sample Preparation and Analytical Procedure

The sample preparation procedure followed in this investigation was designed to ensure that the isotopic analyses of copper solutions represent the minerals of interest and not mixtures of isotopically different minerals. To this end, samples of copper minerals including copper oxide minerals, sulfides and native copper were hand picked for purity from hand samples, drill core, or outcrop. The minerals were carefully examined under a binocular microscope and hand separated for purity. Grains less than 100μm were routinely picked to ensure that the samples were mineralogically pure and free from alteration or intergrowth of sulfide phases. Great care was taken to avoid sampling mineral grains exhibiting the appearance of exsolution textures.

Mineral samples were usually between 0.0003 to 0.004g, generally representing one or two mineral grains, which also helped to ensure mineral purity. Weighed samples were placed in Teflon containers for dissolution. Dissolution of minerals was commonly on a hot plate with a 50:50 solution of distilled concentrated HCl and HNO_3 acids. Concentrated nitric acid is adequate for sulfide dissolution, but the two-acid solution causes chlorine and sulfur to be volatilized during digestion and evaporation. The sample was re-dissolved in 2% HNO_3 and evaporated again. This nearly completely removes S from the sample, thereby decreasing solution matrix for the sulfide samples. Analysis of chalcopyrite prepared by the two-acid and single-acid procedures yields identical results, within analytical reproducibility (sample 1400 18.9 386a,c: Appendix 1). This indicates that sulfur not driven off by the evaporation process in the HNO_3-only dissolution has no analytical effect on the copper ratio. Finally, the sample was diluted to 100ppb (±10ppb) copper concentration for isotope analysis. This concentration produces an optimized signal of approximately 3 volts at mass 63 (^{63}Cu) on the mass spectrometer.

Prior to isotopic analysis, the detectors of the multiple collector ICP-MS (Neptune®) are configured to measure masses 62 (Ni), 63 (Cu), 64 (Ni, Zn), 65 (Cu), 66(Zn), 67(Zn), and 68(Zn). For sample-standard bracketing analyses, only data from mass 63 and 65 are utilized. This "cup" configuration is also used when running samples doped with the zinc isotope standard for machine fractionation correction. Due to technical limitations of the Neptune detector arrangement, mass 60 (Ni) could not be configured with these other masses, and so a different detector configuration was required when analyzing copper solutions doped with the nickel standard. Since ^{64}Zn is isobaric with ^{64}Ni, it is not possible to simultaneously measure Ni and Zn isotope ratios in the same solution.

The Neptune® is tuned to maximize the measured signal with NIST SRM 976 Cu standard prior to peak centering and mass calibration determination. Detector baseline and gain are determined on the Faraday collectors, peak shape is maximized to produce flat-topped scanned peaks, and peak centering of the ion beam and mass calibration are performed at the beginning of the analytical run. Peak centering and shape are checked at times during the course of the run to ensure that the ion beam was centered in the detector. It is important for the scanned peak shape to be as flat and wide on mass as possible (and at the same time maximize ion signal intensity) to allow for minor machine drift to occur without significantly affecting the measured ion beam signal. The most significant cause of day-to-day differences in the intensity of ion beam signals is probably related to the flow rate of Ar carrier gas. Once the other tune factors were optimized, day-to-day changes in signal intensity were generally related to carrier gas flow parameters. Samples are introduced to the plasma at 100ppb (±10ppb) Cu concentration through a ESI PFA-50 nebulizer, which features a cyclonic, double pass introduction system and is self aspirated. Flow rate is nominally 50μl per minute.

Isotope analysis consists of measuring a baseline on a blank 2% HNO_3 solution, which is then subtracted from measured signal intensities on the detectors during sample analysis. After the baseline is measured, the sample is introduced into the nebulizing system. There is a period of detector voltage increase and instability as the sample solution is first introduced into the plasma. The detector voltage is monitored prior to measurement until the ion beam voltage has stabilized (usually in about 30 seconds). Ratio measurement (i.e., measurement of ion beams in the detectors) begins once the copper signal voltage has stablized. Two blocks of 25 ratios (each ratio integrated over approximately 8 seconds) are measured during which statistical calculations are performed by Neptune® software. Individual sample ratios statistically outside of 2σ analytical standard error of the "running" mean are not included in the analytical mean.

Once the sample measurement is complete, the sample introduction system is washed with 2% HNO_3. When the voltage has decreased during the wash out (dropping of background typically to 0.005V on ^{65}Cu), a blank 2% HNO_3 solution is then introduced for the next baseline measurement. The next sample is analyzed following the same procedure. Wash and baseline solutions are periodically changed during the course of an analytical run. All changes of solutions introduced to the Neptune® are performed manually. If standards show considerable drift from one standard to the next, or during the analysis, the intervening sample is re-analyzed (e.g., Fig. 11).

Data reduction

Data files are exported to a common spreadsheet (e.g., Excel) and the data are plotted on a graph of $^{65}Cu/^{63}Cu$ verses time to evaluate machine drift for the analytical run. Although Neptune® software does not include integrated ratios outside of 2σ of the "running" mean (usually 2-4 ratios out of 50), any samples where individual integrated isotope ratios change abruptly during the course of analysis can be examined in the integrated ratio list in each output file. They can also be graphically evaluated by plotting the data and noting any unusually large error bars (Appendix 3). Since sample-standard bracketing requires constant drift during analysis and between bracketing standards, the evaluation of statistical errors is a check for determining reliability of the machine mass fractionation correction. Each mean sample ratio is corrected for machine fractionation relative to the time-corrected standard (linear extrapolation between two bracketing standard means) and the delta value ($\delta^{65}Cu$) is calculated.

IV. Analytical Results

Analysis of NIST SRM 976

Results of analyses of NIST SRM 976 Cu isotope standard on the Neptune® are shown in Figure 9. The actual accuracy of the raw copper isotope ratio measurement of NIST SRM 976 is poor, and $^{65}Cu/^{63}Cu$ varies from 0.469501 to 0.474393 (accepted NIST SRM 976 $^{65}Cu/^{63}Cu$ is 0.4456 ±0.0004: Shields et al., 1965). The machine mass fractionation for NIST SRM 976 is about 3% per amu. Day-to-day reproducibility of the standard can be quite variable. Based on the average ratio from all analyses of NIST SRM 976 (n = 505), the machine fractionation coefficient (β factor - see Section III) is -1.82 and the machine fractionation factor has a mean value of 0.9449. The fractionation factor (see Section III) varies from 0.9393 to 0.9491, and changes for every analysis due to machine drift. This variability makes absolute copper isotope analysis unreliable on the Neptune®. However, the fact that machine stability is generally very good and the drift is relatively constant during the course of an analytical run permits reliable and reproducible isotopic measurements relative to an isotopic standard. In the case of sample-standard bracketing, a fractionation factor for every analysis can be reliably determined by linearly extrapolating (relative to time) between bracketing standards (Fig. 10), assuming nearly linear machine drift is satisfied (e.g., Fig. 19).

Day-to-Day Reproducibility: Internal Standards

Three internal standards that have been used to test reproducibility in measuring copper isotope ratios are native copper samples, RAY-1 and LS-10, and one chalcopyrite sample, SUP-1. Mean delta values for these samples determined from sample-standard bracketing and by elemental doping are presented in Table 5 and shown graphically in Figure 20. The data for RAY-1 derived from elemental doping have been corrected for machine fractionation by a combination of elemental isotope pairs. 2σ standard deviation reproducibility of RAY-1 is better than 0.03 per mil for some isotope pairs, depending on the constancy of β^{Zn}/β^{Cu}. 2σ reproducibility for other isotope pairs is worse than 0.08%, particularly when ^{67}Zn is used as one of the zinc isotopes. This characteristic of ^{67}Zn on the mass fractionation correction has also been noted by Mason et al. (2004b).

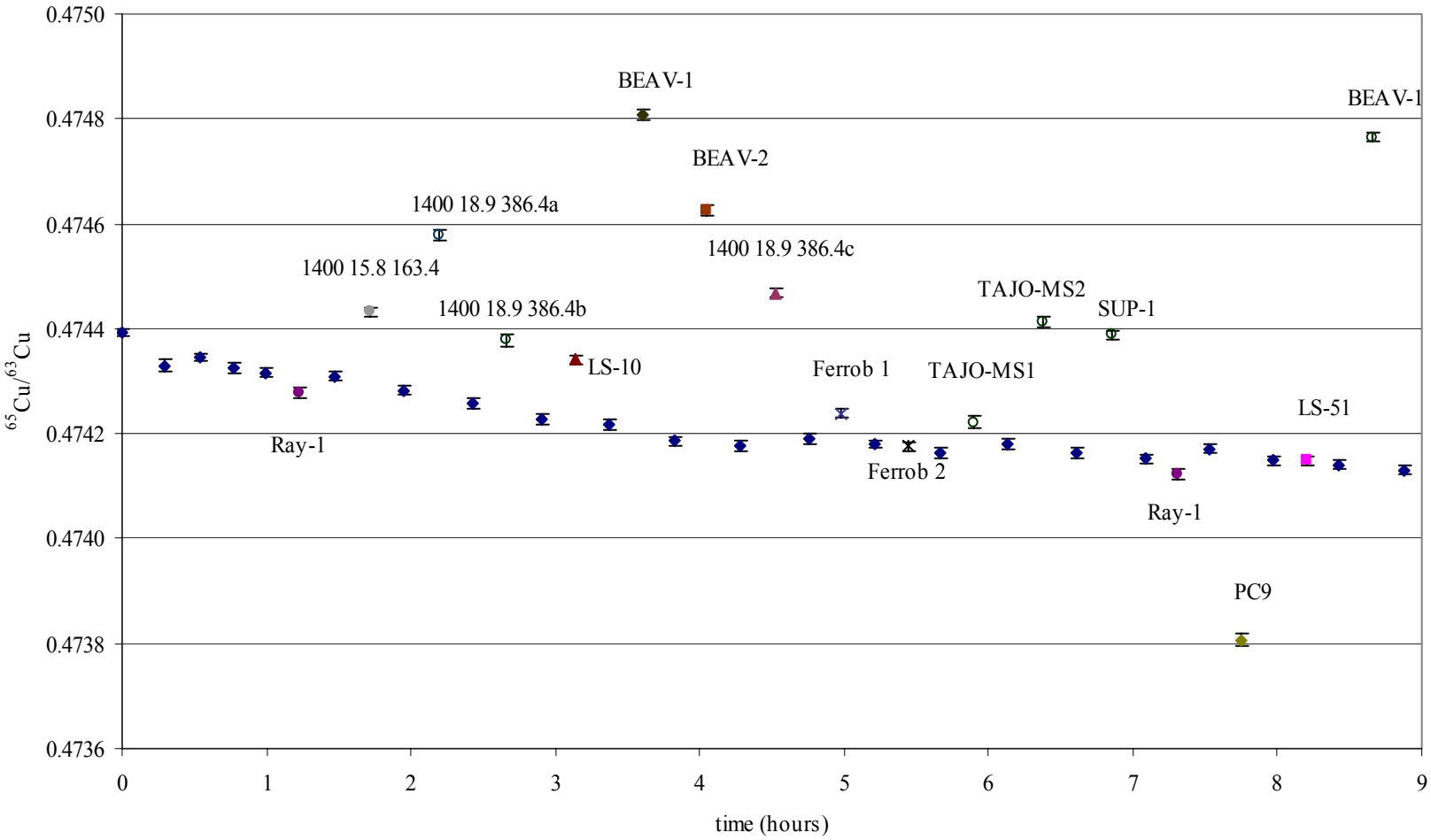

Figure 19. An analytical run (4 Jun 2002) showing very consistent machine drift in $^{65}Cu/^{63}Cu$ over 9 hours. Filled diamonds are NIST SRM 976 (100ppb), other symbols are sample unknowns as labeled.

Table 5. Summary of analyses of internal standards over three years.

Sample-standard bracketing correction

Sample	$\delta^{65}Cu$	Sample	$\delta^{65}Cu$
Ray-1	0.21	LS-10	0.52
"	0.02	"	0.36
"	0.00	"	0.30
"	0.02	"	0.32
"	-0.05	"	0.27
"	-0.04	"	0.30
"	-0.06	"	0.34
"	0.00	"	0.29
"	-0.08	"	0.27
"	-0.09	"	0.22
"	-0.09	"	0.23
"	-0.06	"	0.19
"	-0.10	"	0.25
"	-0.12	"	0.26
"	-0.03	"	0.15
"	-0.11	"	0.34
"	-0.08	"	0.29
"	-0.01	"	0.22
"	0.01	"	0.23
"	-0.08	"	0.22
"	-0.03	**mean[1]**	**0.267**
"	-0.03	**2σ**	**0.09**
"	-0.11	Sup-1	0.51
"	-0.10	"	0.55
"	-0.07	"	0.52
"	-0.07	"	0.54
"	-0.06	"	0.57
"	-0.29	"	0.56
"	-0.16	"	0.57
"	-0.11	"	0.49
"	-0.18	"	0.52
"	-0.17	"	0.51
"	-0.09	"	0.21
"	-0.14	"	0.46
"	-0.06	"	0.44
"	-0.10	"	0.52
"	-0.18	"	0.47
mean[1]	**-0.056**	"	0.52
2σ	**0.08**	"	0.49
		mean[1]	**0.514**
		2σ	**0.07**

Table 5 Cont.

Element doping correction

Sample	$\delta^{65}Cu$	isotope pair	Sample	$\delta^{65}Cu$	isotope pair
Ray-1[2]	-0.04	68/64	Ray-1[3]	-0.13	68/64
"	0.11	68/64	"	-0.13	68/64
"	-0.06	68/64	"	-0.13	68/64
"	-0.07	68/64	"	-0.12	68/64
"	-0.06	68/64	"	-0.12	66/64
"	-0.07	68/64	"	-0.13	66/64
"	0.06	66/64	"	-0.13	66/64
"	1.46	66/64	"	-0.10	66/64
"	-0.03	66/64	"	-0.15	68/66
"	-0.05	66/64	"	-0.14	68/66
"	-0.08	66/64	"	-0.12	68/66
"	-0.07	66/64	"	-0.13	68/66
"	-0.13	68/66	"	0.12	67/68
"	0.62	68/66	"	0.02	67/68
"	-0.09	68/66	"	0.05	67/68
"	-0.10	68/66	"	-0.25	67/66
"	-0.06	68/66	"	-0.55	67/66
"	-0.06	68/66	"	-0.36	67/66
"	0.06	67/68	"	-0.32	67/66
"	0.68	67/68	"	0.02	67/64
"	0.01	67/68	"	-0.26	67/64
"	-0.15	67/68	"	-0.20	67/64
"	-0.08	67/68	"	-0.21	67/64
"	-0.04	67/68	**mean**	**-0.146**	
"	-0.28	67/66	**2σ**	**0.14**	
"	0.53	67/66	Ray-1[4]	0.005	61/62
"	-0.19	67/66	"	-0.162	61/62
"	-0.07	67/66	"	0.034	61/62
"	-0.08	67/66	**mean**	**-0.041**	
"	-0.08	67/66	**2s**	**0.17**	
"	-0.07	67/64	Ray-1[5]	-0.083	61/62
"	0.96	67/64	"	-0.158	61/62
"	-0.11	67/64	"	0.065	61/62
"	-0.04	67/64	"	-0.051	62/60
"	-0.06	67/64	"	0.032	62/60
"	-0.08	67/64	"	-0.064	62/60
mean[6]	**-0.072**		**mean[6]**	**-0.043**	
2σ	**0.12**		**2s**	**0.15**	

[1]Data outliers not considered in the mean.

[2]Analyses from 2005.

[3]Analyses performed by G. Hart (personal communication, 2004).

[4]Poor constancy in β^{Ni}/β^{Cu} (20 Jan 2005).

[5]Analytical run with the best constancy in β^{Ni}/β^{Cu} (27 Jan 2005).

[6]Includes all analyses from the analytical run.

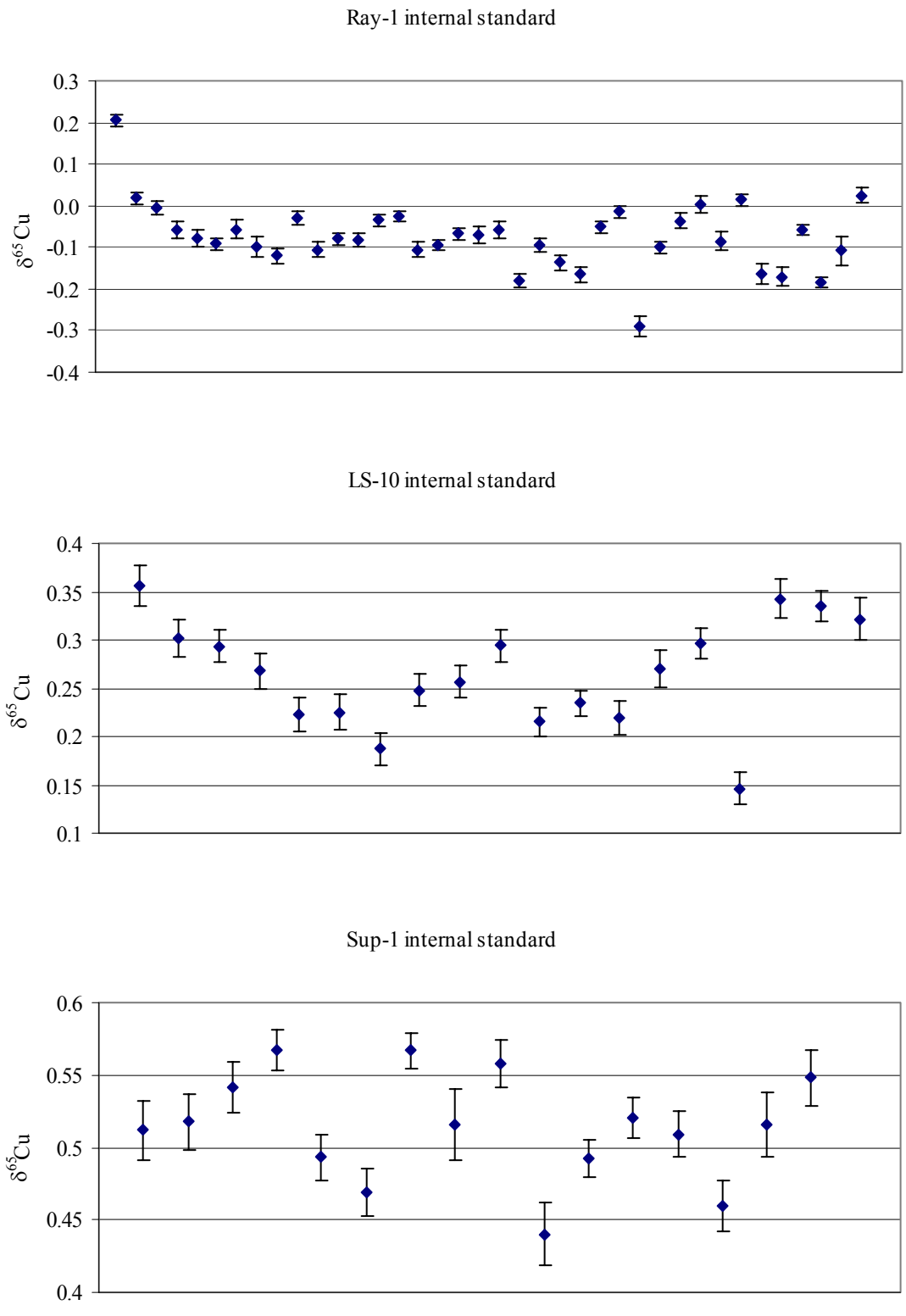

Figure 20. Day-to-day reproducibility of internal standards. (Error bars are 2σ, standard error.)

With the exception of the analytical run using zinc to correct for mass fractionation by G. Hart (personal communication, 2004; Table 5), all correction methods give almost the same mean value for RAY-1 (-0.07 to 0.04‰). The major difference between the methods is that the daily analytical precision may be slightly better with Zn-doping, utilizing $^{68}Zn/^{64}Zn$ or $^{66}Zn/^{64}Zn$ isotope pairs (Table 3). The improved precision of element doping may be related to the improved machine stability of copper isotope ratios induced by the presence of zinc in solution (see data from runs 27 Jan 2005 and 24 Mar 2005 in Appendix 3). It is unclear why this is the case, but it is not always consistently so. The large discrepancy in corrected $\delta^{65}Cu$ values between recently measured RAY-1 analyses and those measured by G. Hart is also not presently well understood. Long-term analytical reproducibility using zinc-doping has not been thoroughly examined due to the limited availability of zinc isotope standard. Thus, this data set prevents comparison of long-term analytical precision using zinc-doping with the sample-standard bracketing method.

Using the sample-standard bracketing technique, a non-chromatographically processed chalcopyrite standard, SUP-1, has been analyzed and gives a mean $\delta^{65}Cu$ value of = 0.52 (±0.077) per mil (2σ standard deviation, n = 12). The same chromatographically purified sample yields a $\delta^{65}Cu$ value of 0.50 (±0.049) per mil (2σ standard deviation, n = 4), analytically identical to the non-purified sample.

With-in Run Reproducibility

For the standard-sample bracketing technique, the within-run precision is usually much better than 2σ standard deviation reproducibility from day-to-day analyses, as long as drift is constant. Table 6 shows in-run reproducibility for several samples. For example, sample 1400 18.9 386.4 has a reproducibility of plus or minus 0.04 per mil. Sample BU-130c has an in-run reproducibility of plus or minus 0.03 per mil. Thus, analyses from Table 6 demonstrate that the analytical reproducibility of a sample during an analytical run by the standard-sample bracketing technique is plus or minus 0.04 per mil $\delta^{65}Cu$, about one half of the day-to-day reproducibility.

Table 6. Summary of analytical run reproducibility from various samples.

sample	δ^{65}Cu (‰)	δ^{65}Cu of repeat (‰)	mineral	date of analysis
LS-10	0.30	0.34	native copper	8 May 2002
Ray-1	-0.05	-0.04	"	8 May 2002
Ray-1	-0.06	0.00	"	11 May 2002
Ray-1	-0.08	-0.09	"	4 Jun 2002
Ray-1	-0.01	0.01	"	17 Jun 2003
1300 16.1 208.65	0.01	-0.06	chalcocite	1 Feb 2003
1400 18.9 386.4	0.69	0.64	chalcopyrite	4 Jun 2002
SUP-1	0.57	0.56	chalcopyrite	17 Jun 2003
Ar-14b	0.00	-0.02	bornite	30 Sep 2004
S27-A 1847	0.45	0.53	bornite	30 Jun 2003
BU-130c	-0.20	-0.17	chalcocite	30 Sep 2004
BEAV-1	1.36	1.41	chalcopyrite	4 Jun 2002

Within-run reproducibility (2σ , standard deviation) is **±0.04‰** and determined by averaging individual sample with-in run reproducibilities.

Drift on the Neptune® MC-ICPMS

Machine drift on the Neptune® is generally linear and may total less than 600ppm (considered minor) over 7 continuous hours of run time (e.g., Fig. 19). Occasionally, the drift is large and inconsistent (e.g., Fig 11). A large jump in drift may occur during a single analysis, or between samples. With the sample-standard bracketing technique the assumption is made that the drift between bracketing standards is constant and linear so that the value of the standard can be extrapolated to the time of analysis. Some question has arisen as to whether the assumption of constant drift is valid for inductively coupled plasma ionization systems (Mason et al., 2004b). Observations during many analytical runs show that an abrupt change in drift almost always occurs between analyses rather than during a single analysis. Statistical errors in reported raw ratios will be much greater if a large change in drift occurs during analysis and thus will be an indication of a suspect analysis. As indicated above, the procedure followed in this investigation was to reanalyze the sample and bracketing standards when any large jump in drift occurred between analyses.

Copper Isotope Ratios

One of the objectives of this investigation was to survey the range of variations in copper isotope ratios from a variety of ore-forming environments. Another objective was to determine copper isotope ratios of reservoirs that could potentially contribute copper to high-temperature hydrothermal systems. Recently, Luck et al. (2003) and Rouxel et al. (2004) have published preliminary copper isotope ratios for some terrestrial reservoirs first determined by C. Maréchal. There appears to be little isotopic variation among different rock types (with all igneous rocks ranging from -0.4 to 0.5‰). Data from this investigation also indirectly leads to similar conclusions, as will be presented later.

Samples from this investigation consist of chalcopyrite, bornite, chalcocite, native copper, cuprite, covellite, azurite and Cu-sulfosalts. These samples come from both supergene and hypogene mineralization in porphyry copper, skarn, “magmatic” sulfide, sediment-hosted, Cu-vein and manto, and sedimentary exhalative deposits. Copper isotope ratios for most of these samples are summarized in terms of δ^{65}Cu in Figure 21, which also

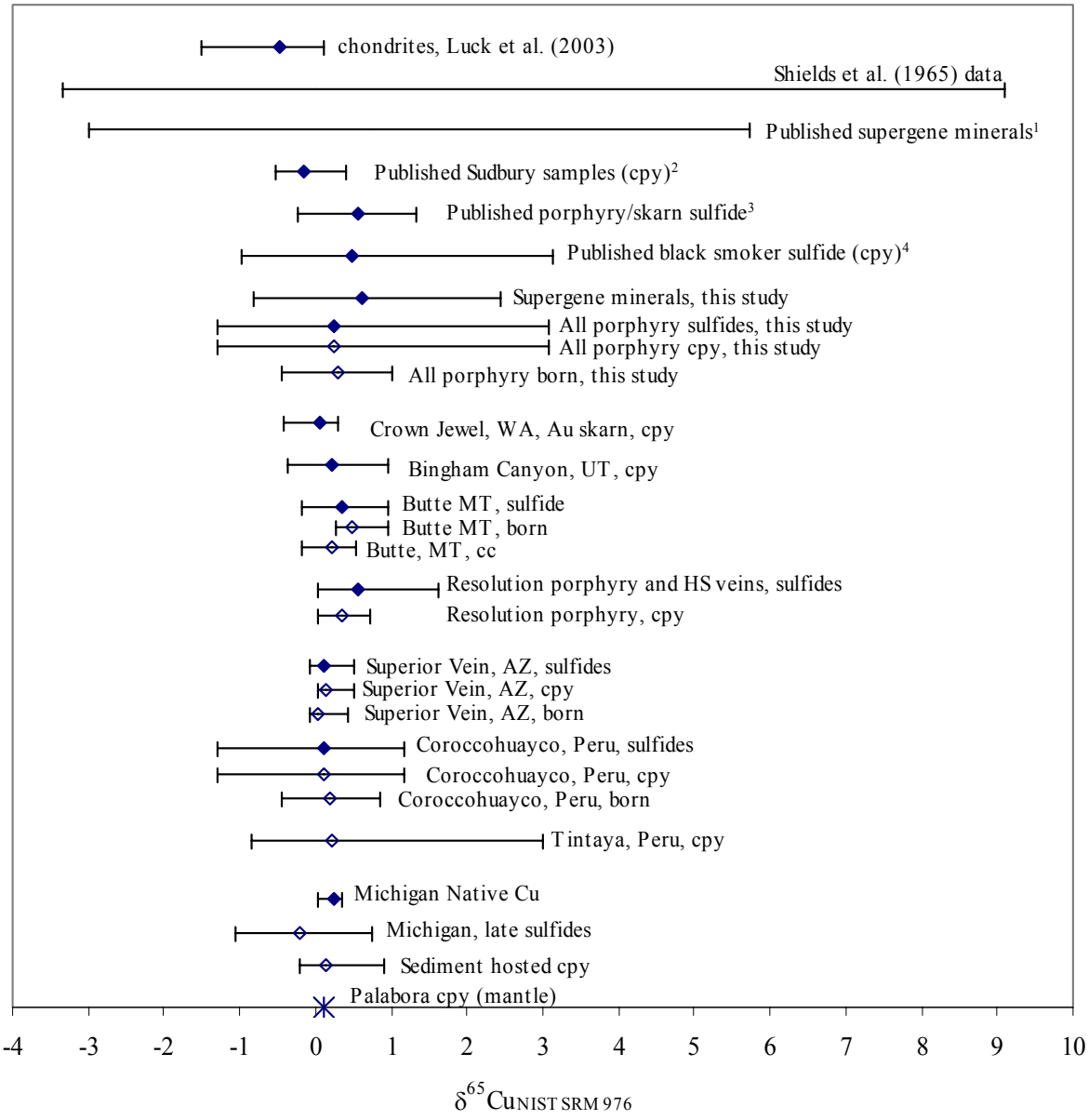

Figure 21. Results of copper isotope analyses as ranges from different deposits and geologic environments. All samples are from this investigation unless otherwise noted. (cpy = chalcopyrite, born = bornite).

[1]Data from Maréchal et al. (1999) and Zhu et al. (2000).

[2]Data from Zhu et al. (1999).

[3]Data from Zhu et al. (1999) and Graham et al. (2004).

[4]Data from Zhu et al. (2000) and Rouxel et al. (2004).

includes data from other published investigations. Figure 22 graphically presents analyses from this study. Appendix 2 presents δ^{65}Cu values for the samples analyzed in this investigation and geologic descriptions. The analytical data are presented in Appendix 3, which lists the raw isotopic ratios, analytical errors, drift of standards, and graphs for each analytical run.

Discussion: Ranges in Copper Isotope Ratios

Since 1999, the published range of copper isotope ratios of copper minerals is about 9 per mil (Fig. 21). Older work of Shields et al. (1965) produced a range of about 12 per mil, with poorer precision (±1.5‰). Even though Shields et al.'s large range of δ^{65}Cu values has not been duplicated by any recent investigation, Figure 21 can not be construed to represent a complete picture of copper isotope ranges from different ore deposit types since several of the deposits (and types) have not been completely sampled. For example, a recent presentation by Asael et al. (2005) showed that analyzed copper sulfides have δ^{65}Cu values as low as -3.5 per mil. It is likely that continued investigation into other ore deposits will expand the range of δ^{65}Cu values for copper minerals in all geologic environments.

The Cu-porphyry/skarn samples from this investigation have a range much larger than those analyzed by Zhu et al. (2000). These investigators reasoned that the δ^{65}Cu range in "continental sulphides" was constrained to a narrow range, and so implied this environment must lack important isotopic fractionation mechanisms at high-temperature. They therefore focused their investigation on black smoker hydrothermal systems. The black smoker sulfide range from Figure 21 represents copper isotope ratios from various massive sulfide hydrothermal systems that vary in chalcopyrite precipitation temperature, fluid geochemistry, and degree of post-depositional oxidation. Rouxel et al. (2004) have shown that chalcopyrite samples from actively forming black smokers generally have relatively small ranges in δ^{65}Cu (<0.4‰) (cf., Zhu et al., 2000). Those with larger ranges are related to copper remobilization processes or higher-salinity hydrothermal systems. Considering the geologic diversity represented by black smoker sulfides, the δ^{65}Cu range in seafloor mineralization is about the same as the δ^{65}Cu range in chalcopyrite from porphyry-related skarn mineralization at Tintaya, Perú. Since the porphyry/skarn copper mineralization has a large range in δ^{65}Cu there must be important high-temperature fractionation mechanisms

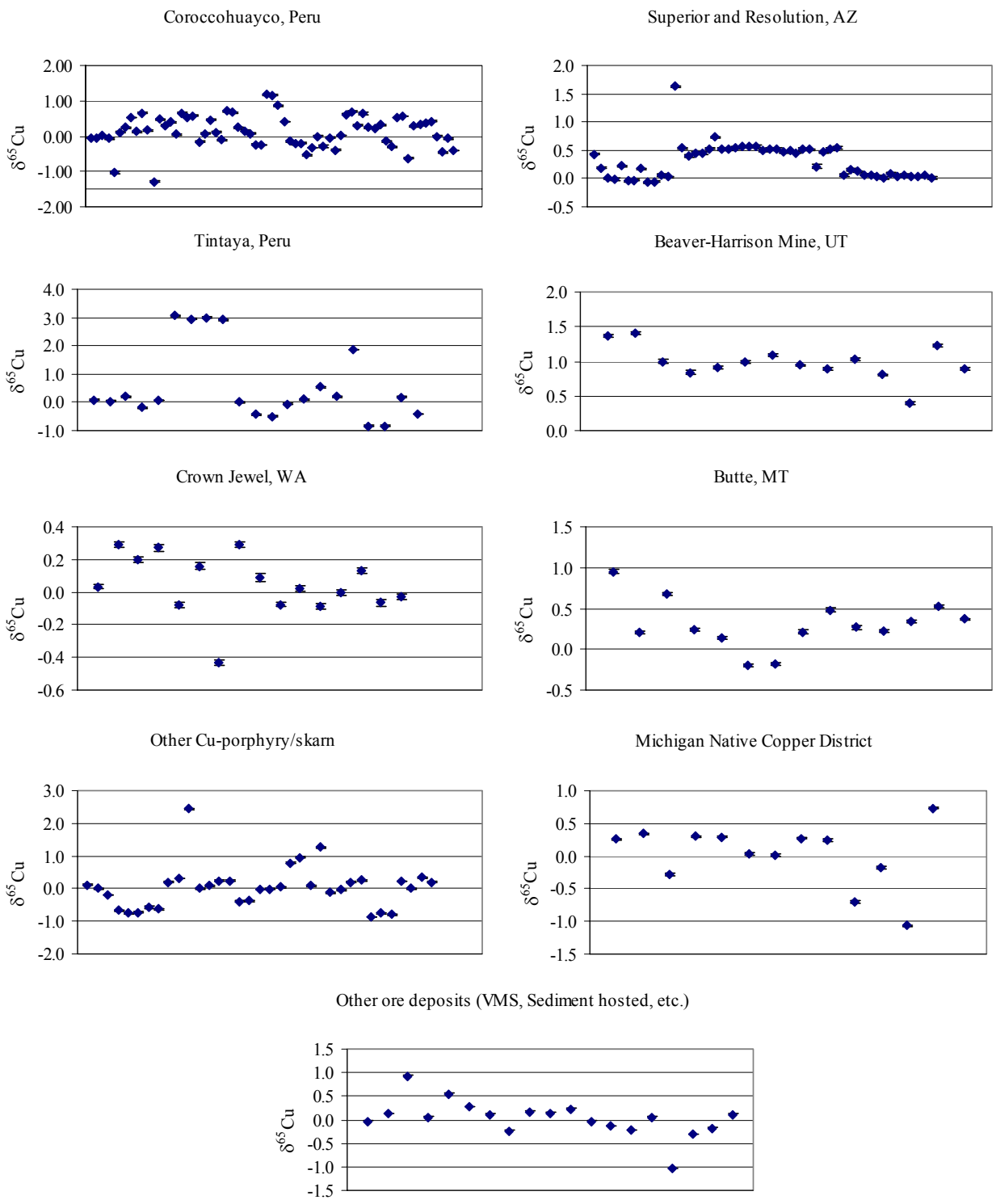

Figure 22. Graphs of calculated delta values for samples analyzed in this study from different ore deposits. Data specifics can be found in Appendix 2.

operating in this geologic environment. These possible fractionation mechanisms are discussed in Sections V and VI.

Mantle and Bulk Earth Copper Isotope Characteristics

Maréchal (1998) investigated the copper isotope characteristics of whole rocks and proposed a terrestrial copper isotope range of -0.4 to 0.5 per mil. The range in values suggests there is more than one copper isotope reservoir in the earth. Basalts in that study were determined to have a more restricted range in δ^{65}Cu of -0.2 to 0.0 per mil. Archer and Vance (2004) determined a value of 0.07 (±0.08) per mil for the basalt standard BCR-1 (Columbia River basalt). Chalcopyrite samples from Sudbury, Canada, the Stillwater mafic igneous complex, Montana, and the Palabora carbonatite, South Africa, were chosen based on their geologic context as potential indicators of a mantle copper isotope ratio. The samples of chalcopyrite from Stillwater and Sudbury were derived from disseminated to massive sulfide clots in igneous rocks (Raedeke and Vian, 1986, and Naldrett, 1989, respectively), and are interpreted to have formed as immiscible sulfide melts during petrogenesis of the magmas.

Figure 21 shows the Sudbury sample range from the published literature (Zhu et al., 2000), including a sample from this study (TL-4 = -0.25‰). A sample from the JM Reef at the Stillwater mine (STILLJM-1) yielded a value of -0.18 per mil (not shown on Fig. 21). Samples from these deposits lie within the bulk earth copper isotope range (-0.4 to 0.5‰), as well as the basalt range (-0.2 to 0.0‰) of Maréchal (1998). An initial interpretation is that mafic igneous rocks, dominantly derived from the mantle, contain isotopically lighter copper ratios than those magmas which have interacted with rocks in the crust (as observed in the BCR-1 analysis of Archer and Vance, 2004).

Other data suggest that the mantle values may be heterogeneous. Chalcopyrite from the Palabora carbonatite has a δ^{65}Cu value of 0.11 per mil, isotopically heavier than the mafic complex values. Ores from the Sudbury complex have been interpreted elsewhere (Molnár et al., 1997) as having a hydrothermal component in their genesis, so the copper isotope ratios in this particular deposit may not be truly representative of a unique mantle copper source. The copper isotopic ratio of the mantle may indeed be heterogeneous, but the present resolution of copper isotope analysis, as well as incomplete sampling, does not presently permit distinctions to be made by this investigation.

Cogenetic Copper Minerals

One of the fundamental objectives of stable isotope geochemistry is to determine the magnitude of mineral-mineral isotopic fractionation. This aspect has been thoroughly investigated for oxygen isotopes and the published oxygen mineral-mineral fractionation factors are routinely used in the interpretation of petrogenetic and hydrothermal processes (e.g., Bottinga and Javoy, 1975; Chacko et al., 2001). Copper mineralization is frequently observed as two or more cogenetic copper phases (i.e., chalcopyrite-bornite, bornite-chalcocite, etc.). Thus, it is conceivable that copper isotope fractionation occurs between co-precipitated copper phases. This has been addressed by Larson et al. (2003) and further developed by Maher and Larson (in review; Appendix 4).

Co-precipitated pairs of chalcopyrite and bornite have been analyzed for copper isotope ratios from several deposits (Table 2 of Appendix 4). The majority of these samples show a fractionation of 0.38 per mil between chalcopyrite and bornite formed in a variety of geologic environments. Bornite has been observed to be isotopically lighter than co-precipitated chalcopyrite in all but one case (Appendix 4). Maher and Larson (in review) have shown that this is likely an equilibrium isotopic fractionation and can be used to evaluate isotopic equilibrium in a sample and the effects of copper remobilization or copper enrichment of existing copper minerals. The temperature dependence of this fractionation is presently unknown, but the observed fractionation is likely produced through equilibrium with hydrothermal fluids in the range of 300ºC plus or minus 50ºC, based on fluid inclusion evidence for mineralization from Coroccohuayco, Perú (Maher, 1999).

Sulfur isotope ratios of two chalcopyrite-bornite pairs that exhibit this approximately 0.38 per mil copper fractionation are isotopically lighter in the chalcopyrite relative to the co-precipitated bornite (Table 7). However, the isotopic variability of S in this isotopically zoned sequence (drill hole 1400 18.9) is much less than that of copper. The fractionation of copper isotopes through this mineralized zone is by a process that does not produce sulfur isotope variations (such as source mixing or kinetic, biologic, or oxidation-reduction induced fractionation). Rouxel et al. (2004) observed similar non-correlation between copper isotope ratios and sulfur isotope ratios in most of the sea-floor hydrothermal systems they examined.

Table 7. Sulfur and copper isotope analyses for chalcopyrite and bornite samples.

sample	mineral	$\delta^{34}S_{VCDT}$ [1]	$\delta^{65}Cu_{NIST\ SRM\ 976}$
1400 18.9 357.2	chalcopyrite	-5.06	-0.21
1400 18.9 365.85	chalcopyrite	-4.08	-0.54
1400 18.9 370	chalcopyrite	-4.85	-0.33
1400 18.9 376.5A	chalcopyrite	-4.64	-0.02
1400 18.9 376.5B	bornite	-4.35	-0.40
1400 18.9 386.4A	chalcopyrite	-4.06	0.69
1400 18.9 386.4B	bornite	-3.91	0.31
T6237E-4	chalcopyrite	-0.46	2.98
T990N080	chalcopyrite	-2.12	-0.43

S analyses courtesy of E. Ripley, University of Indiana. Analytical precision of S isotope ratios ±0.1‰.

V. Variations in Copper Isotope Ratios from Ore Environments

Copper ore deposits can vary considerably in their geochemistry, tectonic setting, paragenesis and size. Copper can also have diverse sources in magmatic and hydrothermal ore deposits. It can be scavenged from magmas by immiscible sulfide melts or it can precipitated from fluids of varying salinities ranging in temperature from 50°C to +450°C (i.e., hydrothermal/hypogene). Copper porphyry/skarn systems form at the upper temperature end of the hydrothermal range, where hydrothermal fluids exsolved from crystallizing magmas may precipitate copper sulfides at temperatures >350°C. Volcanogenic massive sulfide (VMS) deposits, formed by hydrothermal convection cells in the ocean crust, may precipitate copper minerals from active hot-spring vents generally at temperatures <350°C (Rouxel et al., 2004). Other hydrothermal copper ore-forming environments may occur at lower temperature, such as sedimentary exhalative, or clastic and carbonate replacement deposits produced from basinal brines. Redox-type deposits (e.g., roll-front) may border on low, ambient geothermal gradient temperatures of deposition. Finally, supergene deposits form at ambient near-surface temperatures from the oxidation of primary sulfides previously deposited at high temperature. Copper can be transported and deposited as various minerals in a wide range of geologic environments and conditions.

Copper isotope ratios have been measured from a variety of these ore environments and ranges of copper ore minerals have been presented in Maréchal et al. (1999), Zhu et al. (2000), Larson et al. (2003), and Maher et al. (2003). The copper mineral chalcopyrite ($CuFeS_2$) is found in most types of hydrothermal copper deposits and so is an economically important mineral. As noted by Larson et al. (2003), most chalcopyrite from ore deposits average about 0.1 per mil $\delta^{65}Cu$ although the range can be nearly the entire known range in copper isotope ratios (Fig. 21).

Copper ore minerals from oxidized ore zones can vary isotopically from heavy to light. Several ore minerals, such as native copper and supergene chalcocite, can be both isotopically heavy or isotopically light. The copper carbonate, azurite, tends to be isotopically heavy (cf., Asael et al., 2005). However, malachite tends to be lighter, and this is consistent with recent experimental investigations into oxidation-induced equilibrium isotope fractionation (Zhu et al., 2002; Erhlich et al., 2004). The extreme variation in supergene minerals is not the focus of this investigation, but will be touched upon later in this section.

The isotopic ranges of copper mineralization from several of the hydrothermal ore deposits examined as part of this investigation are listed in Table 8. Other published investigations are graphically shown for comparison

Table 8. Comparison of ranges in $\delta^{65}Cu$ from mineralization from several ore deposits.

Deposit	deposit type	total sulfide $\delta^{65}Cu$ range average number	chalcopyrite $\delta^{65}Cu$ range average number	bornite $\delta^{65}Cu$ range average number	Notes
Michigan Native copper district	related to migration of basinal brines?	-1.07 to 0.74 -0.21 6	N/A[1]	N/A[1]	native copper: 0.25/0.31 7
Tintaya, Perú	Cu-porphyry / skarn	-0.84 to 3.00 **0.22** 16	-0.84 to 3.00 **0.23** 15	N/A[1]	Extreme enrichment in ^{65}Cu in cpy from remobilization into distal skarn (?)
Coroccohuayco, Perú	Cu-porphyry / skarn	-1.29 to 1.16 **0.11** 52	-1.29 to 1.16 **0.10** 41	-0.46 to 0.86 0.20 10	
Superior, AZ	vein/manto	-0.07 to 0.51 **0.10** 18	0.02 to 0.51 **0.13** 11	-0.07 to 0.43 **0.04** 6	
Resolution, Az	Cu-porphyry with overprinting high sulfidation veins	0.03 to 1.62 **0.57** 6	0.03 to 0.73 **0.34** 4	0.46 to 1.62 **1.04** 2	Bornite values from high sulfidation veins. Chalcopyrite from both zones.
Butte, MT	Cu-porphyry with overprinting high sulfidation veins	-0.19 to 0.95 **0.34** 13	N/A[1]	0.27 to 0.95 **0.48** 5	chalcocite: -0.19 to 0.53 0.20 6 All samples from hypogene minerals in high-sulfidation veins.
Bingham Canyon, UT	Cu-porphyry /skarn	-0.37 to 0.95 **0.21** **7**	-0.37 to 0.95 **0.21** **7**	N/A[1]	
Millard Co, UT	Cu-Porphyry, breccia pipes	0.00 to 1.36 **0.77** **9**	0.00 to 1.36 0.77 **6**	0.40 to 1.00 **0.76** **3**	data from three deposits in district and metallogenic trend
Crown Jewel, WA	Au skarn	-0.43 to 0.29 **0.06** 13	-0.43 to 0.29 **0.06** 13	N/A[1]	From disseminated mineralization - possibly metamorphosed (M. Gaspar, Pers. comm., 2005)

[1]Insufficient data

in Figure 21. Porphyry copper and skarn systems (i.e., high temperature) appear to have greater variations in $\delta^{65}Cu$ than most other deposit types. The investigation of Rouxel et al. (2004) of sea-floor massive sulfide deposits indicates that actively precipitating sulfide chimneys have limited $\delta^{65}Cu$ values, although combined ranges for all deposits in their study were similar to those observed in some porphyry-related systems. The presence, or lack, of isotopic variations in hypogene mineralization suggests that under certain conditions considerable isotopic variations are produced in high-temperature ore-forming environments. The magnitudes of the isotopic fractionations produced by these processes are also different among ore deposit types (e.g., black smoker verses porphyry, gold skarn verses copper skarn/porphyry, etc.). The remainder of this section will outline the possible causes of variations in copper isotopic ratios from ore systems.

Copper Isotope Variations in Hypogene Mineralization

Theoretical considerations of stable isotope fractionation suggest that equilibrium fractionation between isotopes based on mass is strongly temperature dependent (Urey, 1947). Empirically, several hydrothermal systems contain ranges in copper isotope ratios (Table 8) much greater than that expected through fluid-mineral equilibrium isotope fractionation based on the relative masses of the isotopes involved. One hypothesis suggests that these variations are due to source variations, with ranges in the isotopic composition of copper minerals due to mixing of copper between two or more distinct copper reservoirs (i.e., source rocks), such as is observed for light stable isotopes (e.g., oxygen). Another hypothesis is that variations are due to isotopically distinct and overprinting hydrothermal fluids during the history of the hydrothermal fluid. A corollary to this is that fluids may remobilize copper from rock or existing mineralization and fractionate copper isotopes through some mechanism of the leaching process(es). A third possibility is that fractionation may occur based on fluid parameters, such as between the solution complexes in a fluid (Maréchal and Albarède, 2002), leading to isotopic variations in precipitated minerals. The fourth hypothesis is the possibility that fluid-mineral fractionations are greater than expected from a theoretical standpoint of low mass differences between the isotopes of copper and the decrease of isotopic fractionation with increasing temperature. It is probable that several of these processes or mechanisms operate during the history of an ore deposit, and so it may be difficult to differentiate among them.

Source Variations

Maréchal (1998) suggests that little copper isotopic variation exists in the rocks of the earth (-0.4 to 0.5‰). Using copper isotopes as petrogenetic tracers is somewhat problematic since more significant isotopic fractionation (relative to possible variations in the mantle or bulk earth) occurs through hydrothermal and low-temperature processes. For example, disseminated chalcopyrite in a pre-skarn dioritic mafic rock from Coroccohuayco, Perú, has a δ^{65}Cu value (-0.31‰) similar to, although slightly lower than, the basalt range of Maréchal (1998). However, chalcopyrite analyzed from late, lower-temperature quartz-sulfide veins in Coroccohuayco range from -0.54 to 0.69 per mil. Vein-controlled mineralization elsewhere in the same district locally reaches -1.29 per mil. These data indicate that isotopically light isotope values can be produced through isotopic fractionation processes during metallogenesis and it may be impossible to isotopically distinguish between "magmatic"-source copper and copper fractionated by hydrothermal processes. Therefore, low δ^{65}Cu values in high-temperature hydrothermal environments can not be automatically interpreted as "starting copper isotope values" in ore deposit metallogenesis, which then evolve during the history of mineralization. The "initial" copper isotopic value for any hydrothermal fluid may be a product of not only the initial copper isotope signature of the magma/rock (assuming there is measurable isotopic heterogeneity in magmas), but also the process(es) which lead to the formation of the hydrothermal fluid (i.e., degree of copper leaching of the rock, or stages of fluid exsolution from the magma). Since it is very difficult to discount the role of hydrothermal fluids in interacting with almost all high-temperature sulfides, only through micro-scale sampling of sulfide inclusions in magmatic minerals may it be possible to truly evaluate magmatic copper isotopic ratios. However, this investigation provides no evidence that initial, or "magmatic"-source copper is significantly heavier isotopically than NIST SRM 976.

The small terrestrial copper isotope range observed in igneous rocks (Maréchal, 1998) is likely due to the limitations of fractionating copper through magmatic processes. Although this study does not directly evaluate isotopic variations in potential rock reservoirs, the question of earth reservoirs can be indirectly addressed by looking at the data from several hydrothermal deposits. Most disseminated and vein chalcopyrite hosted by igneous rocks (from porphyry/skarn, Bingham Canyon, Coroccohuayco, Tintaya, and Sudbury, Fig. 21 and Appendix 2) have δ^{65}Cu values in a rather restricted range, and tend to be relatively isotopically light. However, a noticeable exception occurs in the isotopically heavy chalcopyrite and bornite of the Beaver-Harrison Mine, near Milford,

Utah, USA. Disseminated chalcopyrite (BEAV-3) and mineralization from quartz-K feldspar-chalcopyrite-bornite-molybdenite veins (BEAV-1,2,4,5) cutting a nearly equigranular, fine-grained monzonitic rock have been analyzed. Several generations of veins contain elevated chalcopyrite δ^{65}Cu values (up to 1.38‰, Appendix 2), among the most elevated chalcopyrite δ^{65}Cu values analyzed in this investigation. Since isotopically heavy values are uncommon for igneous rock-hosted mineralization of this style, it would indicate that the magmas represented by these rocks may be anomalous in their copper isotope signature. However, mineralization hosted by a late porphyry dike in the breccia pipe deposit in the nearby OK Mine of similar age (K. Krahulec, personal communication, 2005) show chalcopyrite δ^{65}Cu values that are closer to igneous rocks (0.00‰). Also chalcopyrite mineralization in the Cactus Mine, San Francisco Mountains, UT, farther west in the same structural trend, has a "normal" chalcopyrite δ^{65}Cu value (0.23‰) in endoskarn (high-temperature alteration in an igneous intrusion). These observations suggest that the elevated values at the Beaver-Harrison mine were probably not produced by an anomalous copper isotopic source manifested in other parts of the same metallogenic trend, but are a local phenomenon produced through hydrothermal processes.

Evaluation of copper isotope ratios from different areas shows no indication of anomalous copper isotope ratios in different tectonic environments. This includes igneous rock-hosted chalcopyrite from the Stillwater complex (Archean mafic magmatic complex), the Palabora carbonatite (mantle-derived), values from porphyry mineralization in Indonesia (i.e., Grasberg; cf., Graham et al., 2004), the western Cordillera of North America, and the central Andes (Table 8). This is primarily due to the "spreading" effect on isotopic ranges by hydrothermal related isotopic fractionation, but also because igneous rock copper isotope values ordinarily have a limited range in δ^{65}Cu values (Maréchal, 1998).

Isotopically Distinct Fluids

Graham et al. (2004) called upon multiple, isotopically distinct hydrothermal fluids to explain variations they observed in chalcopyrite mineralization near the Grasberg mine, Irian Jaya, Indonesia. They based this interpretation on the general trend of isotopic values relative to distinct mineralizing intrusions in the Grasberg complex and spatially related skarns by using cumulative probability diagrams. Since their sample suite included

mineralization from paragenetically distinct mineralizing events, the variations could also be interpreted based on the temporal and spatial relationship of the mineralization to each fluid source.

Rouxel et al. (2004) also indicated that fluids may isotopically evolve with time due to the temporal isotopic fractionation related to leaching of copper from rocks altered in sea-floor convection at mid-ocean ridges, or leaching of existing sulfides. Since copper isotopes can be fractionated by hydrothermal processes (see below), it seems unlikely that spatially overlapping mineralization could be traced isotopically to specific intrusive rocks (i.e., in a porphyry environment) unless extreme initial isotopic values of exsolved hydrothermal fluids could be confirmed for specific magmas. Thus, the isotopic zonation produced during mineralization would need to be carefully evaluated, both isotopically and paragenetically for determining the likelihood of mineralization from isotopically distinct fluids.

Remobilization of Copper

Copper isotope ratios could assist in tracing remobilization of copper in hydrothermal systems. An influx of copper-undersaturated hydrothermal fluid into previously mineralized zones would be expected to have some kind of remobilization effect, thereby transporting copper to another zone in the deposit. Several samples from this investigation indicate that copper may be less likely to be remobilized than would be expected. One hand sample from the Beaver-Harrison Mine shows three distinct mineralizing events, with two vein sets and also disseminated mineralization (BEAV-1,2,3,5 analyses, Appendix 2). Each of these mineralizing events produced isotopically distinct chalcopyrite, and show a range of about 0.4 per mil in chalcopyrite analyzed from different parts of the sample. Disseminated chalcopyrite shows the lowest δ^{65}Cu value (1.04‰) and is significantly different from the vein chalcopyrite 1cm away (1.22‰) (Fig. 23) (cf., samples from Ajo, Arizona, Appendix 2). However, a sample of strongly sheeted, late chalcopyrite veins cutting garnet skarn with disseminated mineralization from a Cu-skarn deposit (Tintaya Mine, Perú, samples Chab-Este, Chab-Esteb) shows that the late vein and disseminated chalcopyrite in garnet are isotopically identical (Fig. 24). The garnet skarn host shows little evidence of alteration by the late mineralizing fluid here, but also may have had a better rock permeability than the BEAV samples.

Different types of hydrothermal fluids may be more important to mobilizing copper than others, such as acidic quartz-sericite-pyrite (QSP)-forming fluids in porphyries verses earlier potassic fluids. Fluids producing QSP-

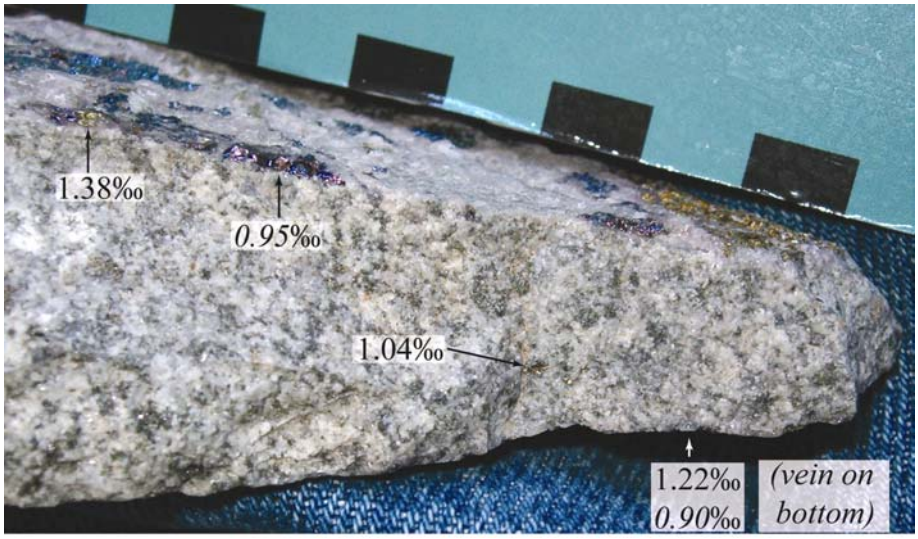

Figure 23. Photo of mineralization sampled in three places centimeters apart for BEAV-1,2,3,5 from the Beaver-Harrison mine, UT, USA. Values are δ^{65}Cu, with those for bornite in italics. The vein on the top of the sample and that on the bottom (not visible) consist of quartz-K feldspar-chalcopyrite-bornite, but the top vein is larger, contains minor amphibole, and is paragenetically later than the vein on the bottom of the sample. Black rectangles on scale are 1cm long.

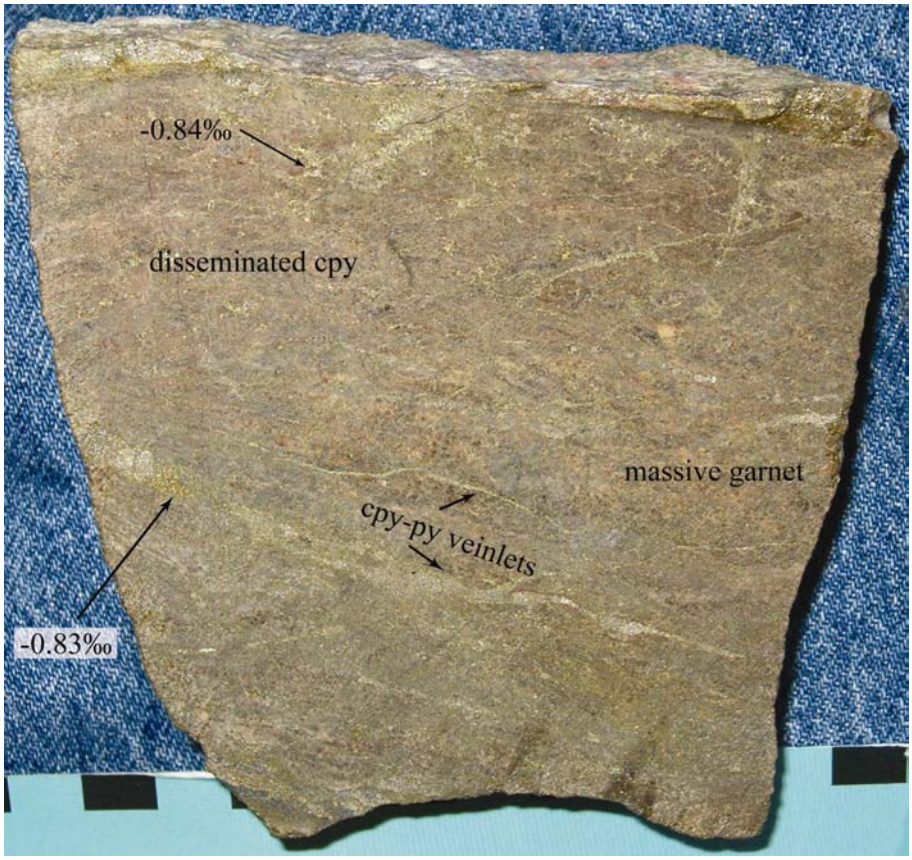

Figure 24. Strongly mineralized sample Chab-Este from Tintaya, Perú, showing δ^{65}Cu values for chalcopyrite from disseminated and vein-controlled mineralization. The late overprinting mineralized veins and veinlets cut through garnet grains but there is little alteration effect on the garnet by the mineralizing fluid. Black rectangles are 1cm long.

style alteration have also been observed to physically remobilize disseminated mineralization in some ore deposits, although the scale is often small (Fig. 25). Measures of isotopic equilibrium between two co-existing ore minerals might be able to help clarify whether a sample has experienced leaching or overprinting mineralization, as proposed in Maher and Larson (in review; Appendix 4). That paper addresses the possibility of using a characteristic bornite-chalcopyrite fractionation, such as is observed in several ore deposits between co-precipitated bornite and chalcopyrite, to define equilibrium precipitation of two copper phases.

One environment where copper remobilization is frequently called upon is high-sulfidation vein systems that post-date earlier porphyry style mineralization (Brimhall, 1980; Manske and Paul, 2002). The source of the late mineralizing fluids forming the high-sulfidation veins is not presently agreed upon. It has been suggested that these fluids may represent porphyry-derived condensed vapor (Rusk et al, 2004), or possibly a distinctly different mineralizing fluid of separate genesis from the porphyry fluids (including the fluids producing potassic and sericitic alteration). The actual source of the metals in these large veins has also been debated. Rusk et al. (2004) suggest the copper may be vapor-transported from phase separation of magmatic low-salinity fluids. Another possibility is that the copper may be produced from remobilization of earlier-precipitated porphyry ores deeper in the system and re-deposited in structurally favorable zones within the phyllic alteration zone above the earlier potassic alteration (Brimhall, 1980).

Several investigations have shown that low- to high-temperature copper leaching of minerals tends to produce a fluid that is initially isotopically heavier than the mineralization (Young and Ruiz, 2003; Rouxel et al. 2004, Erhlich et al., 2004). Rouxel et al. (2004) attributed strong isotopic zonation in individual black smoker chimneys to preferential remobilization of isotopically heavy copper from earlier sulfides by the hydrothermal fluid. Copper isotope variations in late high-sulfidation veins from Butte, Montana (Table 8), show that hypogene bornite, chalcocite, and covellite tend to be isotopically heavier than that expected from the porphyry-style, higher-temperature (potassic) alteration, such as at Coroccohuayco, Perú (Fig. 21). Bornite values of nearly 1 per mil (e.g., sample Bu-10) indicate considerable enrichment in ^{65}Cu. This may be due to preferential remobilization of ^{65}Cu from earlier porphyry copper mineralization. In comparison, disseminated bornite from the prograde copper skarn at Coroccohuayco, Perú, range from -0.46 to 0.40 per mil.

A study of hypogene copper minerals from the potassic and high-sulfidation mineralization in the Resolution porphyry deposit (Superior porphyry of Manske and Paul, 2002), show that $\delta^{65}Cu$ values of chalcopyrite

Figure 25. Drill-core sample from Resolution porphyry, Arizona, USA, showing the removal (remobilization) of disseminated mineralization (chalcocite-digenite) from the vein selvages from late pyrite-sericite (QSP) veins. Barren halos have been outlined for reference. Although this is a small-scale feature, similar processes may operate on the deposit scale in hydrothermal systems with late phyllic alteration remobilizing copper from early potassic alteration-related mineralization into high-sulfidation veins. The mineralization in this sample is too fine grained (approximately 50μm grains) for the sampling procedure utilized in this investigation, and would required laser ablation sampling to analyze.

increase away from the potassic alteration, with relatively high values in chalcopyrite in the high-sulfidation veins (Fig. 26). Bornite from these same veins shows enrichment in ^{65}Cu producing $\delta^{65}Cu$ values as high as 1.62 per mil. This ^{65}Cu enrichment in a non-supergene environment indicates significant fractionation of copper has occurred in the formation of these high-sulfidation veins under hydrothermal conditions. If the hypothesis is accepted that this mineralization results from vapor transport of copper from phase separation of the magmatic fluid then there must exist a large isotopic fractionation effect during the boiling process at high temperatures, and such a fractionation has not yet been documented experimentally. Additionally, this could be explained as mineralization resulting from preferential leaching of ^{65}Cu from earlier porphyry mineralization. Such extreme enrichments in the heavy isotope are probably the products of a leaching process of the earlier porphyry ores in which the leaching Cu-enriched fluid became isotopically heavier than the Cu-leached minerals. Subsequent precipitation of copper from this fluid in the high-sulfidation veins may have resulted in isotopically heavy copper mineralization.

Interestingly, copper mineralization from the nearby and related Superior vein and mantos shows less enrichment in ^{65}Cu than might be expected from isotopic fractionation during remobilization of copper. The maximum $\delta^{65}Cu$ value for bornite observed in this vein/manto system is 0.43 per mil (Ar-6). Chalcopyrite values from this mineralization also reach 0.54 per mil (Sup-1). Although remobilization and re-precipitation of copper derived from the Resolution area to the vein system at Superior can not be completely ruled out, it may have played a smaller role here than in the late, high-sulfidation veins overlying the Resolution porphyry system to the south.

Copper Isotope Fractionation Among Complexes in Solution

Maréchal and Albarède (2002) first suggested the possibility that copper may fractionate among polynuclear copper chloride complexes in solution in their experimental study (at 20°C) of copper isotope fractionation on anion exchange resin. Rouxel et al. (2004) also examined this possible fractionation mechanism at high temperature for producing the $\delta^{65}Cu$ variations they observed in sea-floor massive sulfide deposits. Theoretically, due to the differing ligand geometries of copper-transporting complexes in solution, fractionation between complex species in solution would not be unexpected and has been modeled for iron isotopes by Schauble et al. (2001). The significance of this fractionation mechanism is debatable at high temperature, but Fe isotope

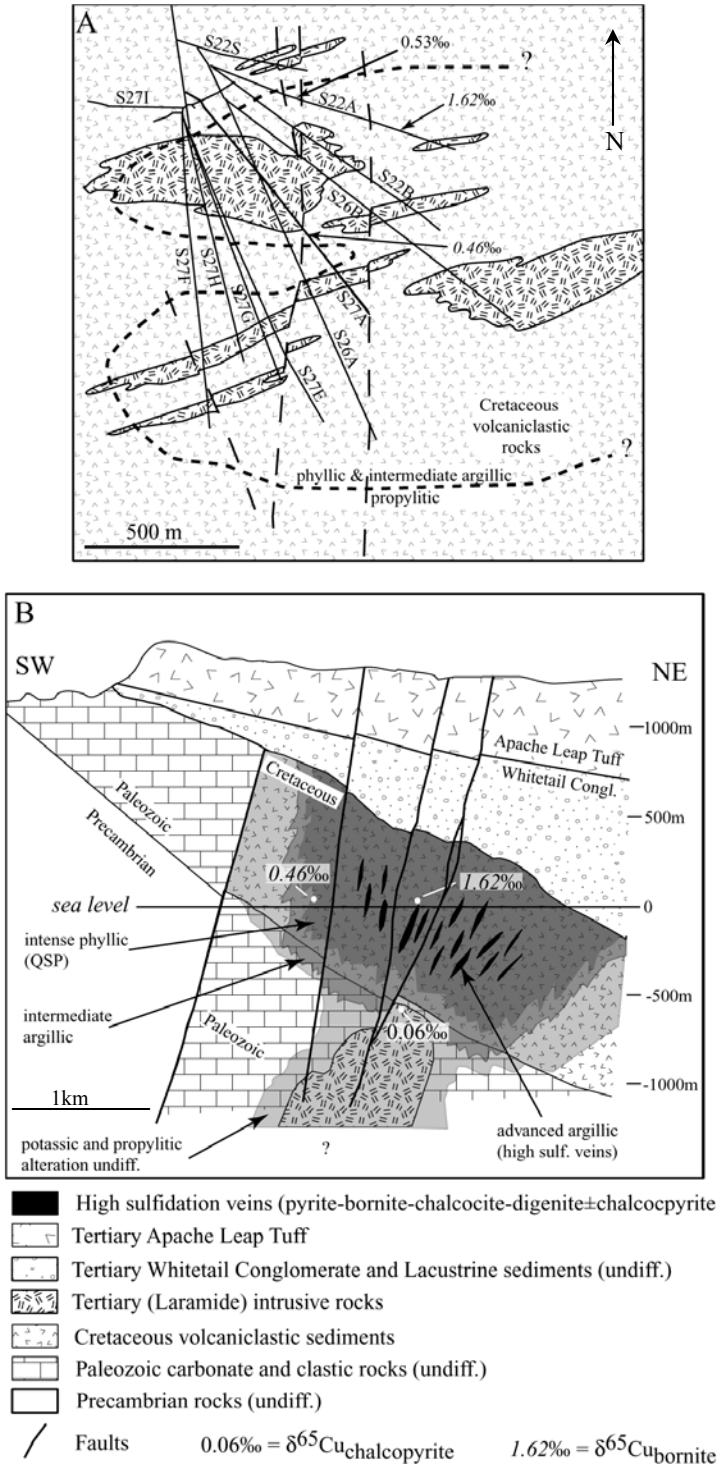

Figure 26. Plan view at sea level (A) and SW-NE cross section (B) of the Resolution porphyry, Arizona (adapted from Manske and Paul, 2002). (A) is taken approximately at sea level (See Manske and Paul, 2002, for deposit specifics). Highest $\delta^{65}Cu$ for bornite is found in the center of the late, overprinting mineralization associated with advanced argillic alteration (not shown in (A)).

fractionations of over 0.5 per mil have been suggested for this process at lower temperature. This, in concert with an equilibrium fluid-mineral fractionation, could conceivably produce significant variations in copper isotope ratios of mineralization. An extensive study of isotopically zoned copper mineralization in a high-temperature hydrothermal skarn system where this fractionation mechanism is called upon is presented in Appendix 4. This Appendix (Maher and Larson, in review) documents isotopic variation in hypogene mineralization with a geologic context in the Tintaya District, Perú.

In summary, based on fluid inclusion evidence and styles of mineralization, isotopically zoned mineralization could have been produced during precipitation of copper from isotopically fractionated copper chloride complexes from a single fluid pulse. It is proposed that isotopic fractionation occurs between predominant chloride species ($CuCl_2^-$ and $CuCl_4^{-3}$) during the synchronous formation of the complexes in high-salinity brine formed by fluid exsolution from a magma or by later phase separation (boiling).

During early precipitation of copper from the fluid, temperature-induced thermodynamic instability of the $CuCl_4^{-3}$ complex produces isotopically lighter chalcopyrite, and later, more massive mineralization is isotopically heavier. Due to the differing ligand geometries of these complexes, $CuCl_2^-$ may be isotopically heavier than $CuCl_4^{-3}$. The later mineralization is derived from the isotopically heavier fluid, dominated by the remaining isotopically heavier copper complexes in solution. The later precipitation is produced by thermodynamic instabilities of the complexes resulting from changes in other fluid variables (i.e., fO_2, pH, etc.) rather than simply a decline in temperature. The isotopic fractionation between copper complexes may produce a larger fractionation than a fluid-mineral fractionation, although the latter likely also operates during precipitation of a copper phase.

It should be noted that isotopic fractionation between transporting complexes have not been experimentally confirmed at high temperatures (i.e., ≈300º C). The significance of this fractionation mechanism under such geologic conditions is hypothesized based on the empirical evidence observed in the spatial variation in $\delta^{65}Cu$ values of mineralization and other geologic and thermodynamic data presented in Maher and Larson (in review, Appendix 4). The supporting geologic context of the isotopic study is more thoroughly presented in Maher (in prep.) and Maher (1999).

As is indicated in Maher and Larson (in review), the significance of the proposed isotopic fractionation between transporting complexes can explain several important features of the data from this and other investigations of ranges in copper isotope ratios. Copper isotopes from several ore deposits listed in Figure 21 show limited $\delta^{65}Cu$

ranges in hypogene copper mineralization. For example, the study of native copper from the Michigan native copper district (Table 8; Larson et al., 2003) indicates that the hypogene native copper from several deposits over 100km strike are isotopically homogenous. This was not expected prior to analysis of the samples, simply because variability within large ore districts was not known. Rouxel et al. (2004) showed that ranges in $\delta^{65}Cu$ for hypogene chalcopyrite from active individual black smoker deposits tends to be limited to individual ranges of about 0.4 per mil. Two important exceptions of a larger spread and higher values in $\delta^{65}Cu$ were observed in this study. The first is from Logatchev field, where strong textural evidence exists for remobilization of copper, and the second from Rainbow field, which Rouxel et al. (2004) indicated was characterized by the highest-salinity hydrothermal fluids. These two examples of larger ranges support the hypothesis that remobilization of copper and the role of fractionation among copper complexes (in higher-salinity fluids) can produce higher and larger ranges in $\delta^{65}Cu$ values relative to systems lacking such features.

Samples of chalcopyrite from the Au-skarn system at Buckhorn Mountain (Crown Jewel), Washington, USA, are also quite restricted in their range, from -0.43 to 0.29 per mil (Table 8). M. Gaspar (personal communication, 2005) indicates that the chalcopyrite-forming solutions were magmatically derived, with fluid salinities approximately 20-24 weight percent NaCl equivalent. Deposits with a more limited range in $\delta^{65}Cu$ values share a common characteristic in that their mineralizing fluid salinity is generally less than that observed for porphyry systems, or their mineralizing fluid(s) is much more homogeneous than those from porphyry deposits. The deposits characterized by high salinities produce primary isotopically zoned mineralization with >1 per mil variations in $\delta^{65}Cu$, even at high depositional temperatures (i.e., Bingham Canyon, Utah, Coroccohuayco and Tintaya, Perú, this study, and Graham et al., 2004). As proposed in Maher and Larson (in review; Appendix 4), thermodynamic calculations indicate that for salinites less than about 40 wt % NaCl equivalent there is only one predominant copper chloride complex of significance under hydrothermal conditions. This implies that the resulting mineralization from lower-salinity fluids will have a smaller isotopic range because the only fractionation mechanism operating during primary precipitation of copper from the fluid would be an equilibrium fluid-mineral fractionation. The fractionation of copper between transporting complexes would still occur, but would be significantly less important, due to the relative lack of other complexes.

Undoubtedly there is isotopic fractionation among all complexes in solution. The difficulty comes in experimentally determining what they might be, or even if they are significant. The example of Coroccohuayco

empirically fits this fractionation model because it is a chloride-dominated system where several of the important fluid and geologic variables that control mineralization are constrained. Copper isotopic variation in hypogene mineralization in other systems, such as Butte, Montana, USA, with two main mineralization events and styles, would be more difficult to explain with this model, although there must be a thermodynamic basis for the variation observed. In systems where copper is transported by other complexes, such as bisulfide, there is likely a copper isotopic fractionation between the different ligands in these solutions. Experimentally it is observed that a simple increase in oxidative capacity of a fluid can produce the difference between a chalcopyrite-pyrite assemblage and a covellite-chalcocite-pyrite assemblage (high-sulfidation type assemblage), even with the same fluid composition (see Section VI). So, even in those systems with high-sulfidation assemblages, chloride complexes likely dominate (Mountain and Seward, 1999) and copper isotopic fractionation may occur between the dominant chloride and other complexes in these solutions.

Copper Isotope Fractionation in Supergene Ore Zones

Shields et al. (1965) first recognized the relationship between oxidation-reduction processes and copper isotope fractionation where they observed the largest range in δ^{65}Cu values from supergene minerals. Several investigators are presently examining the behavior of copper isotopes in the supergene environment (Young and Ruiz, 2003; Asael et al., 2005). Although not the direct focus of this investigation, some important features of copper isotope variations have been observed through the analysis of supergene copper minerals. Several of these aspects have been presented in Larson et al. (2003). However, some important generalizations can be made in relation to the isotopic fractionation of copper in this environment.

Recent analyses of copper minerals from supergene zones have confirmed a larger range in δ^{65}Cu values than for sulfides (Fig. 21). The ranges of δ^{65}Cu values for a single copper mineral from the supergene environment can be considerable. For example, the range in δ^{65}Cu values for supergene native copper from the Ray mine, Arizona, is from -3.03 per mil (Maréchal et al., 1999) to 0.72 per mil (this study). In the supergene environment, the transport (mobility) and deposition of copper is related to oxidation of hypogene and supergene ore minerals and the hydrologic cycle. The large range in supergene mineral δ^{65}Cu values is a function of three processes: the initial leaching, the change in valence of copper (oxidation/reduction if it occurs), and the final precipitation. The leaching

process involves the removal of copper from existing ore minerals (hypogene or supergene). Experimental work (Young and Ruiz, 2003) shows that the first leachate from copper sulfides is isotopically heavier than the minerals. Rouxel et al. (2004) also demonstrate that leaching of sulfides by hydrothermal fluids tends to preferentially remove ^{65}Cu from the existing minerals. Although not presently quantifiable, the leachate will be isotopically heavier than the leached minerals depending on the degree of leaching. Minor leaching will produce more extreme enrichment of ^{65}Cu in the leachate than nearly complete leaching.

Several investigators have observed that supergene copper minerals co-existing in the same sample with hypogene copper minerals are isotopically heavier then their hypogene precursors (Rouxel et al., 2004; Asael et al., 2005). However, the actual direction of the fractionation of copper by oxidation or reduction of the Cu ion in solution is uncertain since at least two fractionation steps are indicated in samples with hypogene and oxidized supergene minerals. Zhu et al. (2002) measured fractionation in an oxidation-reduction process between Cu^{+} and Cu^{2+}. However, their technique involved a precipitation step, so more than one fractionation process may have occurred in their experiment. Other workers (Matthews and Zhu, unpublished data, *in* Erhlich et al., 2004) attempted to chromatographically separate Cu(I) from Cu(II) in solution, and obtained a fractionation factor between isotopically heavier Cu(II) and isotopically lighter Cu(I) of 3.7 per mil. However, there is a question as to whether isotopic fractionation occurred on the column since neither their procedure, nor the the method of determining the mass balance of copper in the two valences, were explained.

The last fractionation step in the supergene environment is during precipitation of a mineral from the solution. This step has been measured for two minerals, malachite and covellite. The low-temperature fractionation factors for malachite (Maréchal and Sheppard, 2002) and covellite (Erhlich et al., 2004) indicate that the precipitation of either of these minerals from cupric copper in solution will precipitate minerals which are isotopically lighter than the fluid. As noted above, these experimental studies are applicable to only part of the total oxidation processes in supergene zones because the experimental fluids were already oxidized (Cu^{2+}). In the case of the study by Erhlich et al. (2004), the precipitation of covellite was accompanied by reduction of the copper so their measured fractionation represents both the reduction of copper and the mineral precipitation from the fluid. The oxidation of copper sulfides in supergene zones is not always accompanied by the oxidation of copper and so the precipitation of covellite in the enriched blanket of supergene zones may, or may not, be accompanied by reduction of copper in the fluid.

Using malachite as an example, and assuming copper is derived from the leaching of chalcopyrite protore, the isotopic fractionation associated with leaching copper from the protore and precipitation of malachite will both enrich the fluid in ^{65}Cu. The direction of fractionation during the oxidation of Cu(I) to Cu(II) is unknown. The fractionation for the reduction reaction of Cu(II) to CuS is nearly an order of magnitude larger than the equilibrium reaction of Cu(II) to malachite at the same temperature, suggesting that the isotopic fractionation from oxidation of Cu^{+} to Cu^{2+} in the fluid may be much larger than the fluid-mineral fractionation during precipitation.

Malachite is isotopically light in several deposits (<0.0‰) (Shields et al., 1965; Maréchal et al., 1999; Zhu et al., 2000). This may indicate that the degree of leaching of the protore (i.e., mature supergene oxidation) and/or that a multi-step precipitation of malachite from the supergene fluid (Zhu et al., 2002) were important in its formation. The lower the $\delta^{65}Cu$ value for malachite, the more extreme the fractionation has been in one of the fractionation processes. Minimal leaching of chalcopyrite (i.e., immature supergene weathering) will produce an isotopically heavy fluid. Precipitation of a small amount of malachite from this solution will produce malachite only slightly isotopically lighter than the fluid (ignoring the oxidation fractionation), but multi-step equilibrium fractionation precipitating small Cu fractions may produce an over-all large fractionation and isotopically light malachite. In addition, a Rayleigh-type fractionation could produce a large variation in the isotope composition of copper minerals. The botryoidal and banded nature of malachite suggests that the bands are a result of several copper precipitation events and possibly even deposit scale oxidation events, each one recording an isotopically distinct fluid or degree of fractionation.

An azurite sample (OKM-1) from the OK Mine, Millard Co., UT, is extremely enriched in ^{65}Cu (2.44‰) relative to porphyry-hosted disseminated chalcopyrite in the same deposit (OKM-2, 0.00‰). As other recently published analyses of azurite (Maréchal et al., 1999; Zhu et al., 2000) indicate that azurite tends to be isotopically heavy, the fluid-azurite fractionation factor may be negative. Since a starting $\delta^{65}Cu$ value of the chalcopyrite can be considered as the chalcopyrite protore value from the OK Mine, considerable fractionation of copper must have occurred in the formation of this azurite. However, this could also be accomplished by precipitation of a large fraction of the copper in the fluid without isotopic re-equilibration of the mineral with the fluid (Rayleigh), by numerous stepwise equilibrium precipitation events over the pathway of the mineralization, or by only very minor leaching of the protore (weakly developed supergene oxidation of the deposit). Certainly more than one of these processes would be required to produce such an isotopically heavy azurite. In this deposit, the azurite is from a zone

of mixed hypogene copper sulfides and supergene copper minerals, and the intensity of oxidation and volume of acid produced during deposit oxidation was not large. Since minor leaching of the hypogene protore is geologically confirmed in this case, the large leaching-related isotopic fractionation likely contributed to the high δ^{65}Cu value of the azurite in this deposit.

The famous azurite mineralization from Chessy, France, has a range in δ^{65}Cu values from 0.44 per mil to 2.05 per mil (Maréchal et al., 1999; Gale et al., 1999; Zhu et al., 2000). Although the δ^{65}Cu value of the chalcopyrite from which copper was leached to form the azurite is unknown, it may have been between 0.0 per mil and 0.5 per mil (similar to the Superior vein, Arizona). The lower δ^{65}Cu values of some Chessy azurite suggest large amounts of copper were leached by supergene processes from the chalcopyrite vein source, but locally more extreme fractionation processes occurred to produce the high values.

Due to the generally high δ^{65}Cu values for azurite, the fluid-azurite fractionation factor is likely to be negative and possibly of larger magnitude than for malachite. A stepwise equilibrium fractionation process at small copper fractions might produce extreme enrichment in ^{65}Cu in azurite. Highly negative or positive δ^{65}Cu values of copper minerals in supergene environments suggests either repetitive, small-batch equilibrium fractionation during precipitation occurred, or precipitation of a large fraction of the copper from a leachate derived from very minor Cu leaching (by a Rayleigh fractionation process). Unfortunately, extreme isotopic values observed in some supergene minerals do not necessarily indicate whether the supergene system is mature or immature. Additional geologic constraints are required to make such interpretations. Supergene environments with other evidence of minor supergene oxidation (e.g., leached cap thickness) would thus imply that less isotopic fractionation “processing” of supergene fluids has occurred (i.e., less maturely oxidized systems). As with other stable isotopic systems, a geologic context of the mineralization is required to correctly identify (or eliminate as reasonable possibilities) the fractionation processes involved in producing a specific copper isotope composition.

The variations observed in copper isotopic ratios between different supergene minerals (such as azurite and malachite) is a result of lower temperatures, large isotopic fractionations resulting from varying degrees of leaching of copper from protore (sulfide or oxide), and large isotopic fractionation between fluid and minerals during precipitation. In addition, further fractionation could be induced between metal-transporting complexes and the conditions of copper precipitation from the fluid (analogous to the proposed fractionation between copper complexes at high temperature). This is then complicated by the cyclic nature of dissolution-precipitation subject to

changes in the hydrologic system over time. Changes in the local hydrologic system, especially due to uplift and erosion, would remobilize the secondary enrichment blanket, exposing it to a new cycle of oxidation of sulfides, mobilization of copper, and a second cycle of fractionation of copper isotopes. This is probably a continuous process in tectonically active regions, such as active continental margins with porphyry systems. Thus, many factors contribute to the complexity and large range of $\delta^{65}Cu$ values in supergene environments.

VI. High-Temperature Fractionation of Copper Isotopes Under Experimental Hydrothermal Conditions

Empirical evidence of high-temperature copper isotope fractionation in hydrothermal ore environments suggests that under certain physicochemical conditions such fractionation could be reproduced experimentally. This investigation measured fractionation of copper isotopes under high-temperature hydrothermal conditions. These experiments were designed to measure the fractionation factors between the hydrothermal fluid and precipitated copper mineral. The experimental approach was to precipitate chalcopyrite from element nutrient in the presence of a simple hydrothermal fluid. A procedure was required to separate the fluid from the precipitate at temperature, since decreasing the temperature would precipitate copper from the solution, possibly changing the fluid isotopic composition from what it was at the temperature of interest. The experimental approach was modified from the closed silica-tube technique of Seward (1976). That investigation measured solubility of AgCl by reacting the material in one half of the silica tube and then inverting the tube, at temperature, and separating the solution from the solid by a filtered constriction in the middle of the tube. Due to high temperatures, the experiments were conducted in sealed bombs to equilibrate the internal tube pressure and prevent rupturing of the tubes. The bomb was carefully inverted at temperature to separate the fluid from the solid.

This investigation synthesized chalcopyrite in the presence of a hydrothermal fluid in one half of the experimental tube and then the tubes were inverted at temperature to separate the fluid from the precipitate. Exact weight proportions of the elements as found in chalcopyrite (iron and copper wires and elemental sulfur powder) were used as nutrient to produce 0.3 to 0.5 grams of precipitate. The copper and iron were small cuttings (approximately 0.5mm lengths) of high-purity wire. The total experimental charge consisted of these nutrients in the presence of a water solution (Appendix 5).

Procedure

Sealed silica tubes provide a closed environment for the reaction of the nutrient and hydrothermal fluid without interaction with the bomb and allow several experiments to be run in the same bomb at once. Six-inch (15.25cm) long silica-glass tubes were constricted in the center by softening the glass with a hydrogen-oxygen torch

flame, and then sealing one of the ends. Each tube was individually marked with its number. Solutions of various hydrochloric acid and NaCl molalities were loaded into the lower half of the tube (Appendix 5). A small amount of silica wool was then placed into the open end of the tube above the constriction and nutrient was placed on top of the silica wool. A small amount of silica wool was placed at the top opening of the tube and then the tube was sealed in the hydrogen-oxygen flame while the previously sealed end of the tube was cooled in an ice-water bath.

The upper silica wool prevented hot gas from entering into the charge area and melting the sulfur powder during sealing of the open end. Melting of the sulfur powder in the charge causes the tube to become sealed by sulfur at that point. After several experiments and variations it became apparent that the sulfur blockage point was the site of sulfide precipitation. This blockage was replaced with sulfide precipitate that would cause incomplete separation of the fluid from the precipitated sulfide when the bomb was inverted.

An ice water bath permitted the tube to be handled by hand during the delicate process of sealing the top. If the tube was heated too far down from the top during sealing, a large bubble would form at the top of the tube, causing the glass walls to stretch and become very fragile. Sealing too far at the top would cause the tube to wrap into itself (apparently under a slight vacuum produced by the cooling effect of the ice water bath?). The tube could still be sealed in this situation, but the volume of the tube would steadily decrease as the tube top was pulling into itself. This could become a problem since a volume of water, based on the relative volume of water to air space in the silica tubes, was put into the bomb to equalize the internal tube pressure with the bomb pressure. Without this pressure equalization the tubes would burst.

Prior to placing the sealed tubes into the bomb, the nutrient was shaken to the end of the tube (the top) if possible, away from the constriction with the silica wool. As mentioned above, it was found that the high temperature precipitation of sulfide occurs at the site of the nutrient. For those tubes in which the nutrient remained at the constriction (where it was initially loaded), the sulfide precipitated at this location tended to block the tube and prevent much of the reacting fluid from separating from the precipitate. Often this was evident from the formation of covellite crystals around the earlier precipitated sulfide during cooling of the experiment (Appendix 5).

Water was placed in the bomb to equalize the internal tube pressure. The bolts on the top of the bomb were tightened to 40ft-lbs torque for experiments at 225º C and 60ft-lbs for 300º C. The bomb was left in an oven (at 225ºC) or a furnace (at 300ºC) for 5-7 days. Temperature fluctuation in the oven was measured with a high-temperature mercury thermometer suspended from the top of the oven, near the bomb. After the bomb came up to

temperature, cyclic heating of the oven produced a temperature fluctuation of approximately plus or minus 0.6ºC from the target temperature. The temperature in the furnace was measured by a thermocouple inserted into the wall of the bomb. Once the bomb in the furnace was up to temperature, its temperature fluctuated less than 1ºC.

Once the reaction was completed, the bomb was carefully inverted and immediately replaced in the oven or furnace. The flipping procedure took less than one minute during which time the bomb cooled less than 5 degrees. The bomb was again placed in the oven or furnace for a minimum of one hour while the solution drained past the silica wool and constriction into the other end of the tube (a process that probably took only one quarter of that time).

At the end of the experimental run the bomb was cooled under a stream of compressed air and then in a cold-water bath. When the bomb was opened each tube was carefully examined and the outside cleaned without tipping the tube and allowing the fluid to get near the precipitate. If a tube leaked fluid into the bomb (due to incomplete sealing of the tube, this occurred only in one case) it was apparent when the bomb was opened from a hydrogen sulfide odor. The tubes were re-labeled based on their position in the bomb. Tubes that did not drain at the experimental temperature due to sulfide blockage would not drain after several months at room temperature, and these samples were not further processed or analyzed. Chalcopyrite was visually observed in all silica tubes in which elemental sulfur, iron and copper were used as nutrient (Appendix 5). Much of the precipitate was finely crystalline, and/or botryoidal in habit.

The tubes were opened at the constriction. In all cases a hydrogen sulfide odor was apparent upon opening. The fluid was pipetted from the end of the tube and whatever fluid remained in the tube was rinsed out with a few ml of nano-filtered de-ionized water. To this fluid from the experiment was added 7N HCl + 0.1% H_2O_2 to dissolve any solid which might have precipitated after the fluid had separated from the precipitate. This solution was evaporated until dry and the residue was dissolved in 2ml of 2% HNO_3. This solution was analyzed, after dilution, for concentration of several elements on a quadrupole ICPMS. Of significance were Fe, Na, and Cu (Appendix 5). The precipitate was rinsed out of the tube (in some cases the solid required chipping out) with nano-filtered de-ionized water into a Teflon container. The water was decanted out of the container along with the very fine fraction of sulfide. This step was repeated twice and most of the smallest precipitate fraction was removed. The sulfide was then wetted with acetone and air-dried. Samples of the solid were analyzed by X-ray diffraction to determine the mineral phases present (Appendix 5). All sample precipitates were dominated by chalcopyrite, with minor fractions

of pyrite, pyrrhotite, and one sample with bornite. The presence of the iron sulfide phases were not of concern to copper isotope analyses. The sample with bornite was not analyzed isotopically since separation of the copper phases was not possible and previous studies of co-precipitated chalcopyrite-bornite indicate a measurable isotopic fractionation exists between them (Section III).

Chomatography of Fluid

Fluid samples from chalcopyrite precipitation were chromatographically purified for copper analysis. Based on the initial concentration analysis by ICPMS, sufficient fluid from each sample to produce a final 100ppb Cu solution (assuming that all the copper would be recovered during the chromatographic purification) was evaporated. The residue from the evaporation always contained NaCl crystals. This was re-dissolved in 7N HCl + 0.1% H_2O_2 to oxidize the Cu in the sample. This was repeated once. The last residue was re-dissolved in 0.1ml of 7N HCl + 0.1% H_2O_2. Due to the chloride concentration in the acid, the NaCl in the residue could not be completely re-dissolved. The solution was loaded on prepared chromatographic columns containing MP-1M resin as two steps. After the first 0.1ml was loaded another 0.1ml of acid was added to the NaCl residue and then loaded on the resin for a total load of 0.2ml. Little difference was observed between loading the sample at once or by loading in two steps. Due to the nature of the separation process, using too much acid (sufficient to dissolve the NaCl) spread out the copper elution, mixing it with the Na elution. This produced significant error during copper collection (see below). Using a lower strength acid to completely dissolve the NaCl would have made the separation impossible since copper is retained on the resin only at high acid normality. At lower acid normality both copper and iron migrate through the column without complete separation from the other matrix (i.e., Na).

Under the circumstances it was considered best to discard the insoluble NaCl and whatever amount of Cu and Fe might have been with it. Residual NaCl was slightly yellow colored and so probably contained some of both iron and copper. There is evidence that during dry-down of the solution in preparation for chromatography that the chlorides of copper and iron may precipitate during the first precipitation of halite and get trapped in the salt (see below).

The chromatographic procedure was similar to that utilized for Cu-Fe sulfides (Appendix 1). The copper elution was evaporated and the residue dissolved in 2% HNO_3 and analyzed by a quadrupole ICPMS. The separation

of copper from iron was always very clean, but not copper from sodium in those cases where the samples were loaded on the resin with more than 0.2ml, or if the beginning of the copper collection overlapped with the matrix elution. Fluids from several samples went through various purification procedures to try to maximize the separation and copper recovery. In most cases the analyzed fluid contained less copper than what was expected based on the multi-element analysis from the quadrupole-MS.

If the columns are not properly calibrated for the conditions of the solution, copper can easily be lost during elution of the sample. If the copper collection begins too early, the final Cu concentration will be low and the copper collected will be isotopically light (e.g., Fig. 6). If the collection starts too late, the final Cu-concentration will also be low but isotopically heavier. Those purified solutions with higher Na (eluted some of the matrix with the Cu) suggest the collection of copper may have began too early. From these samples it is implied that the sample should be relatively isotopically lighter, plus have isobaric interference with ^{63}Cu from $ArNa^+$ causing the meaasured $^{65}Cu/^{63}Cu$ ratio to be isotopically light. However, the samples are actually isotopically heavier than those elutions with low Na, suggesting that the $ArNa^+$ isobar is not significant.

Due to experimental constraints an abbreviated method of chromatographic separation was tested alongside the standard method. This abbreviated method eluted copper more rapidly using 4.5N HCl , rather than 7N HCl+0.1% H_2O_2. The sample was loaded in the same manner and the matrix removed in 7N HCl + 0.1% H_2O_2, but then the copper was eluted in a smaller volume using a lower acid concentration. Iron started to slowly migrate down the column with this lower strength acid but the copper migrated more rapidly, and was removed prior to the iron elution. Fluid samples designated " xx Cu(2)" or "xx chrom" are from the abbreviated elution scheme.

Since the synthesis fluid contains NaCl up to 7.4 moles/kg, halite (NaCl) would precipitate as the synthesis fluid was drying down. Due to the strength of the HCl elution solution, not all halite would dissolve. Thus every sample contained some Cu-Fe in the insoluble residue, possibly as Fe-oxide (and Cu oxide) and/or as chloride salts. There may have been some copper isotopic fractionation at the time of the precipitation of chloride salts and/or the dissolution of the sample for loading on the resin. A modification was made to the procedure to try to load the sample on the resin over 0.2ml in two 0.1ml steps rather than as the whole charge to try to dissolve as much Fe and Cu as possible.

Results

$\delta^{65}Cu$ values for synthesized chalcopyrite samples are shown in Table 9. These samples represent experiments using different temperatures and molalities of NaCl (Cl^-) to try to investigate the effect of salinity on the magnitude of the copper fluid-mineral fractionation. The graphs of the analytical runs for these samples are shown in Figure 27. The analyses of copper concentration in the final fluid indicate that more than 99.96 percent of the starting copper was precipitated as chalcopyrite and very little remained in solution. However, the solubility of chalcopyrite depends on the fluid salinity, with a direct correlation between the salinity and the fluid copper concentration, as other solubility experiments have indicated (Liu et al., 2002). Of particular interest are the two experiments run with 5m NaCl (39 and 40) that give almost identical fluid copper concentrations, although the isotopic composition of the precipitates are quite different.

The measured $\delta^{65}Cu$ values for fluids from experiments 37 and 42 are -1.83 per mil and 0.73 per mil, respectively (using "Cu Chrom" samples). Both fluids have $\delta^{65}Cu$ values lower than the bulk copper composition, and the chalcopyrites are higher. All other samples of synthesized chalcopyrite are also isotopically heavier than the bulk system, with the exception of experiment 40 (repeat synthesis under the conditions of experiment 39). The samples purified from the abbreviated elution scheme have Cu concentrations similar to those from the standard elution scheme but consistently differ from them by approximately 0.36 per mil. This difference is due to fractionation effects, but the actual cause and the reason for the near uniformity in the differences is presently unknown. The $\Delta_{fluid\text{-}mineral}$ values for experiments 27, 39, and 42 are -2.45, 0.16, and -0.70 per mil respectively. Due to the poor chromatographic reproducibility of fluids from these experiments the magnitude of calculated $\Delta_{fluid\text{-}mineral}$ may have large errors, but the direction of the fractionation is probably correct.

Experiment 39 is problematic from the standpoint that both the chalcopyrite and fluid copper isotope ratios are isotopically heavier than the bulk system copper ratio. This may be due to problems in the chromatographic purification. Although this sample was purified twice with nearly the same results in Cu concentration, and both $\delta^{65}Cu$ values of the fluids are high, it is possible from the poor recovery that what copper was left in the halite prior to loading the sample on the resin had been fractionated and was isotopically light. However, if this process occurred with the other experimental fluids, then their $\delta^{65}Cu_{fluid}$ values would be even lower than they are,

Table 9. Isotopic analyses of synthetic chalcopyrite and chromatographically purified fluids.

date	sample	δ^{65}Cu (‰)	fraction of Cu in solution relative to standard	standard drift (ppm)	salinity and temperature of synthesis	total copper (μg) in fluid[1]
			synthetic chalcopyrite			
27-Jun-05	27 cpy	0.629	0.86	56	5m NaCl at 225° C	36.0
24-Jun-05	27 cpy	0.610	0.89	48	repeat analysis	
27-Jun-05	37 cpy	1.370	0.93	-51	3m NaCl at 300° C	2.2
24-Jun-05	39 cpy	0.570	0.93	92	5m NaCl at 300° C	3.9
27-Jun-05	40 cpy	0.427	0.96	-93	5m NaCl at 300° C	3.4
24-Jun-05	42 cpy	0.778	0.92	31	7.4m NaCl at 300° C	15.5
			chromatography			
27-Jun-05	27 Cu(2)	-1.433	0.57	-326	Cu=64ppb, Na=4ppb; eluted Cu in 6.5ml 4.5NHCl, matrix in 3ml; loaded in 0.2ml	
27-Jun-05	27 Cu(2)	-1.476	0.58	35	repeat analysis	
	average	-1.455				
27-Jun-05	27 Cu Chrom	-1.856	0.62	-180	Cu = 62ppb; eluted Cu in 18ml, matrix in 3.5ml; loaded in 0.3ml (0.1 + 0.2)	
27-Jun-05	27 Cu Chrom	-1.805	0.62	-93	repeat analysis	
24-Jun-05	27 Cu Chrom	-1.835	0.62	-66	repeat analysis	
	average	-1.832				
	difference	**0.378**	between purified solutions			
24-Jun-05	39 Cu Chrom	0.733	0.24	-104	Cu = 24ppb; eluted Cu in 18ml, matrix in 3.5; loaded in 0.2ml (0.1+0.1)	
24-Jun-05	39 Cu(2)	1.125	0.24	22	Cu=26ppb, Na=80ppb; eluted Cu in 6.5ml 4.5NHCl, matrix in 3ml; loaded in 0.2ml at once	
	difference	**0.392**	between purified solutions			
24-Jun-05	42 Cu Chrom	0.054	0.68	-93	Cu = 69ppb; eluted Cu in 18ml 7NHCl, matrix in 3.5ml; loaded in 2ml (0.1+0.1)	
27-Jun-05	42 Cu Chrom	0.104	0.69	-153	repeat analysis	
	average	0.079				
27-Jun-05	42 Chrom	0.390	0.77	40	Cu = 83ppb, Na=11ppb, Fe = 15ppb; eluted Cu in 6.5ml 4.5NHCl, matrix in 3ml; loaded in 0.2ml	
	difference	**0.311**	between purified solutions			
			characteristics of copper wire nutrient			
24-Jun-05		0.472	1.32	159		
	Cu wire	0.460	1.32	22		
		0.463	1.33	74		
	mean	**0.465**				
	experiment:	27	39	42		
$\Delta_{fluid-mineral}$:		-2.452	0.163	-0.699		

[1]Determined by relating the Cu concentration analyzed by ICP-MS to the volume of water in the experiment.

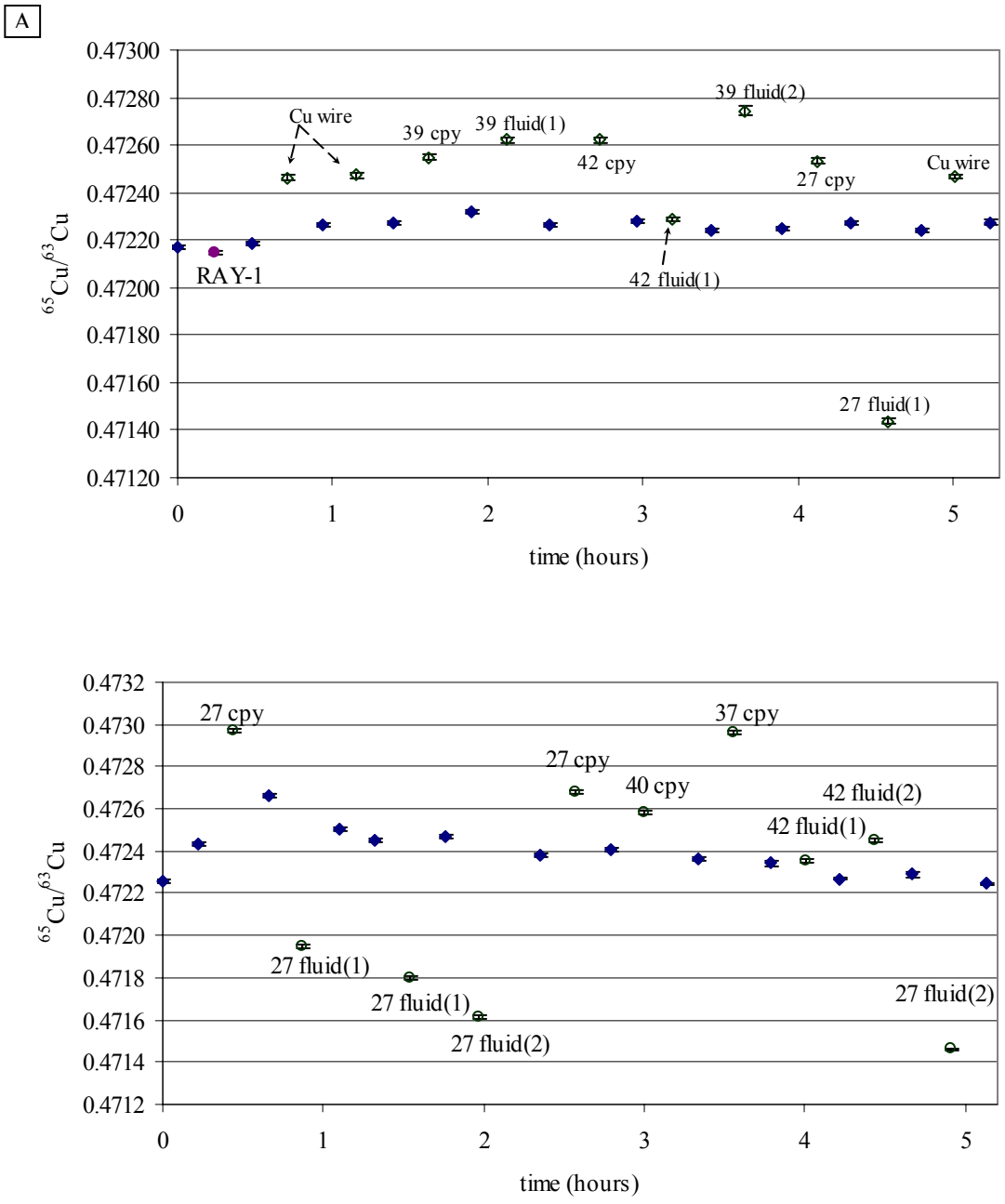

Figure 27. Analytical run from (A) 24 Jun 2005, and (B) from 27 Jun 2005. $^{65}Cu/^{63}Cu$ of synthetic chalcopyrite is greater than that for the purified fluids. Filled diamonds are NIST SRM 976 (100ppb); other symbols as labeled.

[1]39 Cu Chrom
[2]42 Cu Chrom
[3]39 Cu(2)
[4]27 Cu Chrom
[5]27 Cu(2)
[6]42 Chrom

causing the measured fluid-mineral fractionations to be even larger.

Interpretations of Sulfide Synthesis Data

Prior to running the experiments it was expected that an equilibrium fractionation between the fluid and the precipitate would be small (probably <0.5‰). The large fractionation between the fluids and chalcopyrite (to 2‰) is larger in most experiments than what would be expected based on theoretical considerations of equilibrium mass fractionation and even larger than some low-temperature fractionation processes (Erhlich et al., 2004). The direction (mathematical sign) of isotope fractionation derived from all synthesis experiments (with the exception of experiment 40) would also produce chalcopyrite isotopically heavier than the fluid during precipitation. The isotopically zoned mineralization resulting from this process would produce isotopic zonation opposite to that implied for several hydrothermal systems which assume the earliest mineralization commences closest to the fluid source (Section IV).

Although its fluid has not been isotopically analyzed for copper, only the 300ºC 5m NaCl experiment (#40) produced a bulk system-mineral fractionation (based on chalcopyrite being lower than bulk system) consistent with empirically observed isotopic trends where chalcopyrite is isotopically heavier than the fluid (based on paragenetic timing interpretation). However, experiment 39, run under the same chemical conditions as 40, gave a fractionation direction consistent with the other experiments. The bulk system-chalcopyrite fractionation for 39 and 40 are both smaller than the others, suggesting that 5m Cl^- fluids may produce smaller equilibrium fractionations than either 3m or 7.4m Cl^- solutions at the same temperature. It is not clear why this is so.

Based on complex stability constants of Liu et al. (2002), the $CuCl_2^-$ chloride complex was predominant in the hydrothermal fluids in all the experiments reported here. Since none of these experiments were run at temperatures higher than 300ºC, no comment can be made relating the fractionation hypothesis of Maher and Larson (in review) to these experiments. The salinity effect on copper isotopic fractionation should take place at higher temperatures than those explored in the present synthesis experiments.

Implications of Experimental Fluid Mineral Fractionations

Ore deposit literature frequently addresses the causes of metal transport and factors controlling mineralization, but few investigations have examined the paragenesis of the same mineral along a single fluid pathway. Relative to high-temperature copper porphyry and skarn systems, should the fluid-chalcopyrite isotopic fractionations determined from experiments 27, 37, 39, and 42 be correct in their sign, then copper mineralization would have to commence distally first and advance toward the source of the fluids to produce the observed isotopic zonation. The actual timing of monomineralic mineralization along a single fluid pathway is uncertain. For a simple case where mineralization commences due to thermal instabilities of complexes in solution, mineralization should first commence in the lower-temperature part of the system (assuming sulfides are saturated). The mineralization should then progress in the direction of the source of the fluids as the thermal regime collapses toward the center of the system. In many porphyry copper and skarn systems the mineralization is commonly below ore grade in the core of the system or in the proximal garnet, and endoskarn is frequently barren (Meinert, 1993), suggesting that either geochemical conditions for mineralization were not reached, or the mineralizing fluids had already deposited the majority of their copper.

An example of a simple case of a carbonate-hosted Cu-skarn system is presented here. A single pulse of magmatic fluid emanating from a crystallizing magma (Fig. 28) will be too hot to precipitate copper but will produce prograde calc-silicate alteration. As the initial front of the hydrothermal pulse is cooler due to interaction with cooler rocks, this part of the magmatic pulse will initially precipitate copper sulfides due to thermal and chemical constraints, assuming the sulfides are saturated in solution. As the fluid pulse loses heat, the mineralization will migrate toward the core of the system, continuing to precipitate sulfides. The grade variation of disseminated sulfides commonly observed in prograde skarn (Atkinson and Einaudi, 1978) would be due to the available remnant interstitial space between existing calc-silicates.

The equilibrium fluid-mineral fractionation determined by these hydrothermal experiments suggests that the first chalcopyrite mineralization precipitated from a fluid should be isotopically heavier than the fluid. Further precipitation of chalcopyrite from this same fluid would produce chalcopyrite with increasingly negative $\delta^{65}Cu$. Assuming the sign of the fluid-chalcopyrite fractionation is correct in these experiments, only a thermal collapse of a hydrothermal system with mineralization spatially following the shift of isotherms would produce the isotopic

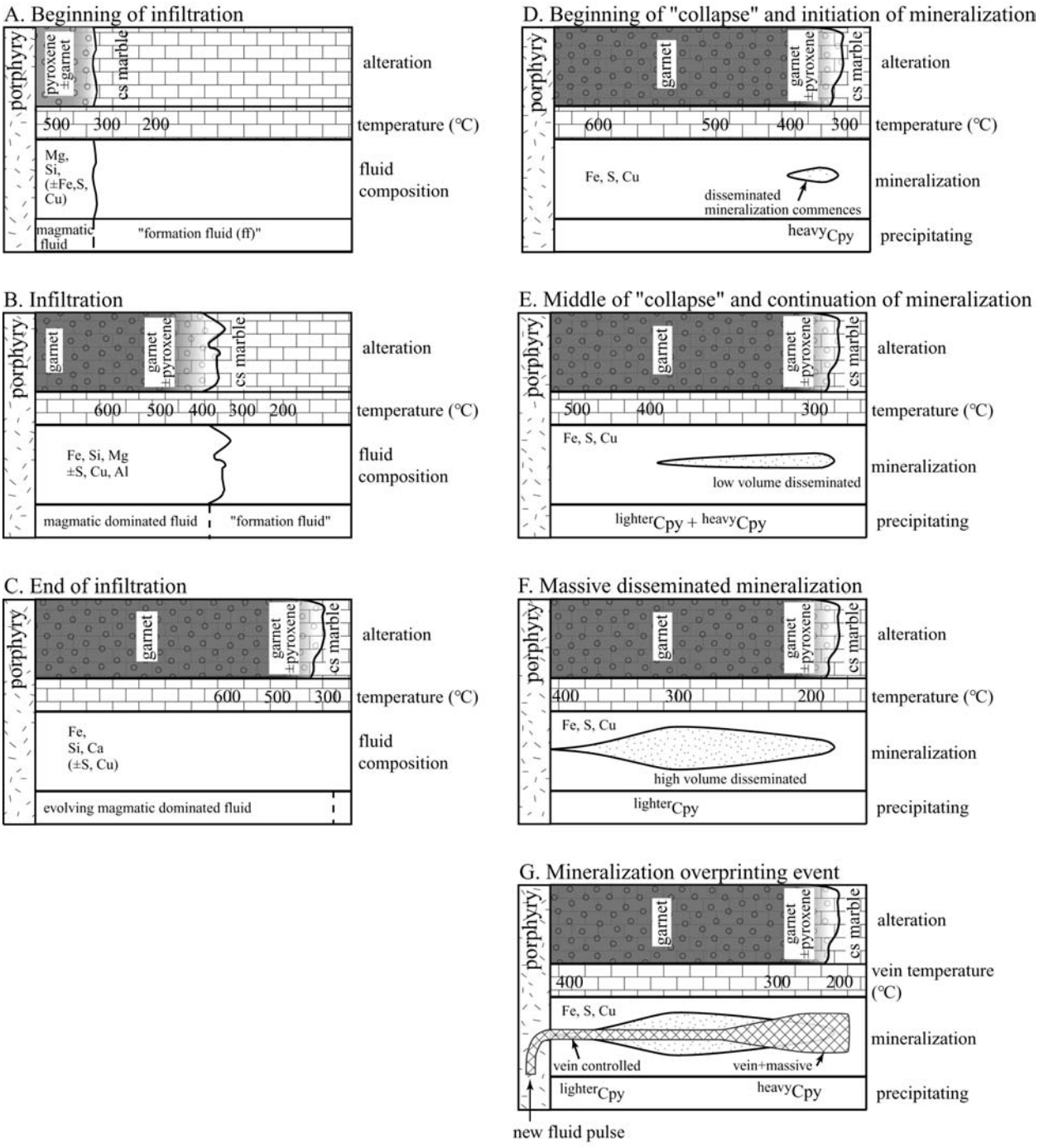

Figure 28. Step-wise diagrams showing the progress of calc-silicate alteration related to porphyry-derived hydrothermal fluid (A-C) and then the progressive mineralization of skarn (D-F) based on the isotopic zonation observed at Coroccohuayco, Perú (Maher and Larson, in review), and experimental fluid-chalcopyrite fractionation determined in this investigation. Note, vein-controlled overprinting of skarn from a second pulse of mineralizing fluid in (G) and temperature trend in each diagram.

zonation observed from systems such as Coroccohuayco, Perú (Appendix 4). Modeling of the late overprinting mineralization at Coroccohuayco, Perú, using the fluid-chalcopyrite fractionation determined from experiment 42 (Table 9), demonstrates the possibility of relating copper isotopes to degree of precipitation of copper from a pulse of mineralizing fluid.

Figure 29 shows the actual data (stippled band) and also two curves representing a step-wise bulk isotope fractionation due to precipitation of copper. The dashed curve represents bulk fractionation with 10% copper precipitated at each step. The orange curve represents unequal bulk fractionation required to model the isotopic data. These models are based on the direction of the experimental fractionation data that indicates that fluid-chalcopyrite fractionation is negative (i.e., chalcopyrite is isotopically heavier than the fluid from which it precipitated). Thus, copper is first precipitated in the more distal (deeper) part of the mineralization and precipitation progresses toward the middle of the intrusion with time (due to shift in isotherms?). The vertical line represents the boundary between mineralizing porphyry and existing skarn. The vertical gray zones represent zones where ore grade is greater than 3 percent Cu (i.e., higher grade). What is evident from this figure is that in the zones where there is very high ore grade, the copper isotopes show very little isotopic fractionation (effectively flat or low slope between the data). These zones correspond to large-scale batch chalcopyrite precipitation (corresponding to the % Cu precipitated) with correspondingly lower fractionation. Lower fractions of copper precipitated in a step (i.e., lower grade ore) will produce steeper slopes between the points. For the sake of simplicity, the role of bornite precipitation and possible copper isotope fractionation between complexes in solution has been ignored (Section IV), but even then the model fits the data well.

This model and the implications for sequence of mineralization are attractive from the standpoint that they are supported by theoretical equilibrium fractionation theory. The heavier isotope is preferentially incorporated into the site with the least vibrational energy (O'Neil, 1986), which can be related to bond type and length (Schauble et al., 2001). All things being equal, the first chalcopyrite to form would be expected to be isotopically heavier than subsequent chalcopyrite, assuming mineralization from the same pulse of fluid. However, this model can not be used to explain isotopic features such as the δ^{65}Cu values of Cu-Fe sulfides observed from paragenetically distinct mineralization from the Beaver-Harrison Mine, UT (Section IV, Fig. 21).

Based on the bornite-chalcopyrite fractionation observed in several of the samples from Coroccohuayco, Perú, the fluid-bornite fractionation may be in the same direction (although of a lower magnitude) as the fluid-

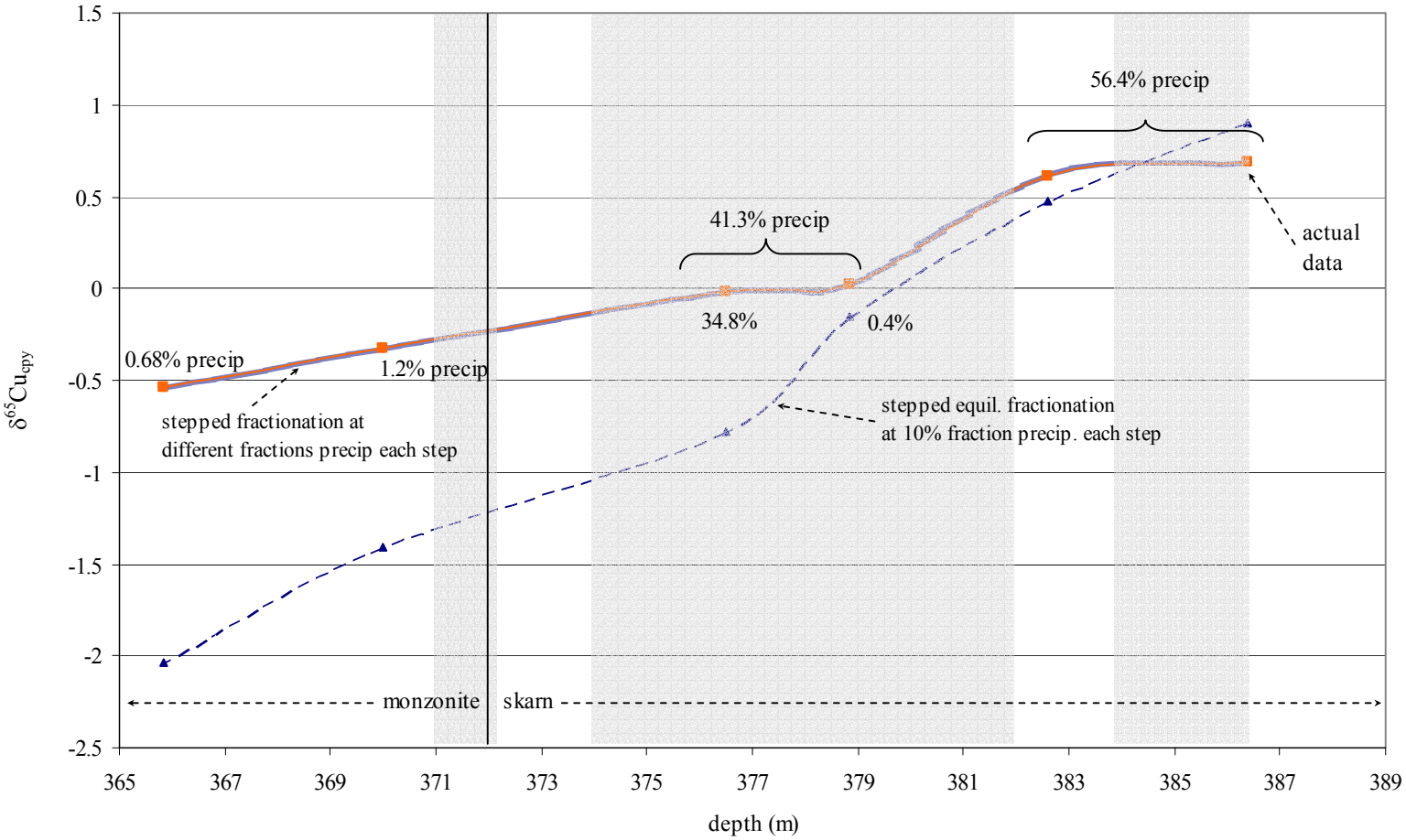

Figure 29. $\delta^{65}Cu$ of chalcopyrite verses depth in drill hole 1400 18.9 of Coroccohuayco, Perú (see Maher, 1999, for more geologic information). Shaded bands are zones in the drill core of high (>3% Cu) ore grade and correspond to zones with large fractionations of copper precipitated out of the fluid. These fractions were determined by calculating stepped equilibrium fractionations based on the fluid-chalcopyrite fractionation factor determined in synthesis experiment 42 (of 7.4m NaCl) and a starting fluid $\delta^{65}Cu$ value of 0.3‰. Starting fluid values <0.2‰ or >0.3 can not be modeled to correlate with the actual data.

chalcopyrite fractionation determined in the synthesis experiments (depending on the reliability of the magnitude of these measured fractionations). Should this be the case, then the isotopic evolution of the fluid would be similar to that presented in the simple model above for chalcopyrite-bornite, or bornite-dominant mineralization.

Finally, it is important to note that the fluid-chalcopyrite fractionations determined from these experiments are for simple H_2O-NaCl-HCl systems at 225ºC and 300ºC. Fluid-chalcopyrite fractionation could deviate significantly from the results presented herein if the temperature or physicochemical (i.e., fO_2, pH, ΣS, etc.) conditions vary from the experimental conditions.

VII. Conclusion

This report has sought to address only a few of the basic questions surrounding copper isotope systematics and has presented data and interpretations primarily relating to copper mineralization in high-temperature hydrothermal systems. This investigation has demonstrated that copper isotope variations can be reliably measured with good analytical reproducibility by multiple collector-inductively coupled plasma mass spectrometry (MC-ICPMS) with the machine mass fractionation corrected by either standard-sample bracketing or by element doping using a zinc isotopic standard. The sample-standard bracketing method has been extensively evaluated over three years with internal standards. The Neptune® shows similar mass fractionation behavior between standard and Cu-Fe sulfides. The sample-standard correction method and can be used reliably for Cu-Fe sulfides as long as Neptune® machine drift between bracketing standards is minor and constant. By this method the machine drift can be corrected at the same time as machine mass fractionation. Reproducibility of internal standards by this technique is plus or minus 0.08 per mil $\delta^{65}Cu_{NIST\ SRM\ 976}$ (2σ, standard deviation). With this precision, even relatively small isotopic variations in hypogene mineralization can be differentiated.

The zinc element doping method for correcting machine mass fractionation may produce better in-run reproducibility than the sample-standard bracketing technique, depending on the zinc isotope pair used in the correction. Preliminary evaluation of the day-to-day reproducibility for the zinc method has not exhibited better long term precision than that observed for the sample-standard bracketing technique. The element doping technique must also utilize some form of the standard-sample bracketing technique to produce highest precision results.

Matrix effects on isotopic analyses of Cu-Fe sulfides have been evaluated by measuring the relative concentrations of other elements to copper in the analyzed solutions, chromatographic purification of samples, and doping of standards with different elements. The conclusion reached in this investigation is that chromatographic purification of Cu-Fe sulfides (and other copper sulfides) is not necessary to produce meaningful MC-ICPMS isotopic analyses when using the standard-sample bracketing technique. Extensive evaluation of matrix effects relative to the zinc doping correction technique has not been pursued as part of this study, although Archer and Vance (2004) suggest the presence of matrix iron may affect Cu-Zn isotope analysis.

Analytical results from this investigation indicate that the range in $\delta^{65}Cu$ values of high-temperature mineralization from individual Cu-porphyry and skarn deposits may be as large as those observed from the whole

class of sea-floor massive sulfide deposits (black smoker) (Rouxel et al., 2004). This investigation also expands the range in $\delta^{65}Cu$ for hypogene mineralization beyond post-1999 publications, and shows that even individual porphyry/skarn systems may have greater than 3 per mil ranges from hypogene mineralization. These data suggest that important isotopic fractionation mechanisms operate in high-temperature hydrothermal systems and may produce isotopically zoned mineralization.

One possible fractionation mechanism is isotopic fractionation between metal-transporting complexes in solution, where differing ligand geometries of the predominant copper complexes lead to fractionation between the complexes. These variations are then recorded in the mineralization arising from differences in the thermodynamic stability of the metal transporting complexes. This fractionation mechanism is most likely to occur where there is more than one predominant copper complex in solution, such as high-salinity hydrothermal fluids (> 40 wt % NaCl equivalent). Other hydrothermal systems of lower salinity or with only one predominant copper complex may not show as large a range in $\delta^{65}Cu$ values because this fractionation mechanism is much less important.

Isotopically heavy copper minerals from high-sulfidation veins overprinting earlier porphyry-style alteration and mineralization may isotopically record the remobilization of earlier copper mineralization from the potassic alteration zone. Examples of this process may be seen in the high-sulfidation copper veins at the Resolution deposit, Arizona, USA, where bornite-pyrite veins with associated silicification and argillic alteration are up to 1.62 per mil heavier than chalcopyrite from the potassic alteration zone. High-sulfidation veins from Butte, Montana, similarly show high bornite $\delta^{65}Cu$ values, which are generally isotopically heavier than high-temperature, co-precipitated bornite-chalcopyrite from high-temperature skarn (e.g., Coroccohuayco, Perú).

High-temperature chalcopyrite synthesis experiments indicate the magnitude of fluid-chalcopyrite fractionation may be as large as 2.45 per mil at 225ºC and 0.7 per mil at 300ºC. Most chalcopyrite produced from these experiments is isotopically heavier than the bulk system copper isotope ratio, suggesting that the fluid-mineral fractionation is negative. Stepwise equilibrium isotopic fractionation from a fluid under these conditions will produce progressively lighter chalcopyrite with extent of copper precipitation. Applying the results of these experiments to actual isotope zonation, such in the late mineralization at Coroccohuayco, Perú, would require that chalcopyrite precipitation commences distally first, probably due to thermal constraints. Deposition of copper (i.e., mineralization) advances toward the source of the fluids with time, with some steps of more massive precipitation. Comparison of copper isotope data and the grade of copper mineralization show that zones with relatively small

changes in $\delta^{65}Cu$ correspond to zones of massive mineralization. This is plausible because small changes in $\delta^{65}Cu$ caused by equilibrium fluid-chalcopyrite fractionation over continuous mineralization require large fractions of copper to be precipitated (resulting in higher ore grade).

Future Avenues of Research in Copper Isotope Systematics

Many questions relating to copper isotope characteristics are beyond the scope of this investigation. These include further experimental measurement of fluid-mineral isotopic fractionations under differing physicochemical conditions and at different temperatures. Specifically pH, fO_2, and the valence of copper (i.e., Cu(I) or Cu(II)) need to be better constrained in these experiments, perhaps by adding buffering assemblages and evacuating the silica tubes prior to sealing. Hydrothermal copper mineral precipitation may occur to +450ºC, and the present experimentally determined fractionations need to be reconfirmed and the data extended to other temperatures. Technical problems relating to chromatographic purification of hydrothermal chalcopyrite synthesis fluids need to be overcome to increase confidence in experimentally derived fractionations.

Equilibrium isotope fractionation between co-precipitated copper minerals is another direction of research with great potential, especially in relationship to addressing fundamental questions of copper remobilization in hydrothermal systems and possible isotopic fractionation during exsolution of different phases from higher-temperature sulfide solutions. Since many copper sulfides are intergrown on a very small scale, new analytical techniques would need to be developed to approach this issue. Specifically, high-precision analytical techniques employing laser ablation micro-sampling would need to be developed to evaluate potential differences between co-precipitated copper mineral pairs over the scale of 10's of microns.

Evaluating low-temperature fractionation mechanisms relevant to supergene mineralization is a large field promising fruitful work for many years. Many copper minerals characterize supergene mineralization under different oxidation-reduction conditions and determining fluid-mineral fractionation factors for these minerals could do much toward understanding the processes within and the evolution of supergene deposits.

Leaching-induced isotopic fractionation has been recognized in several ore deposits (Rouxel et al., 2004; Section IV, this report). Experimental confirmation of such fractionation under different conditions would help

clarify the magnitude of this process relative to other processes, such as oxidation-reduction related fractionation or fluid-mineral equilibrium fractionation.

There are many avenues of research in copper isotope systematics that can be pursued with the present level of analytical precision and await only interest and financial support. As with other isotopic systems, many more questions have been raised during this investigation than have been answered. Although several hypotheses of copper isotope fractionation at high temperature have been presented here, further experimental work and careful isotopic study of copper mineralization in various deposits are required to confirm and expand them. Doubtless, these hypotheses will change with time and some may be embraced or discarded as new data and geological observations are gathered.

References

Albarède, F., Telouk, P., Blichert-Toft, J., Boyet, M., Agranier, A., and Nelson, B., 2004, Precise and accurate isotopic measurements using multiple-collector ICPMS: Geochimica et Cosmochimica Acta, vol. 68, p. 2725-2744.

Archer, C. and Vance, D., 2004, Mass discrimination correction in multiple-collector plasma source mass spectrometry: an example using Cu and Zn isotopes: Journal of Analytical Atomic Spectrometry, vol. 19, p. 656-665.

Asael, D., Matthews, A., Bar-Matthews, M., Halicz, L., Erhlich, S., Teplyakov, N., 2005, Redox fractionation of copper isotopes in sedimentary conditions: Goldschmidt 2005 Conference, Moscow, ID., Goldschmidt Conference Abstracts, A216.

Atkinson, W.W. and Einaudi, M.T., 1978, Skarn formation and mineralization in the contact aureole at Carr Fork, Bingham, Utah: Economic Geology, vol. 73, p. 1326-1365.

Bottinga, Y. and Javoy, M., 1975, Oxygen isotope partitioning among the minerals in igneous and metamorphic rocks: Reviews in Geophysics and Space Physics, vol. 13, p. 401-418.

Brimhall Jr., G.H., 1980, Deep hypogene oxidation of porphyry copper potassium silicate protore at Butte, Montana; a theoretical evaluation of the copper remobilization hypothesis: Economic Geology, vol., 75, p. 384-409.

Chacko, T., Cole, D.R., and Horita, J., 2001, Equilibrium oxygen, hydrogen, and carbon isotope fractionation factors applicable to geologic systems: Mineralogical Society of America, Reviews in Mineralogy and Geochemistry, vol. 43, p. 1-81.

Ehrlich, S., Butler, I., Halicz, L., Rickard, D., Oldroyd, A., and Matthews, A., 2004, Experimental study of the copper isotope fractionation between aqueous Cu (II) and covellite, CuS: Chemical Geology, vol. 209, p. 259-269.

Gale, N.H., Woodhead, A.P., Stos-Gale, Z.A., Wlader, A., and Bowen, 1999, Natural variations detected in the isotopic composition of copper: possible applications to archaeology and geochemistry: International Journal of Mass Spectrometry, vol. 184, p. 1-9.

Graham, S., Pearson, N., Jackson, S., Griffin, W., and O'Reilly, S.Y., 2004, Tracing Cu and Fe from source to porphyry: in situ determination of Cu and Fe isotope ratios in sulfides from the Grasberg Cu-Au deposit: Chemical Geology, vol. 207, p. 147-169.

Larson, P.B., Maher, K., Ramos, F.C., Chang, Z., Gaspar, M., and Meinert, L.D., 2003, Copper isotope ratios in magmatic and hydrothermal ore-forming environments: Chemical Geology, vol. 201, p. 337-350.

Liu, W., Brugger, J., McPhail, D.C., and Spiccia, L., 2002, A spectrophotometric study of aqueous copper(I)-chloride complexes in LiCl solutions between 100 ºC and 250 ºC: Geochimica et Cosmochimica Acta, vol. 66, p. 3615-3633.

Luck, J.M., Ben Othman, D., Barrat, J.A., and Albarède, F., 2003, Coupled ^{63}Cu and ^{16}O excesses in chondrites: Geochimica et Cosmochimica Acta, vol. 67, p. 143-151.

Maher, K.C., 1999, Geology of the Cu-skarn at Coroccohuayco, Peru: Unpublished MS thesis, Washington State University, Pullman, WA, USA. 133 pages.

Maher, K.C., Ramos, F.C., and Larson, P.B., 2003, Copper isotope characteristics of the Cu (+Au, Ag) skarn at Coroccohuayco, Peru: Geological Society of America, Annual Meeting, paper 211-4.

Maher, K.C. and Larson, P.B., 2005, Variation in copper isotope ratios and controls on fractionation in hypogene skarn mineralization at Coroccohuayco and Tintaya, Perú: *In review*, Economic Geology.

Manske, S.L. and Paul, A.H., 2002, Geology of a major new porphyry center in the Superior (Pioneer) district, Arizona: Economic Geology, vol. 97, p. 197-220.

Maréchal, C, 1998, Géochimie de isotopes du cuivre et du zinc: Méthode, variabilité naturelle et application océanographique: Unpublished Ph.D. thesis, Grenoble, France, Universite Joseph Fourier, 261 pages.

Maréchal, C. and Albarède, F., 2002, Ion-exchange fractionation of copper and zinc isotopes: Geochimica et Cosmochimica Acta, vol. 66, p. 1499-1509.

Maréchal, C.N., and Sheppard, S.M.F., 2002. Isotopic fractionation of Cu and Zn between chloride and nitrate solutions and malachite or smithsonite at 30° and 50°C: Goldschmidt 2002 Conference, Davos.Geochim. Cosmochim. Acta 66 (15A), A484.

Maréchal, C. N., Telouk, P., and Albarède, F., 1999, Precise analysis of copper and zinc isotopic compositions by plasma-source mass spectrometry: Chemical Geology, vol. 156, p. 251-273.

Mason, T.F.D., Weiss, D.J., Horstwood, M., Parrish, R.R., Russell, S.S., Mullane, E., and Coles, B., 2004a, High-precision Cu and Zn isotope analysis by plamsa source mass spectrometry. Part 1. Spectral interferences and their correction: Journal of Analytical Atomic Spectrometry, vol. 19, p. 209-217.

Mason, T.F.D., Weiss, D.J., Horstwood, M., Parrish, R.R., Russell, S.S., Mullane, E., and Coles, B., 2004b, High-precision Cu and Zn isotope analysis by plasma source mass spectrometry. Part 2. Correcting for mass discrimination effects: Journal of Analytical Atomic Spectrometry, vol. 19, p. 218-226.

Meinert, L.D., 1993, Skarns and skarn deposits: Geoscience Canada, vol. 19, p. 145-162.

Molnár, F., Watkinson, D.H., Jones, P.C., and Gatter, I., 1997, Fluid inclusion evidence for hydrothermal enrichment of magmatic ore at the contact zone of the Ni-Cu-Platinum-Group element 4b deposit, Lindsley mine, Sudbury, Canada: Economic Geology, vol., 92, p. 674-685.

Mountain, B.W. and Seward, T.M., 2003, Hydrosulfide/sulfide complexes of copper (I): Experimental confirmation of the stoichiometry and stability of $Cu(HS)_2^-$ to elevated temperatures: Geochimica et Cosmochimica Acta, vol. 67, p. 3005-3014.

Naldrett, A.J., 1989, Magmatic sulfide deposits. Oxford, New York, Oxford University Press, 196 pages.

O'Neil, J.R., 1986, Theoretical and experimental aspects of isotopic fractionation, *In* Stable isotopes in high temperature geological processes: Valley, J.W., Taylor-H.P.,Jr., and O'Neil, J.R., eds, Reviews in Mineralogy, vol. 16. p. 1-40.

Raedeke, L.D. and Vian, R.W., 1986, A three-dimensional view of mineralization in the Stillwater J-M Reef: Economic Geology, vol. 81, p 1187-1195.

Rouxel, O., Fouquet, Y., and Ludden, J.N., 2004, Copper isotope systematics of the Lucky Strike, Rainbow, and Logatchev sea-floor hydrothermal fields on the Mid-Atlantic Ridge: Economic Geology, vol. 99, p. 585-600.

Rusk, B.G., Reed, M.H., Dilles, J.H., Klemm, L.M., and Heinrich, C.A., 2004, Compositions of magmatic hydrothermal fluids determined by LA-ICP-MS of fluid inclusions from the porphyry copper-molybdenum deposit at Butte, MT: Chemical Geology, vol., 210, p. 173-199.

Schauble, E.A., Rossman, G.R., and Taylor, H.P., Jr., 2001, Theoretical estimates of equilibrium Fe-isotope fractionations from vibrational spectroscopy: Geochimica et Cosmochimica Acta, vol. 65, p. 2487-2497.

Seward, T.M., 1976, The stability of chloride complexes of silver in hydrothermal solutions up to 350ºC: Geochimica et Cosmochimica Acta, vol., 40, p. 1329-1341.

Shields, W.R., Goldich, S.S., Garner, E.L., and Murphy, T.J., 1965, Natural variations in the abundance ratio and the atomic weight of copper: Journal of Geophysical Research, vol. 70, p. 479-491.

Urey, H.C., 1947, The thermodynamic properties of isotopic substances: Journal of the Chemical Society, vol. 1, p. 562-582.

Walker, D.C., Cuttitta, F., and Senftle, F.E., 1958, Some natural variations in the relative abundance of copper isotopes: Geochimica et Cosmochimica Acta, vol., 15, p. 183-194.

White, W.M., Albarède, F., and Telouk, P., 2000, High-precision analysis of Pb isotope ratios by multi-collector ICP-MS: Chemical Geology, vol. 167, p. 257-270.

Young, S. and Ruiz, J., 2003, Inorganic controls of copper isotope fractionation in supergene environment: Geophysical Research Abstracts, vol 5, number 02045.

Zhu, X.K., O'Nions, R.K., Guo, Y., Belshaw, N.S., and Rickard, D., 2000, Determination of natural Cu-isotope variation by plasma-source mass spectrometry: implication for use as geochemical tracers: Chemical Geology, vol. 163, p. 139-149.

Zhu, X.K., Guo, Y., Williams, R.J.P., O'Nions, R.K., Matthews, A., Belshaw, N.S., Canters, G.W., de Waal, E.C., Weser, U., Burgess, B.K., and Salvato, B., 2002, Mass fractionation processes of transition metal isotopes: Earth and Planetary Science Letters, vol. 200, p. 47-62.

Appendix 1

Chromatographic Purification of Samples

The procedure utilized for the purification of copper in solutions as part of this investigation is based on the copper purification scheme of Maréchal et al. (1999). Chromatographic columns used here are glass with a column length of approximately 7cm. The width of the columns is 5mm. The resin was rinsed several times and the finest particles decanted. The columns were then filled with resin (MP-1M or MP-1) to exactly 7cm.

The resin is initially cleaned with several washings of 3ml distilled and nano-filtered H_2O alternating with 3ml 2% HNO_3. After cleaning the resin, it is prepared for loading of sample by rinsing with 3ml of distilled deionized water and then washing with 6ml of 7N HCl + 0.1% H_2O_2. Changing between water and the high normality acid causes the resin to compact (shrink) thereby decreasing the permeability significantly. The resin is re-suspended by threading a thin Teflon tube into the column while introducing the wash acid (7N HCL + 0.1% H_2O_2). The effect of this process is to suspend the resin, which then again settles down in the column without being compacted. This process significantly aids in solution throughput.

All samples are evaporated until dry and sufficient 7N HCl +0.1% H_2O_2 is added to moisten the sample and then evaporated again. This solution has the effect of oxidizing the reduced species (particularly iron and copper). The sample is again dissolved in as little 7N HCl + 0.1% H_2O_2 solution as possible (generally <200µl for whole rock and sulfide synthesis solutions, and less than 50µl for chalcopyrite solution). The sample is loaded onto the resin bed. With dissolved chalcopyrite this is accomplished with less than 10µl.

Chalcopyrite Purification

The chalcopyrite samples contain a simple matrix. Copper is eluted from the column after about 5ml of 7N HCl + 0.1% H_2O_2. The total copper collection is eluted with an additional 8ml of 7N HCl + 0.1% H_2O_2. The separation of copper and iron is evident in two distinct yellowish color bands on the resin after the addition of about 1.5ml; the faster moving band is copper. As long as the 7N HCl + 0.1% H_2O_2 solution is used the iron band is effectively immobile on the resin, but the copper band slowly migrates down the resin bed. After copper is eluted,

the iron is removed from the resin by changing the eluant solution to 2N HCl + 0.1% H_2O_2, with more than 90 percent of the iron removed in the first milliliter. Other observations suggest that iron will start to slowly migrate down the resin bed with an acid solution of 5N (HCl). Although the samples do not contain significant zinc, zinc can be eluted after iron by changing the acid to 0.5N HNO_3. Since the chalcopyrite samples contain little zinc, and iron isotopic analysis has not been pursued as part of this study, the iron is usually stripped off the resin by washing the resin with 3ml of purified H_2O.

Maréchal et al. (1999) noted that a full chromatographic yield of copper is required for meaningingful copper isotope measurements since extreme isotopic fractionation takes place on the resin. This has also been an observation of this study (Fig. 6), and it is essential that all the copper in the sample be collected. It is also known that incomplete oxidation of copper causes the cuprous copper to pass through the resin almost immediately so care must be maintained to completely oxidize the copper prior to loading on the resin.

Enough sample is loaded onto the column to produce a solution of 100ppb Cu concentration, assuming 100% yield. An estimate of the actual copper yield is determined by measuring the signal intensity of the purified sample relative to the signal from a 100ppb Cu solution, as well as comparing the delta values of purified and unpurified sample. This is tested by analysis on quadrupole ICP-MS and during isotopic analysis on multi-collector-ICPMS. Samples of SUP-1 (internal chalcopyrite standard) have been satisfactorily purified by this process.

Bulk Rock Sample

The matrix of bulk rock samples is considerably more complicated than that of Cu-sulfides. Based on XRD trace element data for BCR-P (Washington State University Geoanalytical lab internal standard), sufficient sample of the trace element solution typically analyzed at WSU for trace element work was evaporated. The residue was then re-dissolved in 7NHCl + 0.1%H_2O_2 + 10µl of 50% H_2O_2. The extra H_2O_2 was required to completely oxidize the sample. However, it also causes the solution to stick to the Teflon container so care is required to remove the solution for the next step. The oxidized solution is centrifuged to remove undissolved solid. A white solid settles out, which may be a compound of Al (Si is driven off during the perchloric leaching of the original rock powder (C. Knaack, personal communication, 2005). Sufficient centrifuged solution is then loaded on the resin to produce a

final 100ppb Cu solution. Because of the low Cu content of BCR-P, this requires much more sample than for a chalcopyrite solution.

The elution curves shown in Figure 7 (Section II) demonstrate the behavior of the different elements on the resin. Most Al and other major elements are eluted in the first 4ml of 7NHCl + 0.1% H_2O_2 solution. Unfortunately, other important elements (such as Co, and Ni) are retained on the resin or are eluted with copper. The other effect is that copper appears to wash off the resin earlier than for a sample with little matrix (i.e., chalcopyrite), and this may be due to reduction (?) of the copper on the resin bed when other significant rock matrix is present.

Since no elution curves or procedures for separating copper from a bulk rock matrix have been published, it is unclear what improvements besides re-purifying the copper eluant might give a cleaner copper separate. Maréchal et al. (1999) only presented an elution scheme for a synthetic mixture of copper-, iron-, and zinc-sulfides, without the rock matrix. Their elution scheme was probably different for the non-ore samples they processed.

Sulfide Synthesis Solution

Sulfide synthesis solutions were completely evaporated and then wetted with 7NHCl + 0.1% H_2O_2 and again dried, as with other solutions. The residues from the drying steps contained large amounts of NaCl (from the synthesis), even when less than 100µl of sample was dried. The final solution prepared for loading on the column contained insoluble halite crystals, which could not be completely dissolved and also satisfy the requirement of loading as little sample as possible on the resin. The approach used here consisted of dissolving as much of the sample as possible in 100µl of 7NHCl + 0.1% H_2O_2, loading that solution and then repeating this step. Insolubility of the halite is due to the large amount of Cl^- in the acid solution. Dissolution of the sample in a lower-normality acid solution (to try to dissolve more salt) would cause the copper to pass through the resin too rapidly. It was impossible to dissolve all the salt in the original dried solution, and undoubtedly some Cu, and certainly Fe, from the sample could not all be loaded on the resin for purification. Thus, it is impossible to know whether a full elution of copper was achieved for the purification of these particular samples.

Since copper may be present in the evaporated residue as Cu-chloride which may be fractionated if other copper species are present (e.g., Cu oxide). Thus, it is possible that without complete solution of the copper, the solution copper loaded on the resin may be fractionated from the true copper value.

Note on the Acid Used

The solution of 7NHCl + 0.1% H_2O_2 used in this study was more oxidized than the 0.001% H_2O_2 solution used by Maréchal et al. (1999). It was noted that this solution tended to lose some of its oxidative capacity with time. In addition, it would produce bubbles in the resin bed, if mixed up and used immediately. These bubbles would then become sites where copper or iron could separate from the rest of the resin, leading to problems in elution. Therefore it was necessary to allow the acid solution to sit in a vented container (as gas build-up occurred during this maturation period) for at least two days prior to use.

Appendix 2

Results of Copper Isotope Analyses with Geologic Context

This Appendix lists the samples analyzed in this investigation with a short description of the geologic context of each. The raw $^{65}Cu/^{63}Cu$ ratio, with its analytical error, the corrected $^{65}Cu/^{63}Cu$ ratio (using standard-sample bracketing or elemental doping), $\delta^{65}Cu$ value and the date analyzed are presented in the tables. Abbreviations include the following:

act	actinolite	hnfls	hornfels
alb	albitized	HS	high sulfidation
altn	alteration	interst	interstitial
amph	amphibole	Kspar	potassium feldspar
anh	anhydrite	magn	magnetite
arg'd	argillized	mal	malachite
bio	biotite	moly/Mo	molybdenite
born	bornite	monz	monzonite
bx	breccia	plag	plagioclase
cal	calcite	prox	proximal
calc	calc-silicate	px	pyroxene
carb	carbonate	py	pyrite
cc	chalcocite	QSP	quartz-sericite-pyrite
chl	chlorite	qtz	quartz
cov	covellite	rb	red-brown
cpy	chalcopyrite	repl.	replacement
ep	epidote	ser	sericite
euhed	euhedral	sid	siderite
gal	galena	sph	sphalerite
garn	garnet	tetrah	tetrahedrite
hem	hematite	Vc	Volcaniclastic sediments

Appendix 2

Table of Results of Copper Isotope Analyses

sample	mineral	location/description	raw $^{65}Cu/^{63}Cu$	2σ error	corrected $^{65}Cu/^{63}Cu$	$\delta^{65}Cu$	date analyzed
		Coroccohuayco, Perú					
1300 16.1 208.65	cc	Interstitial to green-tan garnet (hypogene?)	0.473547	0.000008	0.445575	-0.06	20-Jun-02
1300 16.1 208.65		repeat	0.470605	0.000008	0.445581	-0.04	23-Nov-02
1300 16.1 208.65		repeat	0.471847	0.000010	0.445604	0.01	01-Feb-03
1300 16.1 208.65		repeat	0.471796	0.000008	0.445573	-0.06	01-Feb-03
1300 16.1 252.65	cpy	Cpy vein in gray marble (cuts lamination)	0.472398	0.000011	0.445140	-1.03	30-Sep-04
1400 13.7 300.12	cpy	Cpy in retrograde garnet	0.470899	0.000007	0.445646	0.10	01-Jul-03
1400 13.7 300.6	cpy	Cpy in retrograde garnet (to chl)	0.470968	0.000007	0.445706	0.24	01-Jul-03
1400 14.5 244.45A	cpy	Cpy-born in dissem patches in tan garn+white px	0.471187	0.000006	0.445832	0.52	01-Jul-03
1400 14.5 244.45B	born	from above	0.471021	0.000007	0.445655	0.12	01-Jul-03
1400 14.5 246.1	cpy	Honey-brown garn w/ px-dissem cpy	0.471196	0.000008	0.445891	0.65	01-Jul-03
1400 14.5 313.3	cpy	Magn replacing garn with dissem cpy (cpy came in with magn?)	0.471754	0.000009	0.445669	0.16	03-Feb-03
1400 14.5 340.5	cpy	Qtz-cpy-anh vein cutting px hornfels w/ patchy remnant bio hnfls	0.470323	0.000006	0.445027	-1.29	01-Jul-03
1400 15.3 326.15	cpy	Green garn w/ rb rims, dissem interst. cpy; locally garn to magn-cal	0.471134	0.000008	0.445811	0.47	01-Jul-03
1400 15.8 163.4	cpy	Dark brown to honey brown garnet (distal?) with dissem/vein cpy	0.474433	0.000009	0.445737	0.31	04-Jun-02
1400 15.8 191.25	born	Born interstitial to massive green brown garn; locally minor cpy with born	0.471231	0.000006	0.445778	0.40	06-Mar-04
1400 15.8 246.86	cpy	Massive brown garnet w/ dissem cpy	0.471624	0.000010	0.445621	0.05	03-Feb-03
1400 15.8 248.6	cpy	Granular brown garnet	0.472163	0.000009	0.445888	0.65	20-Feb-03
1400 15.8 248.6		repeat	0.471216	0.000007	0.445842	0.54	01-Jul-03
1400 15.8 248.6		repeat	0.470435	0.000008	0.445855	0.57	07-Jan-04
1400 15.8 306.4	cpy	Cpy veinlets cutting quartz-moly veined endoskarn in monz Z	0.470969	0.000007	0.445529	-0.16	05-Mar-04
1400 16.1 147.35	cpy	Platy magn replacing white px; fine grain dissem cpy in px w/ stringers	0.471259	0.000007	0.445631	0.07	03-Feb-03
1400 16.1 241.6A	cpy	Magn repl. rb garn w/ interst. born-cpy	0.472289	0.000009	0.445802	0.45	20-Feb-03
1400 16.1 241.6B	born	as above	0.472121	0.000010	0.445645	0.10	20-Feb-03
1400 16.8 250.8	cc	Green garnet retrograde to calcite-clay-hem, with interestitial steely cc (supergene or retrograde?)	0.473525	0.000007	0.445552	-0.11	20-Jun-02
1400 17.7 322.6A	cpy	Green garn; classic interstitial cpy and bornite (co-precipitated)	0.471615	0.000008	0.445917	0.71	03-Feb-03
1400 17.7 322.6A #2		repeat	0.471657	0.000007	0.445900	0.67	03-Feb-03
1400 17.7 322.6B	born	as above	0.471439	0.000006	0.445706	0.24	03-Feb-03
1400 17.7 352.7	cpy	Cpy veinlets in chl-amph alt'd px w/ minor green garn w/ hem alt'n	0.471007	0.000008	0.445667	0.15	01-Jul-03
1400 18.9 301.95	cpy	Monz Z; hairline kspar-cpy veinlets in weakly albitized monz	0.473609	0.000010	0.445632	0.07	20-Jun-02

Appendix 2 cont.

1400 18.9 331.75	cpy	Cpy dissem in tan garnet	0.472478	0.000011	0.445490	-0.25	08-Mar-05
1400 18.9 331.75		repeat	0.471813	0.000007	0.445487	-0.25	15-Mar-05
1400 18.9 334.8A	cpy	Px skarn (w/ chl altn) breccia with "frags" (?) of cpy and born (or replacing fragments); cov present in rock, cpy/born may not be coprecip	0.470568	0.000006	0.446121	1.17	18-Feb-04
1400 18.9 334.8A		repeat	0.471542	0.000007	0.446113	1.15	06-Mar-04
1400 18.9 334.8B	born	as above	0.470455	0.000006	0.445984	0.86	18-Feb-04
1400 18.9 350	born	Sheeted born>cpy veins w/ rock silicification in Monz Z	0.470155	0.000006	0.445783	0.41	18-Feb-04
1400 18.9 356.9	cpy	Qtz-cpy-Mo vein cutting alb. Monz Z (w/ chl-ser in feld) - cpy from cpy only vein sub // to qtz-cpy vein	0.471755	0.000009	0.445536	-0.14	20-Feb-03
1400 18.9 356.9		repeat	0.470922	0.000006	0.445501	-0.22	01-Jul-03
1400 18.9 357.2	cpy	Qtz-cpy-Mo vein cutting alb Monz Z	0.470901	0.000007	0.445508	-0.21	01-Jul-03
1400 18.9 365.85	cpy	Strongly albitized Monz Z w/ sheeted qtz-cpy-Mo; 2-3/cm	0.470794	0.000006	0.445359	-0.54	01-Jul-03
1400 18.9 370	cpy	Strongly sheeted qtz-cpy veins in monz Z - 9/cm	0.469804	0.000006	0.445451	-0.33	18-Feb-04
1400 18.9 376.5A	cpy	Massive magn repl. Yellow-green garn w/ cpy-born vns (cut and dissem w/ magn)	0.472044	0.000007	0.445593	-0.02	20-Feb-03
1400 18.9 376.5A#2		repeat	0.471830	0.000011	0.445470	-0.29	20-Feb-03
1400 18.9 376.5A#3		repeat	0.471899	0.000009	0.445582	-0.04	20-Feb-03
1400 18.9 376.5B	born	as above	0.471718	0.000009	0.445420	-0.40	20-Feb-03
1400 18.9 378.85	cpy	Semisilicified (green-bn) garnet skarn with strongly disseminated-stringer cpy and minor disseminated magn (to hem?)	0.470034	0.000007	0.445609	0.02	18-Feb-04
1400 18.9 382.6	cpy	Brown granular garn w/ interst. and repl. Of qtz-magn-cpy and qtz-magn-cpy vein - sample from dissem cpy-magn-qtz	0.471314	0.000006	0.445875	0.62	01-Jul-03
1400 18.9 386.4a	cpy	From sheeted quartz-cpy-born veins cutting brown garnet (nearly bx)	0.474579	0.000011	0.445909	0.69	04-Jun-02
1400 18.9 386.4b	born	As above but the born pair	0.474378	0.000013	0.445736	0.31	04-Jun-02
1400 18.9 386.4c	cpy	From above but cpy from HNO_3-only dissolution	0.474469	0.000010	0.445885	0.64	04-Jun-02
1400 18.9 387.8	cpy	Gran mass. brown-tan-green garn w/ mass. Magn repl. W/ patchy dissem cpy (+- magn) and qtz-cpy-cal vns - from vein	0.471166	0.000006	0.445709	0.24	01-Jul-03
1400 18.9 387.8b		repeat	0.471975	0.000007	0.445697	0.22	01-Apr-04
1400 18.9 387.9	cpy	Silicified brown garnet with quartz veins, disseminated +vein cpy; from vein; oxidized	0.473725	0.000007	0.445743	0.32	20-Jun-02
1400 20.9 324.7	cpy	Stringer dissem cpy in alb. Monz F - from stringers	0.470776	0.000007	0.445533	-0.15	01-Jul-03
1400 20.9 49.7	cpy	Dissem cpy in mafic clot in diorite	0.470872	0.000007	0.445462	-0.31	05-Mar-04
1400 21.7 119.6	cpy	Px-bio skarn, patchy dissem cpy; below diorite	0.473725	0.000008	0.445834	0.52	20-Jun-02
1400 21.7 119.6		repeat	0.471822	0.000006	0.445849	0.56	24-Mar-05
1400 21.7 183.5	cpy	Cpy veinlets cutting px=garn skarn; near Monz F intrusion	0.469812	0.000007	0.445319	-0.63	18-Feb-04
1400 21.7 416.95	cpy	Brown-honey garnet skarn (oxidized); interst. cpy	0.473662	0.000012	0.445722	0.27	20-Jun-02

Appendix 2 cont.

1400 21.7 425.8	cpy	Patchy cpy in in ep-plag-cal-chl-endo (?) F	0.471025	0.000007	0.445744	0.32	01-Jul-03
400 16.0 78.1A	cpy	Qtz-cpy-born-mo w/ garn (?) vein in fine grained diorite	0.471200	0.000007	0.445770	0.38	06-Mar-04
400 16.0 78.1B	born	as above	0.471217	0.000006	0.445789	0.43	06-Mar-04
900 14.8 388.7a	cpy	Banded magnetite-px skarn with patchy and veined cpy-born	0.473581	0.000008	0.445600	0.00	20-Jun-02
900 14.8 388.7b	born	as above (from vein)	0.473381	0.000009	0.445396	-0.46	20-Jun-02
900 15.2 401.9	cpy	Qtz-cpy vien in massive magnetite replacing green garn	0.470990	0.000007	0.445572	-0.06	06-Mar-04
900 16.2A 185.65	cpy	Kspar/qtz-carb-cpy vein assoc. w/ amphibole alt'n in diorite	0.470852	0.000007	0.445419	-0.41	06-Mar-04
		Ccatun Pucara, Tintaya district, Perú					
CCP-1	native Cu	From crystalline supergene native Cu	0.470838	0.000010	0.445357	-0.54	11-May-02
CCP-2	cuprite	From cubes of cuprite occurring with native Cu	0.470738	0.000011	0.445231	-0.83	11-May-02
		Tintaya, Perú					
T1900N-9 21.45	cpy	Coarse crystalline amph skarn with interst cpy and hem; yellow-gn garn may be later	0.470026	0.000006	0.445636	0.08	18-Feb-04
T1900N-9 21.45		repeat	0.471059	0.000006	0.445617	0.04	06-Mar-04
T1975N-4 111.35	cpy	Cpy from massive pyrrh-cpy-py in roca fluidal	0.471916	0.000011	0.445692	0.21	01-Apr-04
T440N255E	cpy	Sheeted cpy+py veins w/ amph halos cutting px skarn; 8351440N,251255E	0.470446	0.000008	0.445512	-0.20	23-Nov-02
T448N268E	cpy	Tajo, sheeted cpy veins in silicified skarn?; 8351448N,251268E	0.470544	0.000008	0.445632	0.07	23-Nov-02
T6237E-4	cpy	Cu skarn; disseminated cpy in pale white pyroxene	0.472353	0.000007	0.446967	3.07	24-Apr-02
T6237E-4		repeat	0.473338	0.000008	0.446915	2.95	30-Apr-02
T6237E-4b	cpy	As above, second dissolution	0.472368	0.000010	0.446933	2.99	11-May-02
T6237E-4c	cpy	Second picking same sample, no cc	0.471863	0.000008	0.446901	2.92	23-Nov-02
T982N042E	cpy	Cpy cutting monz with silicified halo; 8350982N,251042E	0.471297	0.000009	0.445606	0.01	03-Feb-03
T990N080E	cpy	Sheeted cpy veins cutting green garnet skarn; 8350990N,251080E	0.471058	0.000008	0.445411	-0.43	03-Feb-03
T990N080E		repeat	0.471359	0.000007	0.445379	-0.50	24-Mar-05
Tajo	cpy	Cu skarn; disseminated cpy in green garnet host; upper east side Tajo	0.470957	0.000007	0.445576	-0.05	24-Apr-02
TAJO-MS1	born	Bornite from massive lense of bornite-cpy; low east side Tajo pit	0.474222	0.000011	0.445650	0.11	04-Jun-02
TAJO-MS2	cpy	Cpy from above massive sulfide	0.474414	0.000011	0.445843	0.54	04-Jun-02
TT008-214	cpy	vein in PM1b	0.473036	0.000008	0.445687	0.19	30-Sep-04
CHAB-E-MAR	cpy	Cpy -silica-calcite veins in dark gray marble	0.470752	0.000007	0.446432	1.87	18-Feb-04
Chab-Este	cpy	Green garnet w/ cpy+py veinlets	0.470682	0.000008	0.445229	-0.83	06-Mar-04
Chab-Esteb	cpy	Dissem mineralization in above sample	0.471427	0.000007	0.445227	-0.84	01-Apr-04
Chab-Sur-Cp-Ma	cpy	Massive magn with cpy semi-massive	0.471051	0.000008	0.445683	0.19	06-Mar-04
CHE 039424	cpy	Vein cpy; strong kspar alt w/ late cpy-silica vns in PM1a(?)	0.472758	0.000008	0.445416	-0.41	30-Sep-04
		Chalcobamba, Peru					
Chalc	cpy	Massive cpy in massive magnetite; cpy is veined by Cu-pitch but picked sample	0.471148	0.000006	0.445764	0.37	24-Apr-02
CHALC-MAGN1	cpy	Massive magnetite with patchy dissem cpy	0.473651	0.000007	0.445674	0.17	20-Jun-02

Appendix 2 cont.

		Ferrobamba, Peru					
Ferrob-1	cp	Massive sulfide, bornite in skarn hosted lense; w/ cc	0.474239	0.000008	0.445653	0.12	04-Jun-02
Ferrob-2	born	As above but chalcopyrite (possibly replaced by born)	0.474175	0.000010	0.445603	0.01	04-Jun-02
		Empire Mine, ID, USA					
17-389	cpy	Cu skarn	0.470885	0.000004	0.445510	-0.20	24-Apr-02
18-365I	cpy	Cu skarn	0.470513	0.000007	0.445305	-0.66	18-Apr-02
18-365I		repeat	0.470663	0.000007	0.445262	-0.76	24-Apr-02
18-365I		repeat	0.471641	0.000007	0.445278	-0.72	30-Apr-02
18-365II	cpy	Cu skarn	0.470740	0.000019	0.445352	-0.56	24-Apr-02
18-365II		repeat	0.471701	0.000008	0.445319	-0.63	30-Apr-02
		Crown Jewel, WA, USA					
192-56	cpy	Au skarn, Crown Jewel, WA	0.471276	0.000006	0.445614	0.03	21-Apr-03
194-82	cpy	as above	0.471250	0.000007	0.445730	0.29	21-Apr-03
203-350	cpy	as above	0.471223	0.000007	0.445690	0.20	21-Apr-03
204-197	cpy	as above	0.471260	0.000008	0.445721	0.27	21-Apr-03
204-402	cpy	as above	0.471089	0.000007	0.445565	-0.08	21-Apr-03
204-418	cpy	as above	0.471182	0.000009	0.445671	0.16	21-Apr-03
215-448	cpy	as above	0.470922	0.000008	0.445407	-0.43	21-Apr-03
216-485	cpy	as above	0.471256	0.000007	0.445729	0.29	21-Apr-03
C-600-173	cpy	as above	0.471189	0.000011	0.445640	0.09	21-Apr-03
C-722-51	cpy	as above	0.471225	0.000006	0.445565	-0.08	21-Apr-03
C-727-166	cpy	as above	0.471146	0.000007	0.445610	0.02	21-Apr-03
D563-C	cpy	as above	0.471098	0.000007	0.445560	-0.09	21-Apr-03
GAC-12PO	cpy	as above	0.470769	0.000008	0.445597	-0.01	18-Apr-02
GAC-12BD	cpy	as above	0.471023	0.000008	0.445658	0.13	24-Apr-02
GAC-12PO	cpy	as above	0.470962	0.000010	0.445571	-0.07	24-Apr-02
GAC-12 PO 2C	cpy	chromatography	0.471473	0.000007	0.445586	-0.03	11-May-02
		VMS, Portugal					
PAN-1	cpy	Massive cpy from VMS	0.471235	0.000006	0.445583	-0.04	21-Apr-03
NC-5	cpy	as above	0.471206	0.000006	0.445655	0179	21-Apr-03
		Blackbird Mine, ID, USA					
81-4	cpy	Feeder zone sulfides underlying massive exhalative sulfides in black shale basin	0.471442	0.000012	0.446006	0.91	11-May-02
81-4b	cpy	Second handsample of above	0.471394	0.000009	0.445622	0.05	11-May-02
		Ajo, AZ, USA					
Ajo-7a	cpy	Late qtz-cpy veins cutting qtz-monz and earlier hairline qtz-cpy fracts	0.471750	0.000007	0.445691	0.20	01-Apr-04
Ajo-7e	cpy	Early qtz-cpy (+kspar?) fract cutting qtz monz; same sample as above	0.471796	0.000004	0.445739	0.31	01-Apr-04
		Superior mine, AZ, USA					
Ar 32	born	Massive bornite	0.471204	0.000007	0.445793	0.43	06-Mar-04
Ar-14a	cpy	Massive suilfide	0.473024	0.000008	0.445685	0.19	30-Sep-04
Ar-14b	born	as above	0.472919	0.000007	0.445600	0.00	30-Sep-04
Ar-14b #2		repeat	0.472928	0.000007	0.445592	-0.02	30-Sep-04
AR-17a	cpy	Massive sulfide	0.471265	0.000007	0.445699	0.22	01-Jul-03
AR-17b	born	Massive sulfide above	0.471178	0.000007	0.445581	-0.04	01-Jul-03
Ar-37a	born	Massive enargite with minor bornite	0.470984	0.000006	0.445587	-0.03	06-Mar-04
Ar-37b	enargite	as above	0.471067	0.000007	0.445677	0.17	06-Mar-04
Ar-6	born	Massive bornite	0.470963	0.000008	0.445568	-0.07	06-Mar-04
Ar6 #2		repeat dissolution	0.470997	0.000007	0.445574	-0.06	06-Mar-04

Appendix 2 cont.

Resolution Porphyry, AZ, USA							
RES-2A 1885.55	cpy	Biotite altered diabase, with cpy stringers	0.473512	0.000008	0.445627	0.06	20-Jun-02
RES-2A 1927	cpy	Biotite altered diabase, with cpy stringers	0.473508	0.000007	0.445612	0.03	20-Jun-02
S22-A 2137	born	Bornite-py veins in QSP altered Vc	0.471812	0.000008	0.446324	1.62	01-Jul-03
S22-A 969	cpy	Quartz-sph-py-cpy vein (late) cutting Vc and earlier qtz -cpy vein - (related to HS veins?)	0.473815	0.000010	0.445838	0.53	20-Jun-02
S27-A 1847	born	HS py-born vein cutting Vc	0.473750	0.000009	0.445780	0.40	20-Jun-02
S27-A 1847	born	repeat	0.470875	0.000009	0.445800	0.45	23-Nov-02
S27-A 1847	born	repeat	0.472752	0.000009	0.445802	0.45	30-Jan-03
S27-A 1847 #2	born	repeat	0.472717	0.000008	0.445835	0.53	30-Jan-03
S27-I 2897	cpy	Cpy-py vein in green garn skarn	0.471454	0.000007	0.445925	0.73	01-Jul-03
SUP-1	cpy	Massive cpy from the Superior Vein	0.471258	0.000009	0.445828	0.51	11-May-02
SUP-1	cpy	Cpy rimming and replacing py	0.474389	0.000009	0.445831	0.52	04-Jun-02
SUP-1	cpy	repeat	0.473805	0.000008	0.445841	0.54	20-Jun-02
SUP-1 #1	cpy	repeat	0.469824	0.000005	0.445853	0.57	17-Jun-03
SUP-1 #2	cpy	repeat	0.469754	0.000007	0.445849	0.56	17-Jun-03
SUP-1	cpy	repeat	0.470452	0.000006	0.445853	0.57	07-Jan-04
Sup-1	cpy	repeat	0.472807	0.000007	0.445820	0.49	30-Sep-04
Sup-1 #1	cpy	repeat	0.472776	0.000011	0.445830	0.52	08-Mar-05
Sup-1 #2	cpy	repeat	0.472831	0.000010	0.445833	0.52	08-Mar-05
SUP-1	cpy	repeat	0.471741	0.000007	0.445809	0.47	24-Mar-05
SUP-1 #2	cpy	repeat	0.471831	0.000006	0.445820	0.49	24-Mar-05
Sup-1 +Zn	cpy	Zn doped	0.471883	0.000008	0.445802	0.45	15-Mar-05
SUP-1 col	cpy	Chromatographically purified	0.471794	0.000006	0.445832	0.52	24-Mar-05
Sup-1 column #1	cpy	repeat	0.472779	0.000007	0.445827	0.51	08-Mar-05
Sup-1 column #2	cpy	repeat	0.472670	0.000014	0.445696	0.21	08-Mar-05
Sup-1 Column #3	cpy	repeat	0.472818	0.000008	0.445805	0.46	08-Mar-05
Sup-1 column #4	cpy	repeat	0.472128	0.000010	0.445830	0.52	08-Mar-05
SUP-1b	cpy	Second picking of SUP-1	0.471267	0.000009	0.445844	0.55	11-May-02
SUP-2b	cpy	Other massive sulfide (cpy-py)	0.471300	0.000006	0.445627	0.06	21-Apr-03
SUP-3A(1)	cpy	Massive granular cpy - extensive replacement of py	0.470959	0.000011	0.445664	0.14	05-Mar-04
SUP-3A(1)	cpy	repeat	0.471195	0.000008	0.445656	0.12	06-Mar-04
SUP-3A(2)	cpy	as above, same sample	0.470965	0.000008	0.445628	0.06	05-Mar-04
SUP-3A(2)	cpy	repeat	0.471223	0.000009	0.445626	0.06	06-Mar-04
SUP-3A(3)	cpy	as above, same sample	0.471786	0.000008	0.445617	0.04	01-Apr-04
SUP-3A(4)	cpy	as above, same sample	0.471753	0.000010	0.445609	0.02	01-Apr-04
SUP-3B(1)	cpy	as above, same sample	0.470997	0.000006	0.445638	0.09	05-Mar-04
SUP-3B(1)	cpy	repeat	0.471282	0.000006	0.445620	0.04	06-Mar-04
SUP-3C(1)	cpy	as above, same sample	0.471011	0.000006	0.445626	0.06	05-Mar-04
SUP-3C(1)	cpy	repeat	0.471306	0.000006	0.445612	0.03	06-Mar-04
SUP-3C(2)	cpy	as above, same sample	0.471020	0.000006	0.445615	0.03	05-Mar-04
SUP-3C(2)	cpy	repeat	0.471077	0.000008	0.445621	0.05	05-Mar-04
SUP-3C(2)	cpy	repeat	0.471345	0.000006	0.445605	0.01	06-Mar-04
Beaver-Harrison mine, Millard Co., UT, USA							
BEAV-1	cpy	Vein of kspar-quartz-born-cpy cutting fine grained porphyry/monzonite	0.474808	0.000010	0.446207	1.36	04-Jun-02
BEAV-1 #2	cpy	repeat	0.474765	0.000009	0.446230	1.41	04-Jun-02
BEAV-2	born	As above but born	0.474626	0.000011	0.446045	1.00	04-Jun-02
BEAV-2 +Zn	born	repeat	0.472102	0.000013	0.445973	0.84	15-Mar-05
BEAV-2 #2	born	repeat	0.472034	0.000010	0.446005	0.91	24-Mar-05

Appendix 2 cont.

BEAV-2 #1	born	repeat	0.472383	0.000008	0.446043	0.99	25-Mar-05
BEAV-2 #2	born	repeat	0.472433	0.000006	0.446085	1.09	25-Mar-05
BEAV-2 +Zn #1	born	Zn corrected	0.472392	0.000006	0.446022	0.95	25-Mar-05
BEAV-2 +Zn #2	born	repeat	0.472347	0.000007	0.445995	0.89	25-Mar-05
BEAV-3	cpy	Disseminated cpy away from above vein in same sample	0.472317	0.000009	0.446063	1.04	01-Apr-04
BEAV-4a	cpy	Biotite-cpy-born-moly vein in qtz monz (earlier than BEAV-1?)	0.472195	0.000007	0.445958	0.80	01-Apr-04
BEAV-4b	born	above	0.472006	0.000007	0.445776	0.40	01-Apr-04
Beav-5a	cpy	Cpy from earlier thin qtz-cpy-born vein in same sample as BEAV-1, 3	0.473440	0.000009	0.446143	1.22	30-Sep-04
Beav-5b	born	as above	0.473316	0.000009	0.445999	0.90	30-Sep-04
		OK mine, UT, USA					
OKM-1	azurite	OK Mine; from porphyry-related breccia pipe	0.472114	0.000009	0.446688	2.44	11-May-02
OKM-2	cpy	Cpy on interm arg'd late porph with py after mafics w/ dissem cpy-mo	0.471941	0.000009	0.445599	0.00	08-Mar-05
OKM-2		repeat	0.471986	0.000007	0.445640	0.09	15-Mar-05
		Cactus mine, UT, USA					
SFRAN-1	cpy	Cpy in tourmalinized endoskarn	0.471233	0.000008	0.445704	0.23	21-Apr-03
		Grasberg (Ertsberg) district, Irian Jaya, Indonesia					
BG1-6-600	cpy	Cpy interstitial to distal px	0.471486	0.000008	0.445704	0.23	11-May-02
G6	cpy	Stockwork veins in diorite porphyry	0.470906	0.000012	0.445428	-0.39	11-May-02
		Bingham Canyon, UT, USA					
BING-3	cpy	Cpy on fracts in monzonite with abundant secondary bio	0.470750	0.000007	0.445436	-0.37	06-Mar-04
BING-4	cpy	Cpy on fract in biotized monz	0.471737	0.000005	0.445585	-0.03	01-Apr-04
CF-1	cpy	Cpy fract cutting hornfels; cuts other py-cpy-act+/-qtz veinlets	0.471732	0.000004	0.445595	-0.01	01-Apr-04
CF-14	cpy	Minor dissem cpy in massive green garn (prox.?)	0.471738	0.000006	0.445621	0.05	01-Apr-04
CF-16	cpy	Major (>3%) cpy+/-py dissem in light green px>>granular green garn	0.472065	0.000006	0.445952	0.79	01-Apr-04
CF-18	cpy	Granular euhed. brown garn w/ interst. calcite-cpy (<3%)	0.472112	0.000007	0.446022	0.95	01-Apr-04
BING-6	cpy	Cpy in strongly qtz-Mo veined monz porph	0.471973	0.000011	0.445640	0.09	08-Mar-05
		Butte, MT, USA					
Bu-10	born	Cc-born-py-qtz from 3200 level Granite Mtn mine., Butte	0.473088	0.000010	0.446023	0.95	30-Sep-04
Bu-108a	cc	Cc-cov form Leonard mine, Butte	0.472890	0.000008	0.445689	0.20	30-Sep-04
Bu-108b	cov	as above	0.473067	0.000008	0.445903	0.68	30-Sep-04
Bu-120	cc	Cc-born-py from 2600 level Granite Mtn mine, Butte	0.473026	0.000009	0.445708	0.24	30-Sep-04
Bu-130a	cov	Cov-cc-clay from Granite Mtn mine, Butte; 1000 level	0.472963	0.000007	0.445663	0.14	30-Sep-04
Bu-130b	cc	as above	0.472764	0.000006	0.445512	-0.20	30-Sep-04
Bu-130b #2	cc	repeat	0.472488	0.000007	0.445522	-0.17	30-Sep-04
Bu-15	cc	Cc-py-qtz-clay from 2800 level Granite Mtn mine, Butte	0.472715	0.000010	0.445694	0.21	30-Sep-04
Bu-16	born	born-py-rhodocrosite on 2600 level Granite Mtn mine, Butte	0.472856	0.000010	0.445815	0.48	30-Sep-04
Bu-17	born	born-cc-qtz-clay from 2200 level Granite Mtn mine, Butte	0.472860	0.000009	0.445719	0.27	30-Sep-04
Bu-2	cc	2800 level Granite Mtn mine, Butte; cc+py+clay+qtz	0.472796	0.000010	0.445698	0.22	30-Sep-04

Appendix 2 cont.

Bu-28	born	Born-sph-clay from 3400 level Granite Mtn mine, Butte	0.472878	0.000007	0.445750	0.34	30-Sep-04
Bu-5a	cc	Born+cc+qtz+clay; 2200 level Granite Mtn mine, Butte	0.473154	0.000007	0.445836	0.53	30-Sep-04
Bu-5b	born	as above	0.473076	0.000006	0.445763	0.37	30-Sep-04
		Christmas mine, AZ, USA					
CHRIS-1	cpy	Disseminated cpy-sph in green garnet with local magn replacement, Christmas, AZ	0.471554	0.000006	0.446164	1.27	06-Mar-04
		Empire mine, NM, USA					
EMP-1	cpy	Weak kspar-cpy band in qtz-monz (low cpy)	0.471631	0.000005	0.445547	-0.12	01-Apr-04
EMP-3	cpy	Propylitized (?) qtz monz with cpy veins with kspar envelopes	0.471645	0.000006	0.445581	-0.04	01-Apr-04
EMP-5-4	cpy	Course grained, bladed, brown px with dissem sph-py-cpy	0.471741	0.000006	0.445689	0.20	01-Apr-04
		Galena mine, ID, USA					
GALENAM-1	cpy	Cpy from sid-qtz-tetrah-cpy vn	0.471272	0.000008	0.445651	0.12	01-Jul-03
GALENAM-2	tetrah	as above	0.471266	0.000011	0.445621	0.05	01-Jul-03
		Michigan native copper district, MI, USA					
LS-12	native Cu	Centennial Mine	0.470879	0.000007	0.445714	0.26	18-Apr-02
LS-45	native Cu	Isle Royale Mine	0.470847	0.000006	0.445752	0.34	18-Apr-02
LS-46	mohawkite	Mohawk Mine	0.471349	0.000008	0.445476	-0.28	08-May-02
LS-48	native Cu	Wolverine Mine	0.470905	0.000006	0.445732	0.30	18-Apr-02
LS-48 5%	native Cu	Dr. Larson's first dissolution	0.470927	0.000004	0.445729	0.29	18-Apr-02
LS-51	native Cu	Copper Falls Mine	0.471372	0.000009	0.445614	0.03	08-May-02
LS-51	native Cu	repeat	0.474148	0.000010	0.445603	0.01	04-Jun-02
LS-7	native Cu	Tri-Mountain Mine	0.470859	0.000006	0.445722	0.27	18-Apr-02
LS-8	mohawkite	Mohawk Mine	0.471529	0.000010	0.445708	0.24	08-May-02
Mi-10	cpy	Baltic Mine	0.471301	0.000011	0.445285	-0.71	08-May-02
Mi-2	domeykite	Mohawk Mine	0.471426	0.000009	0.445523	-0.17	08-May-02
Mi-6	born	Baltic Mine	0.471111	0.000008	0.445124	-1.07	08-May-02
PL-1	cc	Baltic Mine	0.471879	0.000009	0.445928	0.74	08-May-02
LS-10	native Cu	Baltic Mine	0.471531	0.000007	0.445832	0.52	12-Apr-02
LS-10	native Cu	repeat	0.470773	0.000009	0.445759	0.36	18-Apr-02
LS-10	native Cu	repeat	0.471086	0.000008	0.445734	0.30	27-Apr-02
LS-10	native Cu	repeat	0.472222	0.000008	0.445720	0.27	30-Apr-02
LS-10 #1	native Cu	repeat	0.471773	0.000007	0.445732	0.30	08-May-02
LS-10 #2	native Cu	repeat	0.471402	0.000009	0.445753	0.34	08-May-02
LS-10	native Cu	repeat	0.471290	0.000007	0.445731	0.29	11-May-02
LS-10	native Cu	repeat	0.474341	0.000008	0.445720	0.27	04-Jun-02
LS-10	native Cu	repeat	0.473676	0.000008	0.445699	0.22	20-Jun-02
LS-10	native Cu	repeat	0.472649	0.000008	0.445700	0.23	30-Jan-03
LS-10	native Cu	repeat	0.471671	0.000008	0.445683	0.19	03-Feb-03
LS-10	native Cu	repeat	0.471350	0.000007	0.445710	0.25	21-Apr-03
LS-10	native Cu	repeat	0.471389	0.000007	0.445714	0.26	01-Jul-03
LS-10 #1	native Cu	repeat	0.470357	0.000007	0.445665	0.15	07-Jan-04
LS-10 #2	native Cu	repeat	0.470339	0.000007	0.445749	0.34	07-Jan-04
LS-10	native Cu	repeat	0.470919	0.000008	0.445731	0.29	05-Mar-04
LS-10	native Cu	repeat	0.471746	0.000007	0.445696	0.22	01-Apr-04
LS-10	native Cu	repeat	0.472713	0.000006	0.445704	0.23	30-Sep-04
LS-10	native Cu	repeat	0.471609	0.000008	0.445698	0.22	24-Mar-05
LS-10 fract	native Cu	Baltic Mine; tried to fractionate this sample through dissolutions	0.471086	0.000009	0.445743	0.32	27-Apr-02

Appendix 2 cont.

			Ray mine, AZ, USA				
RAY-1	native Cu	Supergene -from Livingston Fault Zone	0.471354	0.000007	0.445691	0.21	12-Apr-02
Ray-1	native Cu	repeat	0.470589	0.000006	0.445608	0.02	18-Apr-02
RAY-1	native Cu	repeat	0.470981	0.000008	0.445598	0.00	24-Apr-02
Ray-1(b)	native Cu	repeat	0.470996	0.000008	0.445611	0.02	24-Apr-02
Ray-1 #1	native Cu	repeat	0.471610	0.000006	0.445577	-0.05	08-May-02
RAY-1 #2	native Cu	repeat	0.471271	0.000008	0.445584	-0.04	08-May-02
Ray-1	native Cu	repeat	0.471154	0.000009	0.445575	-0.06	11-May-02
Ray-1 #2	native Cu	repeat	0.471441	0.000009	0.445602	0.00	11-May-02
RAY-1	native Cu	repeat	0.474278	0.000010	0.445565	-0.08	04-Jun-02
RAY-1 #2	native Cu	repeat	0.474123	0.000010	0.445562	-0.09	04-Jun-02
RAY-1	native Cu	repeat	0.473454	0.000006	0.445559	-0.09	20-Jun-02
Ray-1	native Cu	repeat	0.470646	0.000010	0.445575	-0.06	23-Nov-02
Ray-1	native Cu	repeat	0.472501	0.000011	0.445555	-0.10	30-Jan-03
Ray-1	native Cu	repeat	0.471776	0.000008	0.445546	-0.12	01-Feb-03
Ray-1	native Cu	repeat	0.471719	0.000008	0.445587	-0.03	03-Feb-03
Ray-1	native Cu	repeat	0.472104	0.000008	0.445553	-0.11	20-Feb-03
RAY-1	native Cu	repeat	0.471189	0.000006	0.445564	-0.08	21-Apr-03
RAY-1 #1	native Cu	repeat	0.469597	0.000006	0.445593	-0.01	17-Jun-03
RAY-1 #2	native Cu	repeat	0.469590	0.000006	0.445606	0.01	17-Jun-03
RAY-1	native Cu	repeat	0.470799	0.000007	0.445563	-0.08	01-Jul-03
RAY-1	native Cu	repeat	0.470365	0.000006	0.445584	-0.03	07-Jan-04
RAY-1	native Cu	repeat	0.469882	0.000005	0.445588	-0.03	18-Feb-04
RAY-1	native Cu	repeat	0.470747	0.000008	0.445553	-0.11	05-Mar-04
RAY-1	native Cu	repeat	0.471269	0.000006	0.445557	-0.10	06-Mar-04
Ray-1	native Cu	repeat	0.471872	0.000007	0.445570	-0.07	01-Apr-04
Ray-1	native Cu	repeat	0.472779	0.000009	0.445568	-0.07	30-Sep-04
Ray-1 #2	native Cu	repeat	0.472340	0.000009	0.445526	-0.17	10-Jan-05
Ray-1	native Cu	repeat	0.472217	0.000010	0.445574	-0.06	20-Jan-05
Ray-1 #1	native Cu	repeat	0.472415	0.000011	0.445470	-0.29	27-Jan-05
Ray-1 #2	native Cu	repeat	0.471984	0.000011	0.445527	-0.16	27-Jan-05
Ray-1 #3	native Cu	repeat	0.471973	0.000015	0.445552	-0.11	27-Jan-05
Ray-1	native Cu	repeat	0.471862	0.000008	0.445520	-0.18	08-Mar-05
Ray-1 #2	native Cu	repeat	0.471863	0.000010	0.445524	-0.17	08-Mar-05
Ray-1	native Cu	repeat	0.471921	0.000007	0.445558	-0.09	15-Mar-05
RAY-1	native Cu	repeat	0.471453	0.000008	0.445539	-0.14	24-Mar-05
RAY-1 #2	native Cu	repeat	0.471571	0.000005	0.445574	-0.06	24-Mar-05
RAY-1 #1	native Cu	repeat	0.471867	0.000006	0.445555	-0.10	25-Mar-05
RAY-1 #2	native Cu	repeat	0.471898	0.000005	0.445518	-0.18	25-Mar-05
Ray-2	native Cu with cuprite	Supergene, from same zone as Ray-1	0.471230	0.000005	0.446163	1.26	18-Apr-02
Ray-2b	native Cu without cuprite	Supergene, as above	0.470963	0.000007	0.445922	0.72	18-Apr-02
			Montana Tunnels mine, MT, USA				
MTTN-1	cpy	Cpy-galena-sphalerite-Au veins in argillized/sericitized volcaniclastics	0.471254	0.000009	0.445840	0.54	06-Mar-04
			Mission mine, AZ, USA				
PBL-0142	cpy	Dissem cpy in wollastonite/green garn skarn	0.473054	0.000008	0.445718	0.26	30-Sep-04
			Pine Creek mine, CA, USA				
PC-9	cpy	Tungsten skarn; disseminated cpy in brown garnet	0.470729	0.000008	0.445213	-0.87	11-May-02
PC9 #2	cpy	repeat	0.470849	0.000009	0.445267	-0.75	11-May-02

Appendix 2 cont.

PC9	cpy	repeat	0.473806	0.000012	0.445246	-0.79	04-Jun-02
		Palabora mine, South Africa					
Phal-1	cpy	Cpy-magn clot in carbonatite from Palabora	0.471996	0.000009	0.445651	0.11	08-Mar-05
		Troy prospect, ID, USA					
TROY-1A	cpy	Endoskarn in monz w/ garn+dark green px and dissem cpy-born	0.471763	0.000006	0.445704	0.23	01-Apr-04
TROY-1B	born	from above	0.471657	0.000006	0.445600	0.00	01-Apr-04
TROY-4A	cpy	Dark-green px=garn band in calc-quartzite (?) with dissem cpy-born	0.471809	0.000004	0.445751	0.34	01-Apr-04
TROY-4B	born	as above	0.471746	0.000007	0.445686	0.19	01-Apr-04
		Sudbury, Canada					
TL-4	cpy	Thayer-Lindsley Mine, Sudbury; sulfide matrix of impact breccia	0.470954	0.000011	0.445489	-0.25	11-May-02
Sd-5	cpy	Sudbury; Massive sulfide from base of Sudbury Intrusive Complex	0.471234	0.000009	0.445673	0.16	11-May-02
		Animas Forks district, Silverton, CO, USA					
SILV-1	cpy	Cpy in qtz-sph-gal-cpy vein	0.471966	0.000009	0.445665	0.15	15-Mar-05
		Spar Lake, MT, USA					
SLAKE-1A	cpy	Massive bornite>cpy in siltstone	0.470902	0.000008	0.445700	0.22	05-Mar-04
SLAKE-1B	born	as above	0.470827	0.000008	0.445579	-0.05	05-Mar-04
SLAKE-1B	born	repeat	0.470961	0.000007	0.445536	-0.14	06-Mar-04
SL-6b	born	Quartzite w/ born-cpy nodule; locally altered w/ malachite	0.471591	0.000008	0.445501	-0.22	01-Apr-04
SL-6c	cpy	Qtz-cpy+/-mal vein cutting qtzite with dissem born (from above)	0.471713	0.000008	0.445621	0.05	01-Apr-04
		Stillwater mine, MT, USA					
SW-22	cpy	Stillwater mine, MT; hydrothermally reworked sulfides at contact of stillwater igenous complex	0.470859	0.000009	0.445136	-1.04	11-May-02
STILLJM-1	cpy	Stillwater mine, cpy from JM Reef; sampled May 2002	0.471496	0.000008	0.445460	-0.31	03-Feb-03
STILLJM-1 #2	cpy	repeat analysis	0.471247	0.000006	0.445518	-0.18	03-Feb-03
		Rammelsberg, Germany					
W4	cpy	Feeder zone sulfide veins underlying massive exhalative sulfides in black shale basin	0.471468	0.000009	0.445651	0.11	11-May-02

Appendix 3

Table of Results of Copper Isotope Analyses

For convenience, all analyses of the NIST SRM 976 are presented before the unknown sample analyses. The second part of this Appendix lists the complete analytical runs with a graph following each run showing all raw ratios relative to time and graphically showing the machine drift during the course of the analytical run. The purpose of the graphs is to facilitate judgement of the reliability of the sample-standard bracketing correction. The raw ratios are shown with 2σ standard error bars. Delta values are calculated with normalized raw isotopic ratios and NIST SRM 976. The actual normalizing factor for the raw ratios is determined by the subtracting the NIST SRM 976 ratio ($^{65}Cu/^{63}Cu = 0.4456$) from the drifted standard ratio determined by linearly extrapolating between the analyses of two standards which bracket the sample unknown at the time of the unknown analysis (see Section II). Two columns in the table show the percent of the sample copper concentration relative to the copper concentration in the standard (See Albarède et al., 2003), and the drift between bracketing standards in ppm. The drift between bracketing standards is somewhat of an indication of the reliability of the standard-sample bracketing correction. Re-analysis of unknown and bracketing standards is required when abrupt changes occur in the drift between standards.

Following the data table for each analytical run is its graph of $^{65}Cu/^{63}Cu$ verses time. Filled diamonds are NIST SRM 976, and the standards are listed in the analytical run tables as “976 #x”. All $\delta^{65}Cu$ values are per mil (‰) relative to NIST SRM 976.

Appendix 3

Date	Analysis	$^{65}Cu/^{63}Cu$	Error (2σ)	β (fractionation coefficient)	Fractionation factor (exponential law)
12-Apr-02	976 #1	0.4710895	6.76E-06	-1.7886	0.94589
	976 #2	0.4711146	5.98E-06	-1.7903	0.94584
	976 #3	0.4711353	7.99E-06	-1.7917	0.94580
	976 #4	0.4711369	6.66E-06	-1.7919	0.94580
	976 #5	0.4711734	6.02E-06	-1.7943	0.94572
	976 #6	0.4712283	7.83E-06	-1.7981	0.94561
	976 #7	0.4712942	7.68E-06	-1.8026	0.94548
	976 #8	0.4713043	6.07E-06	-1.8033	0.94546
18-Apr-2002	976 #1	0.4705045	6.18E-06	-1.7487	0.94707
	976 #2	0.4705574	7.83E-06	-1.7523	0.94696
	976 #3	0.4705909	5.78E-06	-1.7546	0.94689
	976 #4	0.4706188	7.39E-06	-1.7565	0.94684
	976 #5	0.4706610	5.08E-06	-1.7594	0.94675
	976 #6	0.4709082	8.43E-06	-1.7762	0.94626
	976 #7	0.4700600	1.15E-05	-1.7183	0.94796
	976 #8	0.4701943	7.80E-06	-1.7275	0.94769
	976 #9	0.4702726	7.23E-06	-1.7328	0.94754
	976 #10	0.4703901	5.66E-06	-1.7408	0.94730
	976 #11	0.4705012	8.60E-06	-1.7484	0.94708
	976 #12	0.4704956	8.09E-06	-1.7481	0.94709
	976 #13	0.4705227	9.00E-06	-1.7499	0.94703
	976 #14	0.4705517	6.34E-06	-1.7519	0.94697
	976 #15	0.4706069	7.15E-06	-1.7557	0.94686
	976 #16	0.4706229	5.92E-06	-1.7568	0.94683
	976 #17	0.4706585	6.68E-06	-1.7592	0.94676
	976 #18	0.4706771	6.06E-06	-1.7605	0.94672
	976 #19	0.4707127	6.79E-06	-1.7629	0.94665
	976 #20	0.4707582	7.56E-06	-1.7660	0.94656
	976 #21	0.4707709	6.59E-06	-1.7669	0.94653
	976 #22	0.4707760	5.41E-06	-1.7672	0.94652
	976 #23	0.4708146	6.13E-06	-1.7698	0.94644
	976 #24	0.4708010	6.58E-06	-1.7689	0.94647
	976 #25	0.4707406	6.14E-06	-1.7648	0.94659
24-Apr-2002	976 #1	0.4709148	7.49E-06	-1.7767	0.94624
	976 #2	0.4709110	7.81E-06	-1.7764	0.94625
	976 #3	0.4709212	8.37E-06	-1.7771	0.94623
	976 #4	0.4709213	8.93E-06	-1.7771	0.94623
	976 #5	0.4709566	7.60E-06	-1.7795	0.94616
	976 #6	0.4710094	6.72E-06	-1.7831	0.94605
	976 #7	0.4709934	6.84E-06	-1.7821	0.94609
	976 #8	0.4709878	8.91E-06	-1.7817	0.94610
	976 #9	0.4709890	6.43E-06	-1.7818	0.94609
	976 #10	0.4709601	6.47E-06	-1.7798	0.94615
	976 #11	0.4709701		-1.7805	0.94613
24-Apr-2002	976 #12	0.4709853	5.98E-06	-1.7815	0.94610
24-Apr-2002	976 #12	0.4709864	7.47E-06	-1.7816	0.94610
(cont.)	976 #14	0.4709813	6.80E-06	-1.7812	0.94611
	976 #15	0.4709900	6.04E-06	-1.7818	0.94609
27-Apr-2002	976 #1	0.4709599	7.92E-06	-1.7798	0.94615
	976 #2	0.4709431	9.40E-06	-1.7786	0.94619
	976 #3	0.4709428	7.09E-06	-1.7786	0.94619
	976 #4	0.4709494	6.70E-06	-1.7791	0.94617
	976 #5	0.4709370	7.21E-06	-1.7782	0.94620
30-Apr-2002	976 #1	0.4720275	7.33E-06	-1.8526	0.94401
	976 #2	0.4720461	5.79E-06	-1.8538	0.94398
	976 #3	0.4719876	7.57E-06	-1.8499	0.94409
	976 #4	0.4719935	7.51E-06	-1.8503	0.94408
	976 #5	0.4721680	7.83E-06	-1.8621	0.94373
	976 #6	0.4721468	9.28E-06	-1.8607	0.94377
	976 #7	0.4720531	8.24E-06	-1.8543	0.94396
	976 #8	0.4719920	6.77E-06	-1.8502	0.94408
	976 #9	0.4719716	6.42E-06	-1.8488	0.94412
	976 #10	0.4719538	7.43E-06	-1.8476	0.94416
8-May-2002	976 #1	0.4716910	8.03E-06	-1.8296	0.94469
	976 #2	0.4716760	7.08E-06	-1.8286	0.94472
	976 #3	0.4716721	6.66E-06	-1.8284	0.94472
	976 #4	0.4716599	8.48E-06	-1.8275	0.94475
	976 #5	0.4717024	5.96E-06	-1.8304	0.94466
	976 #6	0.4716783	7.58E-06	-1.8288	0.94471
	976 #7	0.4716527	5.19E-06	-1.8270	0.94476
	976 #8	0.4716230	6.78E-06	-1.8250	0.94482
	976 #9	0.4716408	1.23E-05	-1.8262	0.94479
	976 #10	0.4716394	6.47E-06	-1.8261	0.94479
	976 #11	0.4715950	7.60E-06	-1.8231	0.94488
	976 #12	0.4715797	6.84E-06	-1.8221	0.94491
	976 #13	0.4715198	9.58E-06	-1.8180	0.94503
	976 #14	0.4714889	8.68E-06	-1.8159	0.94509
	976 #15	0.4714546	8.72E-06	-1.8135	0.94516
	976 #16	0.4713953	6.44E-06	-1.8095	0.94528
	976 #17	0.4713242	7.46E-06	-1.8046	0.94542
	976 #18	0.4712472	1.01E-05	-1.7994	0.94558
	976 #19	0.4712519	6.81E-06	-1.7997	0.94557
11-May-2002	976 #1	0.4712648	1.00E-05	-1.8006	0.94554
	976 #2	0.4712223	8.59E-06	-1.7977	0.94563
	976 #3	0.4711822	8.88E-06	-1.7949	0.94571
	976 #4	0.4711913	7.52E-06	-1.7956	0.94569
	976 #5	0.4711927	8.37E-06	-1.7957	0.94569
	976 #6	0.4711673	8.98E-06	-1.7939	0.94574
	976 #7	0.4711511	9.49E-06	-1.7928	0.94577
	976 #8	0.4710744	8.92E-06	-1.7876	0.94592

Date	Analysis	$^{65}Cu/^{63}Cu$	Error (2σ)	β (fractionation coefficient)	Fractionation factor (exponential law)
11-May-2002	976 #10	0.4716560	7.65E-06	-1.8273	0.94476
(cont.)	976 #11	0.4716182	7.36E-06	-1.8247	0.94483
	976 #12	0.4715487	7.13E-06	-1.8199	0.94497
	976 #13	0.4714837	8.65E-06	-1.8155	0.94510
	976 #14	0.4713795	9.60E-06	-1.8084	0.94531
	976 #15	0.4712867	8.06E-06	-1.8021	0.94550
	976 #16	0.4712738	8.47E-06	-1.8012	0.94552
	976 #17	0.4712626	9.03E-06	-1.8004	0.94554
	976 #18	0.4711257	8.56E-06	-1.7911	0.94582
	976 #19	0.4710327	9.73E-06	-1.7847	0.94601
	976 #20	0.4710373	1.13E-05	-1.7851	0.94600
	976 #21	0.4710339	1.06E-05	-1.7848	0.94600
	976 #22	0.4710259	1.03E-05	-1.7843	0.94602
	976 #23	0.4710260		-1.7843	0.94602
	976 #24	0.4711319	8.61E-06	-1.7915	0.94581
	976 #25	0.4711319	1.09E-05	-1.7915	0.94581
	976 #26	0.4710843	8.42E-06	-1.7883	0.94590
	976 #27	0.4710765	9.06E-06	-1.7877	0.94592
	976 #28	0.4710543	9.21E-06	-1.7862	0.94596
	976 #29	0.4709925	7.77E-06	-1.7820	0.94609
	976 #30	0.4713911	9.69E-06	-1.8092	0.94529
	976 #31	0.4714434	8.11E-06	-1.8128	0.94518
	976 #32	0.4713224	1.95E-05	-1.8045	0.94543
	976 #33	0.4713398	6.94E-06	-1.8057	0.94539
	976 #34	0.4714075	6.48E-06	-1.8103	0.94525
	976 #35	0.4714710	8.84E-06	-1.8146	0.94513
	976 #36	0.4715027	7.53E-06	-1.8168	0.94506
4-Jun-2002	976 #1	0.4743930	7.64E-06	-2.0133	0.93931
	976 #2	0.4743289	1.17E-05	-2.0090	0.93943
	976 #3	0.4743455	7.17E-06	-2.0101	0.93940
	976 #4	0.4743257	9.79E-06	-2.0087	0.93944
	976 #5	0.4743156	8.30E-06	-2.0081	0.93946
	976 #6	0.4743097	8.62E-06	-2.0077	0.93947
	976 #7	0.4742828	7.98E-06	-2.0058	0.93952
	976 #8	0.4742572	1.02E-05	-2.0041	0.93957
	976 #9	0.4742266	1.06E-05	-2.0020	0.93964
	976 #10	0.4742167	9.39E-06	-2.0014	0.93965
	976 #11	0.4741862	8.63E-06	-1.9993	0.93972
	976 #12	0.4741762	9.14E-06	-1.9986	0.93974
	976 #13	0.4741909	9.54E-06	-1.9996	0.93971
	976 #14	0.4741809	7.72E-06	-1.9989	0.93973
	976 #15	0.4741644	1.02E-05	-1.9978	0.93976
	976 #16	0.4741790	1.02E-05	-1.9988	0.93973
	976 #17	0.4741635	9.53E-06	-1.9977	0.93976
	976 #18	0.4741526	8.16E-06	-1.9970	0.93978
	976 #19	0.4741709	9.08E-06	-1.9982	0.93975
	976 #20	0.4741488	9.03E-06	-1.9968	0.93979
	976 #21	0.4741408	8.45E-06	-1.9962	0.93981
	976 #22	0.4741299	8.44E-06	-1.9955	0.93983

Date	Analysis	$^{65}Cu/^{63}Cu$	Error (2σ)	β (fractionation coefficient)	Fractionation factor (exponential law)
20-Jun-2002	976 #1	0.4734837	7.79E-06	-1.9516	0.94111
	976 #2	0.4735023	9.73E-06	-1.9529	0.94107
	976 #3	0.4734971	9.15E-06	-1.9525	0.94108
	976 #4	0.4734948	8.38E-06	-1.9524	0.94109
	976 #5	0.4734962	9.58E-06	-1.9525	0.94108
	976 #6	0.4734859	8.79E-06	-1.9518	0.94111
	976 #7	0.4734840	7.04E-06	-1.9516	0.94111
	976 #8	0.4735074	7.87E-06	-1.9532	0.94106
	976 #9	0.4735740	7.74E-06	-1.9577	0.94093
	976 #10	0.4735884	8.07E-06	-1.9587	0.94090
	976 #11	0.4735803	8.60E-06	-1.9582	0.94092
	976 #12	0.4735748	8.22E-06	-1.9578	0.94093
	976 #13	0.4735730	8.14E-06	-1.9577	0.94093
	976 #14	0.4735803	7.08E-06	-1.9582	0.94092
	976 #15	0.4735828	7.38E-06	-1.9583	0.94091
	976 #16	0.4735703	9.27E-06	-1.9575	0.94094
	976 #17	0.4735699	8.10E-06	-1.9575	0.94094
	976 #18	0.4735828	8.59E-06	-1.9583	0.94091
	976 #19	0.4735622	7.62E-06	-1.9569	0.94095
	976 #20	0.4735638	7.51E-06	-1.9571	0.94095
23-Nov-2002	976 #1	0.4706402	1.41E-05	-1.7579	0.94680
	976 #2	0.4706581	9.42E-06	-1.7592	0.94676
	976 #3	0.4706568	1.28E-05	-1.7591	0.94676
	976 #4	0.4706544	8.99E-06	-1.7589	0.94677
	976 #5	0.4706529	1.23E-05	-1.7588	0.94677
	976 #6	0.4706879	1.28E-05	-1.7612	0.94670
	976 #7	0.4706602	1.41E-05	-1.7593	0.94676
	976 #8	0.4706292	8.70E-06	-1.7572	0.94682
	976 #9	0.4706241	9.72E-06	-1.7568	0.94683
	976 #10	0.4706235	9.09E-06	-1.7568	0.94683
	976 #11	0.4706199	7.95E-06	-1.7565	0.94684
	976 #12	0.4705756	8.01E-06	-1.7535	0.94693
	976 #13	0.4705723	9.14E-06	-1.7533	0.94693
	976 #14	0.4705586	8.63E-06	-1.7524	0.94696
	976 #15	0.4705722	8.20E-06	-1.7533	0.94693
	976 #16	0.4705698	7.92E-06	-1.7531	0.94694
	976 #17	0.4705537	8.53E-06	-1.7520	0.94697
	976 #18	0.4705136	7.84E-06	-1.7493	0.94705
	976 #19	0.4705101	7.47E-06	-1.7490	0.94706
30-Jan-2003	976 #2	0.4725574	9.68E-06	-1.8886	0.94295
	976 #3	0.4725568	1.08E-05	-1.8886	0.94296
	976 #4	0.4725466	1.06E-05	-1.8879	0.94298
	976 #5	0.4725449	8.32E-06	-1.8878	0.94298
	976 #6	0.4725531	9.93E-06	-1.8884	0.94296
	976 #7	0.4725469	7.25E-06	-1.8879	0.94298
	976 #8	0.4725417	9.73E-06	-1.8876	0.94299
	976 #9	0.4725485	7.81E-06	-1.8880	0.94297
	976 #10	0.4725229	9.83E-06	-1.8863	0.94302
	976 #11	0.4724803	8.63E-06	-1.8834	0.94311

Date	Analysis	$^{65}Cu/^{63}Cu$	Error (2σ)	β (fractionation coefficient)	Fractionation factor (exponential law)
30-Jan-2003	976 #12	0.4724847	9.42E-06	-1.8837	0.94310
1-Feb-2003	976 #1	0.4716524	7.16E-06	-1.8270	0.94476
	976 #2	0.4717322	1.33E-05	-1.8324	0.94460
	976 #3	0.4717907	1.19E-05	-1.8364	0.94449
	976 #4	0.4718807	8.14E-06	-1.8426	0.94431
	976 #5	0.4718178	1.08E-05	-1.8383	0.94443
	976 #6	0.4718326	9.26E-06	-1.8393	0.94440
	976 #7	0.4718276	9.75E-06	-1.8390	0.94441
	976 #8	0.4718604	8.17E-06	-1.8412	0.94435
	976 #9	0.4718387	1.09E-05	-1.8397	0.94439
	976 #10	0.4718276	9.64E-06	-1.8390	0.94441
	976 #11	0.4718613	1.11E-05	-1.8413	0.94435
	976 #12	0.4718107	9.64E-06	-1.8378	0.94445
	976 #13	0.4718325	8.82E-06	-1.8393	0.94440
3-Feb-2003	976 #1	0.4716785	8.24E-06	-1.8288	0.94471
	976 #2	0.4716809	1.04E-05	-1.8290	0.94471
	976 #3	0.4716930	1.01E-05	-1.8298	0.94468
	976 #4	0.4717077	7.30E-06	-1.8308	0.94465
	976 #5	0.4717554	7.56E-06	-1.8340	0.94456
	976 #6	0.4716202	9.11E-06	-1.8248	0.94483
	976 #7	0.4715850	1.15E-05	-1.8224	0.94490
	976 #8	0.4715894	7.91E-06	-1.8227	0.94489
	976 #9	0.4716826	9.73E-06	-1.8291	0.94470
	976 #10	0.4713409	7.62E-06	-1.8058	0.94539
	976 #11	0.4713156	7.05E-06	-1.8040	0.94544
	976 #12	0.4712673	8.90E-06	-1.8007	0.94554
	976 #13	0.4712276	9.74E-06	-1.7980	0.94562
	976 #14	0.4712297	7.76E-06	-1.7982	0.94561
	976 #15	0.4713660	6.84E-06	-1.8075	0.94534
	976 #16	0.4713482	6.04E-06	-1.8063	0.94537
	976 #17	0.4713177	9.16E-06	-1.8042	0.94543
20-Feb-2003	976 #1	0.4720679	2.25E-05	-1.8553	0.94393
	976 #2	0.4721576	1.85E-05	-1.8614	0.94375
	976 #3	0.4721693	1.58E-05	-1.8622	0.94373
	976 #4	0.4721478	1.16E-05	-1.8608	0.94377
	976 #5	0.4721653	1.15E-05	-1.8620	0.94374
	976 #6	0.4721372	1.06E-05	-1.8600	0.94379
	976 Nsoln	0.4721075	9.05E-06	-1.8580	0.94385
	976 #7	0.4721100	1.06E-05	-1.8582	0.94385
	976 #8	0.4720654	8.46E-06	-1.8552	0.94394
	976 Nsoln#2	0.4720548	7.33E-06	-1.8544	0.94396
	976 #9	0.4720972	6.51E-06	-1.8573	0.94387
	976 #10	0.4720026	8.82E-06	-1.8509	0.94406
	976 #11	0.4719166	7.67E-06	-1.8450	0.94423
	976 #12	0.4719162	8.39E-06	-1.8450	0.94424
	976 #13	0.4718805	9.24E-06	-1.8426	0.94431
	976 #14	0.4718694	1.20E-05	-1.8418	0.94433
	976 #15	0.4717335	1.89E-05	-1.8325	0.94460
21-Apr-2003	976 #1	0.4712564	6.89E-06	-1.8000	0.94556
21-Apr-2003 (cont.)	976 #2	0.4712281	6.34E-06	-1.7981	0.94561
	976 #3	0.4712299	5.56E-06	-1.7982	0.94561
	976 #4	0.4712299	7.11E-06	-1.7982	0.94561
	976 #5	0.4712197	6.52E-06	-1.7975	0.94563
	976 #6	0.4712615	5.98E-06	-1.8004	0.94555
	976 #7	0.4712857	5.66E-06	-1.8020	0.94550
	976 #8	0.4712609	6.09E-06	-1.8003	0.94555
	976 #9	0.4712583	7.36E-06	-1.8001	0.94555
	976 #10	0.4712649	5.53E-06	-1.8006	0.94554
	976 #11	0.4712361	6.71E-06	-1.7986	0.94560
	976 #12	0.4710815	5.96E-06	-1.7881	0.94591
	976 #13	0.4711472	6.91E-06	-1.7926	0.94578
	976 #14	0.4711322	6.05E-06	-1.7915	0.94581
	976 #15	0.4711160	6.77E-06	-1.7904	0.94584
	976 #16	0.4711045	7.18E-06	-1.7896	0.94586
	976 #17	0.4711352	6.82E-06	-1.7917	0.94580
	976 #18	0.4711313	7.62E-06	-1.7915	0.94581
	976 #19	0.4711226	6.63E-06	-1.7909	0.94583
	976 #20	0.4711086	6.74E-06	-1.7899	0.94585
	976 #21	0.4711503	6.70E-06	-1.7928	0.94577
	976 #22	0.4711516	7.20E-06	-1.7929	0.94577
	976 #23	0.4711244	8.35E-06	-1.7910	0.94582
	976 #24	0.4711467	7.46E-06	-1.7925	0.94578
	976 #25	0.4711511	6.17E-06	-1.7928	0.94577
17-Jun-2003	976 #1	0.4695485	5.54E-06	-1.6833	0.94900
	976 #2	0.4695917	6.34E-06	-1.6862	0.94891
	976 #3	0.4695972	6.68E-06	-1.6866	0.94890
	976 #4	0.4696182	6.22E-06	-1.6880	0.94886
	976 #5	0.4695888	5.51E-06	-1.6860	0.94892
	976 #6	0.4696086	6.59E-06	-1.6874	0.94888
	976 #7	0.4696086	5.98E-06	-1.6874	0.94888
	976 #8	0.4695969	6.78E-06	-1.6866	0.94890
	976 #9	0.4695698	6.74E-06	-1.6847	0.94895
	976 #10	0.4695738	6.25E-06	-1.6850	0.94895
	976 #11	0.4695595	5.72E-06	-1.6840	0.94897
	976 #12	0.4695205	6.18E-06	-1.6813	0.94905
	976 #13	0.4695015	5.53E-06	-1.6800	0.94909
	976 #14	0.4695097	7.56E-06	-1.6806	0.94908
	976 #15	0.4695040	5.82E-06	-1.6802	0.94909
1-Jul-2003	976 #1	0.4720674	5.07E-06	-1.8553	0.94393
	976 #2	0.4720918	6.92E-06	-1.8570	0.94388
	976 #3	0.4708681	5.52E-06	-1.7735	0.94634
	976 #4	0.4708440	6.96E-06	-1.7719	0.94639
	976 #5	0.4708362	7.91E-06	-1.7713	0.94640
	976 #6	0.4708359	5.20E-06	-1.7713	0.94640
	976 #7	0.4708504	7.84E-06	-1.7723	0.94637
	976 #8	0.4708554	6.86E-06	-1.7726	0.94636
	976 #9	0.4708686	6.52E-06	-1.7735	0.94634
	976 #10	0.4708941	6.42E-06	-1.7753	0.94628

Date	Analysis	$^{65}Cu/^{63}Cu$	Error (2σ)	β (fractionation coefficient)	Fractionation factor (exponential law)
1-Jul-2003	976 #11	0.4708975	5.75E-06	-1.7755	0.94628
(cont.)	976 #12	0.4709124	6.65E-06	-1.7765	0.94625
	976 #13	0.4709338	6.45E-06	-1.7780	0.94621
	976 #14	0.4709463	7.18E-06	-1.7788	0.94618
	976 #15	0.4709645	5.40E-06	-1.7801	0.94614
	976 #16	0.4709679	5.06E-06	-1.7803	0.94614
	976 #17	0.4709819	5.99E-06	-1.7813	0.94611
	976 #18	0.4710054	6.06E-06	-1.7829	0.94606
	976 #19	0.4710350	6.80E-06	-1.7849	0.94600
	976 #20	0.4710347	7.52E-06	-1.7849	0.94600
	976 #21	0.4710434	6.71E-06	-1.7855	0.94598
	976 #22	0.4710718	7.71E-06	-1.7874	0.94593
	976 #23	0.4711032	6.73E-06	-1.7895	0.94587
	976 #24	0.4711496	6.43E-06	-1.7927	0.94577
	976 #25	0.4711827	6.68E-06	-1.7950	0.94571
	976 #26	0.4712129	5.20E-06	-1.7970	0.94564
	976 #27	0.4712105	6.40E-06	-1.7969	0.94565
	976 #28	0.4712298	7.14E-06	-1.7982	0.94561
	976 #29	0.4712625	7.58E-06	-1.8004	0.94555
	976 #30	0.4712879	6.24E-06	-1.8022	0.94549
7-Jan-2004	976 #1	0.4704369	6.58E-06	-1.7440	0.94720
	976 #2	0.4704083	6.08E-06	-1.7421	0.94726
	976 #3	0.4703847	4.51E-06	-1.7405	0.94731
	976 #4	0.4703807	6.28E-06	-1.7402	0.94732
	976 #5	0.4703803	5.53E-06	-1.7402	0.94732
	976 #6	0.4702047	7.03E-06	-1.7282	0.94767
	976 #7	0.4701940	5.98E-06	-1.7274	0.94769
	976 #8	0.4701842	6.12E-06	-1.7268	0.94771
	976 #9	0.4701766	6.90E-06	-1.7262	0.94773
18-Feb-2004	976 #1	0.4699031		-1.7075	0.94828
	976 #2	0.4698848	5.70E-06	-1.7063	0.94832
	976 #3	0.4699027	6.65E-06	-1.7075	0.94828
	976 #4	0.4699354	5.95E-06	-1.7097	0.94822
	976 #5	0.4699728	6.56E-06	-1.7123	0.94814
	976 #6	0.4699713	7.80E-06	-1.7122	0.94814
	976 #7	0.4700087	7.60E-06	-1.7148	0.94807
	976 #8	0.4700407	6.99E-06	-1.7169	0.94800
	976 #9	0.4700535	5.90E-06	-1.7178	0.94798
	976 #10	0.4700882	5.78E-06	-1.7202	0.94791
	976 #11	0.4700969	5.65E-06	-1.7208	0.94789
5-Mar-2004	976 #1	0.4707325	7.83E-06	-1.7642	0.94661
	976 #2	0.4707622	6.47E-06	-1.7663	0.94655
	976 #3	0.4708035	9.63E-06	-1.7691	0.94647
	976 #4	0.4707623	7.16E-06	-1.7663	0.94655
	976 #5	0.4707989	7.43E-06	-1.7688	0.94648
	976 #6	0.4707890	6.08E-06	-1.7681	0.94650
	976 #7	0.4707875	8.01E-06	-1.7680	0.94650
	976 #8	0.4708185	7.10E-06	-1.7701	0.94644
5-Mar-2004	976 #9	0.4708766	5.93E-06	-1.7741	0.94632
5-Mar-2004	976 #10	0.4709138	7.12E-06	-1.7766	0.94625
(cont.)	976 #11	0.4709586	6.48E-06	-1.7797	0.94616
	976 #12	0.4709583	6.62E-06	-1.7797	0.94616
	976 #13	0.4710093	6.52E-06	-1.7831	0.94605
	976 #14	0.4709997	6.13E-06	-1.7825	0.94607
	976 #15	0.4710205	6.63E-06	-1.7839	0.94603
	976 #16	0.4710587	8.05E-06	-1.7865	0.94595
	976 #17	0.4710533	7.88E-06	-1.7861	0.94597
6-Mar-2004	976 #1	0.4711897	8.17E-06	-1.7955	0.94569
	976 #2	0.4712693	8.15E-06	-1.8009	0.94553
	976 #3	0.4712857	6.77E-06	-1.8020	0.94550
	976 #4	0.4713367	9.06E-06	-1.8055	0.94540
	976 #5	0.4711357	7.52E-06	-1.7918	0.94580
	976 #6	0.4711423	6.60E-06	-1.7922	0.94579
	976 #7	0.4712494	8.12E-06	-1.7995	0.94557
	976 #8	0.4712751	7.37E-06	-1.8013	0.94552
	976 #9	0.4713107	7.42E-06	-1.8037	0.94545
	976 #10	0.4713689	7.53E-06	-1.8077	0.94533
	976 #11	0.4708822	6.88E-06	-1.7745	0.94631
	976 #12	0.4709475	8.04E-06	-1.7789	0.94618
	976 #13	0.4709865	7.79E-06	-1.7816	0.94610
	976 #14	0.4710447	6.62E-06	-1.7856	0.94598
	976 #15	0.4710610	8.95E-06	-1.7867	0.94595
	976 #16	0.4710457	7.57E-06	-1.7856	0.94598
	976 #17	0.4710145	6.96E-06	-1.7835	0.94604
	976 #18	0.4710409	6.36E-06	-1.7853	0.94599
	976 #19	0.4710259	6.80E-06	-1.7843	0.94602
	976 #20	0.4710112	6.39E-06	-1.7833	0.94605
	976 #21	0.4710090	7.80E-06	-1.7831	0.94605
	976 #22	0.4709854	7.11E-06	-1.7815	0.94610
	976 #23	0.4709959	5.93E-06	-1.7822	0.94608
	976 #24	0.4709940	7.21E-06	-1.7821	0.94608
	976 #25	0.4709856	6.59E-06	-1.7815	0.94610
	976 #26	0.4710422	6.50E-06	-1.7854	0.94599
	976 #27	0.4710409	6.71E-06	-1.7853	0.94599
	976 #28	0.4710157	7.00E-06	-1.7836	0.94604
	976 #29	0.4710353	5.60E-06	-1.7849	0.94600
1-Apr-2004	976 #2+Zn	0.4718858	6.40E-06	-1.8429	0.94430
	976 #3 +Zn	0.4718880	6.65E-06	-1.8431	0.94429
	976 #4 +Zn	0.4719149	6.40E-06	-1.8449	0.94424
	976 #5	0.4718963	4.90E-06	-1.8436	0.94428
	976 #6	0.4718586	6.23E-06	-1.8411	0.94435
	976 #7	0.4718497	6.13E-06	-1.8405	0.94437
	976 #8	0.4718249	6.77E-06	-1.8388	0.94442
	976 #9	0.4718350	6.38E-06	-1.8395	0.94440
	976 #10	0.4718128	5.27E-06	-1.8379	0.94444
	976 #11	0.4717873	6.26E-06	-1.8362	0.94449
	976 #12	0.4717496	7.94E-06	-1.8336	0.94457
	976 #13	0.4717386	7.57E-06	-1.8329	0.94459

Date	Analysis	$^{65}Cu/^{63}Cu$	Error (2σ)	β (fractionation coefficient)	Fractionation factor (exponential law)
1-Apr-2004	976 #14	0.4717612	5.48E-06	-1.8344	0.94455
(cont.)	976 #15	0.4717119	5.22E-06	-1.8311	0.94464
	976 #16	0.4717210	5.91E-06	-1.8317	0.94463
	976 #17	0.4717042	5.17E-06	-1.8305	0.94466
	976 #18	0.4716764	7.29E-06	-1.8287	0.94472
	976 #19	0.4717017	5.95E-06	-1.8304	0.94466
	976 #20	0.4716816	4.43E-06	-1.8290	0.94470
	976 #21	0.4716865	5.94E-06	-1.8293	0.94470
	976 #22	0.4716420	5.38E-06	-1.8263	0.94478
	976 #23	0.4716614	5.39E-06	-1.8276	0.94475
	976 #24	0.4716572	5.53E-06	-1.8273	0.94475
	976 #25	0.4716568	4.99E-06	-1.8273	0.94475
	976 #26	0.4716605	5.62E-06	-1.8276	0.94475
	976 #27	0.4716583	6.88E-06	-1.8274	0.94475
	976 #28	0.4716612	6.34E-06	-1.8276	0.94475
	976 #29	0.4716526	5.83E-06	-1.8270	0.94476
	976 #30	0.4716465	5.69E-06	-1.8266	0.94478
30-Sep-2004	976 #1	0.4726118	1.58E-05	-1.8924	0.94285
	976 #2	0.4727454	8.57E-06	-1.9014	0.94258
	976 #3	0.4727695	7.61E-06	-1.9031	0.94253
	976 #4	0.4727898	9.68E-06	-1.9045	0.94249
	976 #5	0.4728311	9.57E-06	-1.9073	0.94241
	976 #6	0.4728824	7.14E-06	-1.9108	0.94231
	976 #7	0.4729112	9.41E-06	-1.9127	0.94225
	976 #8	0.4729216	7.60E-06	-1.9134	0.94223
	976 #9	0.4729493	7.46E-06	-1.9153	0.94217
	976 #10	0.4729483	6.70E-06	-1.9152	0.94217
	976 #11	0.4729350	7.08E-06	-1.9143	0.94220
	976 #12	0.4729433	6.62E-06	-1.9149	0.94218
	976 #13	0.4728873	8.10E-06	-1.9111	0.94230
	976 #14	0.4729469	7.79E-06	-1.9151	0.94218
	976 #15	0.4729253	8.25E-06	-1.9137	0.94222
	976 #16	0.4729122	7.64E-06	-1.9128	0.94225
	976 #17	0.4729134	7.82E-06	-1.9129	0.94224
	976 #18	0.4728870	7.77E-06	-1.9111	0.94230
	976 #19	0.4728165	7.87E-06	-1.9063	0.94244
	976 #20	0.4727835	7.31E-06	-1.9040	0.94250
	976 #21	0.4727431	7.92E-06	-1.9013	0.94258
	976 #22	0.4727384	7.00E-06	-1.9010	0.94259
	976 #23	0.4727175	7.47E-06	-1.8995	0.94263
	976 #24	0.4726767	5.70E-06	-1.8968	0.94272
	976 #25	0.4726534	8.29E-06	-1.8952	0.94276
	976 #26	0.4726279	7.43E-06	-1.8934	0.94281
	976 #27	0.4726134	7.66E-06	-1.8925	0.94284
	976 #28	0.4726038	8.53E-06	-1.8918	0.94286
	976 #29	0.4725697	8.59E-06	-1.8895	0.94293
	976 #30	0.4725612	8.50E-06	-1.8889	0.94295
10-Jan-2005	976 #1	0.4724525	7.89E-06	-1.8815	0.94316
	976 #2	0.4724345	8.71E-06	-1.8803	0.94320
10-Jan-2005	976 #3	0.4723931	1.01E-05	-1.8775	0.94328
20-Jan-2005	976 #1	0.4722239	1.03E-05	-1.8660	0.94362
	976 #2	0.4722411	1.02E-05	-1.8671	0.94359
	976 #3	0.4722439	8.74E-06	-1.8673	0.94358
	976 #4	0.4722765	7.35E-06	-1.8695	0.94352
	976 #5	0.4722843	8.32E-06	-1.8701	0.94350
	976 #6	0.4723255	8.44E-06	-1.8729	0.94342
	976 #7	0.4723388	6.79E-06	-1.8738	0.94339
	976 #8	0.4723400	7.33E-06	-1.8739	0.94339
	976 #9	0.4724329	7.30E-06	-1.8802	0.94320
	976 #10	0.4724295	6.80E-06	-1.8799	0.94321
	976 #11	0.4725354	6.18E-06	-1.8872	0.94300
27-Jan-2005	976 #1	0.4725557		-1.8885	0.94296
	976 #2	0.4725307	1.34E-05	-1.8868	0.94301
	976 #3	0.4724772	8.98E-06	-1.8832	0.94311
	976 #4	0.4726121	1.70E-05	-1.8924	0.94285
	976 #5	0.4720939	1.81E-05	-1.8571	0.94388
	976 #6	0.4720314	1.54E-05	-1.8528	0.94401
	976 #7	0.4720101	1.58E-05	-1.8514	0.94405
1-Feb-2005	976 #1	0.4722584	1.53E-05	-1.8683	0.94355
	976 #2	0.4721739	1.40E-05	-1.8625	0.94372
	976 #3	0.4721814	1.48E-05	-1.8631	0.94371
	976 #4	0.4721410	1.31E-05	-1.8603	0.94379
	976 #5	0.4721566	1.29E-05	-1.8614	0.94375
	976 #6	0.4721692	1.08E-05	-1.8622	0.94373
	976 #7	0.4721565	1.34E-05	-1.8614	0.94375
8-Mar-2005	976 #1	0.4711011	7.41E-06	-1.7894	0.94587
	976 #2	0.4714169	7.87E-06	-1.8110	0.94524
	976 #3	0.4714581	9.76E-06	-1.8138	0.94515
	976 #4	0.4715520	9.11E-06	-1.8202	0.94496
	976 #5	0.4715852	7.61E-06	-1.8224	0.94490
	976 #6	0.4715843	7.87E-06	-1.8224	0.94490
	976 #7	0.4715980	6.59E-06	-1.8233	0.94487
	976 #8	0.4725800	7.03E-06	-1.8902	0.94291
	976 #9	0.4716402	1.41E-05	-1.8262	0.94479
	976 #10	0.4725737	7.04E-06	-1.8898	0.94292
	976 #11	0.4725749	7.42E-06	-1.8898	0.94292
	976 #12	0.4726007	6.95E-06	-1.8916	0.94287
	976 #13	0.4726251	7.07E-06	-1.8933	0.94282
	976 #14	0.4718542	9.53E-06	-1.8408	0.94436
	976 #15	0.4719403	7.35E-06	-1.8466	0.94419
	976 #16	0.4719435	7.55E-06	-1.8468	0.94418
	976 #17	0.4719350	7.87E-06	-1.8463	0.94420
	976 #18	0.4719546	8.35E-06	-1.8476	0.94416
	976 #19	0.4719291	7.29E-06	-1.8459	0.94421
	976 #20	0.4719383	8.00E-06	-1.8465	0.94419
15-Mar-2005	976 #1	0.4715753	7.29E-06	-1.8218	0.94492
	976 #2	0.4715646	6.51E-06	-1.8210	0.94494
	976 #3	0.4718552	6.38E-06	-1.8408	0.94436

Date	Analysis	$^{65}Cu/^{63}Cu$	Error (2σ)	β (fractionation coefficient)	Fractionation factor (exponential law)
15-Mar-2005	976 #4	0.4718875	6.98E-06	-1.8430	0.94429
(cont.)	976 #5	0.4719157	5.38E-06	-1.8450	0.94424
	976 #6	0.4719363	7.37E-06	-1.8464	0.94420
	976 #7	0.4719558	6.91E-06	-1.8477	0.94416
	976 #8	0.4719709	5.54E-06	-1.8487	0.94413
24-Mar-2005	976 #1	0.4714823	7.22E-06	-1.8154	0.94510
	976 #2	0.4715000	8.20E-06	-1.8166	0.94507
	976 #3	0.4715038	9.58E-06	-1.8169	0.94506
	976 #4	0.4715177	7.01E-06	-1.8178	0.94503
	976 #5	0.4715106	7.67E-06	-1.8173	0.94505
	976 #6	0.4715526	6.08E-06	-1.8202	0.94496
	976 #7	0.4715709	6.58E-06	-1.8215	0.94493
	976 #8	0.4715763	7.15E-06	-1.8218	0.94492
24-Mar-2005	976 #9	0.4715838	5.90E-06	-1.8223	0.94490
(cont.)	976 #10	0.4716108	7.67E-06	-1.8242	0.94485
	976 #11	0.4716117	6.36E-06	-1.8242	0.94485
25-Mar-2005	976 #1	0.4718112	6.86E-06	-1.8378	0.94445
	976 #2	0.4718639	8.61E-06	-1.8414	0.94434
	976 #3	0.4718882	5.52E-06	-1.8431	0.94429
	976 #4	0.4719366	8.47E-06	-1.8464	0.94419
	976 #5	0.4719440	7.34E-06	-1.8469	0.94418
	976 #6	0.4720139	7.41E-06	-1.8516	0.94404
	976 #7	0.4719865	6.52E-06	-1.8498	0.94409
	mean	0.4716060	7.96E-06	-1.8238	0.94486
		n=505		high	0.94909
				low	0.93931

Appendix 3 cont.

date	analysis	raw $^{65}Cu/^{63}Cu$	error(2σ)	$\delta^{65}Cu$ (‰)	^{65}Cu voltage	%Cu of sample relative to standard	drift between bracketing standards (ppm)
12-Apr-02	976 #1	0.4710895	6.76E-06		1.567		
	976 #2	0.4711146	5.98E-06		1.557		
	976 #3	0.4711353	7.99E-06		1.546		
	976 #4	0.4711369	6.66E-06		1.524		
	976 #5	0.4711734	6.02E-06		1.515		
	976 #6	0.4712283	7.83E-06		1.503		
	RAY-1	0.4713540	6.72E-06	0.205	1.496	99.24	140
	976 #7	0.4712942	7.68E-06		1.512		
	LS-10	0.4715311	6.63E-06	0.520	1.417	94.04	21
	976 #8	0.4713043	6.07E-06		1.502		

Appendix 3 cont

12 Apr 2002

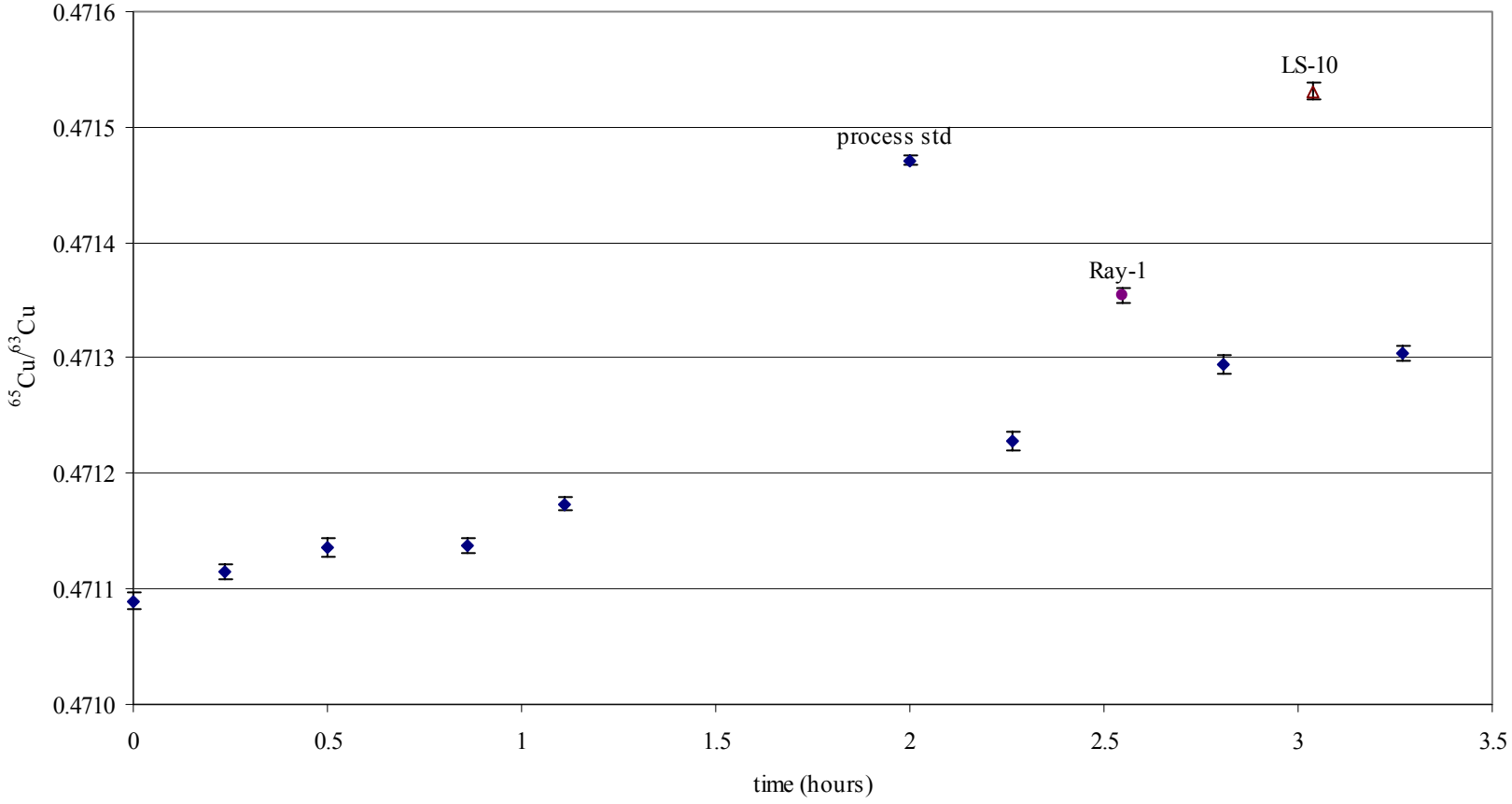

Appendix 3 cont.

date	analysis	raw $^{65}Cu/^{63}Cu$	error (2σ)	$\delta^{65}Cu$ (‰)	^{65}Cu voltage	%Cu of sample relative to standard	drift between bracketing standards (ppm)
18-Apr-02	976 #1	0.4705045	6.18E-06		1.907		
	976 #2	0.4705574	7.83E-06		1.876		
	976 #3	0.4705909	5.78E-06		1.878		
	976 #4	0.4706188	7.39E-06		1.855		
	976 #5	0.4706610	5.08E-06		1.860		
	976 #6	0.4709082	8.43E-06		1.368		
	976 #7	0.4700600	1.15E-05		2.072		
	976 #8	0.4701943	7.80E-06		2.019		
	976 #9	0.4702726	7.23E-06		2.002		
	976 #10	0.4703901	5.66E-06		1.955		
	976 #11	0.4705012	8.60E-06		1.333		
	976 #12	0.4704956	8.09E-06		1.447		
	976 #13	0.4705227	9.00E-06		1.421		
	976 #14	0.4705517	6.34E-06		1.410		
	Ray-1	0.4705885	6.18E-06	0.018	1.370	98.72	117
	976 #15	0.4706069	7.15E-06		1.365		
	LS-10	0.4707733	9.12E-06	0.356	1.292	94.06	34
	976 #16	0.4706229	5.92E-06		1.382		
	Ray-2b	0.4709625	6.76E-06	0.722	1.447	105.41	76
	976 #17	0.4706585	6.68E-06		1.363		
	Ray-2	0.4712302	5.36E-06	1.263	1.609	118.95	40
	976 #18	0.4706771	6.06E-06		1.342		
	LS-45	0.4708471	6.30E-06	0.342	1.651	123.58	76
	976 #19	0.4707127	6.79E-06		1.330		
	LS-7	0.4708590	5.78E-06	0.273	1.265	95.13	97
	976 #20	0.4707582	7.56E-06		1.329		
	LS-12	0.4708791	6.61E-06	0.256	1.454	109.74	27
	976 #21	0.4707709	6.59E-06		1.321		
	LS-48	0.4709053	6.47E-06	0.297	1.519	115.37	11
	976 #22	0.4707760	5.41E-06		1.312		
	LS-48 5%	0.4709274	4.42E-06	0.289	4.507	341.92	82
	976 #23	0.4708146	6.13E-06		1.324		
	18-365I	0.4705132	7.31E-06	-0.662	1.131	85.89	-29
	976 #24	0.4708010	6.58E-06		1.310		
	GAC-12PO	0.4707690	7.91E-06	-0.006	0.791	62.42	-128
	976 #25	0.4707406	6.14E-06		1.227		

Appendix 3 cont

18 Apr 2002

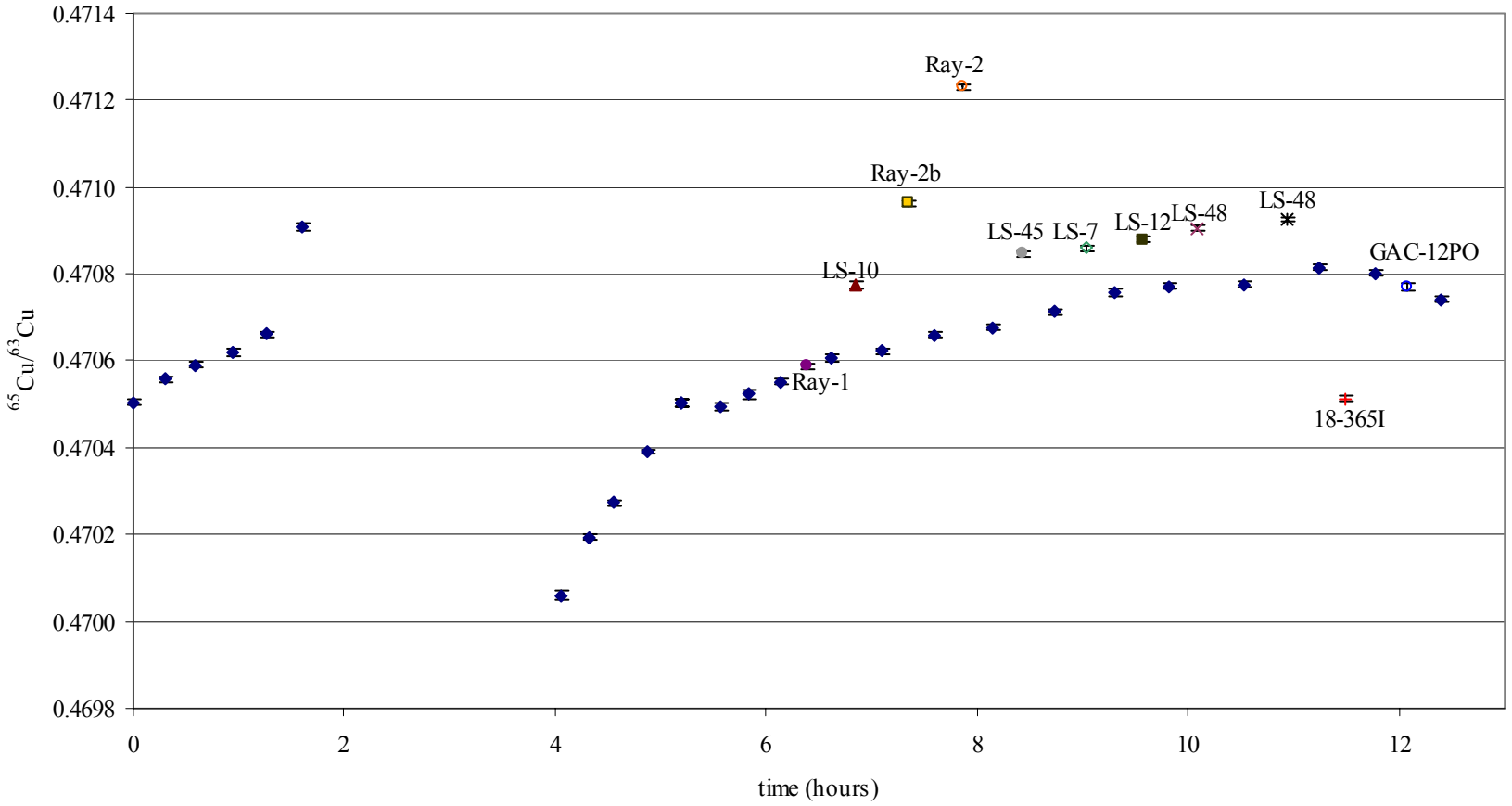

Appendix 3 cont.

date	analysis	raw $^{65}Cu/^{63}Cu$	error (2σ)	$\delta^{65}Cu$ (‰)	^{65}Cu voltage	%Cu of sample relative to standard	drift between bracketing standards (ppm)
24-Apr-02	976 #1	0.4709148	7.49E-06		1.383		
	976 #2	0.4709110	7.81E-06		1.358		
	976 #3	0.4709212	8.37E-06		1.362		
	976 #4	0.4709213	8.93E-06		1.347		
	976 #5	0.4709566	7.60E-06		1.353		
	RAY-1	0.4709808	7.67E-06	-0.004	1.305	96.22	112
	976 #6	0.4710094	6.72E-06		1.360		
	18-365I	0.4706625	6.91E-06	-0.759	1.114	82.39	-34
	976 #7	0.4709934	6.84E-06		1.345		
	GAC-12PO	0.4709616	9.90E-06	-0.065	0.831	62.25	-12
	976 #8	0.4709878	8.91E-06		1.326		
	18-365II	0.4707402	1.89E-05	-0.557	1.086	81.28	3
	976 #9	0.4709890	6.43E-06		1.346		
	17-389	0.4708852	4.19E-06	-0.201	2.678	198.64	-61
	976 #10	0.4709601	6.47E-06		1.350		
	GAC-12BD	0.4710230	8.14E-06	0.131	0.962	71.36	21
	976 #11	0.4709701	1.35E-05		1.348		
	Tajo	0.4709566	6.63E-06	-0.055	1.084	80.38	32
	976 #12	0.4709853	5.98E-06		1.351		
	T6237E-4	0.4723525	6.86E-06	3.067	1.202	88.63	2
	976 #13	0.4709864	7.47E-06		1.362		
	Chalc	0.4711477	5.99E-06	0.367	1.311	96.59	-11
	976 #14	0.4709813	6.80E-06		1.353		
	Ray-1(b)	0.4709961	8.12E-06	0.024	1.269	94.44	19
	976 #15	0.4709900	6.04E-06		1.334		
	Cu-Fe	0.4709855	8.52E-06		1.027	NIST SRM 976 (100ppb Cu) doped with 1ppm Fe	
	Cu-S	0.4709445	6.29E-06		1.403	NIST SRM 976 (100ppb Cu) doped with 9ppm S	

Appendix 3 cont

24 Apr 2002

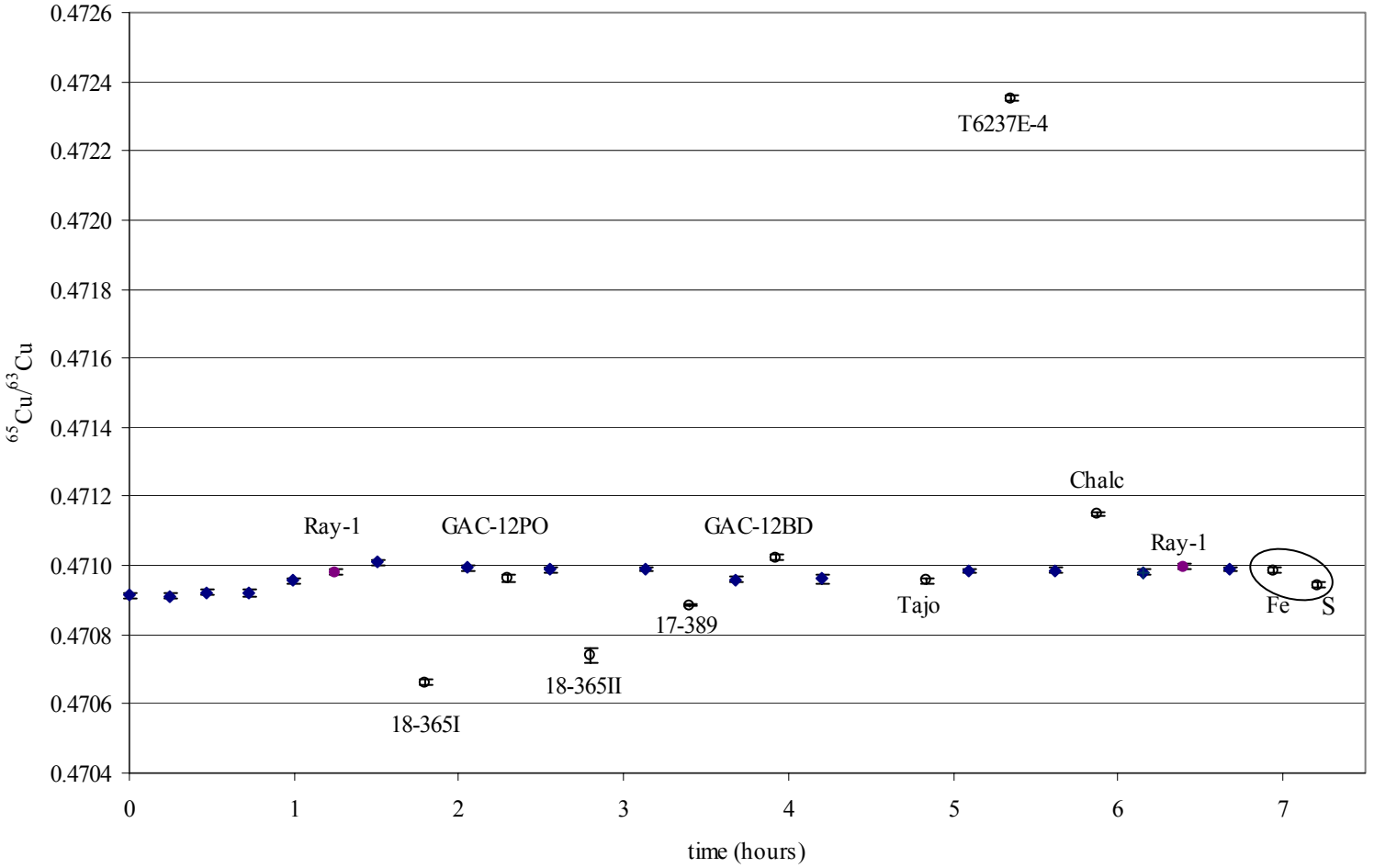

Appendix 3 cont.

date	analysis	raw $^{65}Cu/^{63}Cu$	error (2σ)	$\delta^{65}Cu$ (‰)	^{65}Cu voltage	%Cu of sample relative to standard	drift between bracketing standards (ppm)
27-Apr-02	976 #1	0.4709599	7.92E-06		1.440		
	LS-10	0.4710862	8.43E-06	0.301	1.578	108.95	-36
	976 #2	0.4709431	9.40E-06		1.457		
	LS-10 fract	0.4710864	9.44E-06	0.322	1.593	108.48	-1
	976 #3	0.4709428	7.09E-06		1.479		
	976 col1	0.4710099	7.80E-06	0.143[1]	3.403	229.12	14
	976 #4	0.4709494	6.70E-06		1.492		
	976 col2	0.4683856	2.61E-05	-5.747[1]	0.140		
	976 col3	0.4711783	2.87E-05	0.528[1]	0.088		
	976 col4	0.4711915	3.49E-05	0.564[1]	0.085		
	976 #5	0.4709370	7.21E-06		1.434		

[1]strongly chromatographically fractionated

Appendix 3 cont

27 Apr 2002

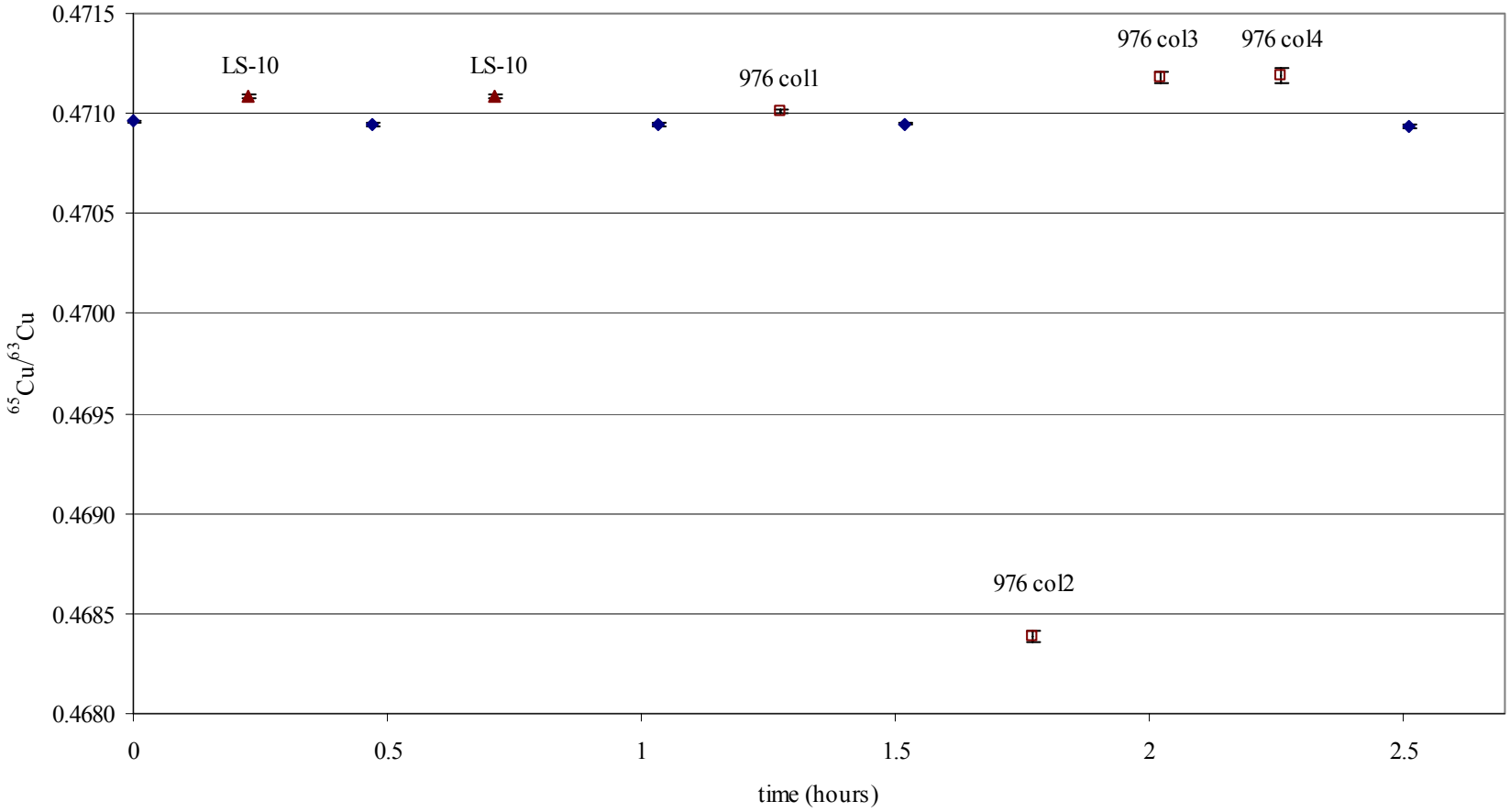

Appendix 3 cont.

date	analysis	raw $^{65}Cu/^{63}Cu$	error (2σ)	$\delta^{65}Cu$ (‰)	^{65}Cu voltage	%Cu of sample relative to standard	drift between bracketing standards (ppm)
30-Apr-02	976 #1	0.4720275	7.33E-06		1.119		
	976 #2	0.4720461	5.79E-06		1.128		
	col1	0.4743518	2.23E-05	5.186[1]	0.196		
	col2	0.4737547	5.02E-06	3.856[1]	3.451		
	col3	0.4732379	5.36E-06	2.717[1]	2.262		
	col4	0.4723982	3.64E-06	0.843[1]	5.461		
	col5	0.4708210	3.84E-06	-2.684[1]	3.472		
	col6	0.4681724	9.36E-06	-8.616[1]	0.727		
	col7	0.4661471	2.16E-05	-13.150[1]	0.158		
	col8	0.4715582	6.34E-05	-0.995[1]	0.038		
	col9	0.4723052	5.95E-05	0.691[1]	0.052		
	col10	0.4721371	7.08E-05	0.325[1]	0.032		
	976 #3	0.4719876	7.57E-06		1.105		
	976 #4	0.4719935	7.51E-06		1.097		
	976 #5	0.4721680	7.83E-06		0.986		
	976 #6	0.4721468	9.28E-06		0.994		
	LS-10	0.4722222	8.32E-06	0.270	0.974	96.54	-199
	976 #7	0.4720531	8.24E-06		1.023		
	T6237E-4	0.4733377	8.08E-06	2.951	0.956	93.32	-129
	976 #8	0.4719920	6.77E-06		1.026		
	18-365II	0.4717013	8.42E-06	-0.629	0.901	86.94	-43
	976 #9	0.4719716	6.42E-06		1.047		
	18-365I	0.4716412	7.01E-06	-0.723	0.941	89.40	-38
	976 #10	0.4719538	7.43E-06		1.057		

[1]strongly chromatographically fractionated

Appendix 3 cont

30 Apr 2002

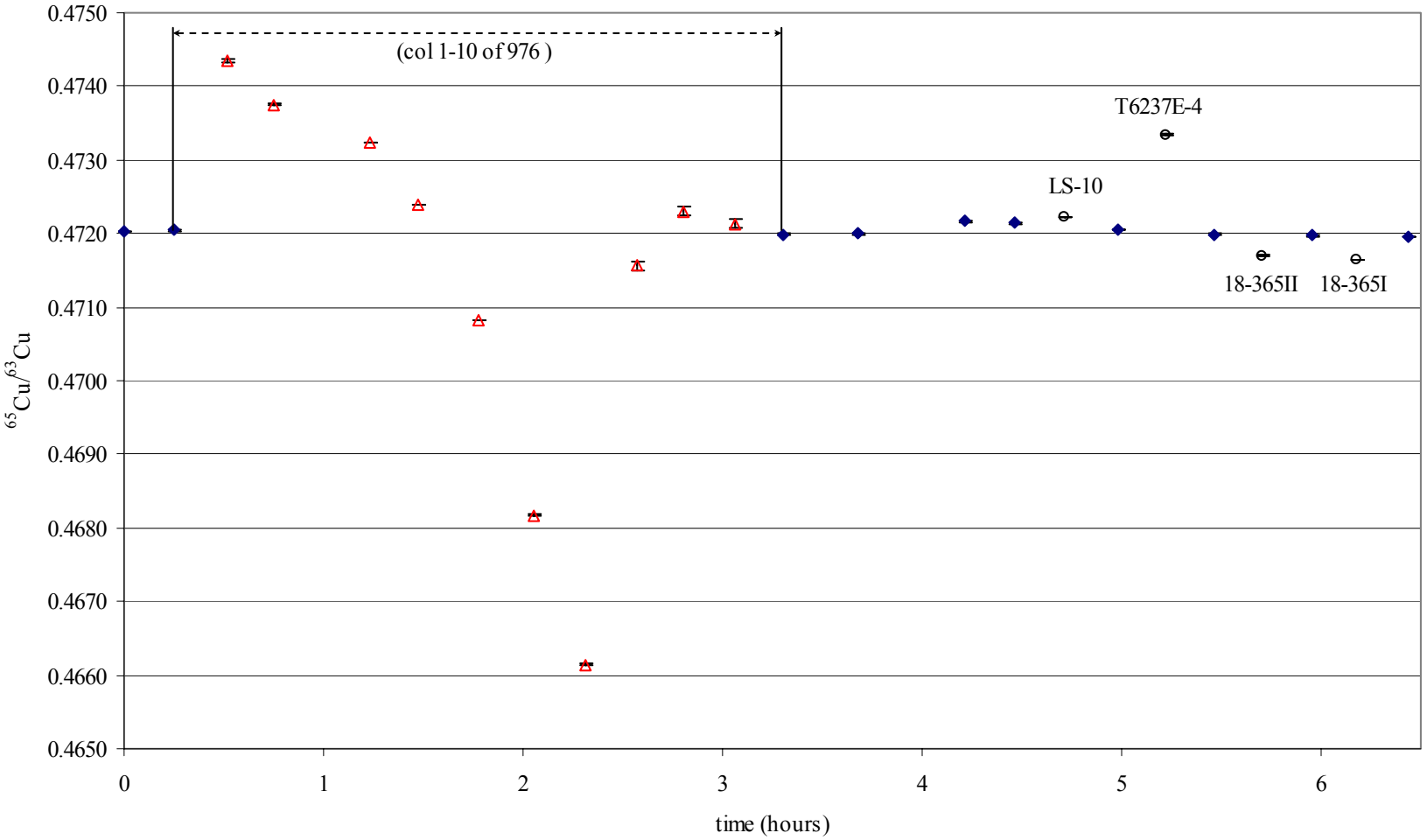

Appendix 3 cont.

date	analysis	raw $^{65}Cu/^{63}Cu$	error (2σ)	$\delta^{65}Cu$ (‰)	^{65}Cu voltage	%Cu of sample relative to standard	drift between bracketing standards (ppm)
8-May-02	976 #1	0.4716910	8.03E-06		1.377		
	976 #2	0.4716760	7.08E-06		1.402		
	976 #3	0.4716721	6.66E-06		1.402		
	976 #4	0.4716599	8.48E-06		1.398		
	976 #5	0.4717024	5.96E-06		1.407		
	976 #6	0.4716783	7.58E-06		1.369		
	976 #7	0.4716527	5.19E-06		1.349		
	976 #8	0.4716230	6.78E-06		1.329		
	Ray-1 #1	0.4716096	6.17E-06	-0.051	1.443	107.79	38
	976 #9	0.4716408	1.23E-05		1.348		
	LS-10 #1	0.4717726	6.99E-06	0.297	1.280	94.56	-3
	976 #10	0.4716394	6.47E-06		1.360		
	Mi-10	0.4713008	1.07E-05	-0.706	1.343	100.43	-94
	976 #11	0.4715950	7.60E-06		1.314		
	Mi-6	0.4711112	8.41E-06	-1.068	0.888	67.02	-32
	976 #12	0.4715797	6.84E-06		1.337		
	PL-1	0.4718786	8.66E-06	0.736	1.206	92.58	-127
	976 #13	0.4715198	9.58E-06		1.268		
	Mi-2	0.4714264	8.80E-06	-0.173	0.847	67.27	-66
	976 #14	0.4714889	8.68E-06		1.250		
	LS-46	0.4713494	8.39E-06	-0.279	1.097	88.75	-73
	976 #15	0.4714546	8.72E-06		1.222		
	LS-8	0.4715286	1.04E-05	0.243	0.824	70.34	-126
	976 #16	0.4713953	6.44E-06		1.120		
	LS-51	0.4713719	8.97E-06	0.030	0.705	65.54	-151
	976 #17	0.4713242	7.46E-06		1.032		
	RAY-1 #2	0.4712707	8.14E-06	-0.037	1.096	107.23	-163
	976 #18	0.4712472	1.01E-05		1.012		
	LS-10 #2	0.4714022	9.10E-06	0.342	0.959	97.52	10
	976 #19	0.4712519	6.81E-06		0.955		

Appendix 3 cont

8 May 2002

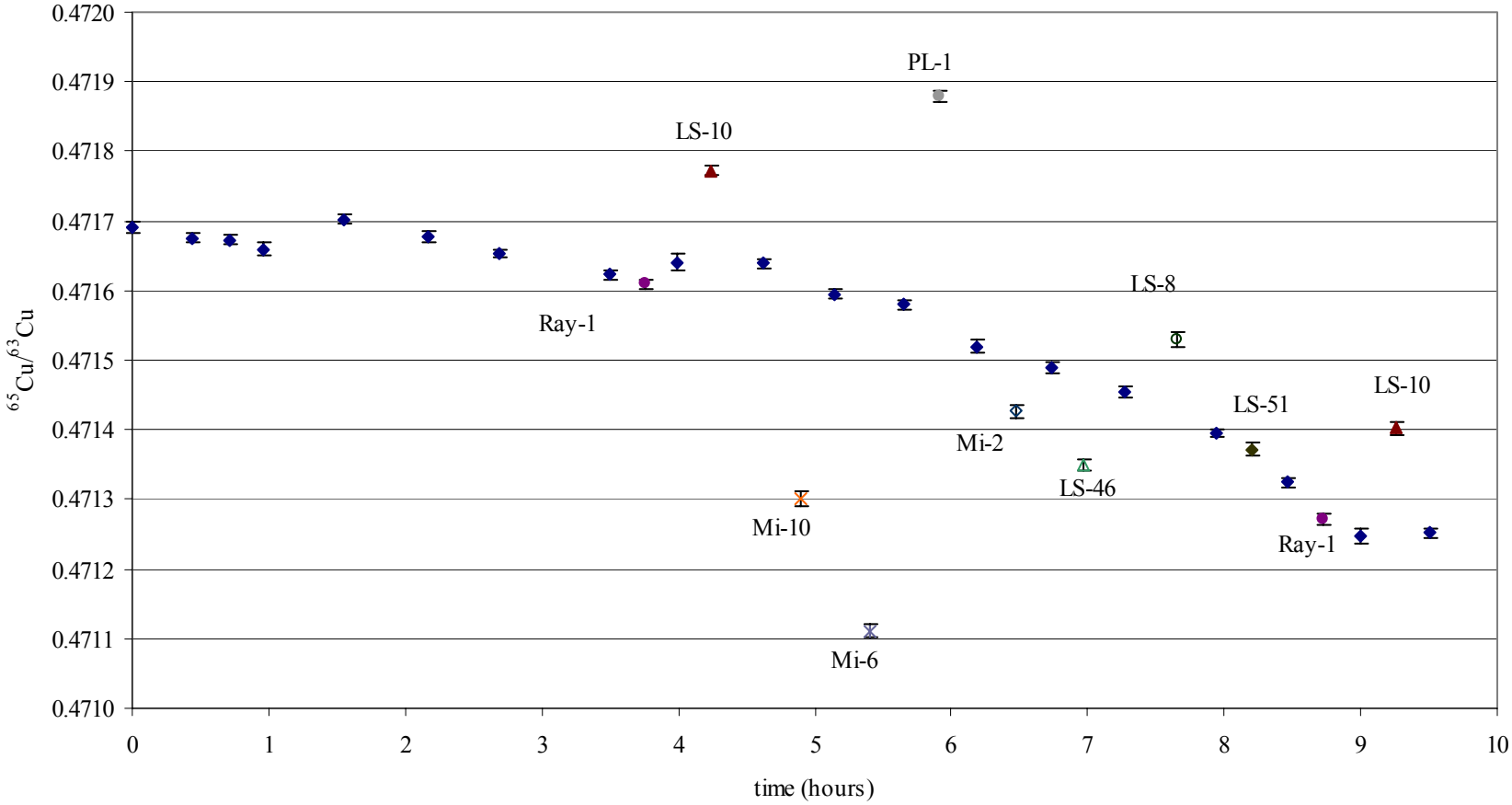

Appendix 3 cont.

date	analysis	raw $^{65}Cu/^{63}Cu$	error (2σ)	$\delta^{65}Cu$ (‰)	^{65}Cu voltage	%Cu of sample relative to standard	drift between bracketing standards (ppm)
11-May-02	976 #1	0.4712648	1.00E-05		1.449		
	976 #2	0.4712223	8.59E-06		1.429		
	976 #3	0.4711822	8.88E-06		1.383		
	976 #4	0.4711913	7.52E-06		1.351		
	976 #5	0.4711927	8.37E-06		1.382		
	Ray-1	0.4711544	9.19E-06	-0.057	1.436	106.39	-54
	976 #6	0.4711673	8.98E-06		1.318		
	LS-10	0.4712900	7.22E-06	0.294	1.291	97.18	-34
	976 #7	0.4711511	9.49E-06		1.338		
	PC-9	0.4707286	7.83E-06	-0.869	0.972	78.14	-163
	976 #8	0.4710744	8.92E-06		1.148		
	976 #10	0.4716560	7.65E-06		1.061		
	976 #11	0.4716182	7.36E-06		1.073		
	976 #12	0.4715487	7.13E-06		1.014		
	976 #13	0.4714837	8.65E-06		0.928		
	976 #14	0.4713795	9.60E-06		0.940		
	976 #15	0.4712867	8.06E-06		0.872		
	976 #16	0.4712738	8.47E-06		0.882		
	976 #17	0.4712626	9.03E-06		0.960		
	PC9 #2	0.4708490	9.45E-06	-0.747	0.883	95.57	-291
	976 #18	0.4711257	8.56E-06		0.886		
	G6	0.4709060	1.22E-05	-0.386	0.811	93.05	-197
	976 #19	0.4710327	9.73E-06		0.857		
	T6237E-4b	0.4723681	9.53E-06	2.992	0.859	95.86	10
	976 #20	0.4710373	1.13E-05		0.935		
	81-4	0.4714419	1.18E-05	0.912	0.764	81.50	-7
	976 #21	0.4710339	1.06E-05		0.939		
	SUP-1	0.4712580	9.13E-06	0.512	0.795	85.47	-17
	976 #22	0.4710259	1.03E-05		0.920		
	OKM-1	0.4721144	9.35E-06	2.443	0.913	94.70	0
	976 #23	0.4710260	1.14E-05		1.007	40 ratios	
	976 #24	0.4711319	8.61E-06		1.410		
	976 #25	0.4711319	1.09E-05		1.397		
	CCP-2	0.4707384	1.08E-05	-0.828	1.241	91.61	-101
	976 #26	0.4710843	8.42E-06		1.312		
	CCP-1	0.4708376	1.01E-05	-0.545	1.110	84.83	-17
	976 #27	0.4710765	9.06E-06		1.305		
	TL-4	0.4709543	1.10E-05	-0.248	1.075	82.85	-47
	976 #28	0.4710543	9.21E-06		1.291		
	SUP-1b	0.4712668	8.71E-06	0.548	1.153	93.01	-131
	976 #29	0.4709925	7.77E-06		1.189		
	Sd-5	0.4712343	9.24E-06	0.163	1.195	97.07	846

Appendix 3 cont.

date	analysis	raw $^{65}Cu/^{63}Cu$	error (2σ)	$\delta^{65}Cu$ (‰)	^{65}Cu voltage	%Cu of sample relative to standard	drift between bracketing standards (ppm)
11-May-02	976 #30	0.4713911	9.69E-06		1.273		
(cont.)	W4	0.4714675	8.58E-06	0.113	0.767	72.50	111
	976 #31	0.4714434	8.11E-06		0.843		
	BG1-6-600	0.4714863	8.32E-06	0.234	0.863	89.14	-257
	976 #32	0.4713224	1.95E-05		1.094		
	SW-22	0.4708585	9.31E-06	-1.041	0.873	76.85	37
	976 #33	0.4713398	6.94E-06		1.179		
	81-4b	0.4713942	8.98E-06	0.049	0.964	85.27	144
	976 #34	0.4714075	6.48E-06		1.083		
	Ray-1 #2	0.4714406	9.01E-06	0.004	1.103	104.11	135
	976 #35	0.4714710	8.84E-06		1.036		
	GAC-12 PO 2C	0.4714728	6.84E-06	-0.031	1.400	138.23	67
	976 #36	0.4715027	7.53E-06		0.989		

Appendix 3 cont

11 May 2002

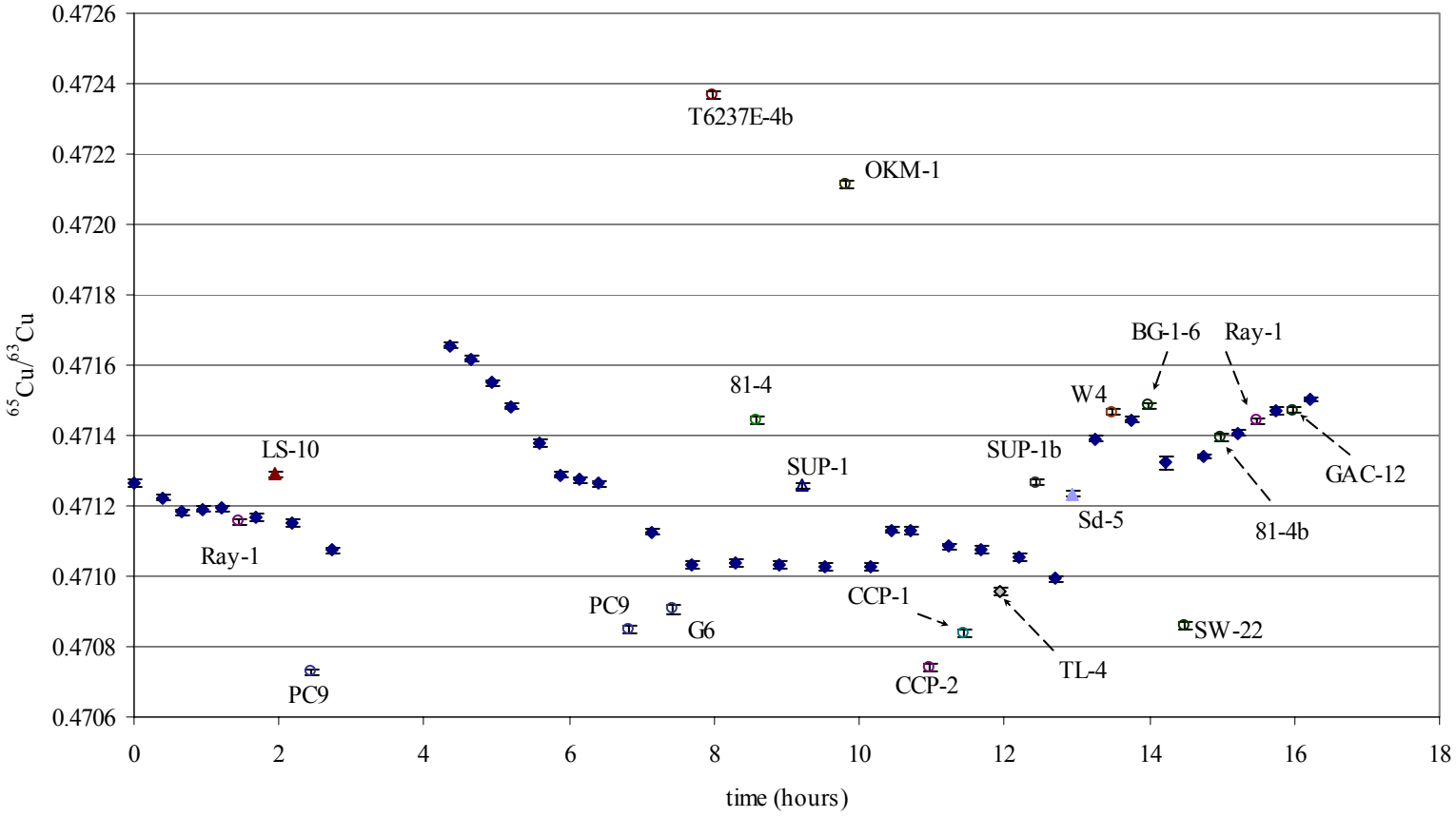

Appendix 3 cont.

date	analysis	raw $^{65}Cu/^{63}Cu$	error (2σ)	$\delta^{65}Cu$ (‰)	^{65}Cu voltage	%Cu of sample relative to standard	drift between bracketing standards (ppm)
4-Jun-02	976 #1	0.4743930	7.64E-06		0.755		
	976 #2	0.4743289	1.17E-05		0.732		
	976 #3	0.4743455	7.17E-06		0.745		
	976 #4	0.4743257	9.79E-06		0.741		
	976 #5	0.4743156	8.30E-06		0.735		
	RAY-1	0.4742778	9.81E-06	-0.078	0.750	102.20	-13
	976 #6	0.4743097	8.62E-06		0.733		
	1400 15.8 163.4	0.4744327	8.91E-06	0.307	0.619	84.62	-57
	976 #7	0.4742828	7.98E-06		0.731		
	1400 18.9 386.4a	0.4745787	1.08E-05	0.693	0.612	84.42	-54
	976 #8	0.4742572	1.02E-05		0.720		
	1400 18.9 386.4b	0.4743780	1.29E-05	0.306	0.597	83.31	-65
	976 #9	0.4742266	1.06E-05		0.714		
	LS-10	0.4743411	8.24E-06	0.268	0.651	90.87	-21
	976 #10	0.4742167	9.39E-06		0.719		
	BEAV-1	0.4748077	9.79E-06	1.362	0.623	86.49	-64
	976 #11	0.4741862	8.63E-06		0.722		
	BEAV-2	0.4746262	1.08E-05	0.999	0.605	83.28	-21
	976 #12	0.4741762	9.14E-06		0.731		
	1400 18.9 386.4c	0.4744687	1.01E-05	0.640	0.571	78.46	31
	976 #13	0.4741909	9.54E-06		0.724		
	Ferrob-1	0.4742385	8.10E-06	0.118	0.694	95.41	-21
	976 #14	0.4741809	7.72E-06		0.730		
	Ferrob-2	0.4741752	1.01E-05	0.006	0.623	85.04	-35
	976 #15	0.4741644	1.02E-05		0.736		
	TAJO-MS1	0.4742219	1.14E-05	0.112	0.632	86.26	31
	976 #16	0.4741790	1.02E-05		0.728		
	TAJO-MS2	0.4744138	1.09E-05	0.545	0.647	88.47	-33
	976 #17	0.4741635	9.53E-06		0.733		
	SUP-1	0.4743885	8.58E-06	0.518	0.618	84.32	-23
	976 #18	0.4741526	8.16E-06		0.733		
	RAY-1 #2	0.4741234	9.98E-06	-0.086	0.745	101.67	39
	976 #19	0.4741709	9.08E-06		0.732		
	PC9	0.4738060	1.17E-05	-0.794	0.666	91.05	-47
	976 #20	0.4741488	9.03E-06		0.730		
	LS-51	0.4741483	9.50E-06	0.008	0.464	63.79	-17
	976 #21	0.4741408	8.45E-06		0.726		
	BEAV-1 #2	0.4747654	9.03E-06	1.414	0.617	84.74	-23
	976 #22	0.4741299	8.44E-06		0.730		

Appendix 3 cont

4 Jun 2002

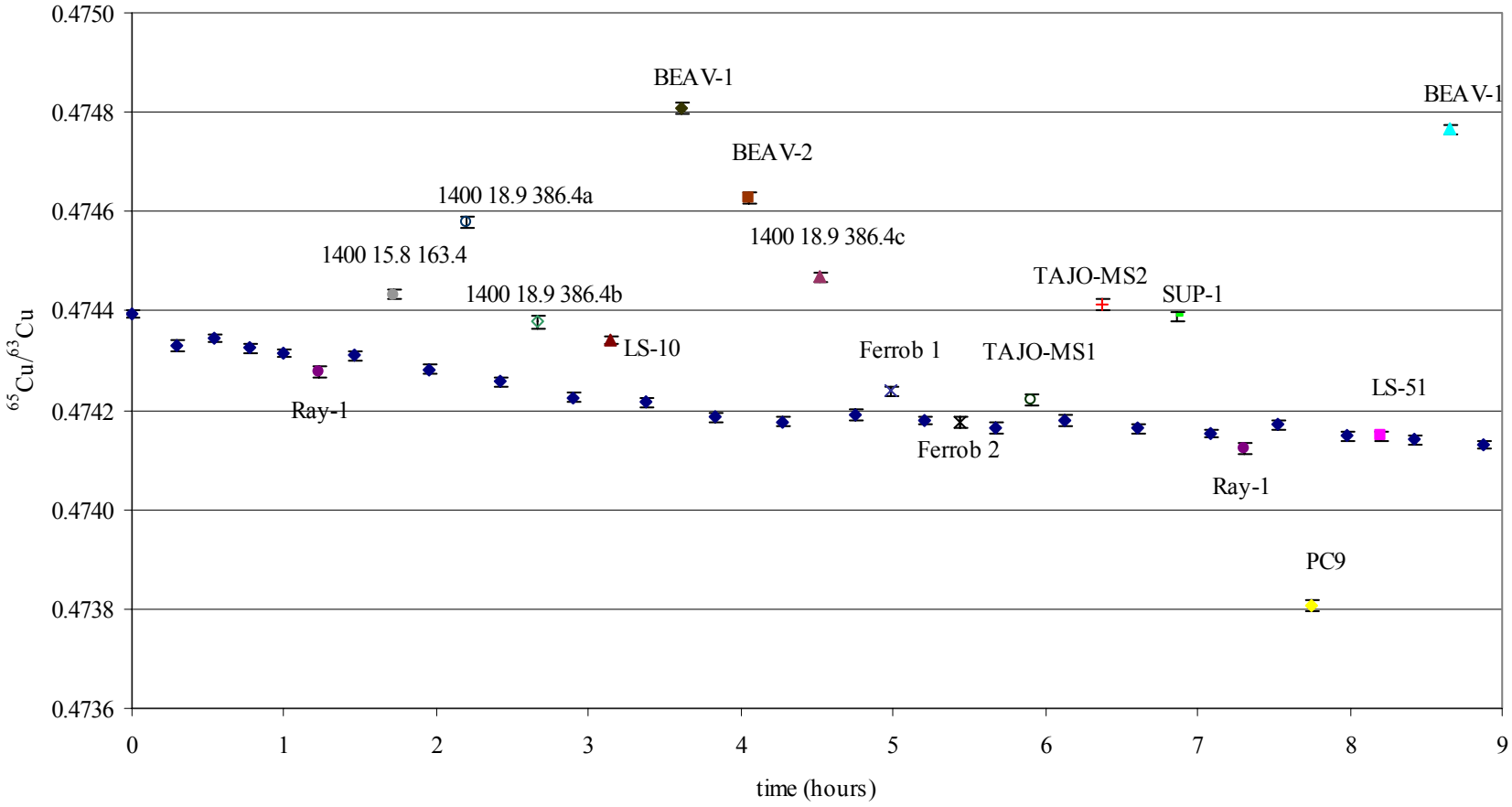

Appendix 3 cont.

date	analysis	raw $^{65}Cu/^{63}Cu$	error (2σ)	$\delta^{65}Cu$ (‰)	^{65}Cu voltage	%Cu of sample relative to standard	drift between bracketing standards (ppm)
20-Jun-02	976 #1	0.4734837	7.79E-06		0.956		
	976 #2	0.4735023	9.73E-06		0.947		
	976 #3	0.4734971	9.15E-06		0.932		
	976 #4	0.4734948	8.38E-06		0.918		
	RAY-1	0.4734544	6.23E-06	-0.092	1.068	116.14	3
	976 #5	0.4734962	9.58E-06		0.922		
	1400 21.7 119.6	0.4737247	7.63E-06	0.525	0.953	103.32	-22
	976 #6	0.4734859	8.79E-06		0.924		
	RES-2A 1885.55	0.4735121	7.71E-06	0.061	0.996	106.36	-4
	976 #7	0.4734840	7.04E-06		0.949		
	RES-2A 1927	0.4735082	7.22E-06	0.028	0.965	101.55	49
	976 #8	0.4735074	7.87E-06		0.951		
	1400 21.7 416.95	0.4736617	1.20E-05	0.274	0.899	95.69	141
	976 #9	0.4735740	7.74E-06		0.927		
	900 14.8 388.7a	0.4735811	8.10E-06	0.000	0.937	100.74	30
	976 #10	0.4735884	8.07E-06		0.934		
	900 14.8 388.7b	0.4733809	9.09E-06	-0.457	0.973	104.36	-17
	976 #11	0.4735803	8.60E-06		0.932		
	1400 18.9 301.95	0.4736091	1.01E-05	0.071	0.654	70.47	-12
	976 #12	0.4735748	8.22E-06		0.926		
	1400 16.8 250.8	0.4735254	7.00E-06	-0.109	0.797	85.92	-4
	976 #13	0.4735730	8.14E-06		0.931		
	LS-10	0.4736763	7.73E-06	0.223	0.947	101.44	15
	976 #14	0.4735803	7.08E-06		0.937		
	1400 18.9 387.9	0.4737246	7.17E-06	0.321	0.959	102.27	5
	976 #15	0.4735828	7.38E-06		0.939		
	S22-A 969	0.4738145	9.69E-06	0.534	0.710	75.92	-26
	976 #16	0.4735703	9.27E-06		0.931		
	S27-A 1847	0.4737504	8.55E-06	0.405	0.937	100.69	-1
	976 #17	0.4735699	8.10E-06		0.931		
	CHALC-MAGN1	0.4736506	6.65E-06	0.166	0.887	94.85	27
	976 #18	0.4735828	8.59E-06		0.939		
	1300 16.1 208.65	0.4735470	8.17E-06	-0.057	0.872	93.77	-43
	976 #19	0.4735622	7.62E-06		0.921		
	SUP-1	0.4738045	7.76E-06	0.542	0.892	96.75	3
	976 #20	0.4735638	7.51E-06		0.924		

Appendix 3 cont

20 Jun 2002

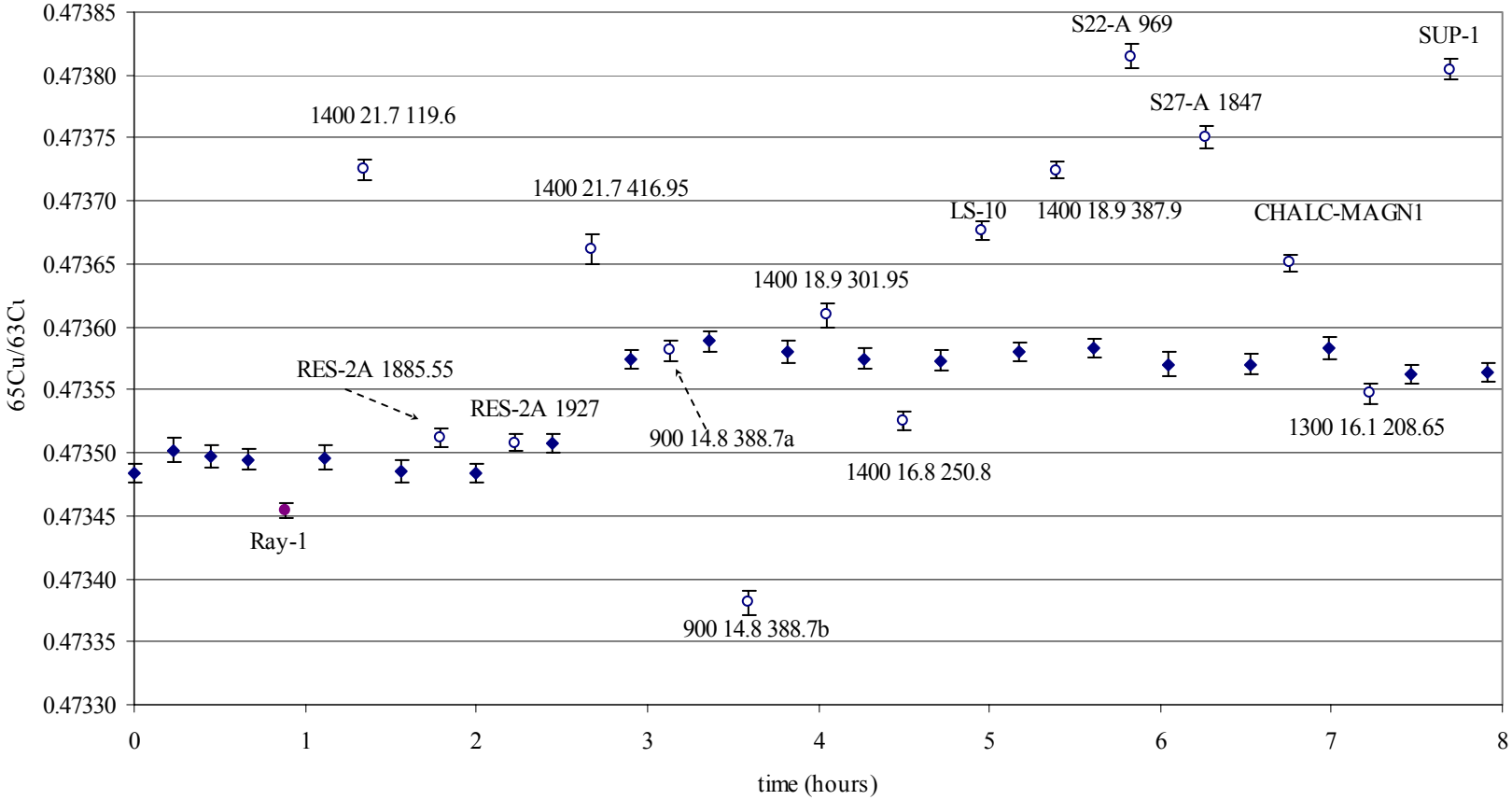

Appendix 3 cont.

date	analysis	raw $^{65}Cu/^{63}Cu$	error (2σ)	$\delta^{65}Cu$ (‰)	^{65}Cu voltage	%Cu of sample relative to standard	drift between bracketing standards (ppm)
23-Nov-02	976 #1	0.4706402	1.41E-05		1.321		
	976 #2	0.4706581	9.42E-06		1.320		
	976 #3	0.4706568	1.28E-05		1.299		
	976 #4	0.4706544	8.99E-06		1.311		
	976 #5	0.4706529	1.23E-05		1.305		
	Ray-1	0.4706462	1.02E-05	-0.057	1.737	131.29	74
	976 #6	0.4706879	1.28E-05		1.342		
	S27-A 1847	0.4708750	9.48E-06	0.449	3.293	248.64	-59
	976 #7	0.4706602	1.41E-05		1.307		
	976 #8	0.4706292	8.70E-06		1.331		
	S27-A 1847 col2	0.4708172	8.69E-06	0.428	2.075	156.16	-11
	976 #9	0.4706241	9.72E-06		1.326		
	1300 16.1 208.65	0.4706048	8.34E-06	-0.043	1.394	104.85	-1
	976 #10	0.4706235	9.09E-06		1.334		
	1300 col2	0.4705543	8.38E-06	-0.151	1.949	146.38	-8
	976 #11	0.4706199	7.95E-06		1.330		
	976 #12	0.4705756	8.01E-06		1.349		
	1300 col1	0.4720115	6.56E-06	3.226[1]	2.611	192.39	-7
	976 #13	0.4705723	9.14E-06		1.365		
	S27-A 1847 col1	0.4736547	7.54E-06	6.936[1]	1.965	144.32	-29
	976 #14	0.4705586	8.63E-06		1.357		
	1300 col3	0.4646913	8.22E-06	-13.187[1]	1.283	94.62	29
	976 #15	0.4705722	8.20E-06		1.355		
	S27-A 1847 col3	0.4615544	2.59E-05	-20.235[1]	0.330	24.31	-5
	976 #16	0.4705698	7.92E-06		1.357		
	T6237E-4c	0.4718627	8.07E-06	2.920	1.386	101.56	-34
	976 #17	0.4705537	8.53E-06		1.372		
	T440N255E	0.4704455	7.70E-06	-0.197	1.349	98.94	-85
	976 #18	0.4705136	7.84E-06		1.356		
	T448N268E	0.4705440	7.70E-06	0.072	1.607	117.45	-7
	976 #19	0.4705101	7.47E-06		1.380		

[1]strongly chromatographically fractionated

Appendix 3 cont

23 Nov 2002

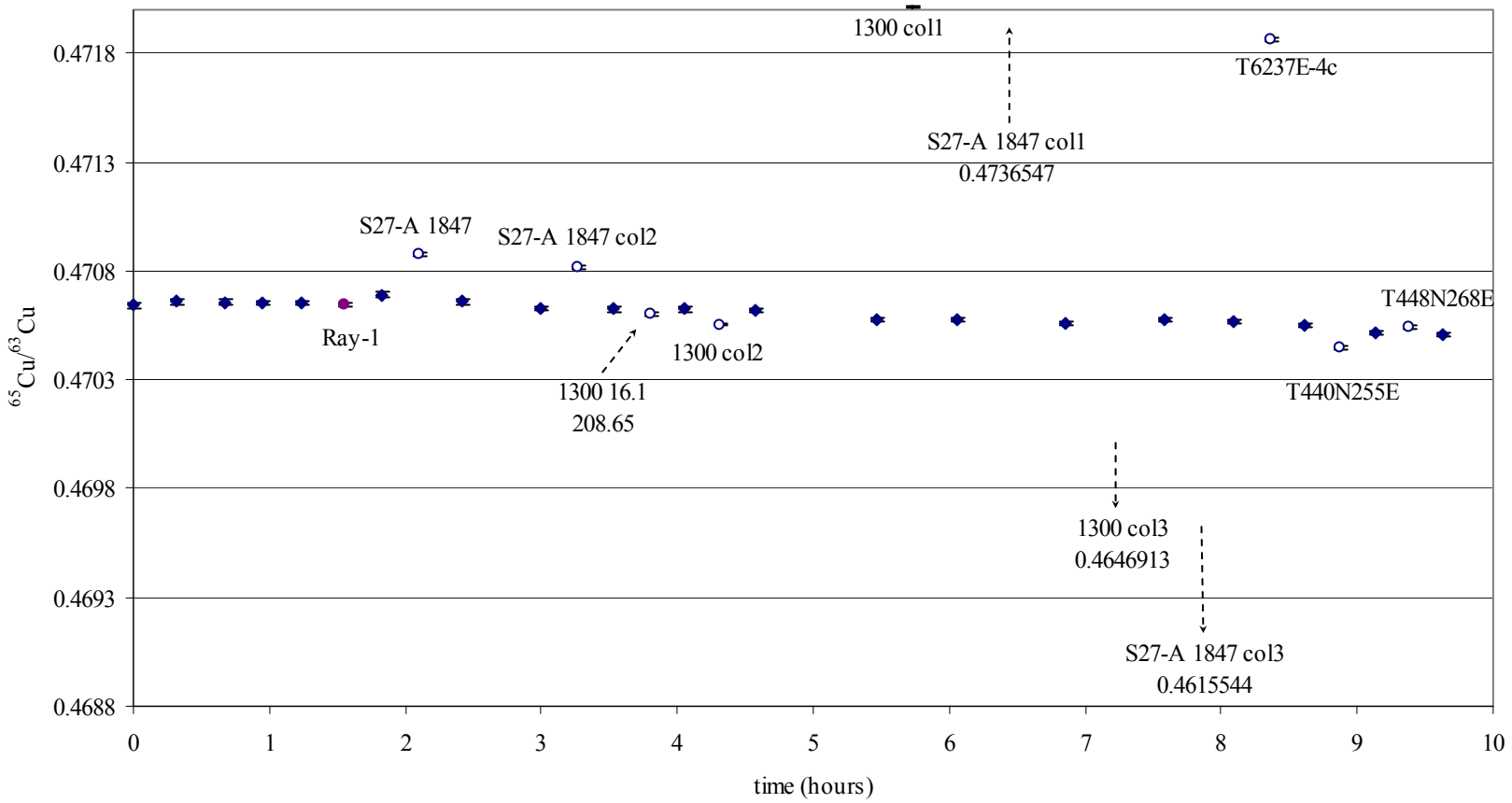

Appendix 3 cont.

date	analysis	raw $^{65}Cu/^{63}Cu$	error (2σ)	$\delta^{65}Cu$ (‰)	^{65}Cu voltage	%Cu of sample relative to standard	drift between bracketing standards (ppm)
30-Jan-03	976 #2	0.4725574	9.68E-06		1.090		
	976 #3	0.4725568	1.08E-05		1.089		
	976 #4	0.4725466	1.06E-05		1.088		
	Ray-1	0.4725011	1.05E-05	-0.100	1.384	127.43	-4
	976 #5	0.4725449	8.32E-06		1.084		
	LS-10	0.4726494	8.46E-06	0.225	1.223	112.48	17
	976 #6	0.4725531	9.93E-06		1.091		
	S27-A 1847	0.4727524	9.10E-06	0.454	1.253	114.58	-13
	976 #7	0.4725469	7.25E-06		1.096		
	S27-A col2	0.4748673	8.86E-06	5.213[1]	1.376	125.57	-11
	976 #8	0.4725417	9.73E-06		1.096		
	S27-A col3	0.4733192	9.11E-06	1.737[1]	3.441	312.85	14
	976 #9	0.4725485	7.81E-06		1.104		
	S27-A col4	0.4714196	7.94E-06	-2.505[1]	1.303	117.93	-54
	976 #10	0.4725229	9.83E-06		1.105		
	S27-A col5	0.4674094	8.42E-06	-11.428[1]	3.169	286.29	-90
	976 #11	0.4724803	8.63E-06		1.109		
	S27-A 1847 #2	0.4727172	7.82E-06	0.527	1.278	115.06	9
	976 #12	0.4724847	9.42E-06		1.113		

[1]strongly chromatographically fractionated

Appendix 3 cont

30 Jan 2003

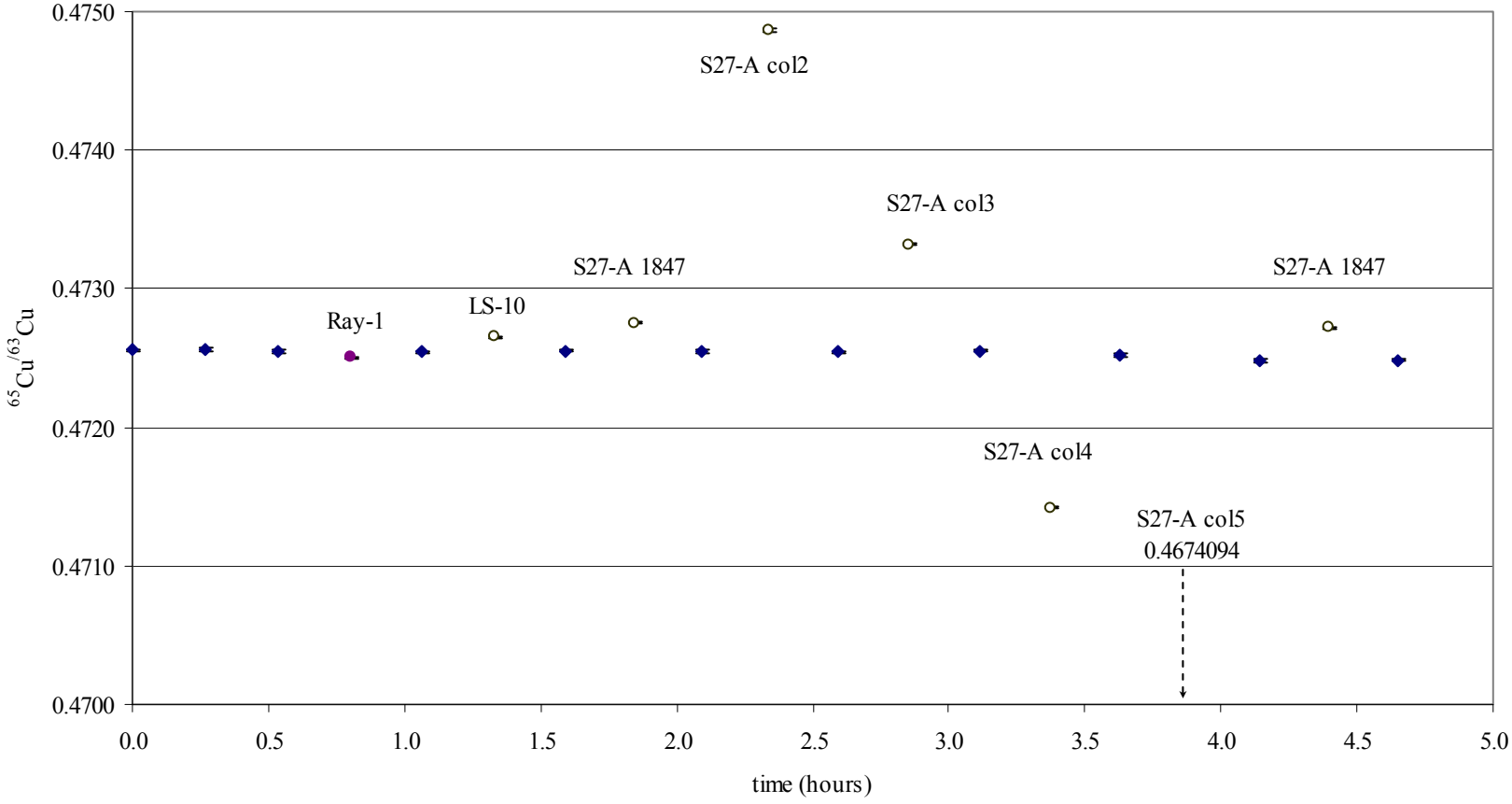

Appendix 3 cont.

date	analysis	raw $^{65}Cu/^{63}Cu$	error (2σ)	$\delta^{65}Cu$ (‰)	^{65}Cu voltage	%Cu of sample relative to standard	drift between bracketing standards (ppm)
1-Feb-03	976 #1	0.4716524	7.16E-06		1.127		
	976 #2	0.4717322	1.33E-05		1.147		
	976 #3	0.4717907	1.19E-05		1.174		
	976 #4	0.4718807	8.14E-06		1.198		
	976 #5	0.4718178	1.08E-05		1.134		
	976 #6	0.4718326	9.26E-06		1.132		
	Ray-1	0.4717762	7.55E-06	-0.121	1.436	127.64	-11
	976 #7	0.4718276	9.75E-06		1.117		
	1300 16.1	0.4718474	1.04E-05	0.008	1.155	103.09	70
	976 #8	0.4718604	8.17E-06		1.123		
	1300 col1	0.4726594	1.23E-05	1.818[1]	1.733	153.85	-46
	976 #9	0.4718387	1.09E-05		1.130		
	1300 col2	0.4717427	8.26E-06	-0.203[1]	2.877	253.77	-23
	976 #10	0.4718276	9.64E-06		1.138		
	1300 col3	0.4702833	9.21E-06	-3.504[1]	1.247	108.87	71
	976 #11	0.4718613	1.11E-05		1.153		
	1300 col4	0.4683505	8.23E-06	-7.822[1]	2.158	188.56	-107
	976 #12	0.4718107	9.64E-06		1.136		
	1300 16.1 #2	0.4717958	7.90E-06	-0.060	1.172	102.69	46
	976 #13	0.4718325	8.82E-06		1.146		

[1]strongly chromatographically fractionated

Appendix 3 cont

1 Feb 2003

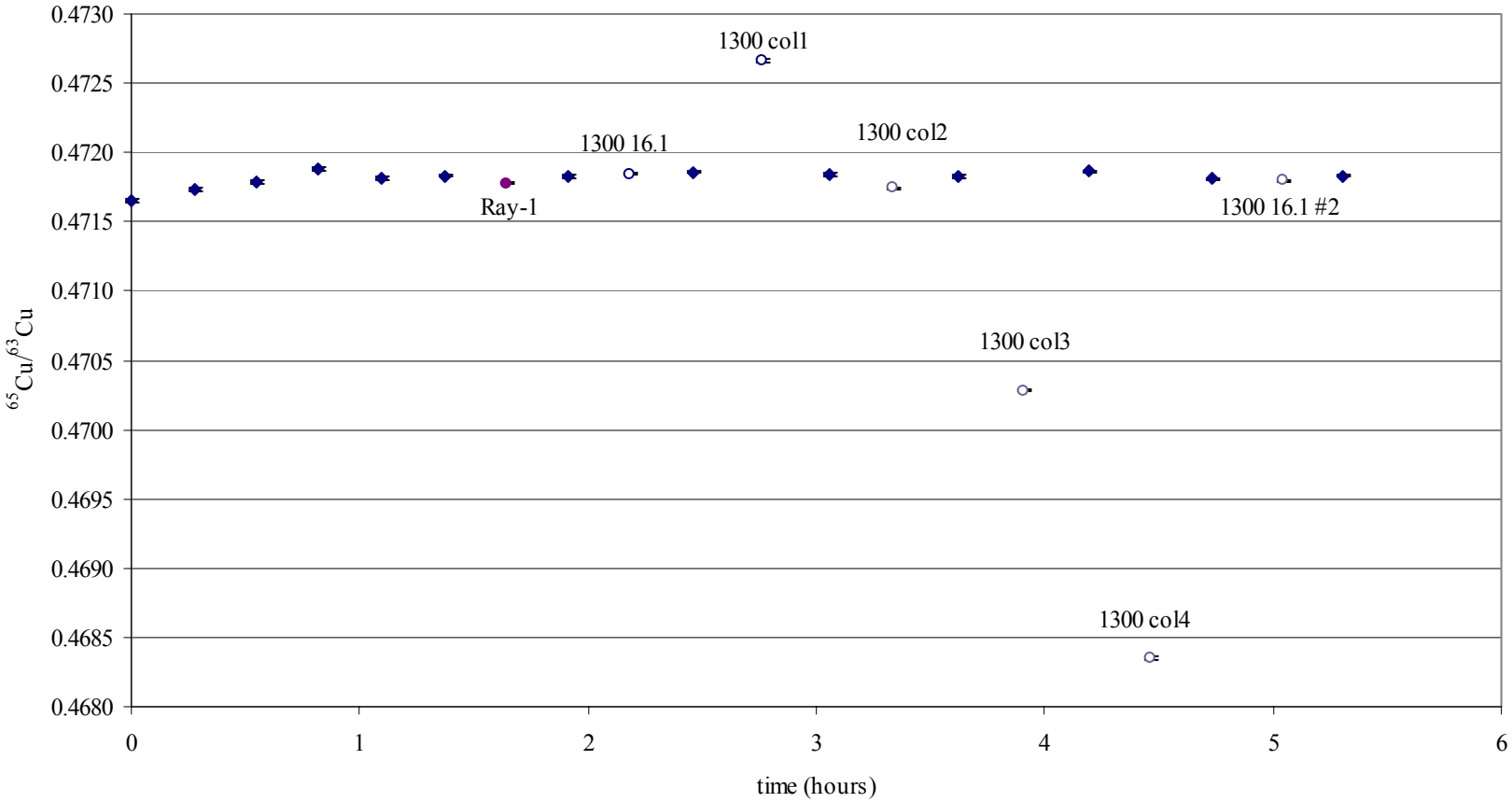

Appendix 3 cont.

date	analysis	raw $^{65}Cu/^{63}Cu$	error (2σ)	$\delta^{65}Cu$ (‰)	^{65}Cu voltage	%Cu of sample relative to standard	drift between bracketing standards (ppm)
3-Feb-03	976 #1	0.4716785	8.24E-06		1.245		
	976 #2	0.4716809	1.04E-05		1.232		
	976 #3	0.4716930	1.01E-05		1.232		
	976 #4	0.4717077	7.30E-06		1.231		
	Ray-1	0.4717187	7.64E-06	-0.030	1.580	127.01	101
	976 #5	0.4717554	7.56E-06		1.257		
	1400 14.5 313.3	0.4717543	8.89E-06	0.155	1.540	122.95	-287
	976 #6	0.4716202	9.11E-06		1.249		
	1400 15.8 246.86	0.4716235	1.04E-05	0.048	1.389	110.64	-75
	976 #7	0.4715850	1.15E-05		1.262		
	LS-10	0.4716706	7.64E-06	0.187	1.402	111.01	9
	976 #8	0.4715894	7.91E-06		1.263		
	STILLJM-1	0.4714959	8.46E-06	-0.314	1.163	92.71	198
	976 #9	0.4716826	9.73E-06		1.246		
	976 #10	0.4713409	7.62E-06		1.325		
	STILLJM-1 #2	0.4712466	6.39E-06	-0.184	1.218	91.63	-54
	976 #11	0.4713156	7.05E-06		1.333		
	T982N042E	0.4712974	8.92E-06	0.014	1.344	100.64	-103
	976 #12	0.4712673	8.90E-06		1.337		
	T990N080E	0.4710580	7.52E-06	-0.425	1.293	96.83	-84
	976 #13	0.4712276	9.74E-06		1.333		
	1400 16.1 147.35	0.4712592	7.48E-06	0.069	1.272	94.63	5
	976 #14	0.4712297	7.76E-06		1.355		
	1400 17.7 322.6A	0.4716146	7.91E-06	0.711	1.591	112.53	289
	976 #15	0.4713660	6.84E-06		1.473		
	1400 17.7 322.6A #2	0.4716571	7.26E-06	0.673	1.632	110.92	-38
	976 #16	0.4713482	6.04E-06		1.471		
	1400 17.7 322.6B	0.4714385	6.23E-06	0.238	2.908	198.36	-65
	976 #17	0.4713177	9.16E-06		1.461		

Appendix 3 cont

3 Feb 2003

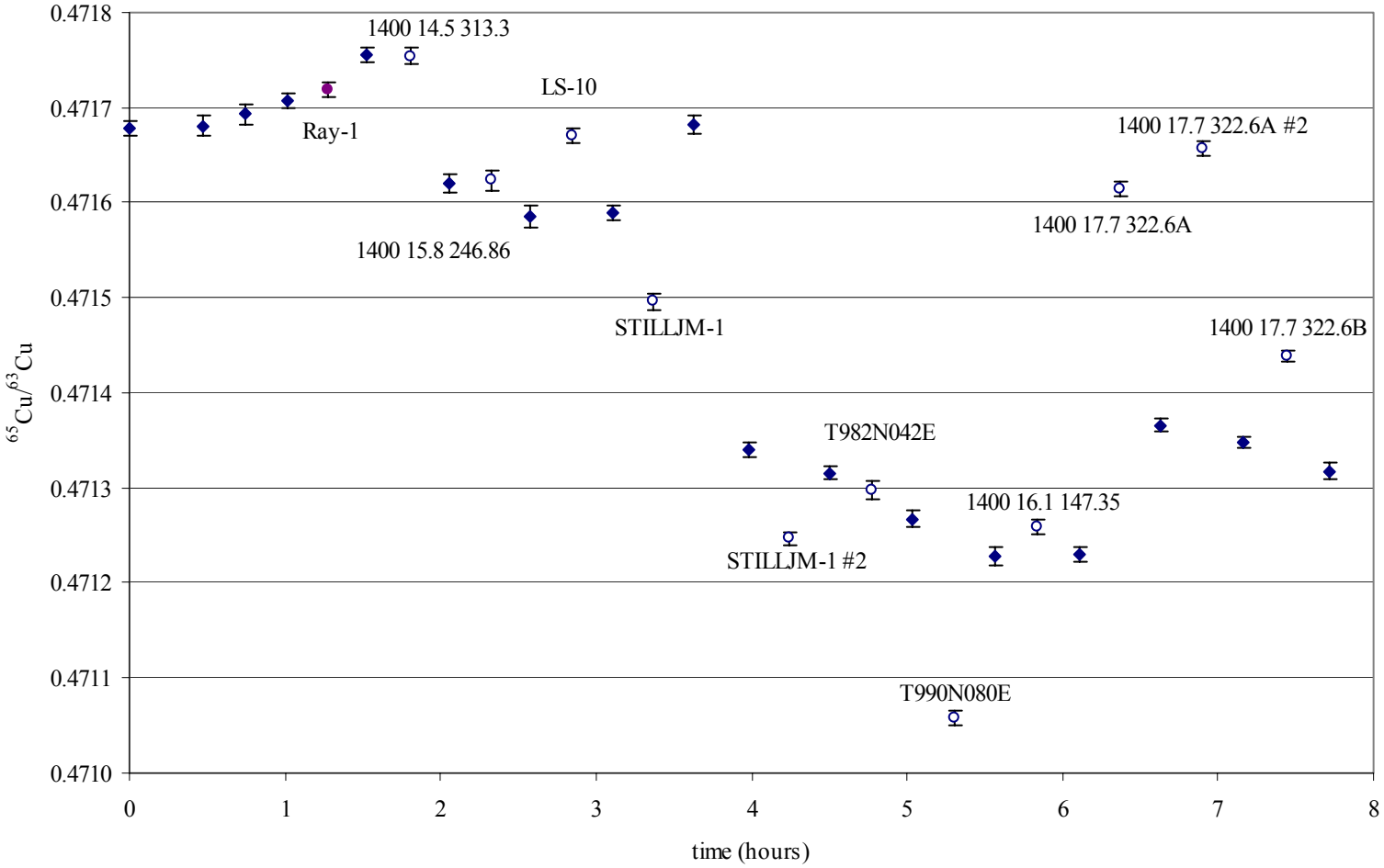

Appendix 3 cont.

date	analysis	raw $^{65}Cu/^{63}Cu$	error (2σ)	$\delta^{65}Cu$ (‰)	^{65}Cu voltage	%Cu of sample relative to standard	drift between bracketing standards (ppm)
20-Feb-03	976 #1	0.4720679	2.25E-05		1.157		
	976 #2	0.4721576	1.85E-05		1.148		
	976 #3	0.4721693	1.58E-05		1.138		
	976 #4	0.4721478	1.16E-05		1.148		
	976 #5	0.4721653	1.15E-05		1.158		
	Ray-1	0.4721040	8.35E-06	-0.106	1.464	125.66	-60
	976 #6	0.4721372	1.06E-05		1.172		
	976 Nsoln	0.4721075	9.05E-06	-0.037	1.244	105.36	-58
	976 #7	0.4721100	1.06E-05		1.189		
	1400 16.1 241.6A	0.4722891	8.60E-06	0.453	0.949	79.38	-95
	976 #8	0.4720654	8.46E-06		1.201		
	976 Nsoln#2	0.4720548	7.33E-06		1.260		
	1400 16.1 241.6B	0.4721206	9.63E-06	0.101	0.890	70.35	90
	976 #9	0.4720972	6.51E-06		1.272		
	1400 18.9 376.5A	0.4720435	7.32E-06	-0.016	1.284	101.84	-201
	976 #10	0.4720026	8.82E-06		1.251		
	1400 18.9 376.5A#2	0.4718299	1.13E-05	-0.291	1.211	97.51	-182
	976 #11	0.4719166	7.67E-06		1.233		
	1400 18.9 376.5A#3	0.4718986	8.67E-06	-0.040	1.254	102.00	-1
	976 #12	0.4719162	8.39E-06		1.226		
	1400 18.9 376.5B	0.4717188	8.81E-06	-0.403	1.383	112.89	-76
	976 #13	0.4718805	9.24E-06		1.225		
	1400 15.8 248.6	0.4721630	9.48E-06	0.646	1.156	93.33	-23
	976 #14	0.4718694	1.20E-05		1.251		
	1400 18.9 356.9	0.4717553	9.46E-06	-0.144	1.453	117.52	-288
	976 #15	0.4717335	1.89E-05		1.221		

Appendix 3 cont

20 Feb 2003

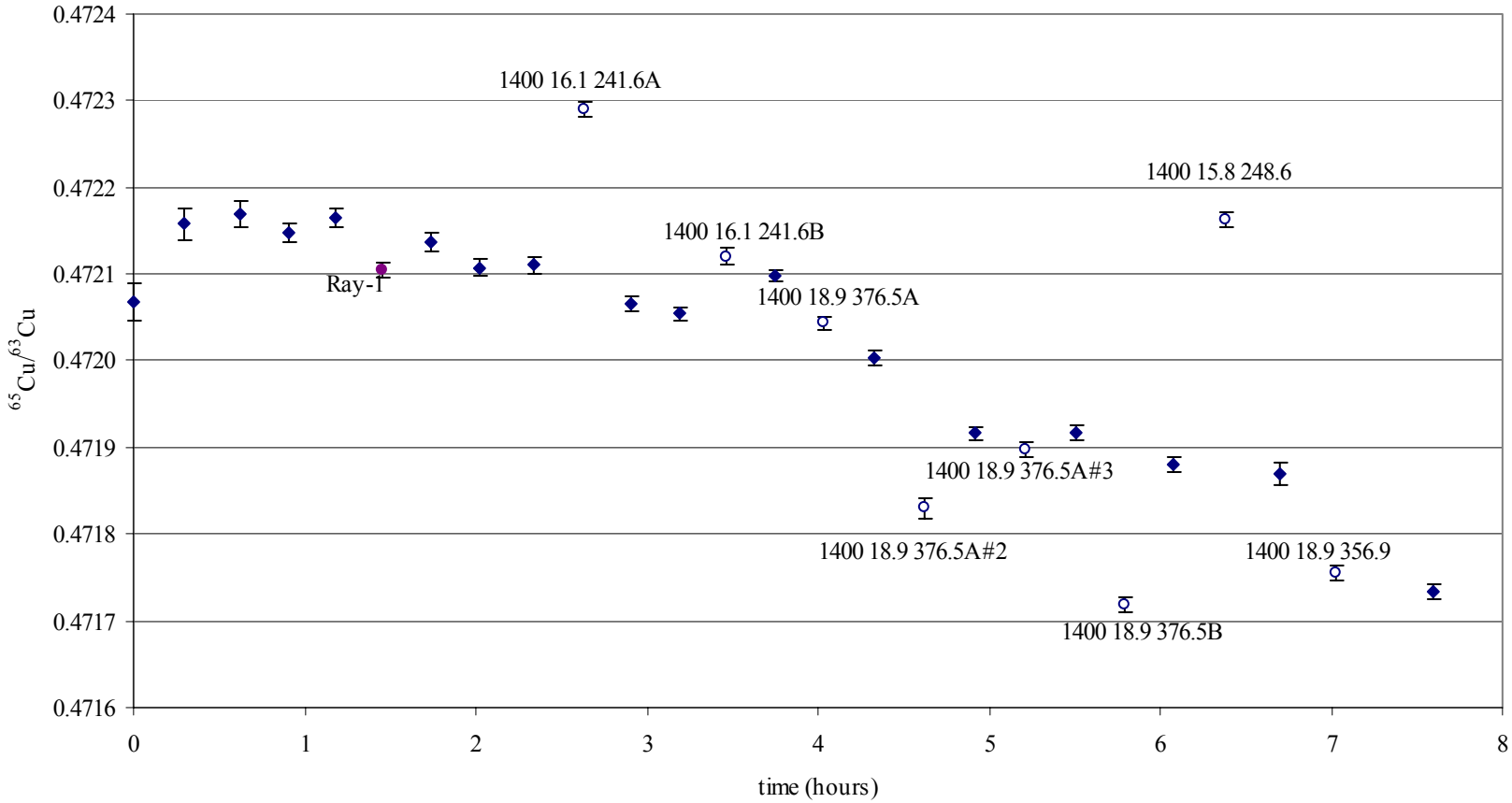

Appendix 3 cont.

date	analysis	raw $^{65}Cu/^{63}Cu$	error (2σ)	$\delta^{65}Cu$	^{65}Cu voltage	%Cu of sample relative to standard	drift between bracketing standards (ppm)
21-Apr-03	976 #1	0.4712564	6.89E-06		1.531		
	976 #2	0.4712281	6.34E-06		1.515		
	976 #3	0.4712299	5.56E-06		1.512		
	976 #4	0.4712299	7.11E-06		1.500		
	RAY-1	0.4711891	5.84E-06	-0.080	1.730	116.52	-22
	976 #5	0.4712197	6.52E-06		1.470		
	LS-10	0.4713503	7.37E-06	0.248	1.503	102.14	89
	976 #6	0.4712615	5.98E-06		1.474		
	SUP-2b	0.4713001	6.11E-06	0.060	1.544	104.84	51
	976 #7	0.4712857	5.66E-06		1.471		
	976 #8	0.4712609	6.09E-06		1.448		
	C-722-51	0.4712248	5.94E-06	-0.078	2.351	165.58	-6
	976 #9	0.4712583	7.36E-06		1.392		
	192-56	0.4712758	5.75E-06	0.032	1.497	108.07	14
	976 #10	0.4712649	5.53E-06		1.378		
	PAN-1	0.4712345	6.10E-06	-0.038	2.887	210.25	-61
	976 #11	0.4712361	6.71E-06		1.368		
	976 #12	0.4710815	5.96E-06		1.462		
	976 #13	0.4711472	6.91E-06		1.408		
	204-197	0.4712599	8.45E-06	0.271	1.058	76.05	-32
	976 #14	0.4711322	6.05E-06		1.373		
	204-402	0.4710889	7.00E-06	-0.079	1.333	96.81	-34
	976 #15	0.4711160	6.77E-06		1.381		
	204-418	0.4711816	9.31E-06	0.160	0.803	58.55	-24
	976 #16	0.4711045	7.18E-06		1.363		
	194-82	0.4712499	7.12E-06	0.292	1.221	89.45	65
	976 #17	0.4711352	6.82E-06		1.366		
	203-350	0.4712230	7.18E-06	0.201	1.454	106.51	-8
	976 #18	0.4711313	7.62E-06		1.364		
	216-485	0.4712564	7.25E-06	0.290	1.333	97.95	-18
	976 #19	0.4711226	6.63E-06		1.358		
	215-448	0.4709224	8.40E-06	-0.433	1.391	102.08	-30
	976 #20	0.4711086	6.74E-06		1.367		
	SFRAN-1	0.4712329	8.27E-06	0.232	1.328	97.33	89
	976 #21	0.4711503	6.70E-06		1.363		
	NC-5	0.4712058	6.44E-06	0.123	1.438	105.46	3
	976 #22	0.4711516	7.20E-06		1.365		
	D563-C	0.4710983	6.92E-06	-0.090	1.337	98.35	-58
	976 #23	0.4711244	8.35E-06		1.354		
	C-727-166	0.4711460	6.97E-06	0.023	1.346	99.26	47
	976 #24	0.4711467	7.46E-06		1.358		
	C-600-173	0.4711888	1.08E-05	0.089	0.700	51.60	9
	976 #25	0.4711511	6.17E-06		1.354		

Appendix 3 cont

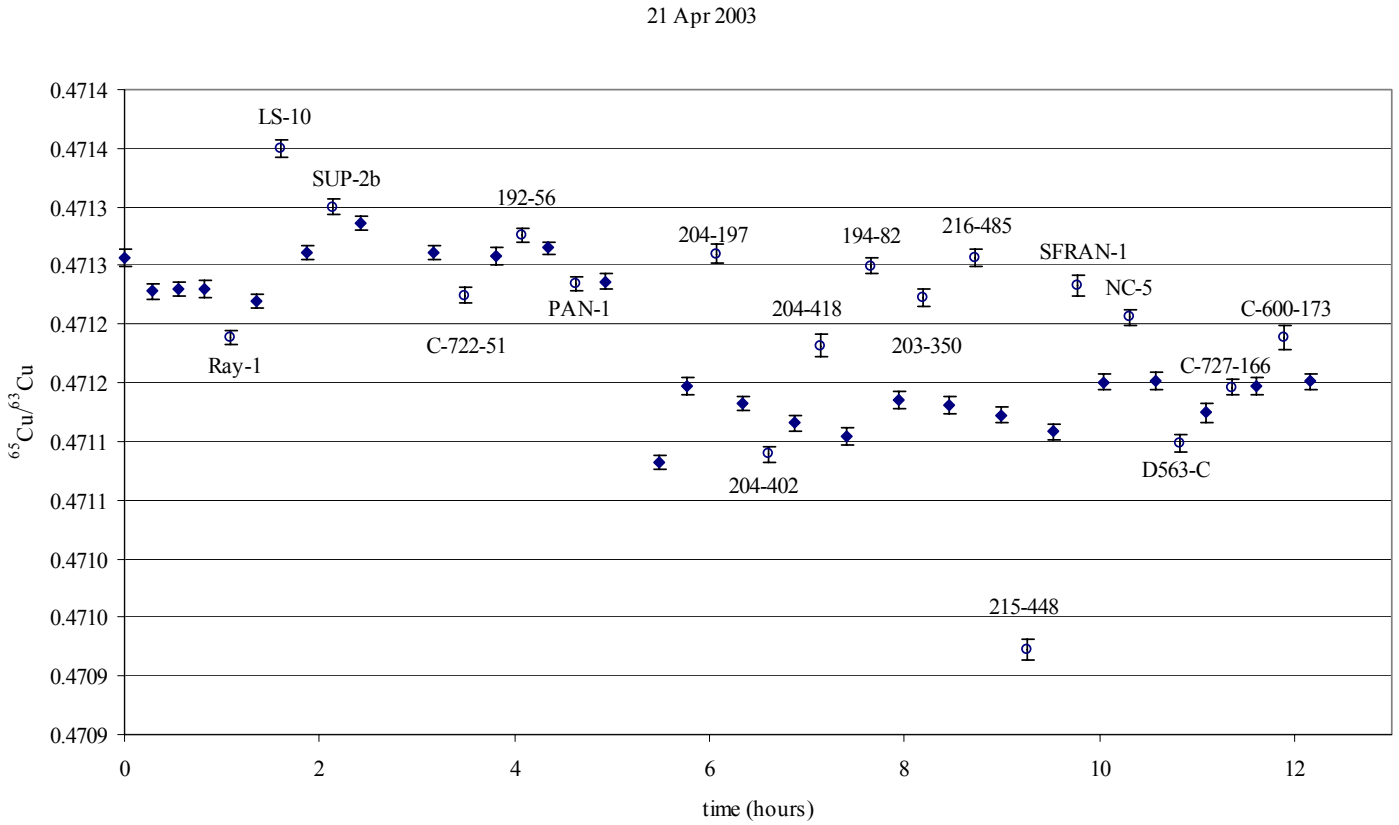

Appendix 3 cont.

date	analysis	raw $^{65}Cu/^{63}Cu$	error (2σ)	$\delta^{65}Cu$	^{65}Cu voltage	%Cu of sample relative to standard	drift between bracketing standards (ppm)
17-Jun-03	976 #1	0.4695485	5.54E-06		1.684		
	976 #2	0.4695917	6.34E-06		1.661		
	976 #3	0.4695972	6.68E-06		1.651		
	976 #4	0.4696182	6.22E-06		1.631		
	RAY-1 #1	0.4695969	5.96E-06	-0.015	1.907	115.81	-63
	976 #5	0.4695888	5.51E-06		1.661		
	RAY-1 10ppb Pb	0.4695680	4.00E-06	-0.068	4.928	297.37	42
	976 #6	0.4696086	6.59E-06		1.653		
	RAY-1 100ppb Pb	0.4695977	4.45E-06	-0.024	4.758	289.83	0
	976 #7	0.4696086	5.98E-06		1.630		
	RAY-1 1ppm Pb	0.4696360	4.58E-06	0.076	4.787	292.39	-25
	976 #8	0.4695969	6.78E-06		1.644		
	RAY-1 #2	0.4695898	5.91E-06	0.014	1.911	115.64	-58
	976 #9	0.4695698	6.74E-06		1.662		
	SUP-1 #1	0.4698244	5.48E-06	0.567	1.588	95.75	9
	976 #10	0.4695738	6.25E-06		1.656		
	SUP-1 10ppb Pb	0.4698349	4.45E-06	0.602	2.313	139.80	-31
	976 #11	0.4695595	5.72E-06		1.654		
	SUP-1 100ppb Pb	0.4697822	6.84E-06	0.544	2.172	130.07	-83
	976 #12	0.4695205	6.18E-06		1.685		
	SUP-1 1ppm	0.4697835	6.00E-06	0.612	2.307	137.70	-40
	976 #13	0.4695015	5.53E-06		1.665		
	SUP-1 #2	0.4697543	7.33E-06	0.558	1.598	96.09	18
	976 #14	0.4695097	7.56E-06		1.661		
	RAY-1 1ppm Pb #2	0.4695155	4.33E-06	0.019	4.899	294.13	-12
	976 #15	0.4695040	5.82E-06		1.670		

Appendix 3 cont

17 Jun 2003

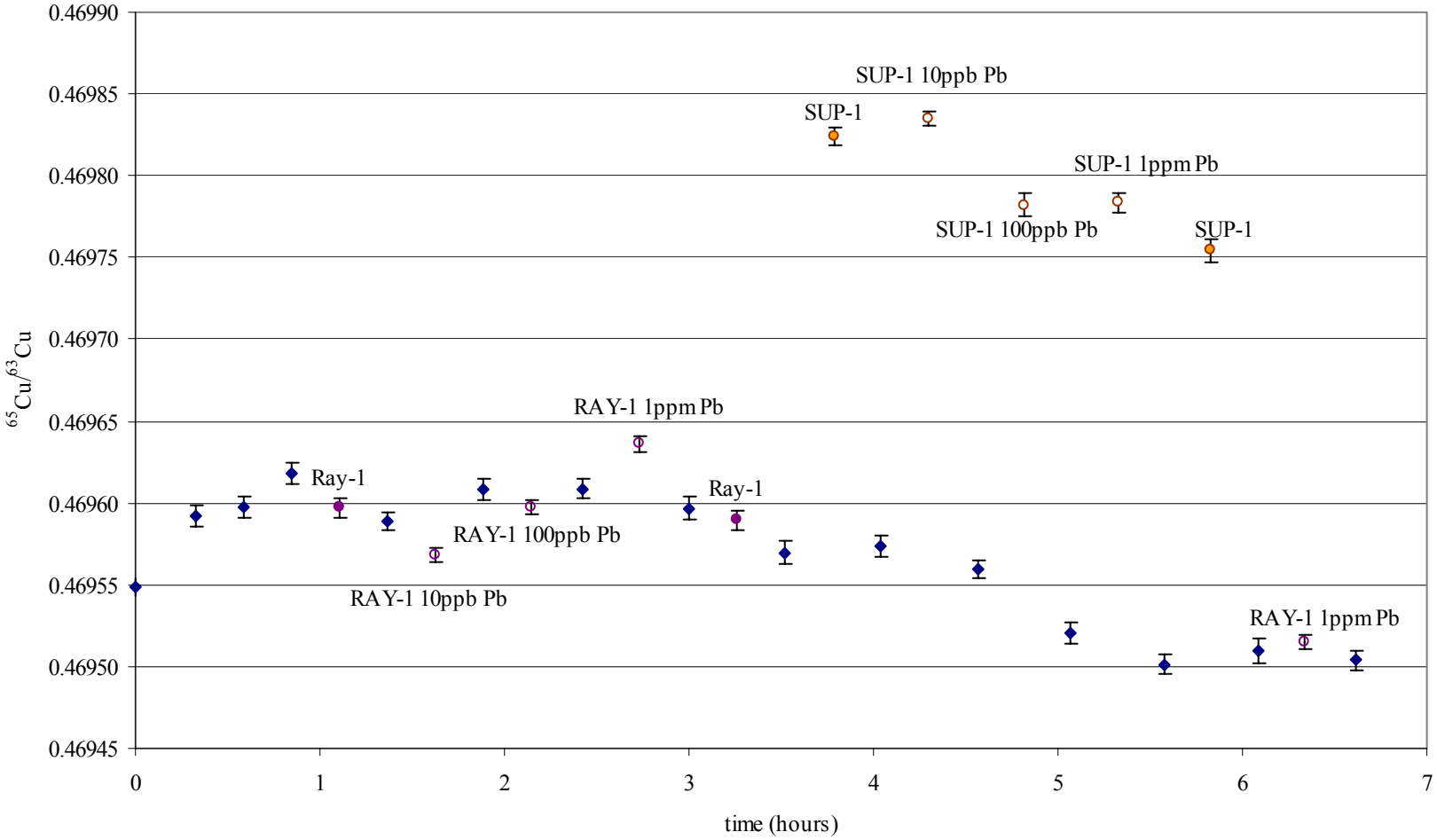

Appendix 3 cont.

date	analysis	raw $^{65}Cu/^{63}Cu$	error (2σ)	$\delta^{65}Cu$	^{65}Cu voltage	%Cu of sample relative to standard	drift between bracketing standards (ppm)
1-Jul-03	976 #1	0.4720674	5.07E-06		1.487		
	976 #2	0.4720918	6.92E-06		1.410		
	976 #3	0.4708681	5.52E-06		1.293		
	976 #4	0.4708440	6.96E-06		1.305		
	976 #5	0.4708362	7.91E-06		1.312		
	RAY-1	0.4707994	6.98E-06	-0.082	1.416	106.79	0
	976 #6	0.4708359	5.20E-06		1.340		
	1400 20.9 324.7	0.4707762	6.53E-06	-0.150	1.204	89.28	31
	976 #7	0.4708504	7.84E-06		1.358		
	1400 13.7 300.12	0.4708986	7.14E-06	0.103	1.306	96.41	11
	976 #8	0.4708554	6.86E-06		1.351		
	1400 13.7 300.6	0.4709679	7.24E-06	0.238	1.212	89.46	28
	976 #9	0.4708686	6.52E-06		1.360		
	1400 21.7 425.8	0.4710252	6.70E-06	0.324	1.255	92.83	54
	976 #10	0.4708941	6.42E-06		1.344		
	1400 14.5 340.5	0.4703226	6.48E-06	-1.286	1.299	96.59	7
	976 #11	0.4708975	5.75E-06		1.346		
	1400 14.5 246.1	0.4711960	7.87E-06	0.654	1.161	86.54	32
	976 #12	0.4709124	6.65E-06		1.338		
	1400 15.3 326.15	0.4711340	7.73E-06	0.473	1.212	90.79	45
	976 #13	0.4709338	6.45E-06		1.331		
	1400 17.7 352.7	0.4710071	7.68E-06	0.150	1.223	91.79	27
	976 #14	0.4709463	7.18E-06		1.333		
	1400 14.5 244.45A	0.4711874	6.11E-06	0.520	1.205	90.57	39
	976 #15	0.4709645	5.40E-06		1.328		
	1400 14.5 244.45B	0.4710214	6.62E-06	0.124	1.235	93.16	7
	976 #16	0.4709679	5.06E-06		1.323		
	1400 15.8 248.6	0.4712164	7.40E-06	0.543	1.093	82.94	30
	976 #17	0.4709819	5.99E-06		1.314		
	1400 18.9 357.2	0.4709013	7.15E-06	-0.208	1.213	92.32	50
	976 #18	0.4710054	6.06E-06		1.313		
	1400 18.9 356.9	0.4709218	5.98E-06	-0.222	1.344	102.07	63
	976 #19	0.4710350	6.80E-06		1.320		
	1400 18.9 365.85	0.4707937	6.05E-06	-0.541	1.156	88.20	0
	976 #20	0.4710347	7.52E-06		1.301		
	1400 18.9 382.6	0.4713142	6.06E-06	0.617	1.238	94.93	18
	976 #21	0.4710434	6.71E-06		1.307		
	1400 18.9 387.8	0.4711655	6.31E-06	0.244	0.977	74.96	60
	976 #22	0.4710718	7.71E-06		1.300		
	S22-A 2137	0.4718117	7.90E-06	1.624	1.098	85.63	66
	976 #23	0.4711032	6.73E-06		1.265		
	S27-I 2897	0.4714542	6.57E-06	0.729	1.164	91.42	99

Appendix 3 cont.

date	analysis	raw $^{65}Cu/^{63}Cu$	error (2σ)	$\delta^{65}Cu$	^{65}Cu voltage	%Cu of sample relative to standard	drift between bracketing standards (ppm)
1-Jul-03	976 #24	0.4711496	6.43E-06		1.283		
(cont.)	AR-17a	0.4712649	6.99E-06	0.222	1.323	103.85	70
	976 #25	0.4711827	6.68E-06		1.265		
	AR-17b	0.4711783	6.62E-06	-0.043	1.233	97.67	64
	976 #26	0.4712129	5.20E-06		1.259		
	976 #27	0.4712105	6.40E-06		1.271		
	GALENAM-1	0.4712715	8.45E-06	0.115	0.977	76.46	41
	976 #28	0.4712298	7.14E-06		1.285		
	GALENAM-2	0.4712664	1.11E-05	0.046	0.491	39.34	69
	976 #29	0.4712625	7.58E-06		1.209		
	LS-10	0.4713894	7.32E-06	0.257	1.167	95.17	54
	976 #30	0.4712879	6.24E-06		1.244		

Appendix 3 cont

1 Jul 2003

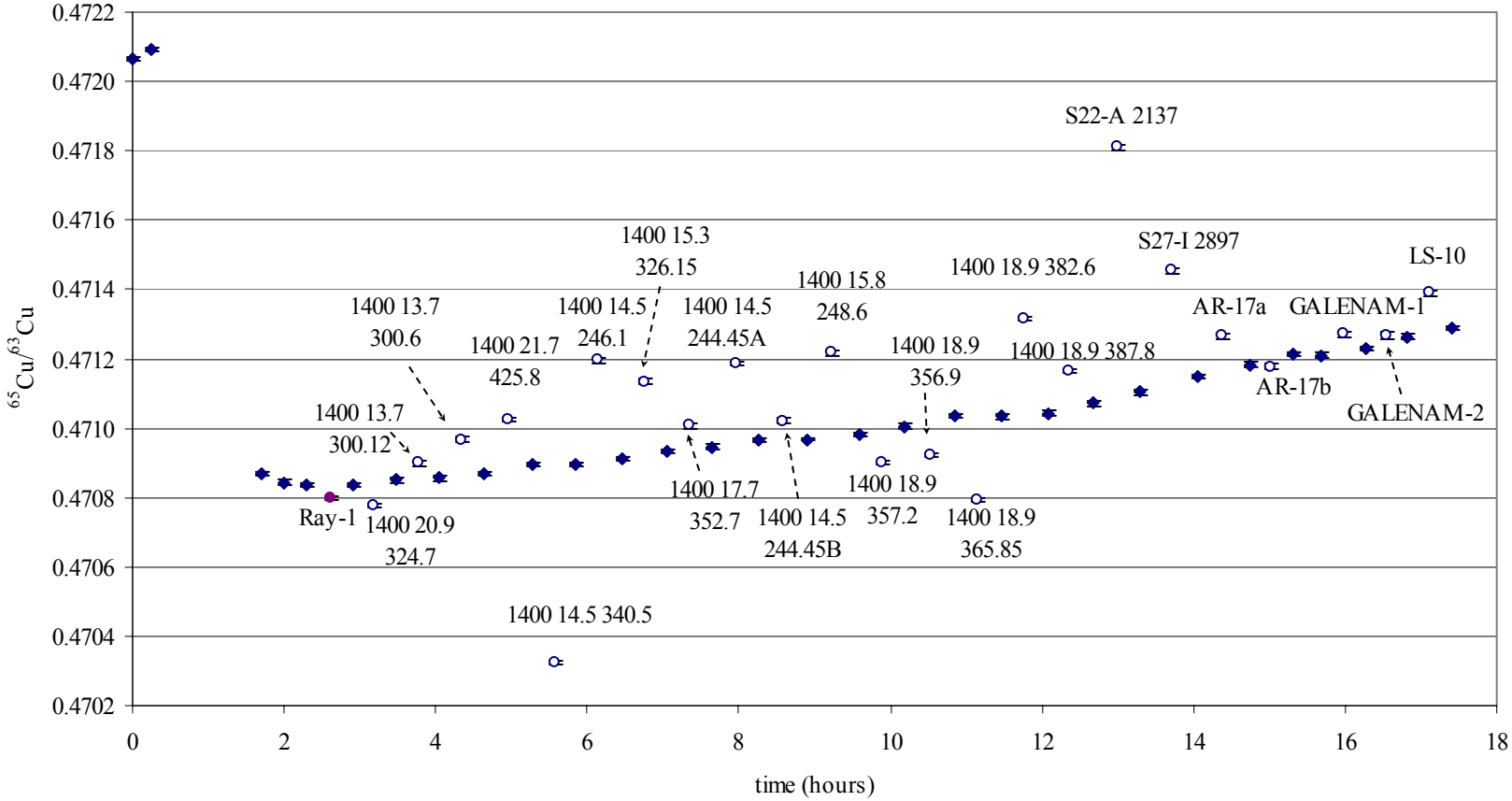

Appendix 3 cont.

date	analysis	raw $^{65}Cu/^{63}Cu$	error (2σ)	$\delta^{65}Cu$	^{65}Cu voltage	%Cu of sample relative to standard	drift between bracketing standards (ppm)
7-Jan-04	NBS976 #1	0.4704369	6.58E-06		1.458		
	NBS976 #2	0.4704083	6.08E-06		1.490		
	NBS976 #3	0.4703847	4.51E-06		1.494		
	NBS976 #4	0.4703807	6.28E-06		1.482		
	RAY-1	0.4703649	5.91E-06	-0.035	1.563	105.58	-1
	NBS976 #5	0.4703803	5.53E-06		1.479		
	LS-10 #1	0.4703574	7.21E-06	0.146	1.398	93.03	-373
	NBS976 #6	0.4702047	7.03E-06		1.526		
	SUP-1	0.4704521	6.22E-06	0.567	1.322	86.81	-23
	NBS976 #7	0.4701940	5.98E-06		1.520		
	LS-10 #2	0.4703385	6.90E-06	0.335	1.384	91.01	-21
	NBS976 #8	0.4701842	6.12E-06		1.521		
	1400 15.8 248.6	0.4704349	8.17E-06	0.572	1.237	81.29	-16
	NBS976 #9	0.4701766	6.90E-06		1.522		

Appendix 3 cont

7 Jan 2004

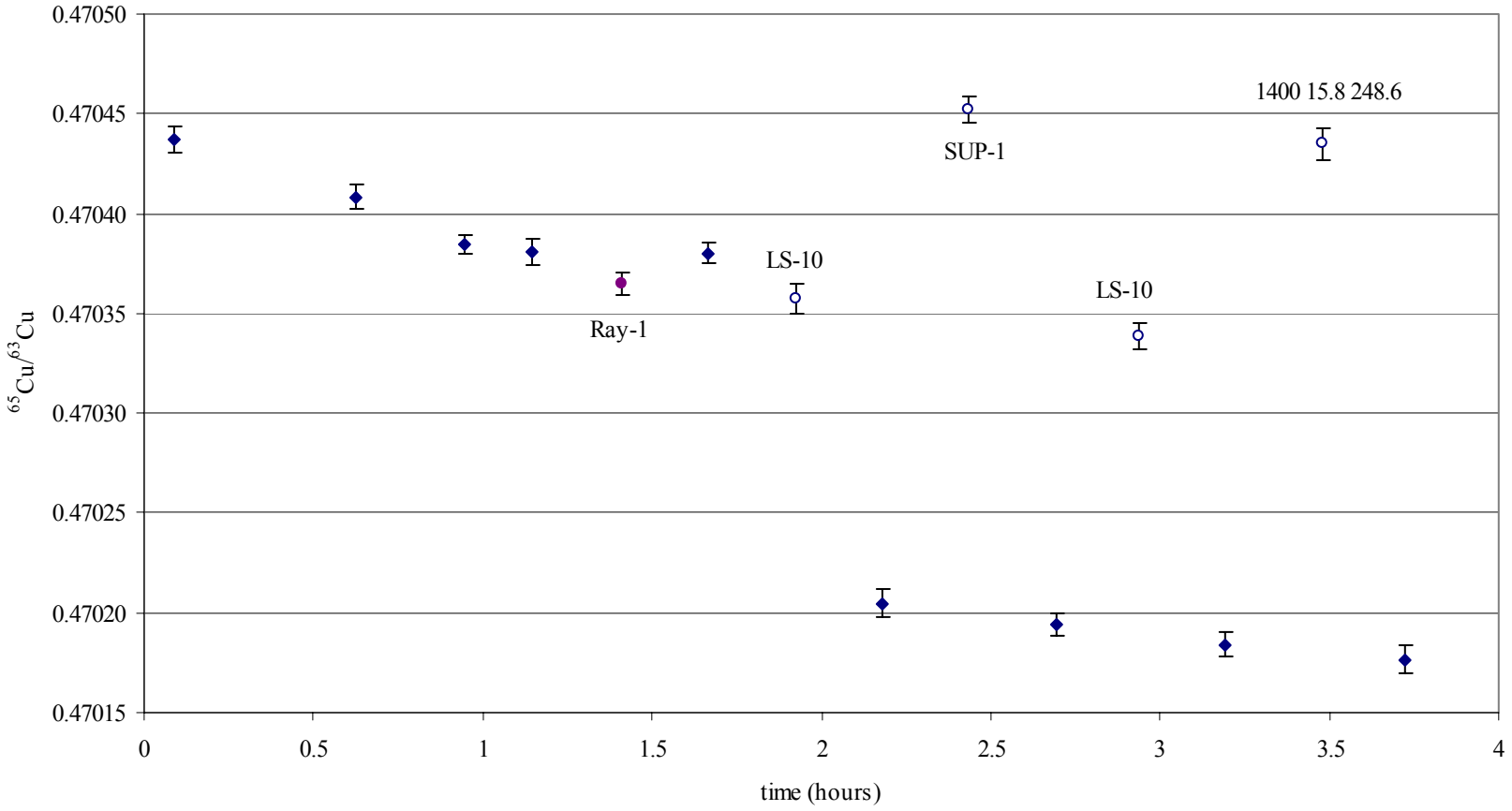

Appendix 3 cont.

date	analysis	raw $^{65}Cu/^{63}Cu$	error (2σ)	$\delta^{65}Cu$	^{65}Cu voltage	%Cu of sample relative to standard	drift between bracketing standards (ppm)
18-Feb-04	976 #1	0.4699031	8.17E-06		1.824		
	976 #2	0.4698848	5.70E-06		1.801		
	RAY-1	0.4698821	5.31E-06	-0.026	1.838	102.95	38
	976 #3	0.4699027	6.65E-06		1.770		
	CHAB-E-MAR	0.4707516	6.57E-06	1.868	1.623	91.61	70
	976 #4	0.4699354	5.95E-06		1.775		
	1400 18.9 370	0.4698043	6.02E-06	-0.335	1.737	99.12	80
	976 #5	0.4699728	6.56E-06		1.730		
	1400 18.9 350	0.4701546	5.91E-06	0.410	1.925	111.99	-3
	976 #6	0.4699713	7.80E-06		1.708		
	T1900N-9 21.45	0.4700264	6.11E-06	0.081	2.442	143.75	80
	976 #7	0.4700087	7.60E-06		1.690		
	1400 18.9 378.85	0.4700339	6.53E-06	0.021	1.597	93.71	68
	976 #8	0.4700407	6.99E-06		1.719		
	1400 18.9 334.8A	0.4705682	6.27E-06	1.170	1.420	83.02	27
	976 #9	0.4700535	5.90E-06		1.701		
	1400 18.9 334.8B	0.4704547	6.37E-06	0.862	1.480	87.24	74
	976 #10	0.4700882	5.78E-06		1.692		
	1400 21.7 183.5	0.4698115	6.90E-06	-0.631	1.570	93.19	19
	976 #11	0.4700969	5.65E-06		1.678		

Appendix 3 cont

18 Feb 2004

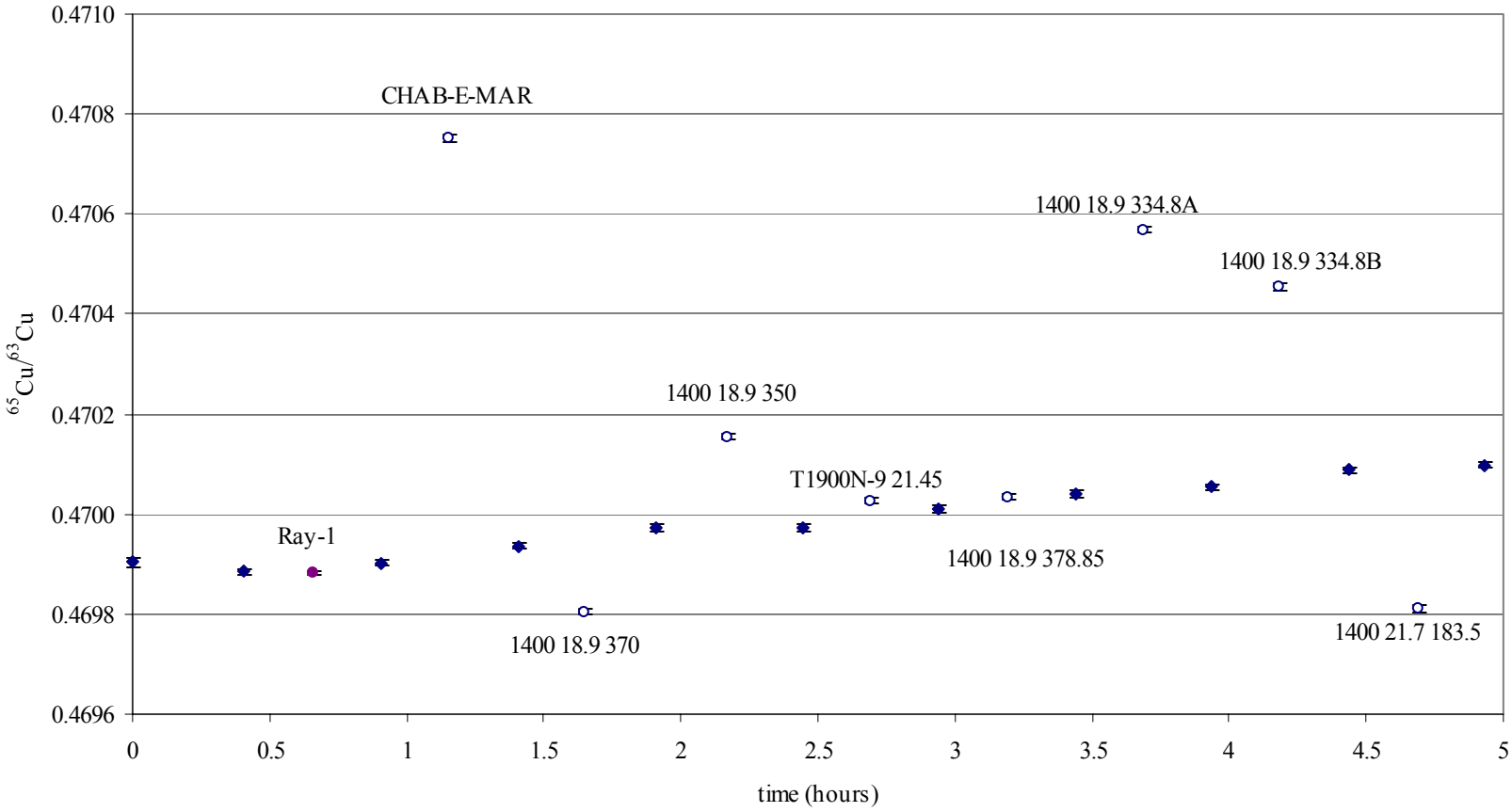

Appendix 3 cont.

date	analysis	raw $^{65}Cu/^{63}Cu$	error (2σ)	$\delta^{65}Cu$	^{65}Cu voltage	%Cu of sample relative to standard	drift between bracketing standards (ppm)
5-Mar-04	976 #1	0.4707325	7.83E-06		1.372		
	976 #2	0.4707622	6.47E-06		1.363		
	976 #3	0.4708035	9.63E-06		1.362		
	976 #4	0.4707623	7.16E-06		1.404		
	976 #5	0.4707989	7.43E-06		1.401		
	RAY-1	0.4707467	7.82E-06	-0.106	1.445	103.19	-21
	976 #6	0.4707890	6.08E-06		1.401		
	LS-10	0.4709193	7.57E-06	0.294	1.253	89.49	-3
	976 #7	0.4707875	8.01E-06		1.398		
	SLAKE-1A	0.4709020	7.52E-06	0.223	1.319	94.47	66
	976 #8	0.4708185	7.10E-06		1.393		
	SLAKE-1B	0.4708270	8.17E-06	-0.046	0.942	67.68	123
	976 #9	0.4708766	5.93E-06		1.392		
	SUP-3A(1)	0.4709591	1.07E-05	0.144	0.416	30.09	79
	976 #10	0.4709138	7.12E-06		1.374		
	SUP-3A(2)	0.4709647	7.58E-06	0.064	1.015	73.83	95
	976 #11	0.4709586	6.48E-06		1.376		
	SUP-3B(1)	0.4709968	5.82E-06	0.086	1.643	119.52	0
	976 #12	0.4709583	6.62E-06		1.373		
	SUP-3C(1)	0.4710107	6.20E-06	0.059	1.454	106.35	108
	976 #13	0.4710093	6.52E-06		1.362		
	SUP-3C(2)	0.4710198	6.06E-06	0.034	1.351	99.19	-20
	976 #14	0.4709997	6.13E-06		1.362		
	1400 20.9 49.7	0.4708718	7.00E-06	-0.310	1.090	80.03	44
	976 #15	0.4710205	6.63E-06		1.362		
	1400 15.8 306.4	0.4709687	6.54E-06	-0.160	1.272	93.53	81
	976 #16	0.4710587	8.05E-06		1.357		
	SUP-3C(2)	0.4710768	7.94E-06	0.047	1.331	98.79	-12
	976 #17	0.4710533	7.88E-06		1.338		

Appendix 3 cont

5 Mar 2004

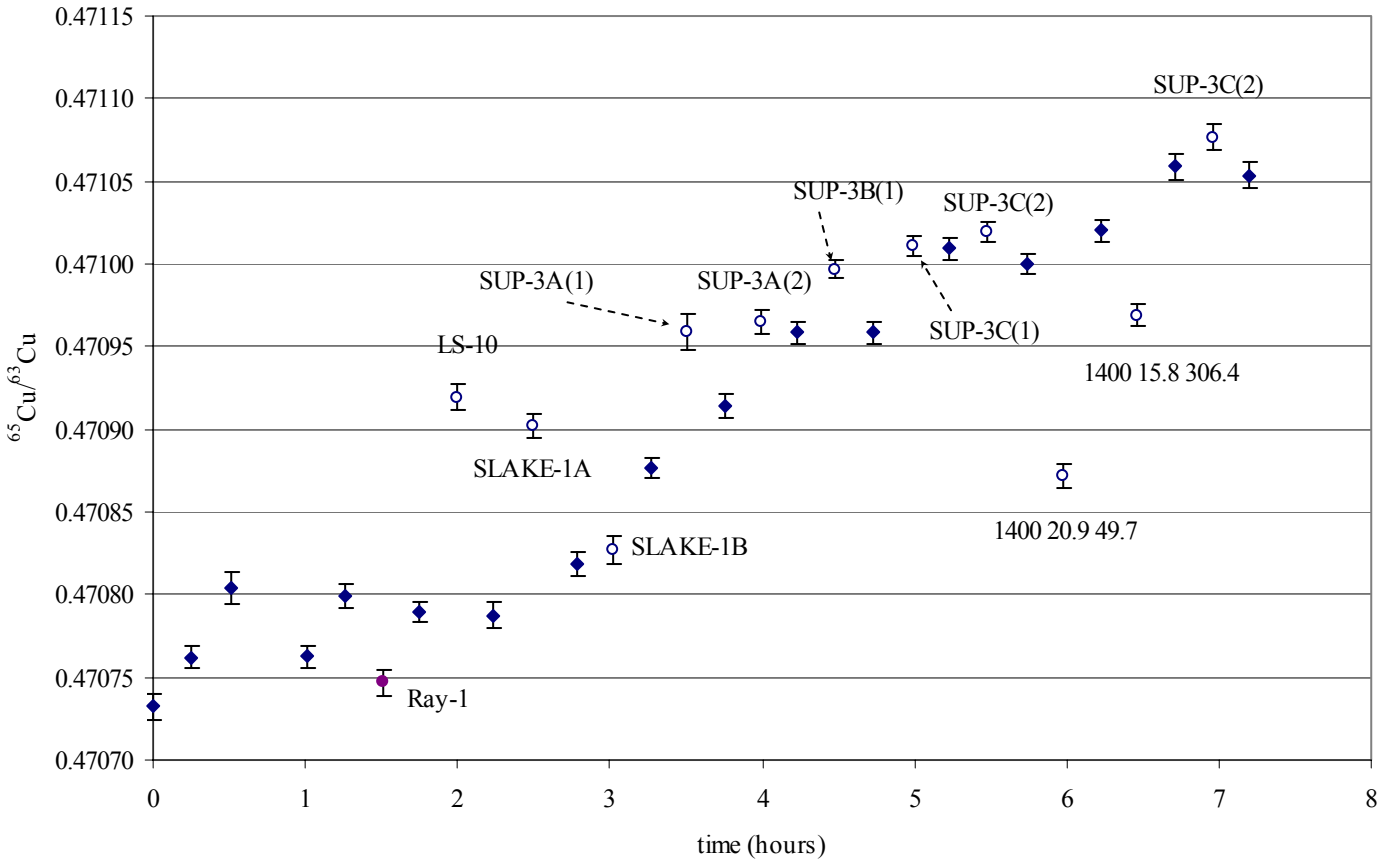

Appendix 3 cont.

date	analysis	raw $^{65}Cu/^{63}Cu$	error (2σ)	$\delta^{65}Cu$	^{65}Cu voltage	%Cu of sample relative to standard	drift between bracketing standards (ppm)
6-Mar-04	976 #1	0.4711897	8.17E-06		1.232		
	976 #2	0.4712693	8.15E-06		1.218		
	976 #3	0.4712857	6.77E-06		1.201		
	RAY-1	0.4712690	5.84E-06	-0.095	1.377	115.38	108
	976 #4	0.4713367	9.06E-06		1.186		
	976 #5	0.4711357	7.52E-06		1.228		
	SUP-3A(1)	0.4711946	7.52E-06	0.125	1.281	104.91	14
	976 #6	0.4711423	6.60E-06		1.213		
	SUP-3A(2)	0.4712228	8.55E-06	0.059	0.993	82.73	227
	976 #7	0.4712494	8.12E-06		1.187		
	SUP-3B(1)	0.4712820	5.84E-06	0.044	1.622	136.78	55
	976 #8	0.4712751	7.37E-06		1.185		
	SUP-3C(1)	0.4713061	5.94E-06	0.026	1.421	120.66	76
	976 #9	0.4713107	7.42E-06		1.170		
	SUP-3C(2)	0.4713447	6.10E-06	0.010	1.315	112.83	124
	976 #10	0.4713689	7.53E-06		1.161		
	976 #11	0.4708822	6.88E-06		1.195		
	BING-3	0.4707502	7.40E-06	-0.368	1.188	99.55	139
	976 #12	0.4709475	8.04E-06		1.192		
	Chab-Sur-Cp-Ma	0.4710507	7.70E-06	0.187	1.198	100.91	83
	976 #13	0.4709865	7.79E-06		1.182		
	976 #14	0.4710447	6.62E-06		1.185		
	Chab-Este	0.4706823	8.08E-06	-0.832	1.347	113.77	35
	976 #15	0.4710610	8.95E-06		1.183		
	1400 15.8 191.25	0.4712311	6.29E-06	0.399	1.396	118.36	-33
	976 #16	0.4710457	7.57E-06		1.176		
	400 16.0 78.1A	0.4712001	6.72E-06	0.381	1.419	120.78	-66
	976 #17	0.4710145	6.96E-06		1.174		
	400 16.0 78.1B	0.4712174	5.90E-06	0.425	1.074	91.43	56
	976 #18	0.4710409	6.36E-06		1.176		
	900 16.2A 185.65	0.4708521	7.15E-06	-0.407	1.030	87.77	-32
	976 #19	0.4710259	6.80E-06		1.170		
	900 15.2 401.9	0.4709901	7.10E-06	-0.063	1.020	87.22	-31
	976 #20	0.4710112	6.39E-06		1.169		
	Ar 32	0.4712036	6.75E-06	0.434	1.434	122.45	-4
	976 #21	0.4710090	7.80E-06		1.173		
	Ar-37a	0.4709843	6.08E-06	-0.029	1.198	102.76	-50
	976 #22	0.4709854	7.11E-06		1.159		
	Ar-37b	0.4710674	7.16E-06	0.172	0.873	75.67	22
	976 #23	0.4709959	5.93E-06		1.148		
	Ar-6	0.4709631	7.97E-06	-0.072	1.183	103.19	-4
	976 #24	0.4709940	7.21E-06		1.145		

Appendix 3 cont.

date	analysis	raw $^{65}Cu/^{63}Cu$	error (2σ)	$\delta^{65}Cu$	^{65}Cu voltage	%Cu of sample relative to standard	drift between bracketing standards (ppm)
6-Mar-04	CHRIS-1	0.4715542	6.30E-06	1.267	0.861	75.28	-18
(cont.)	976 #25	0.4709856	6.59E-06		1.143		
	MTTN-1	0.4712540	8.68E-06	0.539	0.998	86.48	120
	976 #26	0.4710422	6.50E-06		1.165		
	T1900N-9	0.4710589	6.16E-06	0.039	1.834	158.38	-3
	976 #27	0.4710409	6.71E-06		1.151		
	1400 18.9 334.8A	0.4715415	7.25E-06	1.152	1.043	91.19	-54
	976 #28	0.4710157	7.00E-06		1.137		
	SLAKE-1B	0.4709613	7.50E-06	-0.144	0.856	75.14	42
	976 #29	0.4710353	5.60E-06		1.141		
	Ar6 #2	0.4709968	7.25E-06	-0.059	1.133	99.28	

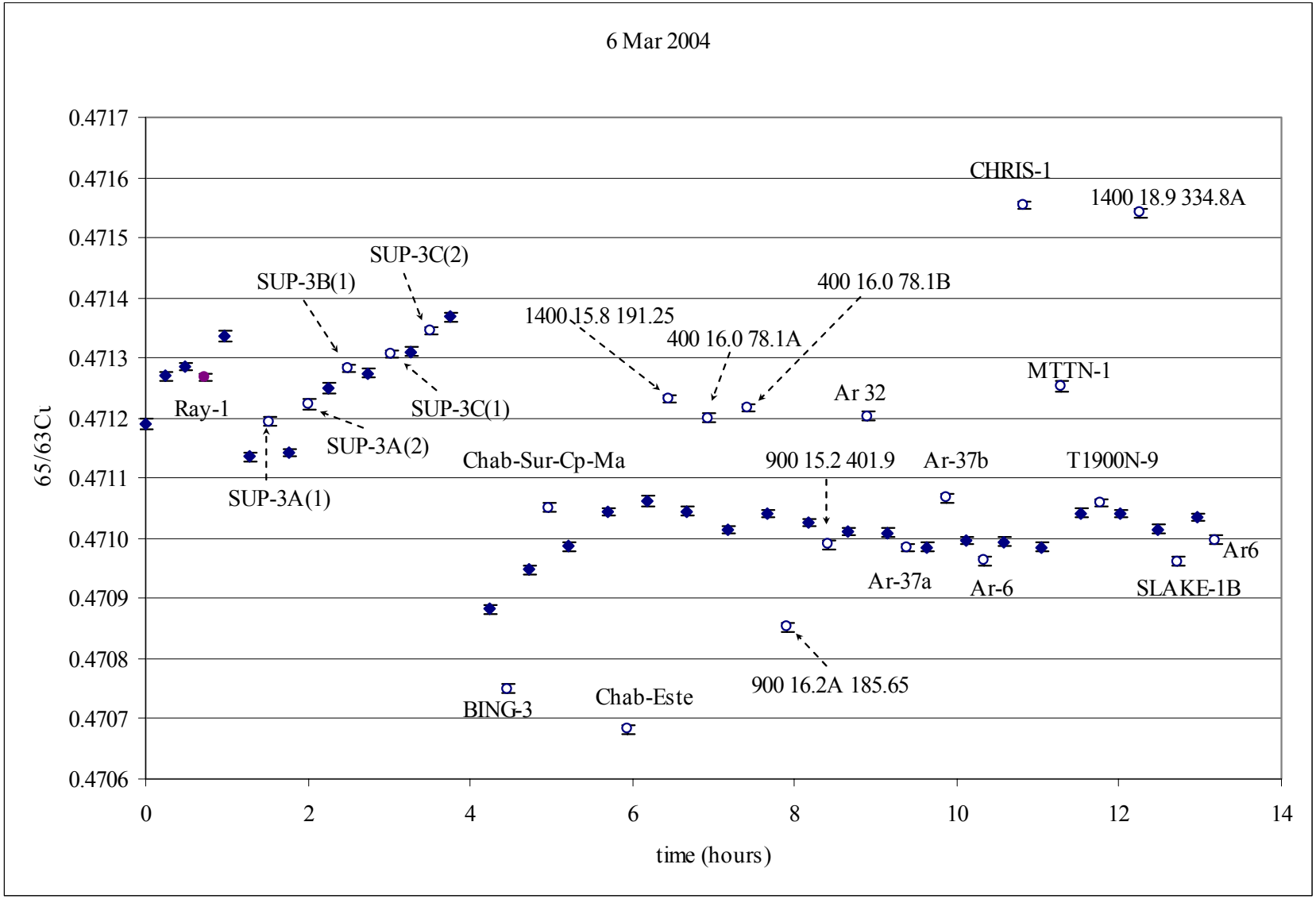
6 Mar 2004
65/63Cu
time (hours)
0.4717
0.4716
0.4715
0.4714
0.4713
0.4712
0.4711
0.4710
0.4709
0.4708
0.4707
0.4706
0
2
4
6
8
10
12
14
CHRIS-1
1400 18.9 334.8A
SUP-3C(2)
SUP-3B(1)
400 16.0 78.1B
1400 15.8 191.25
400 16.0 78.1A
MTTN-1
Ar 32
Ray-1
SUP-3C(1)
SUP-3A(2)
SUP-3A(1)
Chab-Sur-Cp-Ma
900 15.2 401.9
Ar-37b
T1900N-9
Ar6
Ar-37a
Ar-6
SLAKE-1B
900 16.2A 185.65
BING-3
Chab-Este

Appendix 3 cont.

date	analysis	raw $^{65}Cu/^{63}Cu$	error (2σ)	$\delta^{65}Cu$	^{65}Cu voltage	%Cu of sample relative to standard	drift between bracketing standards (ppm)
1-Apr-04	976 #2 +Zn	0.4718858	6.40E-06		1.088		
	976 #3 +Zn	0.4718880	6.65E-06		1.087		
	Ray-1	0.4718715	6.80E-06	-0.067	1.278	116.81	57
	976 #4 +Zn	0.4719149	6.40E-06		1.102		
	976 #5	0.4718963	4.90E-06		1.184		
	1400 18.9 387.8b	0.4719746	7.31E-06	0.218	2.302	192.40	-80
	976 #6	0.4718586	6.23E-06		1.209		
	BEAV-3	0.4723173	8.81E-06	1.039	0.651	53.81	-19
	976 #7	0.4718497	6.13E-06		1.211		
	BEAV-4a	0.4721947	6.76E-06	0.803	1.649	136.00	-52
	976 #8	0.4718249	6.77E-06		1.214		
	BEAV-4b	0.4720063	6.68E-06	0.396	1.060	86.96	21
	976 #9	0.4718350	6.38E-06		1.224		
	T1975N-4 111.35	0.4719162	1.10E-05	0.207	0.349	28.74	-47
	976 #10	0.4718128	5.27E-06		1.201		
	Chab-Esteb	0.4714273	6.50E-06	-0.836	1.037	86.03	-54
	976 #11	0.4717873	6.26E-06		1.208		
	SUP-3A(3)	0.4717860	7.62E-06	0.039	1.095	91.01	-80
	976 #12	0.4717496	7.94E-06		1.198		
	SUP-3A(4)	0.4717530	1.03E-05	0.020	0.571	47.45	-23
	976 #13	0.4717386	7.57E-06		1.209		
	BING-4	0.4717371	5.44E-06	-0.033	1.782	146.47	48
	976 #14	0.4717612	5.48E-06		1.223		
	CF-1	0.4717322	4.24E-06	-0.010	2.817	228.80	-104
	976 #15	0.4717119	5.22E-06		1.239		
	CF-14	0.4717377	6.50E-06	0.048	1.228	98.83	19
	976 #16	0.4717210	5.91E-06		1.247		
	CF-16	0.4720649	5.93E-06	0.791	1.122	89.96	-36
	976 #17	0.4717042	5.17E-06		1.248		
	CF-18	0.4721121	7.47E-06	0.946	1.003	80.62	-59
	976 #18	0.4716764	7.29E-06		1.240		
	SL-6b	0.4715905	7.79E-06	-0.222	0.845	67.89	54
	976 #19	0.4717017	5.95E-06		1.250		
	SL-6c	0.4717128	8.07E-06	0.048	0.926	74.61	-43
	976 #20	0.4716816	4.43E-06		1.231		
	EMP-1	0.4716314	5.40E-06	-0.118	1.121	90.64	10
	976 #21	0.4716865	5.94E-06		1.243		
	EMP-3	0.4716447	6.10E-06	-0.044	1.004	81.30	-94
	976 #22	0.4716420	5.38E-06		1.226		
	EMP-5-4	0.4717409	6.36E-06	0.200	0.941	75.99	41
	976 #23	0.4716614	5.39E-06		1.251		
	TROY-1A	0.4717629	6.02E-06	0.233	1.089	87.24	-9

Appendix 3 cont.

date	analysis	raw $^{65}Cu/^{63}Cu$	error (2σ)	$\delta^{65}Cu$	^{65}Cu voltage	%Cu of sample relative to standard	drift between bracketing standards (ppm)
1-Apr-04	976 #24	0.4716572	5.53E-06		1.246		
	TROY-1B	0.4716572	5.53E-06	0.000	1.246	100.41	-1
	976 #25	0.4716568	4.99E-06		1.236		
	TROY-4A	0.4718094	4.29E-06	0.338	3.031	244.78	8
	976 #26	0.4716605	5.62E-06		1.241		
	TROY-4B	0.4717457	7.13E-06	0.194	1.097	88.83	-5
	976 #27	0.4716583	6.88E-06		1.230		
	Ajo-7a	0.4717504	7.12E-06	0.203	0.884	71.95	6
	976 #28	0.4716612	6.34E-06		1.227		
	Ajo-7e	0.4717957	4.31E-06	0.312	2.201	179.00	-18
	976 #29	0.4716526	5.83E-06		1.232		
	LS-10	0.4717456	6.63E-06	0.215	1.149	93.45	-13
	976 #30	0.4716465	5.69E-06		1.227		
	blank	0.4715941	3.08E-04	-0.111	0.0065		

Appendix 3 cont.

1 Apr 2004

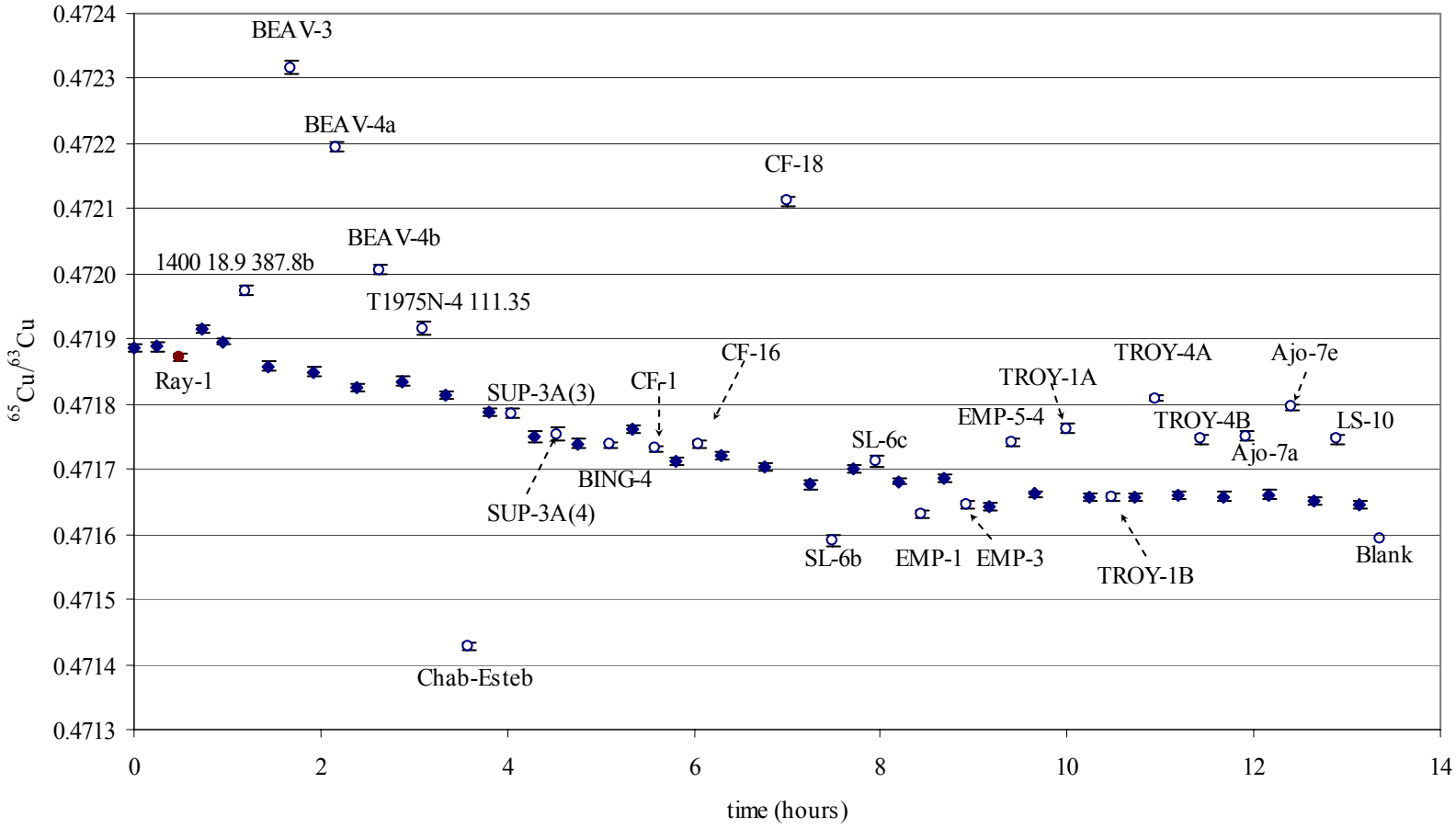

Appendix 3 cont.

date	analysis	raw $^{65}Cu/^{63}Cu$	error (2σ)	$\delta^{65}Cu$	^{65}Cu voltage	%Cu of sample relative to standard	drift between bracketing standards (ppm)
30-Sep-04	976 #1	0.4726118	1.58E-05		1.522		
	976 #2	0.4727454	8.57E-06		1.481		
	976 #3	0.4727695	7.61E-06		1.468		
	976 #4	0.4727898	9.68E-06		1.454		
	Ray-1	0.4727789	8.77E-06	-0.071	1.570	108.08	87
	976 #5	0.4728311	9.57E-06		1.451		
	1300 16.1 252.65	0.4723977	1.06E-05	-1.032	1.423	98.38	109
	976 #6	0.4728824	7.14E-06		1.442		
	Beav-5a	0.4734398	8.86E-06	1.218	1.020	71.44	61
	976 #7	0.4729112	9.41E-06		1.414		
	Beav-5b	0.4733157	8.70E-06	0.896	1.112	78.77	22
	976 #8	0.4729216	7.60E-06		1.410		
	PBL-0142	0.4730535	8.38E-06	0.264	1.132	79.73	59
	976 #9	0.4729493	7.46E-06		1.429		
	TT008-214	0.4730355	7.61E-06	0.194	1.513	105.71	-2
	976 #10	0.4729483	6.70E-06		1.434		
	CHE 039424	0.4727578	7.60E-06	-0.412	1.154	80.80	-28
	976 #11	0.4729350	7.08E-06		1.421		
	Ar-14a	0.4730237	7.92E-06	0.190	1.421	99.79	18
	976 #12	0.4729433	6.62E-06		1.427		
	Ar-14b	0.4729191	7.17E-06	0.000	1.381	98.35	-118
	976 #13	0.4728873	8.10E-06		1.382		
	Bu-120	0.4730255	8.71E-06	0.243	1.106	78.71	126
	976 #14	0.4729469	7.79E-06		1.429		
	Ar-14b #2	0.4729279	7.49E-06	-0.018	1.411	98.85	-46
	976 #15	0.4729253	8.25E-06		1.426		
	Bu-5a	0.4731543	7.29E-06	0.529	1.305	91.97	-28
	976 #16	0.4729122	7.64E-06		1.411		
	Bu-5b	0.4730761	6.44E-06	0.366	1.673	118.19	3
	976 #17	0.4729134	7.82E-06		1.419		
	Bu-130a	0.4729626	6.98E-06	0.141	1.209	85.30	-56
	976 #18	0.4728870	7.77E-06		1.415		
	Bu-130b	0.4727636	5.90E-06	-0.197	1.397	100.27	-149
	976 #19	0.4728165	7.87E-06		1.371		
	Bu-108a	0.4728894	8.20E-06	0.201	1.084	79.00	-70
	976 #20	0.4727835	7.31E-06		1.373		
	Bu-108b	0.4730669	7.89E-06	0.681	1.407	102.37	-86
	976 #21	0.4727431	7.92E-06		1.375		
	Bu-17	0.4728594	9.15E-06	0.266	0.828	59.93	-10
	976 #22	0.4727384	7.00E-06		1.387		
	Bu-28	0.4728778	6.76E-06	0.337	1.336	96.06	-44
	976 #23	0.4727175	7.47E-06		1.394		
	Bu-2	0.4727957	9.96E-06	0.220	1.314	94.39	-86
	976 #24	0.4726767	5.70E-06		1.390		

Appendix 3 cont.

date	analysis	raw $^{65}Cu/^{63}Cu$	error (2σ)	$\delta^{65}Cu$	^{65}Cu voltage	%Cu of sample relative to standard	drift between bracketing standards (ppm)
30-Sep-04	Bu-10	0.4730875	1.04E-05	0.949	1.256	90.45	-49
(cont.)	976 #25	0.4726534	8.29E-06		1.387		
	Bu-16	0.4728559	9.74E-06	0.483	0.989	71.07	-54
	976 #26	0.4726279	7.43E-06		1.395		
	Bu-15	0.4727153	1.03E-05	0.212	1.242	88.87	-31
	976 #27	0.4726134	7.66E-06		1.401		
	LS-10	0.4727131	6.12E-06	0.234	1.297	92.26	-20
	976 #28	0.4726038	8.53E-06		1.411		
	Sup-1	0.4728070	7.16E-06	0.493	1.232	87.52	-72
	976 #29	0.4725697	8.59E-06		1.404		
	Bu-130b #2	0.4724875	6.90E-06	-0.174	1.398	99.61	-18
	976 #30	0.4725612	8.50E-06		1.403		

Appendix 3 cont

30 Sep 2004

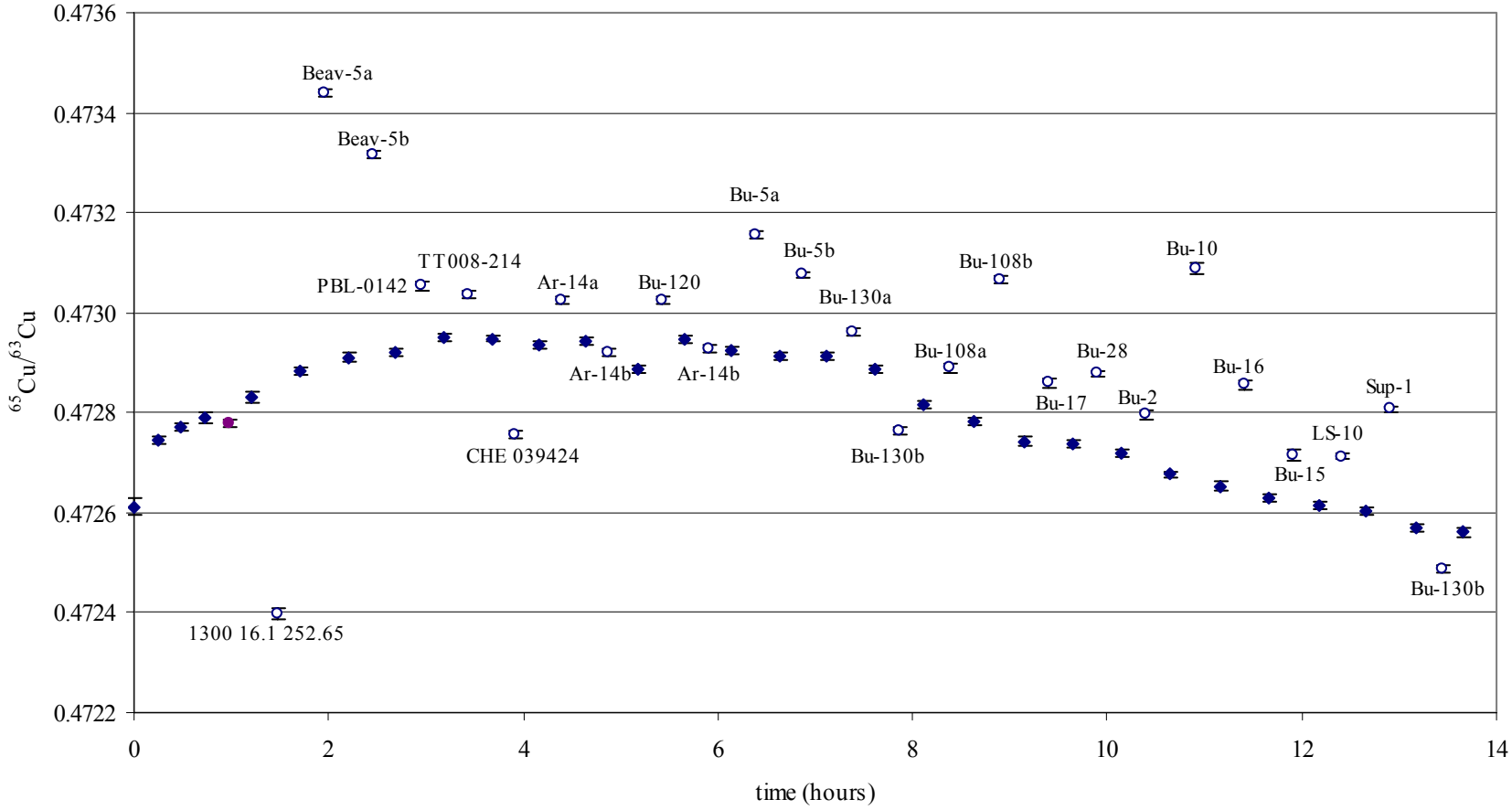

Appendix 3 cont.

date	analysis	raw $^{65}Cu/^{63}Cu$	error (2σ)	$\delta^{65}Cu$	^{65}Cu voltage	$^{61}Ni/^{62}Ni$	error (2σ)	%Cu of sample relative to standard	drift between bracketing standards (ppm)
10-Jan-05	NIST 976-986 #1	0.4715321	1.01E-05		1.279	0.3061191	4.25E-05		
	NIST 976-986 #2	0.4715746	9.51E-06		1.271	0.3061031	3.95E-05		
	Ray-1 #1 +Ni	0.4714960	9.10E-06	-0.190	1.317	0.3061632	3.89E-05	104.15	-25
	NIST 976-986 #3	0.4715863	7.40E-06		1.257	0.3060479	3.30E-05		
	LS-10 +Ni	0.4716356	7.14E-06	0.067	1.170	0.3060928	2.87E-05	93.07	-83
	NIST 976-986 #4	0.4716255	8.24E-06		1.257	0.3060920	2.57E-05		
	NISt 976-986 #5	0.4716345	8.10E-06		1.262	0.3060921	3.41E-05		
	NBS 976 #1	0.4724525	7.89E-06		1.320	0.4957476	4.87E-03		
	NBS 976 #2	0.4724345	8.71E-06		1.325	0.4957424	4.28E-03		
	Ray-1 #2	0.4723403	8.59E-06	-0.165	1.399	0.6199940	7.72E-03	105.68	87
	NBS 976 #3	0.4723931	1.01E-05		1.323	0.5065936	4.21E-03		
	NIST 976-986 #6	0.4715764	8.31E-06		1.258	0.3060119	3.62E-05		
	NIST 986	0.4494565	1.71E-04		0.009	0.3060935	3.00E-05		
	NIST 976-986 #7	0.4716106	8.26E-06		1.259	0.3061140	2.95E-05		
	Ray-1 #2 doped	0.4715434	7.55E-06	-0.175	1.309	0.3061455	2.90E-05	104.28	-44
	NIST 976-986 #8	0.4716312	6.74E-06		1.251	0.3060814	3.48E-05		

Appendix 3 cont

10 Jan 2005

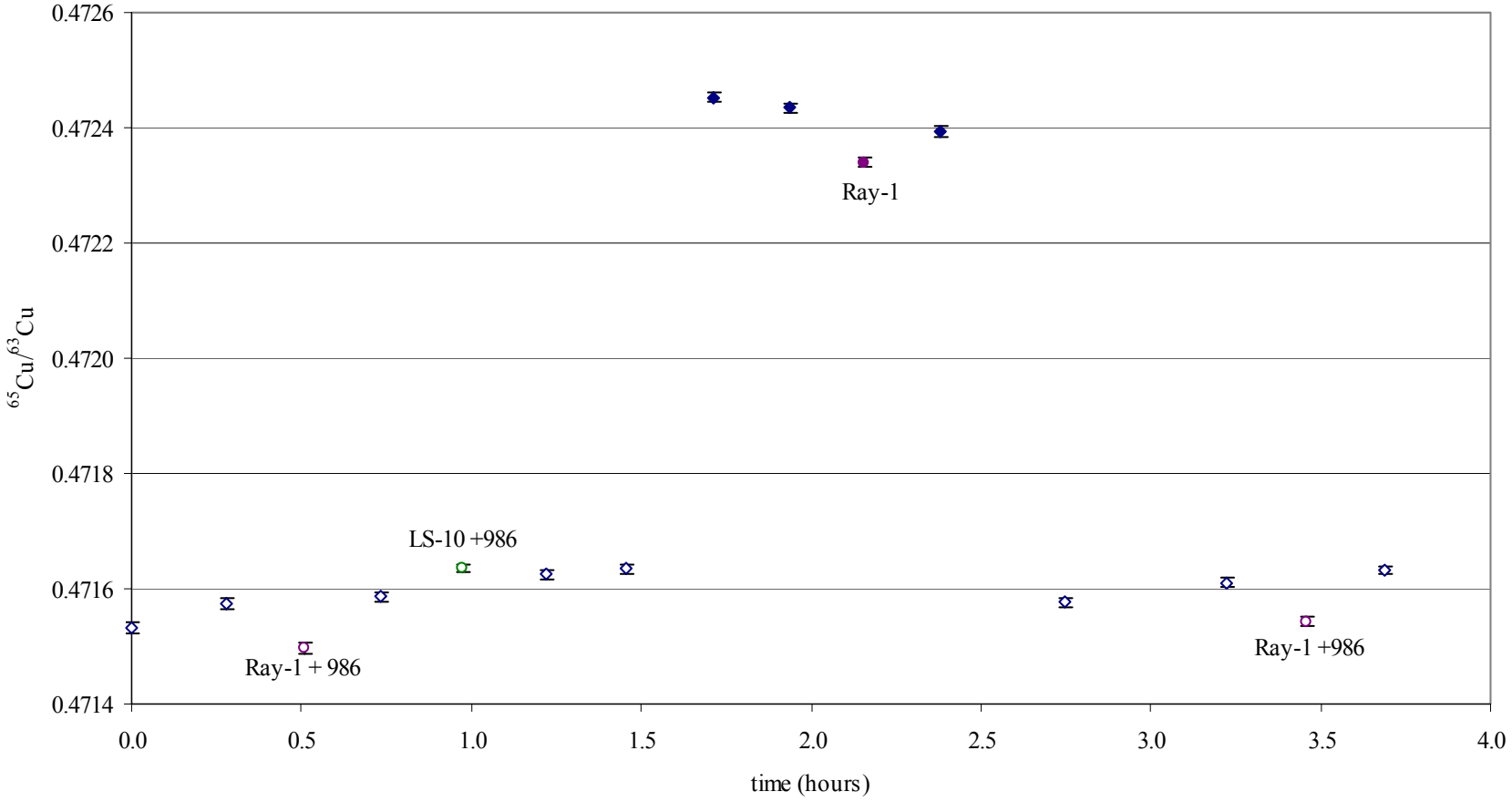

10 Jan 2005

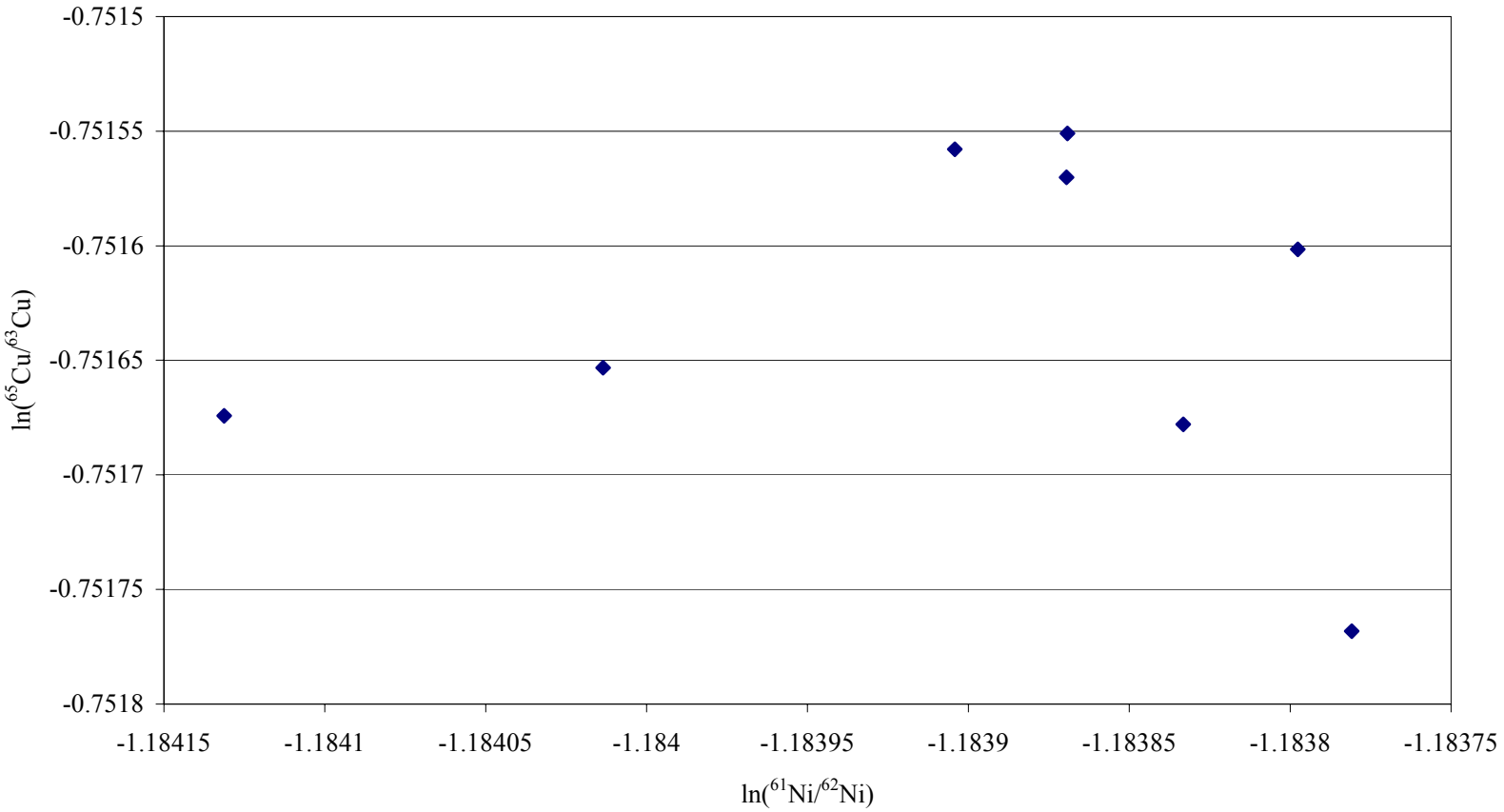
-0.7515
-0.75155
-0.7516
-0.75165
-0.7517
-0.75175
-0.7518
ln(65Cu/63Cu)
-1.18415
-1.1841
-1.18405
-1.184
-1.18395
-1.1839
-1.18385
-1.1838
-1.18375
ln(61Ni/62Ni)

Appendix 3 cont.

date	analysis	raw $^{65}Cu/^{63}Cu$	error (2σ)	$\delta^{65}Cu$	^{65}Cu voltage	%Cu of sample relative to standard	drift between bracketing standards (ppm)	raw $^{61}Ni/^{62}Ni$	error (2σ)	$\delta^{65}Cu$ (from Ni doping)
20-Jan-05	976 #1	0.4722239	1.03E-05		1.412			0.5050218	4.31E-03	
	976 #2	0.4722411	1.02E-05		1.407			0.5141953	4.05E-03	
	Ray-1	0.4722165	9.72E-06	-0.06	1.485	106.28	-6	0.6537761	9.28E-03	
	976 #3	0.4722439	8.74E-06		1.387			0.5077151	5.22E-03	
	976 986 1ppb	0.4722580	1.00E-05	0.00	1.273	92.32	-69	0.3851413	2.01E-03	
	976 #4	0.4722765	7.35E-06		1.372			0.5002314	5.10E-03	
	976 986 10 ppb	0.4722333	6.91E-06	-0.11	1.252	91.56	-17	0.3152798	2.91E-04	
	976 #5	0.4722843	8.32E-06		1.363			0.5107810	4.63E-03	
	976 986 30ppb	0.4713290	9.25E-06	-2.19	1.323	97.68	-87	0.3089545	7.88E-05	
	976 #6	0.4723255	8.44E-06		1.346			0.4940655	4.56E-03	
	976 986 60ppb	0.4713723	9.32E-06	-2.15	1.288	95.90	-28	0.3068406	6.03E-05	
	976 #7	0.4723388	6.79E-06		1.341			0.4951267	5.27E-03	
	976 986 100ppb	0.4714219	1.11E-05	-2.06	1.295	96.97	-2	0.3060301	4.17E-05	
	976 #8	0.4723400	7.33E-06		1.331			0.5038181	4.75E-03	
	976 986 500ppb	0.4714784	1.08E-05	-2.04	1.281	96.72	-197	0.3050243	1.07E-05	
	976 #9	0.4724329	7.30E-06		1.317			0.5084755	5.05E-03	
	976 #10	0.4724295	6.80E-06		1.317			0.5180557	4.20E-03	
	976 986 1000ppb	0.4715889	1.41E-05	-2.00	1.288	99.00	-224	0.3048655	8.00E-06	
	976 #11	0.4725354	6.18E-06		1.285			0.4962243	4.14E-03	
	976 986 100ppb #2	0.4716552	8.20E-06		1.265			0.3059128	3.68E-05	
	Ray-1 986 100ppb #1	0.4715902	8.31E-06	-0.20	1.314	104.54	-104	0.3059906	2.85E-05	0.021
	976 986 100ppb #3	0.4717045	6.22E-06		1.249			0.3059826	3.78E-05	
	Ray-1 986 100ppb #2	0.4716204	7.10E-06	-0.22	1.297	104.16	-59	0.3059606	3.03E-05	-0.051
	976 986 100ppb #4	0.4717324	7.74E-06		1.241			0.3059185	3.48E-05	
	Ray-1 986 100ppb #3	0.4716619	6.39E-06	-0.19	1.295	104.32	-70	0.3059737	3.01E-05	0.096
	976 986 100ppb #5	0.4717655	6.40E-06		1.241			0.3059325	3.28E-05	

Appendix 3 cont

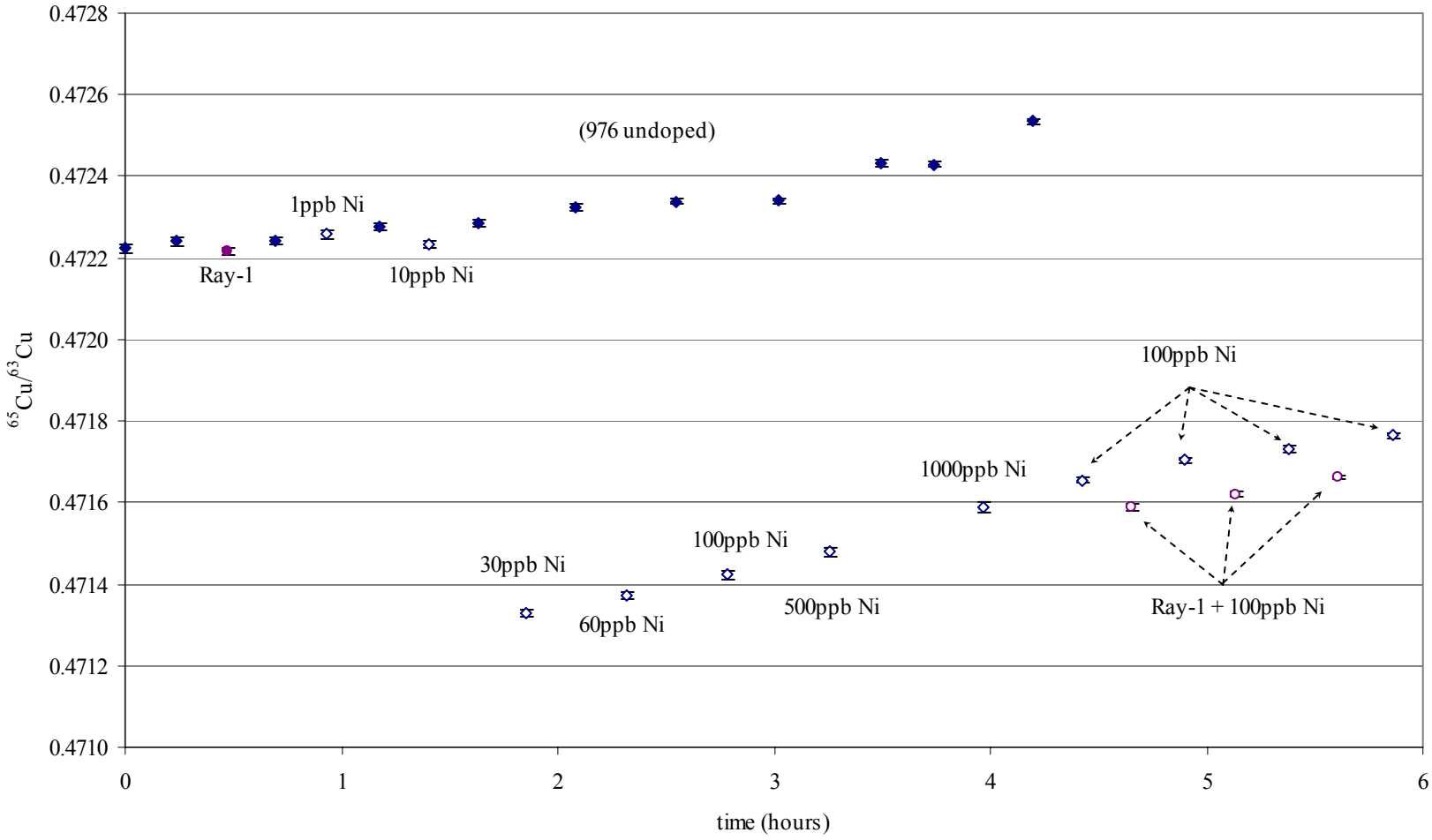

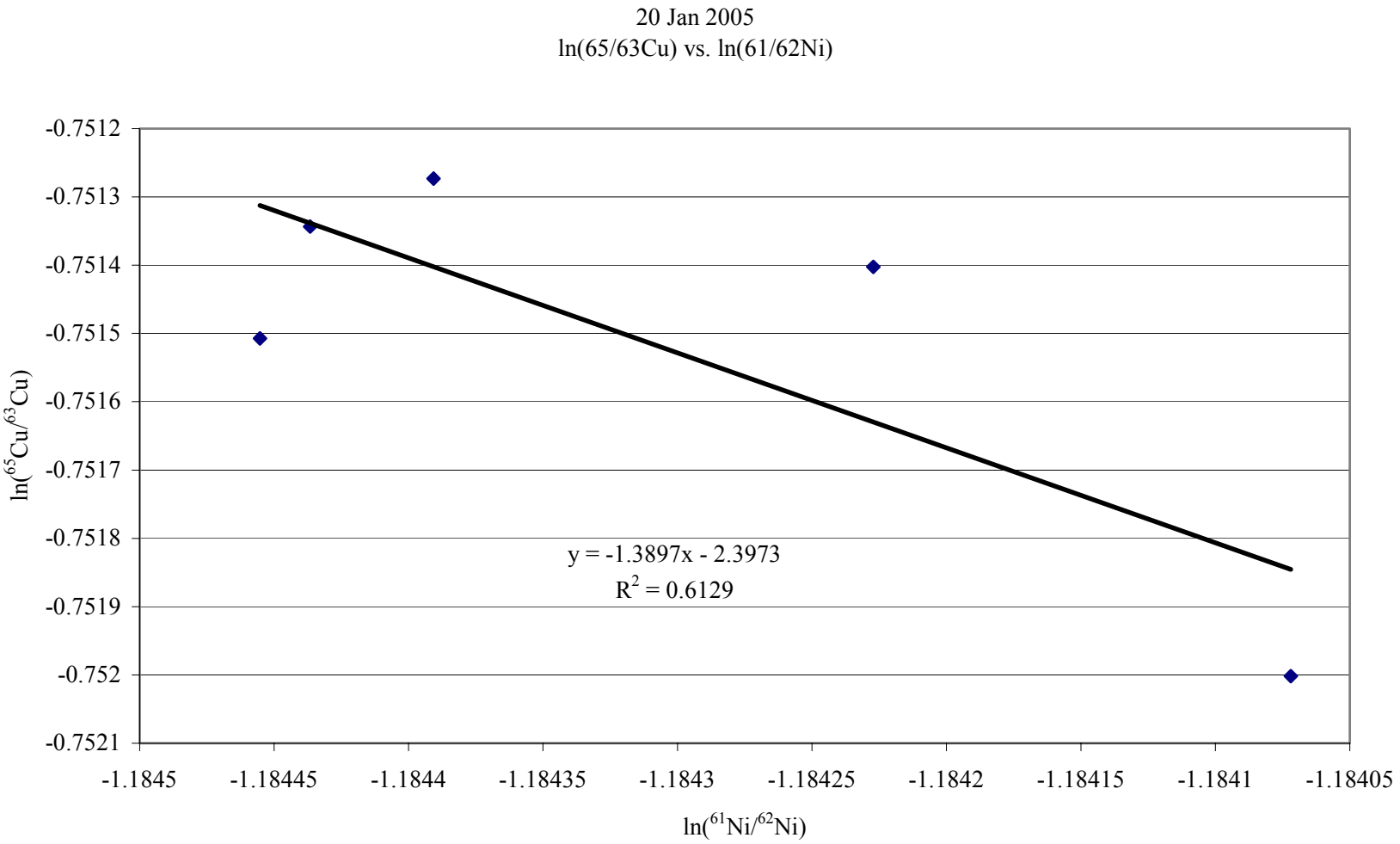
20 Jan 2005
ln(65/63Cu) vs. ln(61/62Ni)
-0.7512
-0.7513
-0.7514
-0.7515
-0.7516
-0.7517
-0.7518
-0.7519
-0.752
-0.7521
ln(65Cu/63Cu)
y = -1.3897x - 2.3973
R2 = 0.6129
-1.1845
-1.18445
-1.1844
-1.18435
-1.1843
-1.18425
-1.1842
-1.18415
-1.1841
-1.18405
ln(61Ni/62Ni)

Appendix 3 cont

20 Jan 2005
Ni isotope ratio relative to Cu:Ni concentration ratio

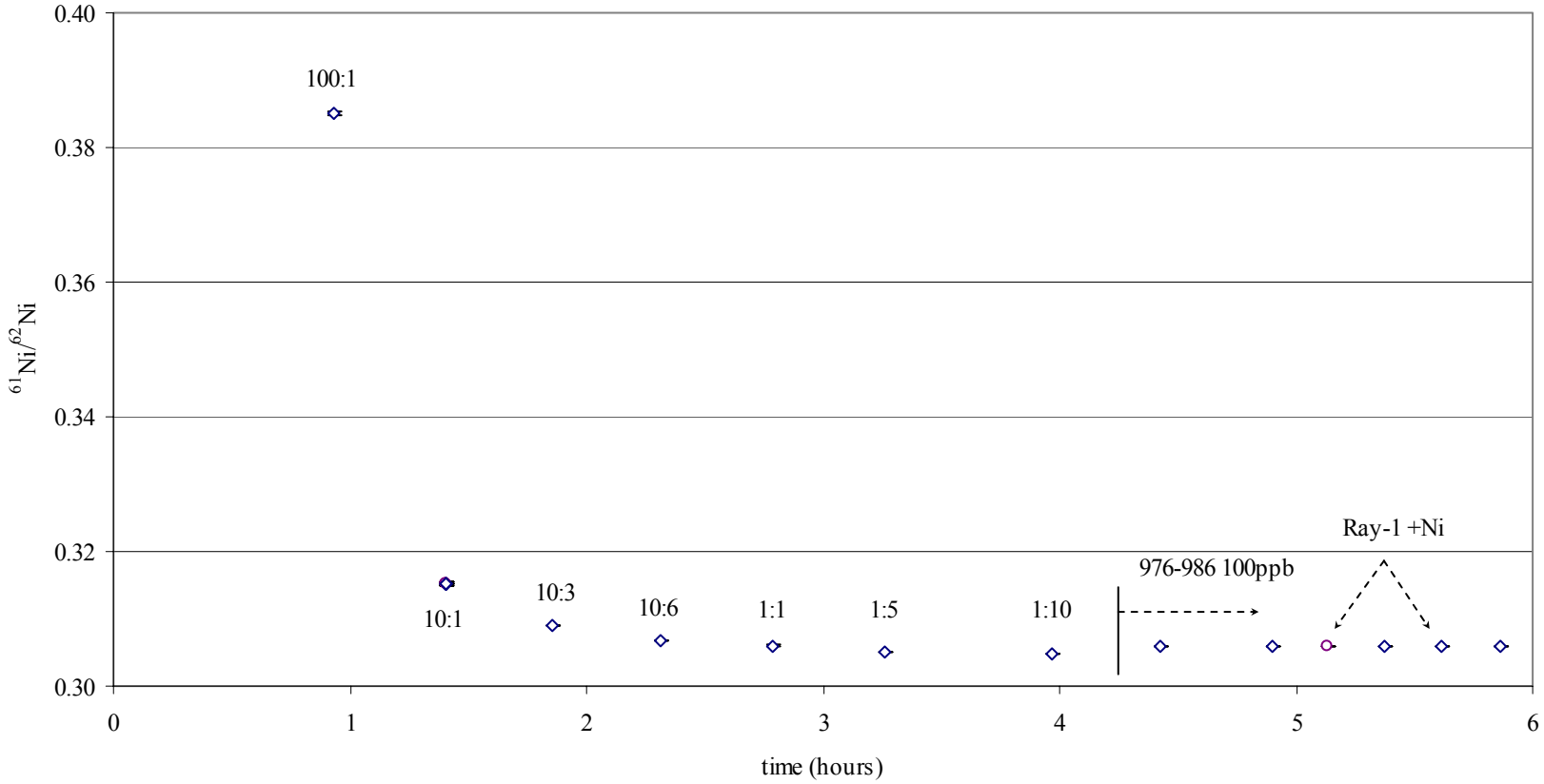

Appendix 3 cont.

date	analysis	raw $^{65}Cu/^{63}Cu$	error (2σ)	$\delta^{65}Cu$	^{65}Cu voltage	%Cu of sample relative to standard	drift between bracketing standards (ppm)	raw $^{61}Ni/^{62}Ni$	error (2σ)	$\delta^{65}Cu$ (from $^{61}Ni/^{62}Ni$ doping)	raw $^{62}Ni/^{60}Ni$	error (2σ)	$\delta^{65}Cu$ (from $^{62}Ni/^{60}Ni$ doping)
27-Jan-05	976 #1	0.4725550	1.27E-05		1.299			0.5625276	5.34E-03		0.1735619	7.39E-04	
	976 #2	0.4725307	1.34E-05		1.306			0.4996450	3.40E-03		0.1752193	9.81E-04	
	976 #3	0.4724772	8.98E-06		1.305			0.4957607	5.02E-03		0.1783077	7.35E-04	
	Ray-1 #1	0.4724152	1.11E-05	-0.291	1.366	108.24	285	0.6263383	1.03E-02		0.2097246	1.52E-03	
	976 #4	0.4726121	1.70E-05		1.220			0.4806428	5.79E-03		0.1750268	7.96E-04	
	976 #5	0.4720939	1.81E-05		1.365			0.5059227	3.54E-03		0.1817213	7.66E-04	
	Ray-1 #2	0.4719838	1.11E-05	-0.163	1.442	105.61	-132	0.6424589	7.44E-03		0.2186224	1.64E-03	
	976 #6	0.4720314	1.54E-05		1.367			0.4979707	3.28E-03		0.1835186	8.39E-04	
	Ray-1 #3	0.4719726	1.50E-05	-0.108	1.432	104.48	-45	0.6515200	5.86E-03		0.2191498	1.67E-03	
	976 #7	0.4720101	1.58E-05		1.374			0.5045963	4.69E-03		0.1836595	7.04E-04	
	976-986 #1	0.4710757	8.44E-06		1.226			0.3062406	3.73E-05		0.1469619	6.67E-06	
	976-986 #2	0.4711077	9.62E-06		1.224			0.3062719	3.67E-05		0.1469800	6.88E-06	
	976-986 #3	0.4714117	9.27E-06		1.238			0.3060025	3.00E-05		0.1470376	7.03E-06	
	976-986 #4	0.4714226	9.53E-06		1.216			0.3060471	3.94E-05		0.1470420	7.26E-06	
	Ray-1 +986 #1	0.4713170	8.84E-06	-0.240	1.246	102.32	6	0.3060931	3.84E-05	-0.083	0.1470274	5.78E-06	-0.051
	976-986 #5	0.4714253	6.28E-06		1.220			0.3060515	2.82E-05		0.1470497	3.93E-06	
	Ray-1 +986 #2	0.4713500	9.83E-06	-0.226	1.254	102.78	111	0.3060653	3.85E-05	-0.158	0.1470259	6.20E-06	0.032
	976-986 #6	0.4714777	7.54E-06		1.220			0.3060441	2.98E-05		0.1470542	5.94E-06	
	Ray-1 +986 #3	0.4713849	7.87E-06	-0.234	1.247	102.84	46	0.3061294	3.41E-05	0.065	0.1470403	5.94E-06	-0.064
	976-986 #7	0.4714996	1.06E-05		1.204			0.3060413	4.13E-05		0.1470593	7.37E-06	
	T6237E-4 +986 #1	0.4727138	8.03E-06	2.746	1.497	124.44	-40	0.3061410	3.48E-05	2.979	0.1470386	7.52E-06	2.741
	976-986 #8	0.4714809	8.91E-06		1.202			0.3060073	3.42E-05		0.1470486	5.21E-06	
	LS-10 +986 #1	0.4714905	9.44E-06	0.059	1.078	89.85	-69	0.3061231	3.04E-05	0.390	0.1470312	6.21E-06	0.262
	976-986 #9	0.4714483	7.74E-06		1.196			0.3060351	2.85E-05		0.1470576	7.36E-06	

Appendix 3 cont

27 Jan 2005
CuNi

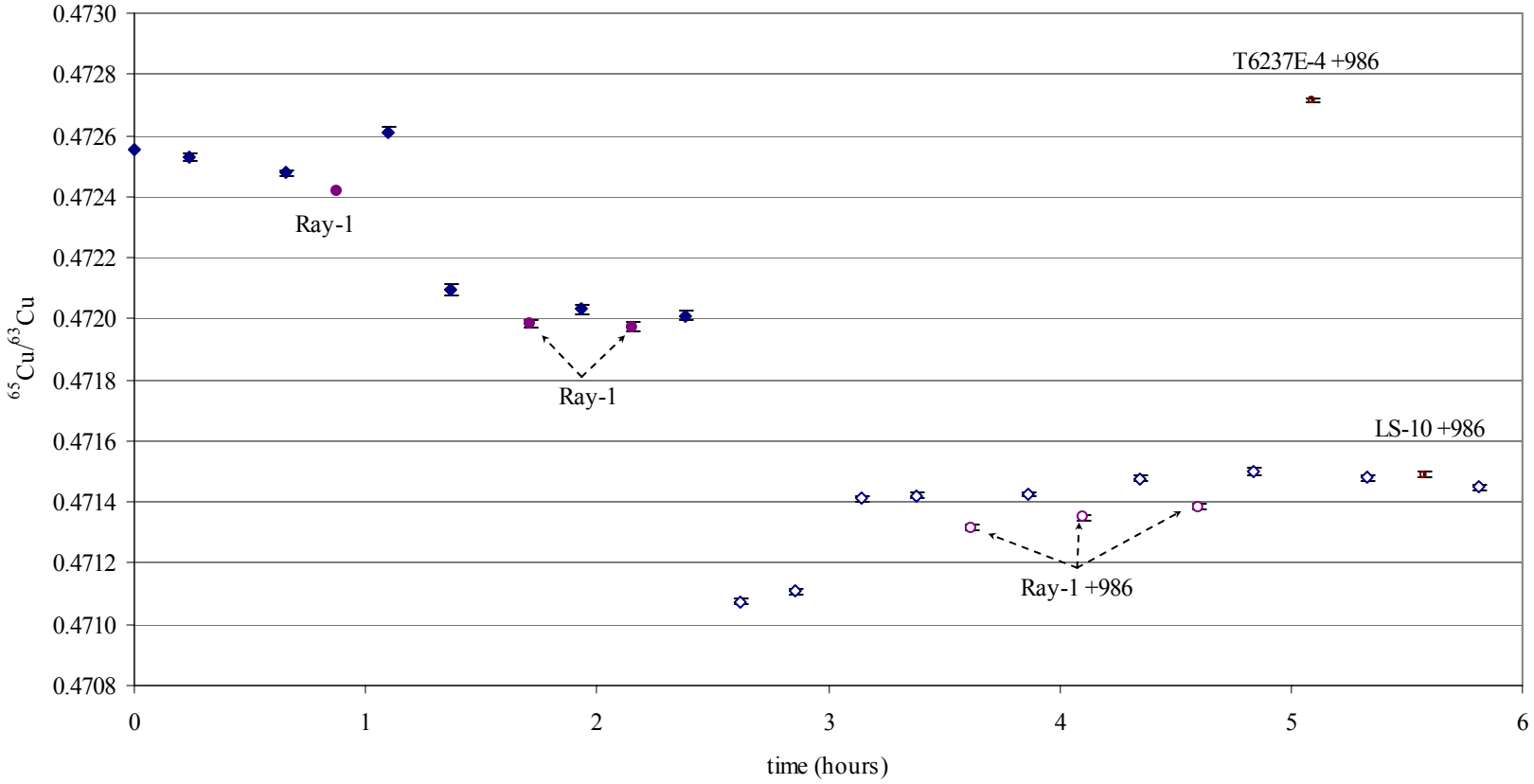

Appendix 3 cont.

date	analysis	raw $^{65}Cu/^{63}Cu$	error (2σ)	$\delta^{65}Cu$	^{65}Cu voltage	%Cu of sample relative to standard	drift between bracketing standards (ppm)	$^{68}Zn/^{64}Zn$	error (2σ)
1-Feb-05	Zn sol #1	0.4553960	4.55E-04		0.005			0.4182343	3.44E-05
	Zn sol + 986 10ppb	0.4551682	3.76E-04		0.005			0.4167854	3.22E-05
	Zn sol #2	0.4555038	3.25E-04		0.005			0.4182509	3.49E-05
	Zn sol + 986 30ppb	0.4540889	4.46E-04		0.005			0.4134513	2.68E-05
	Zn sol #3	0.4555594	4.07E-04		0.005			0.4181367	3.31E-05
	Zn sol + 986 60ppb	0.4550105	3.26E-04		0.005			0.4088182	2.42E-05
	Zn sol #4	0.4555989	4.11E-04		0.004			0.4182993	3.27E-05
	Zn sol +986 100ppb	0.4550126	4.59E-04		0.005			0.4024557	1.76E-05
	Zn sol #5	0.4561924	4.10E-04		0.005			0.4180196	3.13E-05
	Zn sol #6	0.4546833	3.79E-04		0.005			0.4181051	2.81E-05
	976 #1	0.4722584	1.53E-05		1.470			0.4920797	
	976 #2	0.4721739	1.40E-05		1.458			0.4902026	
	976 +30ppbZn	0.4720900	1.17E-05	-0.197	1.281	87.51	16	0.4199539	3.84E-05
	976 #3	0.4721814	1.48E-05		1.470			0.4893762	
	976 +60ppb Zn	0.4720912	1.39E-05	-0.157	1.302	88.86	-86	0.4184747	2.79E-05
	976 #4	0.4721410	1.31E-05		1.461			0.4864732	
	976 +100ppbZn #1	0.4720562	3.68E-05	-0.206	1.301	88.94	33	0.4187331	3.16E-04
	976 #5	0.4721566	1.29E-05		1.464			0.4757804	
	976 +200ppbZn	0.4720834	1.13E-05	-0.178	1.282	87.39	27	0.4173438	2.15E-05
	976 #6	0.4721692	1.08E-05		1.470			0.4799534	
	976 +30ppbZn #2	0.4720858	1.21E-05	-0.173	1.290	87.68	-27	0.4199885	9.39E-05
	976 #7	0.4721565	1.34E-05		1.473			0.4956214	
	976 +30ppbZn #3	0.4720702	1.15E-05		1.288			0.4203934	8.05E-05
	976 + 100ppbZn #2	0.4721149	1.45E-05		1.313			0.4179986	3.34E-05
	976 + 100ppbZn #3	0.4721262	1.24E-05		1.311			0.4181320	3.77E-05

Appendix 3 cont

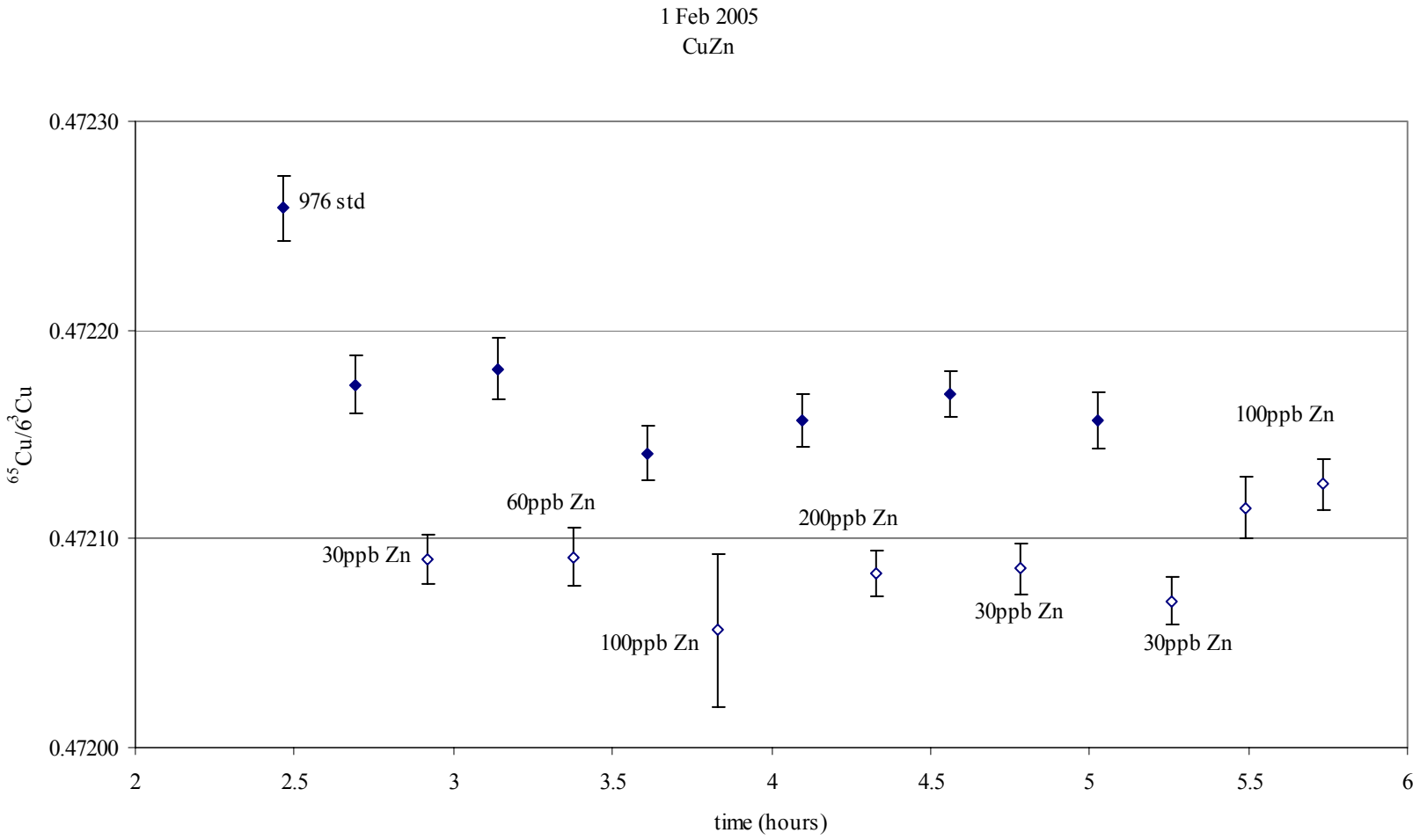

Appendix 3 cont.

date	analysis	raw $^{65}Cu/^{63}Cu$	error (2σ)	$\delta^{65}Cu$	^{65}Cu voltage	%Cu of sample relative to standard	drift between bracketing standards (ppm)
8-Mar-05	976 #1	0.4720620	7.41E-06		1.428		
	976 #2	0.4723778	7.87E-06		1.451		
	976 #3	0.4724190	9.76E-06		1.390		
	976 #4	0.4725128	9.11E-06		1.448		
	976 #5	0.4725461	7.61E-06		1.452		
	Sup-1 #1	0.4727755	1.10E-05	0.516	1.243	85.67	-2
	976 #6	0.4725451	7.87E-06		1.451		
	Sup-1 column #1	0.4727787	7.07E-06	0.509	1.219	84.28	29
	976 #7	0.4725589	6.59E-06		1.441		
	976 #8	0.4725800	7.03E-06		1.425		
	976 #9	0.4726010	1.41E-05		1.427		
	976 #10	0.4725737	7.04E-06		1.416		
	Sup-1 column #2	0.4726698	1.38E-05	0.214	1.123	79.10	2
	976 #11	0.4725749	7.42E-06		1.423		
	1400 18.9 331.75	0.4724775	1.06E-05	-0.246	0.624	44.15	55
	976 #12	0.4726007	6.95E-06		1.403		
	Sup-1 Column #3	0.4728177	7.72E-06	0.460	1.169	84.10	52
	976 #13	0.4726251	7.07E-06		1.377		
	Sup-1 #2[2]	0.4728310	9.66E-06	1.250	1.190	79.98	-1634
	976 #14	0.4718542	9.53E-06		1.598		
	Sup-1 column #4	0.4721277	9.83E-06	0.516	1.334	83.38	182
	976 #15	0.4719403	7.35E-06		1.603		
	Ray-1	0.4718618	7.63E-06	-0.180	1.645	102.42	7
	976 #16	0.4719435	7.55E-06		1.610		
	Ray-1 #2	0.4718633	9.88E-06	-0.170	1.639	101.84	-18
	976 #17	0.4719350	7.87E-06		1.608		
	Phal-1	0.4719958	9.20E-06	0.115	0.826	51.40	42
	976 #18	0.4719546	8.35E-06		1.605		
	OKM-2	0.4719411	9.48E-06	-0.002	1.067	66.50	-54
	976 #19	0.4719291	7.29E-06		1.604		
	BING-6	0.4719732	1.08E-05	0.089	1.949	121.29	20
	976 #20	0.4719383	8.00E-06		1.609		

[1]These standards were corrected to standard #8.

[2](0.44‰) delta calculated from projection of the trend of the standards.

Appendix 3 cont

8 Mar 2005

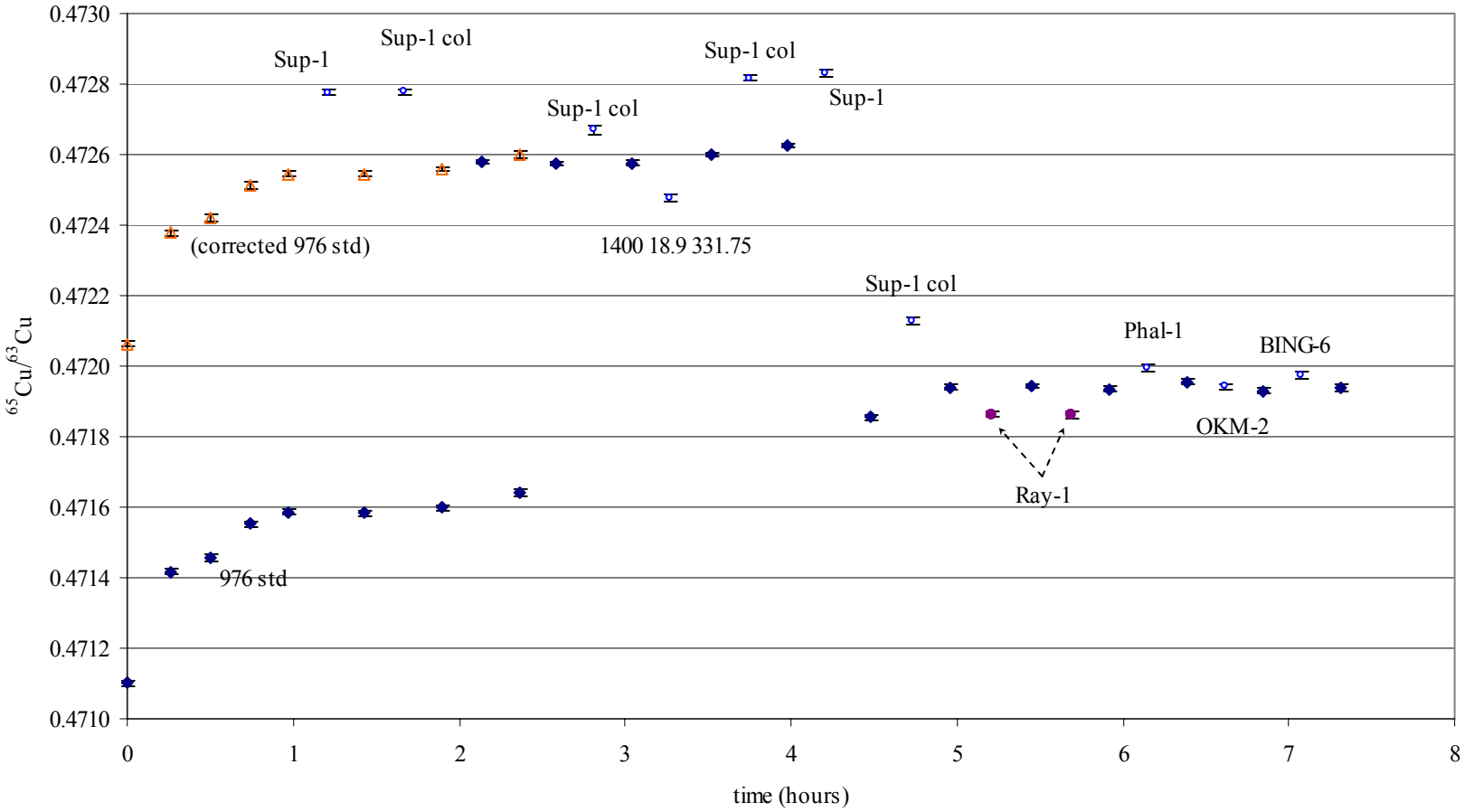

Appendix 3 cont.

date	analysis	raw $^{65}Cu/^{63}Cu$	error (2σ)	$\delta^{65}Cu$	^{65}Cu voltage	%Cu of sample relative to standard	drift between bracketing standards (ppm)	$^{68}Zn/^{64}Zn$	error (2σ)	$\delta^{65}Cu$ from $^{68}Zn/^{64}Zn$	$^{66}Zn/^{64}Zn$	error (2σ)	$\delta^{65}Cu$ from $^{66}Zn/^{64}Zn$
15-Mar-05	976 #1	0.4715753	7.29E-06		1.582								
	976 #2	0.4715646	6.51E-06		1.583								
	976 +Zn #1	0.4715784	7.18E-06		1.458			0.4157067	1.08E-05		0.5958970	1.22E-05	
	976 +Zn #2	0.4716245	6.82E-06		1.457			0.4158031	1.14E-05		0.5959679	1.17E-05	
	976 +Zn #3	0.4716694	6.28E-06		1.462			0.4158954	1.32E-05		0.5960286	1.15E-05	
	Sup-1 +Zn	0.4718834	7.75E-06	0.45	1.404	96.25	51	0.4158276	1.60E-05	0.523	0.5959652	1.08E-05	0.543
	976 +Zn #4	0.4716933	5.29E-06		1.457			0.4159598	1.18E-05		0.5960690	8.80E-06	
	BEAV-2 +Zn	0.4721018	1.26E-05	0.84	1.674	115.28	164	0.4158801	2.46E-05	0.931	0.5960006	1.85E-05	0.949
	976 +Zn #5	0.4717708	6.00E-06		1.448			0.4161041	1.01E-05		0.5961736	8.57E-06	
	Ray-1 +Zn	0.4717418	7.49E-06	-0.04	1.421	98.16	-47	0.4161015	1.14E-05	-0.037	0.5961062	9.50E-06	0.058
	976 +Zn #6	0.4717487	8.78E-06		1.447			0.4161041	1.75E-05		0.5961791	1.44E-05	
	976 #3	0.4718552	6.38E-06		1.340								
	976 #4	0.4718875	6.98E-06		1.552								
	SILV-1	0.4719663	8.70E-06	0.15	1.174	75.41	60						
	976 #5	0.4719157	5.38E-06		1.561								
	1400 18.9 331.75	0.4718126	6.66E-06	-0.25	1.561	100.24	44						
	976 #6	0.4719363	7.37E-06		1.554								
	OKM-2	0.4719861	7.49E-06	0.09	1.565	101.25	41						
	976 #7	0.4719558	6.91E-06		1.537								
	Ray-1	0.4719211	7.44E-06	-0.09	1.560	101.32	32						
	976 #8	0.4719709	5.54E-06		1.543								

analysis	$^{68}Zn/^{66}Zn$	error (2σ)	$\delta^{65}Cu$ from $^{68}Zn/^{66}Zn$	$^{67}Zn/^{68}Zn$	error (2σ)	$\delta^{65}Cu$ from $^{67}Zn/^{68}Zn$	$^{67}Zn/^{66}Zn$	error (2σ)	$\delta^{65}Cu$ from $^{67}Zn/^{66}Zn$	$^{67}Zn/^{64}Zn$	error (2σ)	$\delta^{65}Cu$ from $^{67}Zn/^{64}Zn$
976 #1												
976 #2												
976 +Zn #1	0.6976154	1.32E-05		0.2141409	8.17E-06		0.1493892	5.61E-06		0.0890212	3.31E-06	
976 +Zn #2	0.6976996	1.05E-05		0.2141402	8.14E-06		0.1494039	5.68E-06		0.0890398	3.68E-06	
976 +Zn #3	0.6977728	1.42E-05		0.2141125	8.23E-06		0.1494027	4.49E-06		0.0890486	2.64E-06	

Appendix 3 cont.

	analysis	$^{68}Zn/^{66}Zn$	error (2σ)	$\delta^{65}Cu$ from $^{68}Zn/^{66}Zn$	$^{67}Zn/^{68}Zn$	error (2σ)	$\delta^{65}Cu$ from $^{67}Zn/^{68}Zn$	$^{67}Zn/^{66}Zn$	error (2σ)	$\delta^{65}Cu$ from $^{67}Zn/^{66}Zn$	$^{67}Zn/^{64}Zn$	error (2σ)	$\delta^{65}Cu$ from $^{67}Zn/^{64}Zn$
15-Mar-05	Sup-1 +Zn	0.6977330	1.66E-05	0.503	0.2141419	8.79E-06	0.672	0.1494139	5.36E-06	0.337	0.0890461	3.56E-06	0.467
(cont.)	976 +Zn #4	0.6978250	1.45E-05		0.2141018	8.40E-06		0.1494072	5.09E-06		0.0890567	3.13E-06	
	BEAV-2 +Zn	0.6977755	2.38E-05	0.914	0.2141311	9.56E-06	0.997	0.1494162	5.55E-06	0.807	0.0890513	4.18E-06	0.898
	976 +Zn #5	0.6979572	1.29E-05		0.2140923	7.16E-06		0.1494270	4.77E-06		0.0890849	2.70E-06	
	Ray-1 +Zn	0.6980362	1.29E-05	-0.129	0.2141087	7.08E-06	0.060	0.1494558	5.19E-06	-0.281	0.0890915	3.03E-06	-0.070
	976 +Zn #6	0.6979531	1.71E-05		0.2140984	8.85E-06		0.1494309	5.95E-06		0.0890872	4.00E-06	

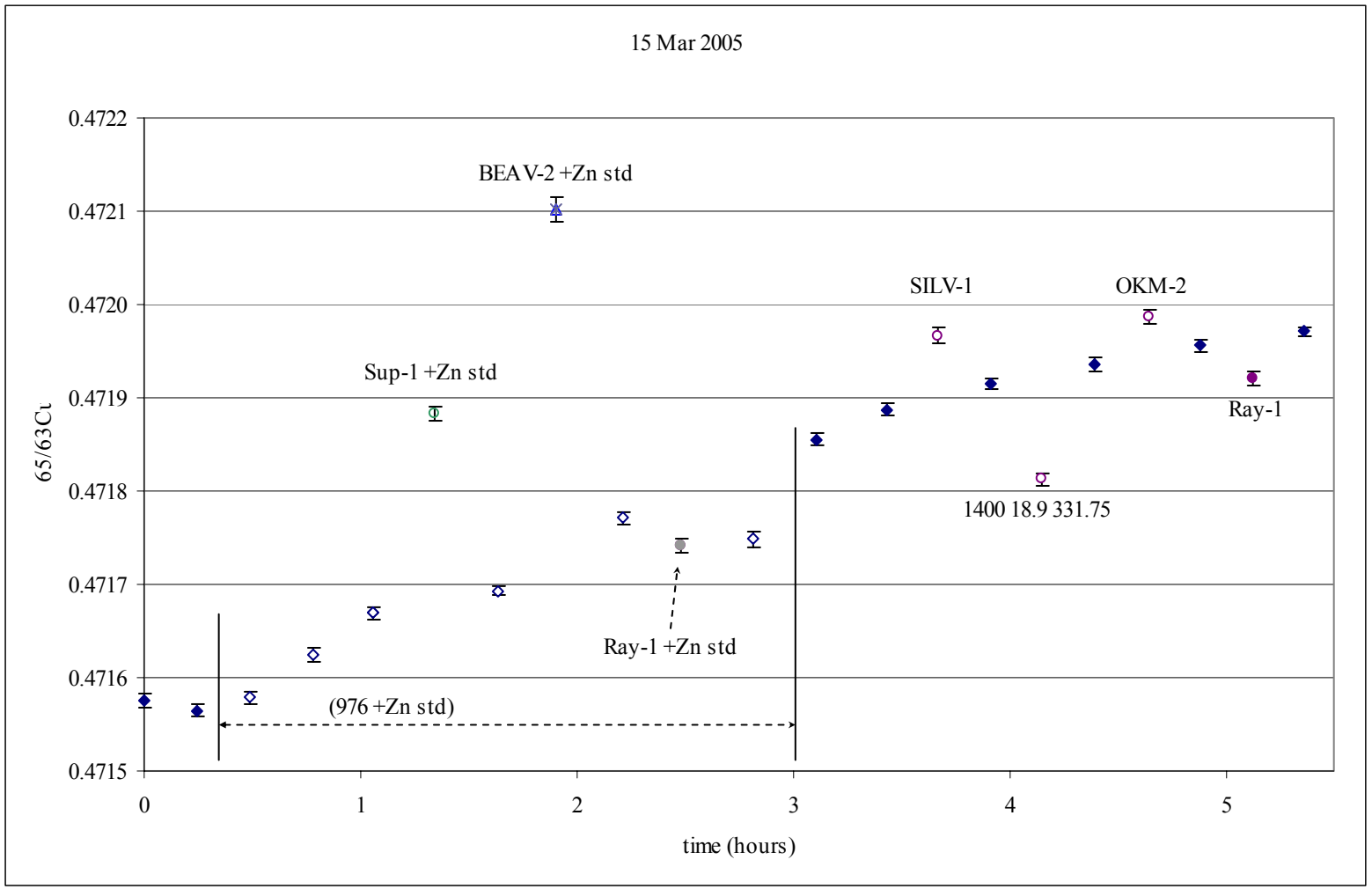
15 Mar 2005
0.4722
0.4721
0.4720
0.4719
0.4718
0.4717
0.4716
0.4715
65/63Cu
BEAV-2 +Zn std
Sup-1 +Zn std
SILV-1
OKM-2
Ray-1
1400 18.9 331.75
Ray-1 +Zn std
(976 +Zn std)
0
1
2
3
4
5
time (hours)

Appendix 3 cont

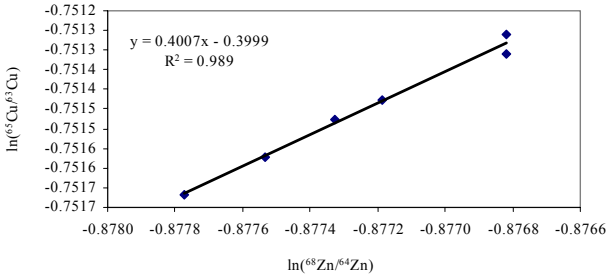

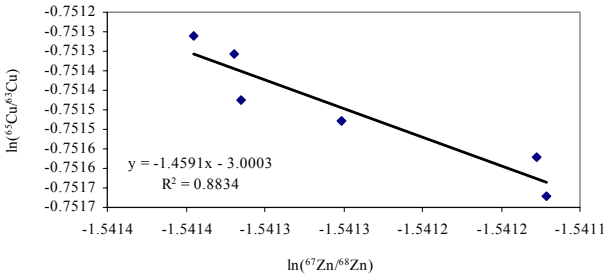

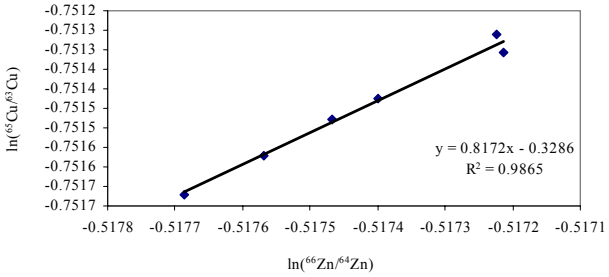

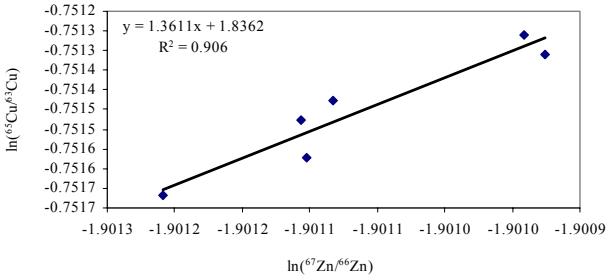

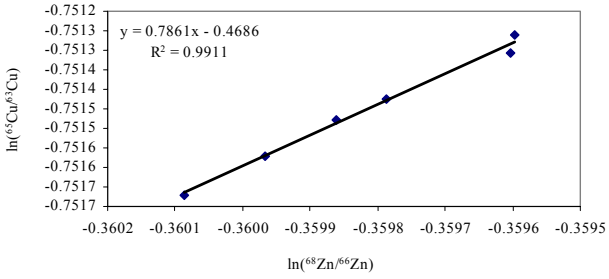

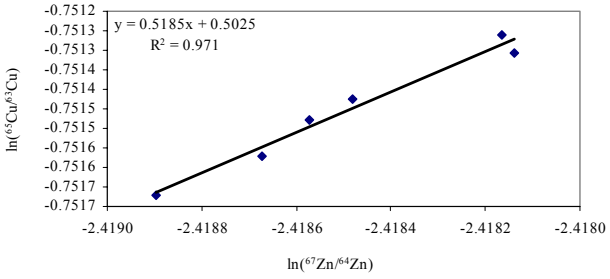

Appendix 3 cont.

date	analysis	raw $^{65}Cu/^{63}Cu$	error (2σ)	$\delta^{65}Cu$	^{65}Cu voltage	%Cu of sample relative to standard	drift between bracketing standards (ppm)	$^{68}Zn/^{64}Zn$	error (2σ)	$\delta^{65}Cu$ from $^{68}Zn/^{64}Zn$	$^{66}Zn/^{64}Zn$	error (2σ)	$\delta^{65}Cu$ from $^{66}Zn/^{64}Zn$
24-Mar-05	976 #1	0.4714823	7.22E-06		1.537								
	976 #2	0.4715000	8.20E-06		1.535								
	976 #3	0.4715038	9.58E-06		1.531								
	LS-10	0.4716086	7.68E-06	0.22	1.336	86.89	30						
	976 #4	0.4715177	7.01E-06		1.544								
	RAY-1	0.4714532	8.40E-06	-0.14	1.545	100.02	-15						
	976 #5	0.4715106	7.67E-06		1.544								
	SUP-1	0.4717406	7.44E-06	0.47	1.276	82.51	89						
	976 #6	0.4715526	6.08E-06		1.548								
	SUP-1 col	0.4717940	6.27E-06	0.52	1.295	83.77	39						
	976 #7	0.4715709	6.58E-06		1.545								
	1400 21.7 119.6	0.4718223	6.22E-06	0.56	1.368	88.56	11						
	976 #8	0.4715763	7.15E-06		1.545								
	T990N080E	0.4713589	6.81E-06	-0.50	1.181	76.50	16						
	976 #9	0.4715838	5.90E-06		1.541								
	RAY-1 #2	0.4715707	5.44E-06	-0.06	1.544	100.12	57						
	976 #10	0.4716108	7.67E-06		1.543								
	SUP-1 #2	0.4718308	5.81E-06	0.49	1.278	82.70	2						
	976 #11	0.4716117	6.36E-06		1.547								
	976 +Zn #1	0.4716172	6.48E-06		1.487			0.4157529	8.50E-06		0.5959304	9.83E-06	
	976 +Zn #2	0.4716253	6.13E-06		1.478			0.4157947	8.85E-06		0.5959481	7.74E-06	
	976 +Zn #3	0.4716221	5.93E-06		1.477			0.4157788	9.34E-06		0.5959465	9.13E-06	
	RAY-1 +Zn	0.4715399	6.89E-06	-0.187	1.372	93.04	4	0.4154394	1.15E-05	0.105	0.5953823	1.13E-05	1.459
	976 +Zn #4	0.4716240	4.75E-06		1.473			0.4157754	8.63E-06		0.5959471	9.61E-06	
	BEAV-2 #2	0.4720343	9.94E-06	0.908	1.623	109.97	24	0.4157341	2.11E-05	1.073	0.5958756	1.75E-05	1.719
	976 +Zn #5	0.4716355	7.26E-06		1.479			0.4157955	1.13E-05		0.5959534	1.11E-05	

Appendix 3 cont.

	analysis	$^{68}Zn/^{66}Zn$	error (2σ)	$\delta^{65}Cu$ from $^{68}Zn/^{66}Zn$	$^{67}Zn/^{68}Zn$	error (2σ)	$\delta^{65}Cu$ from $^{67}Zn/^{68}Zn$	$^{67}Zn/^{66}Zn$	error (2σ)	$\delta^{65}Cu$ from $^{67}Zn/^{66}Zn$	$^{67}Zn/^{64}Zn$	error (2σ)	$\delta^{65}Cu$ from $^{67}Zn/^{64}Zn$
24-Mar-05	976 +Zn #1	0.697657	1.18E-05		0.214129	9.41E-06		0.149391	5.89E-06		0.089026	3.6E-06	
(cont.)	976 +Zn #2	0.697700	1.30E-05		0.214121	7.61E-06		0.149392	5.12E-06		0.089030	2.96E-06	
	976 +Zn #3	0.697684	1.47E-05		0.214129	8.86E-06		0.149394	6.39E-06		0.089030	4E-06	
	RAY-1 +Zn	0.697769	1.45E-05	0.619	0.214149	7.52E-06	0.683	0.149426	5.93E-06	0.529	0.088965	3.88E-06	0.96
	976 +Zn #4	0.697679	1.34E-05		0.214129	7.72E-06		0.149392	5.55E-06		0.089029	3.72E-06	
	BEAV-2 #2	0.697681	2.19E-05	1.619	0.214142	8.00E-06	1.622	0.149403	6.26E-06	1.578	0.089025	4.84E-06	1.64
	976 +Zn #5	0.697693	1.17E-05		0.214129	5.87E-06		0.149395	4.61E-06		0.089033	2.93E-06	

Appendix 3 cont

24 Mar 2005

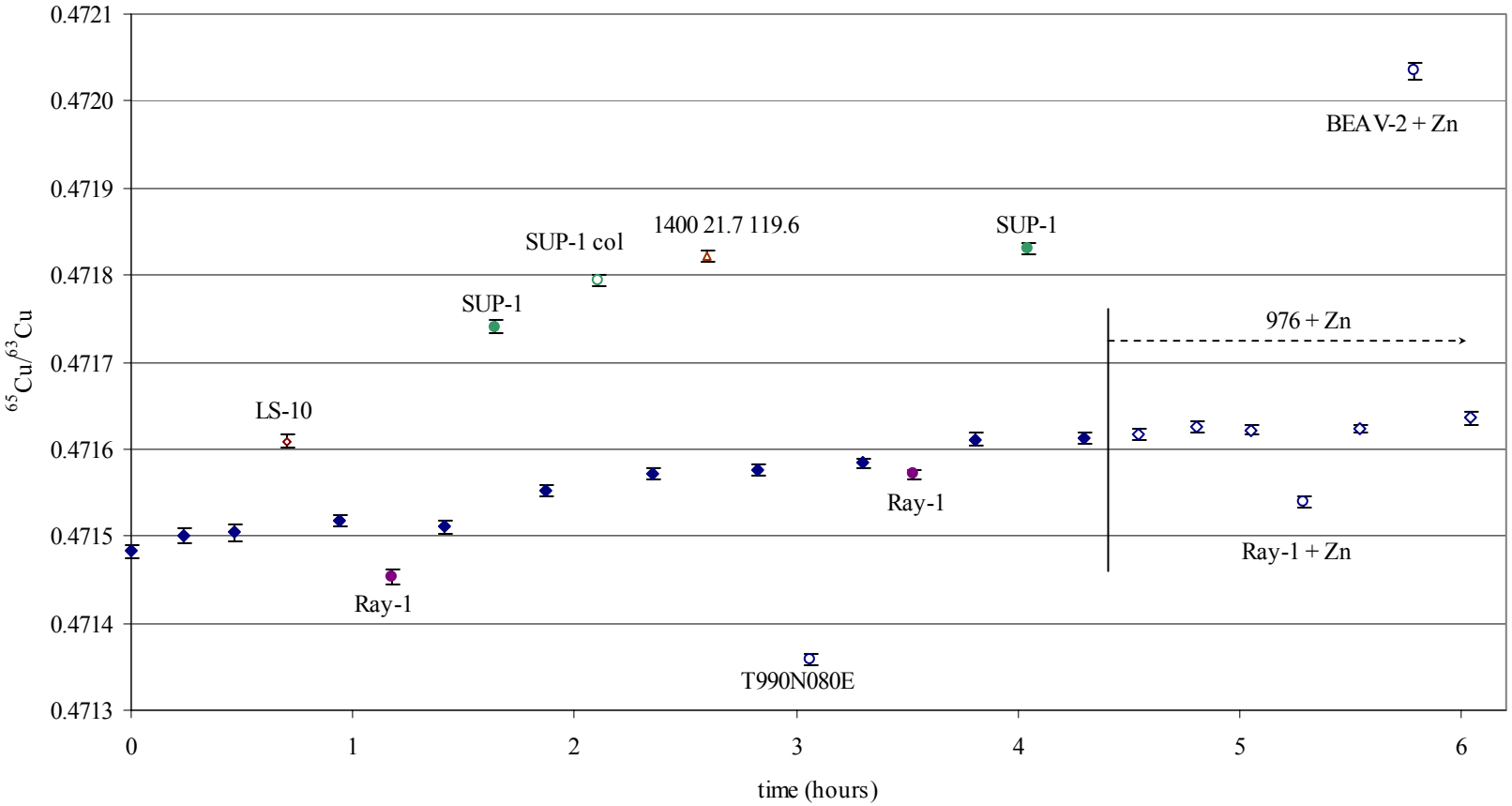

Appendix 3 cont

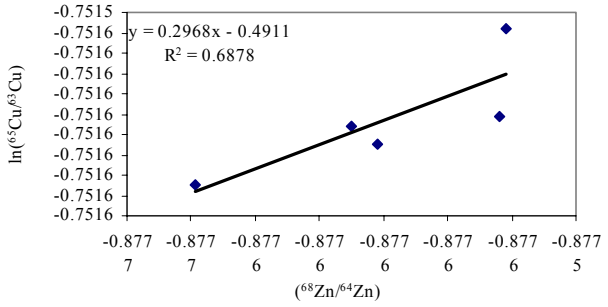

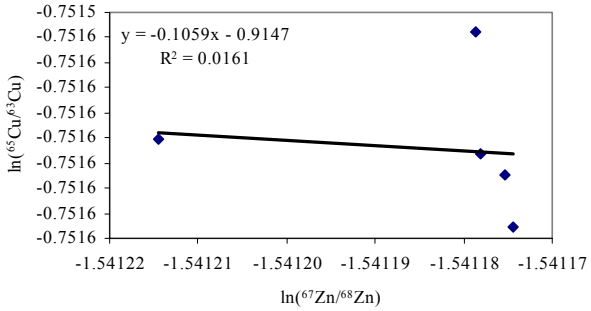

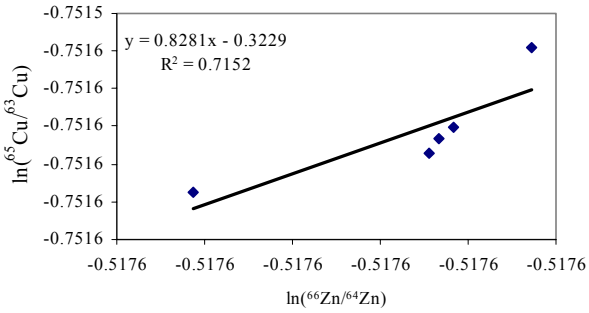

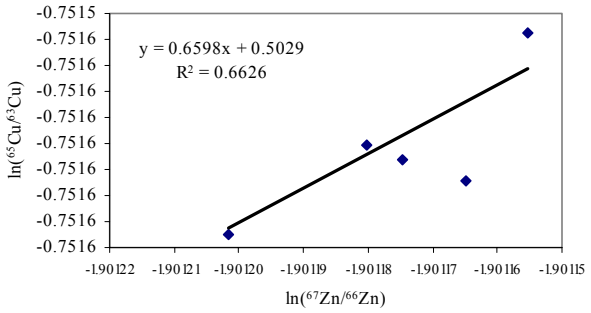

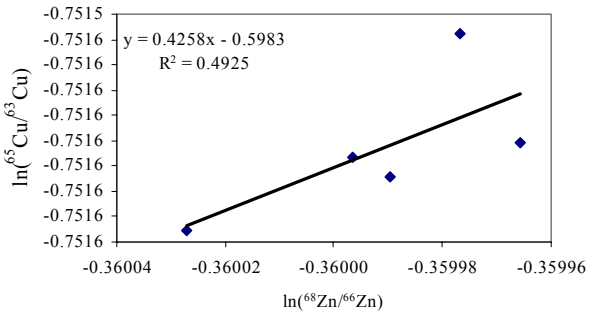

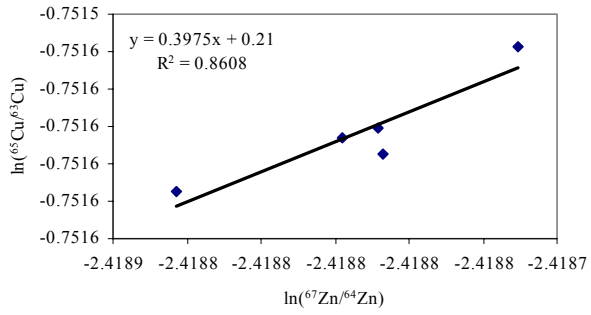

Appendix 3 cont.

date	analysis	raw $^{65}Cu/^{63}Cu$	error (2σ)	$\delta^{65}Cu$	^{65}Cu voltage	%Cu of sample relative to standard	drift between bracketing standards (ppm)	$^{68}Zn/^{64}Zn$	error (2σ)	$\delta^{65}Cu$ from $^{68}Zn/^{64}Zn$	$^{66}Zn/^{64}Zn$	error (2σ)	$\delta^{65}Cu$ from $^{66}Zn/^{64}Zn$
25-Mar-05	976 #1	0.4718112	6.86E-06		1.628								
	976 #2	0.4718639	8.61E-06		1.612								
	976 #3	0.4718882	5.52E-06		1.602								
	RAY-1 #1	0.4718674	5.83E-06	-0.101	1.596	100.08	103						
	976 #4	0.4719366	8.47E-06		1.588								
	BEAV-2 #1	0.4723830	7.83E-06	0.993	1.279	80.69	16						
	976 #5	0.4719440	7.34E-06		1.583								
	RAY-1 #2	0.4718984	5.36E-06	-0.183	1.585	100.81	148						
	976 #6	0.4720139	7.41E-06		1.562								
	976 #7	0.4719865	6.52E-06		1.614								
	976 +Zn #1	0.4719999	6.73E-06		1.546			0.4166462	9.91E-06		0.5965529	1.01E-05	
	976 +Zn #2	0.4719928	7.00E-06		1.541			0.4166241	1.02E-05		0.5965325	1.11E-05	
	976 +Zn #3	0.4719921	6.64E-06		1.529			0.4166202	9.41E-06		0.5965439	9.32E-06	
	RAY-1 +Zn #1	0.4719405	8.38E-06	-0.095	1.443	94.62	-39	0.4165737	1.00E-05	-0.062	0.5964908	9.85E-06	-0.032
	976 +Zn #4	0.4719739	6.02E-06		1.522			0.4165845	9.35E-06		0.5965191	8.04E-06	
	RAY-1 +Zn #2	0.4719165	7.26E-06	-0.129	1.436	94.21	1	0.4165349	1.24E-05	-0.071	0.5964640	1.27E-05	-0.051
	976 +Zn#5	0.4719745	6.09E-06		1.526			0.4165910	9.30E-06		0.5965087	9.05E-06	
	RAY-1 +Zn #3	0.4719103	5.58E-06	-0.143	1.402	91.75	-1	0.4165073	9.75E-06	-0.060	0.5964654	9.34E-06	-0.078
	976 +Zn #6	0.4719740	6.20E-06		1.530			0.4165783	9.30E-06		0.5965022	9.39E-06	
	BEAV-2 +Zn #1	0.4723917	6.02E-06	0.947	1.719	112.99	-17	0.4165457	1.32E-05	0.921	0.5964748	1.47E-05	0.938
	976 +Zn #7	0.4719658	6.16E-06		1.513			0.4165699	9.16E-06		0.5965093	9.58E-06	
	BEAV-2 +Zn #2	0.4723473	7.17E-06	0.886	1.674	110.67	-56	0.4164509	1.22E-05	0.919	0.5964149	8.22E-06	0.934
	976 +Zn #8	0.4719394	7.30E-06		1.511			0.4165027	8.68E-06		0.5964572	9.30E-06	
	RAY-1 +Zn #4	0.4719021	6.23E-06	-0.085	1.385	91.54	2	0.4164972	1.01E-05	-0.065	0.5964580	1.00E-05	-0.073
	976 +Zn #9	0.4719402	7.77E-06		1.515			0.4165216	1.05E-05		0.5964687	9.64E-06	
	BEAV-2 #2	0.4724333	5.64E-06	1.088	1.291	85.11	34	0.4171931	1.22E-05		0.5964149	8.22E-06	
	976 +Zn #10	0.4719564	6.69E-06		1.519			0.4165492	8.72E-06		0.5964962	6.71E-06	

Appendix 3 cont.

	analysis	$^{68}Zn/^{66}Zn$	error (2σ)	$\delta^{65}Cu$ from $^{68}Zn/^{66}Zn$	$^{67}Zn/^{68}Zn$	error (2σ)	$\delta^{65}Cu$ from $^{67}Zn/^{68}Zn$	$^{67}Zn/^{66}Zn$	error (2σ)	$\delta^{65}Cu$ from $^{67}Zn/^{66}Zn$	$^{67}Zn/^{64}Zn$	error (2σ)	$\delta^{65}Cu$ from $^{67}Zn/^{64}Zn$
25-Mar-05	976 +Zn #1	0.6984306	1.30E-05		0.2140170	7.34E-06		0.1494757	5.3E-06		0.0890180	1.93E-05	
(cont.)	976 +Zn #2	0.6984064	1.32E-05		0.2140211	8.09E-06		0.1494737	5.57E-06		0.0891656	3.36E-06	
	976 +Zn #3	0.6983995	1.50E-05		0.2140106	8.83E-06		0.1494639	6.11E-06		0.0891611	3.58E-06	
	RAY-1 +Zn #1	0.6983761	1.15E-05	-0.091	0.2140400	8.77E-06	0.010	0.1494802	6.19E-06	-0.187	0.0891636	4.11E-06	-0.107
	976 +Zn #4	0.6983512	1.41E-05		0.2140263	6.98E-06		0.1494652	4.98E-06		0.0891591	3.22E-06	
	RAY-1 +Zn #2	0.6983421	1.44E-05	-0.100	0.2140222	7.57E-06	-0.147	0.1494622	5.31E-06	-0.069	0.0891488	3.43E-06	-0.040
	976 +Zn#5	0.6983761	1.35E-05		0.2140287	6.91E-06		0.1494724	4.89E-06		0.0891613	3.13E-06	
	RAY-1 +Zn #3	0.6982992	1.54E-05	-0.056	0.2140362	8.62E-06	-0.081	0.1494611	6.07E-06	-0.083	0.0891488	3.62E-06	-0.064
	976 +Zn #6	0.6983751	1.20E-05		0.2140204	7.66E-06		0.1494674	5.89E-06		0.0891563	3.77E-06	
	BEAV-2 +Zn #1	0.6983537	1.38E-05	0.899	0.2140255	8.78E-06	0.908	0.1494665	6.36E-06	0.887	0.0891524	3.84E-06	0.923
	976 +Zn #7	0.6983417	1.26E-05		0.2140245	7.78E-06		0.1494613	5.21E-06		0.0891549	3.38E-06	
	BEAV-2 +Zn #2	0.6982573	1.58E-05	0.902	0.2140426	7.15E-06	0.885	0.1494568	5.11E-06	0.877	0.0891138	3.18E-05	0.921
	976 +Zn #8	0.6983005	1.06E-05		0.2140397	6.48E-06		0.1494634	4.52E-06		0.0891482	2.92E-06	
	RAY-1 +Zn #4	0.6982871	1.53E-05	-0.055	0.2140429	7.67E-06	-0.044	0.1494627	4.97E-06	-0.081	0.0891476	3.41E-06	-0.080
	976 +Zn #9	0.6983228	1.36E-05		0.2140306	7.61E-06		0.1494620	5.13E-06		0.0891491	3.55E-06	
	BEAV-2 #2	0.6982573	1.58E-05		0.2140426	7.15E-06		0.1494568			0.0892971		
	976 +Zn #10	0.6983288	1.43E-05		0.2140314	9.78E-06		0.1494638	6.53E-06		0.0891545	4.18E-06	

Appendix 3 cont.

25 Mar 2005

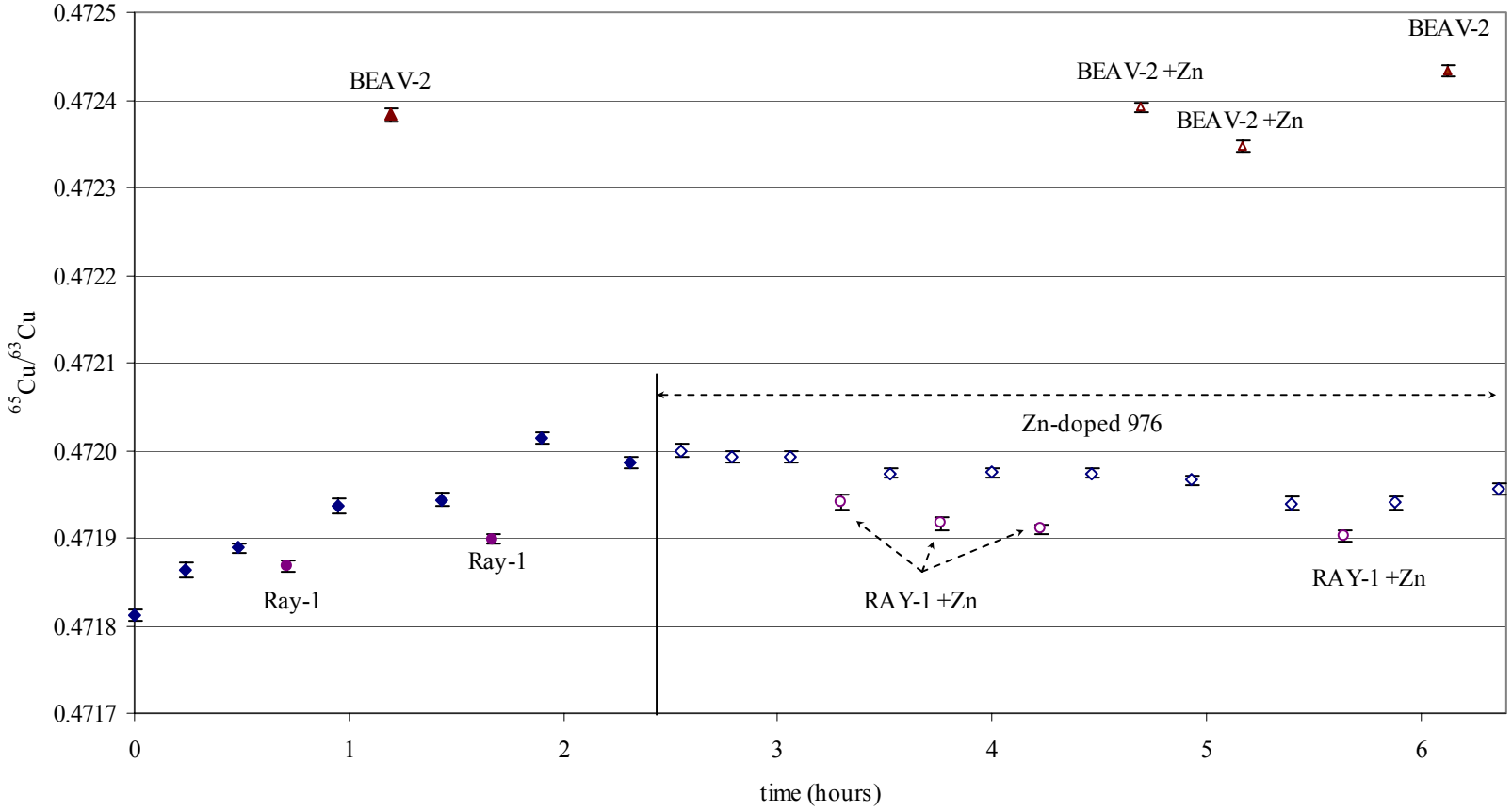

25 Mar 2005
drift of Zn doped samples

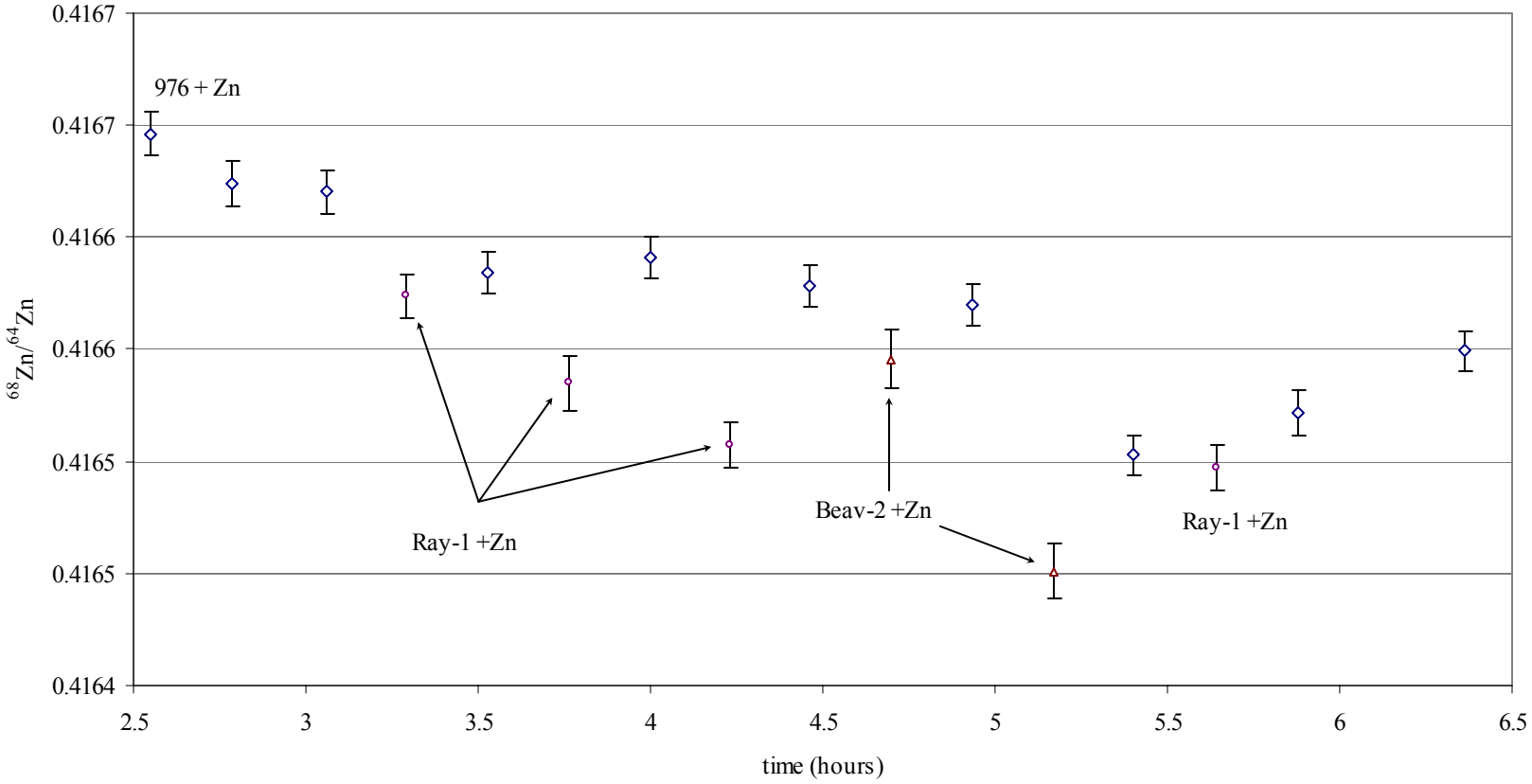

Appendix 3 cont.

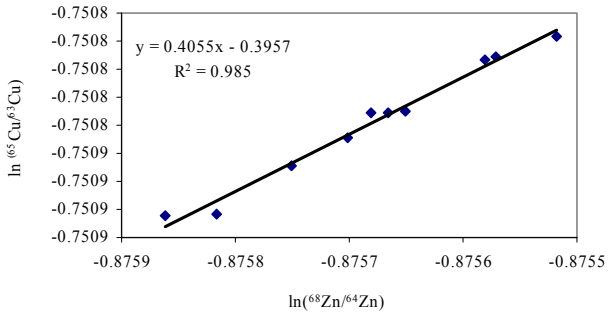

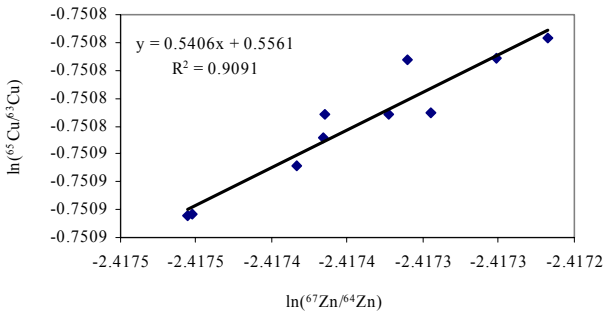

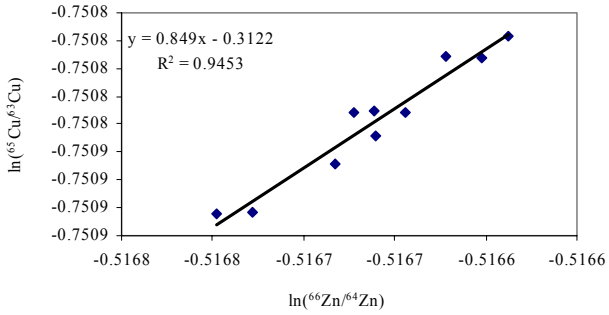

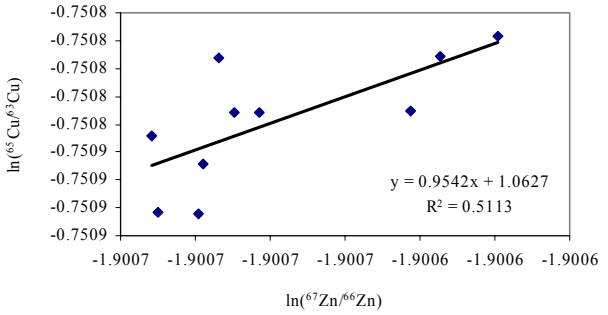

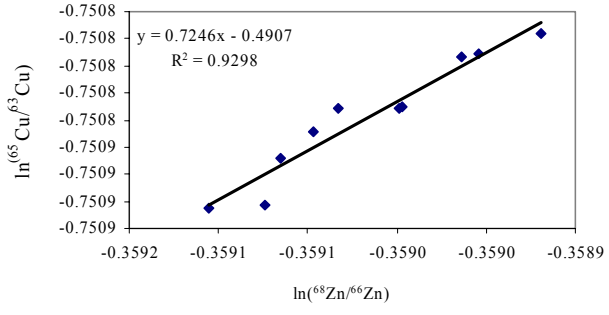

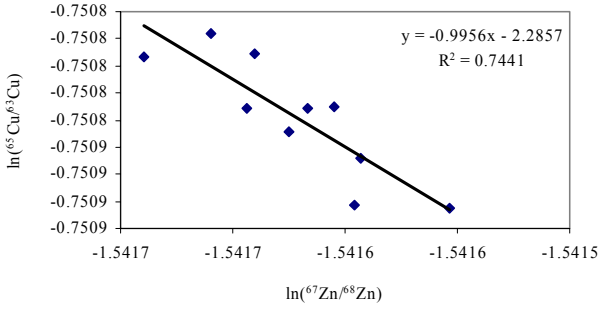

Appendix 4

Manuscript of Maher and Larson (in review)

The following manuscript describes the copper isotope variations in the Tintaya district, Perú, and proposes a high temperature fractionation mechanism to explain isotopic zonation in these deposits. This manuscript was submitted to Economic Geology (April. 2005) and is currently in review.

Variation in copper isotope ratios and controls on fractionation in hypogene skarn mineralization at Coroccohuayco and Tintaya, Perú

Kierran C. Maher

Peter B. Larson

Department of Geology

PO Box 642812

Washington State University

Pullman, WA 99164

Submitted to Economic Geology

April 2005

Abstract

Hypogene chalcopyrite and bornite in copper skarn and related porphyry ore from Coroccohuayco and Tintaya, Perú, have been analyzed for copper isotope ratios. Fifty-six samples of chalcopyrite and bornite mineralization show a copper isotope range of -1.29 to 2.98 per mil δ^{65}Cu (relative to NIST SRM 976) utilizing the sample-standard bracketing technique to correct for machine drift and machine isotope fractionation. Veins and porphyry-hosted mineralization tend to be isotopically lighter than disseminated skarn-hosted mineralization. Based on zoned skarn mineralogy and proximity to mineralizing fluid sources, copper isotope ratios locally show considerable isotopic zonation in hypogene ores from isotopically lighter early/proximal mineralization to isotopically heavier later/distal mineralization. In addition, most co-precipitated chalcopyrite-bornite mineral pairs show a consistent copper fractionation of 0.38 per mil (± 0.04‰, 1σ), even though there is significant range in their chalcopyrite values. This indicates that an important and consistent equilibrium copper isotope fractionation mechanism occurred during co-precipitation. Based on geologic constraints from Coroccohuayco and Tintaya, the most important cause of copper fractionation in these deposits may be related to isotopic fractionation among the dominant copper complexes in the hydrothermal fluid. Due to preferential thermodynamic instability of these different complexes, both temporal and spatial copper isotopic variations were produced during hypogene precipitation of the copper minerals in the deposits. Since copper isotopes appear to fractionate under certain physicochemical conditions, it is expected that copper isotopes can be used as mineralization zonation guides for exploration and development purposes. In addition, the probable relationship of copper isotope fractionation to physicochemical conditions of the hydrothermal fluids allows copper isotopes to be used to improve understanding of mineral precipitation mechanisms and controls.

Introduction

Several recent studies have examined copper isotope ratios in ore-forming environments (Rouxel et al., 2004; Graham et al., 2004). Previous investigations have outlined analytical techniques and the general ranges of copper isotope variations in nature (Marechel et al., 1999; Zhu et al., 2000; Larson et al., 2003). In addition, several experimental studies have been published that shed light on copper isotopic fractionation and isotopic fractionation mechanisms at low temperatures (Maréchal and Albarède, 2002; Young and Ruiz, 2003; Ehrlich et al., 2004). Research reported here demonstrates copper isotope fractionations in the hypogene ore-forming environment in copper deposits of the Tintaya district, Perú, and describes some general features of Cu-isotopic fractionation in these higher-temperature environments.

Earlier work has shown that measurable variability in the copper isotope ratios exists in hypogene (>200º C) ore-forming systems. Based on theoretical considerations of equilibrium isotopic fractionation (Urey, 1947), fractionation at elevated temperature will become less significant when mass differences between isotopes are small (such as for Cu, Fe and Zn). However, studies such as Larson et al. (2003) and Graham et al. (2004) indicate that significant fractionation of copper and iron isotopes occurs at high temperature (>200º C) in ore-forming systems. Possible causes for isotopic variations in ore systems proposed by these and other workers include equilibrium fractionation, source heterogeneity, mixing of isotopic reservoirs, and redox-controlled fractionation in elements of more than one valence. Interpretation of high-temperature isotopic fractionation mechanisms of transition elements to a certain extent awaits the characterization of isotopic reservoirs in the earth and experimental studies of Cu-fractionation at high temperatures. This paper presents copper isotopic data in a geologic context for two high-temperature skarn-forming systems in the Tintaya district, Perú, and provides a possible fractionation mechanism for copper isotopes in these systems.

Geology of the Deposits

The Tintaya district lies in the Department of Cusco in the southeastern Andes of Perú (Fig. 1). The district consists of several porphyry-related copper skarn deposits including Tintaya, Coroccohuayco, Quechas, Antapaccay, Ccatun Pucara and other prospects in the mineral concession operated by BHP Billiton Tintaya S.A. The district lies

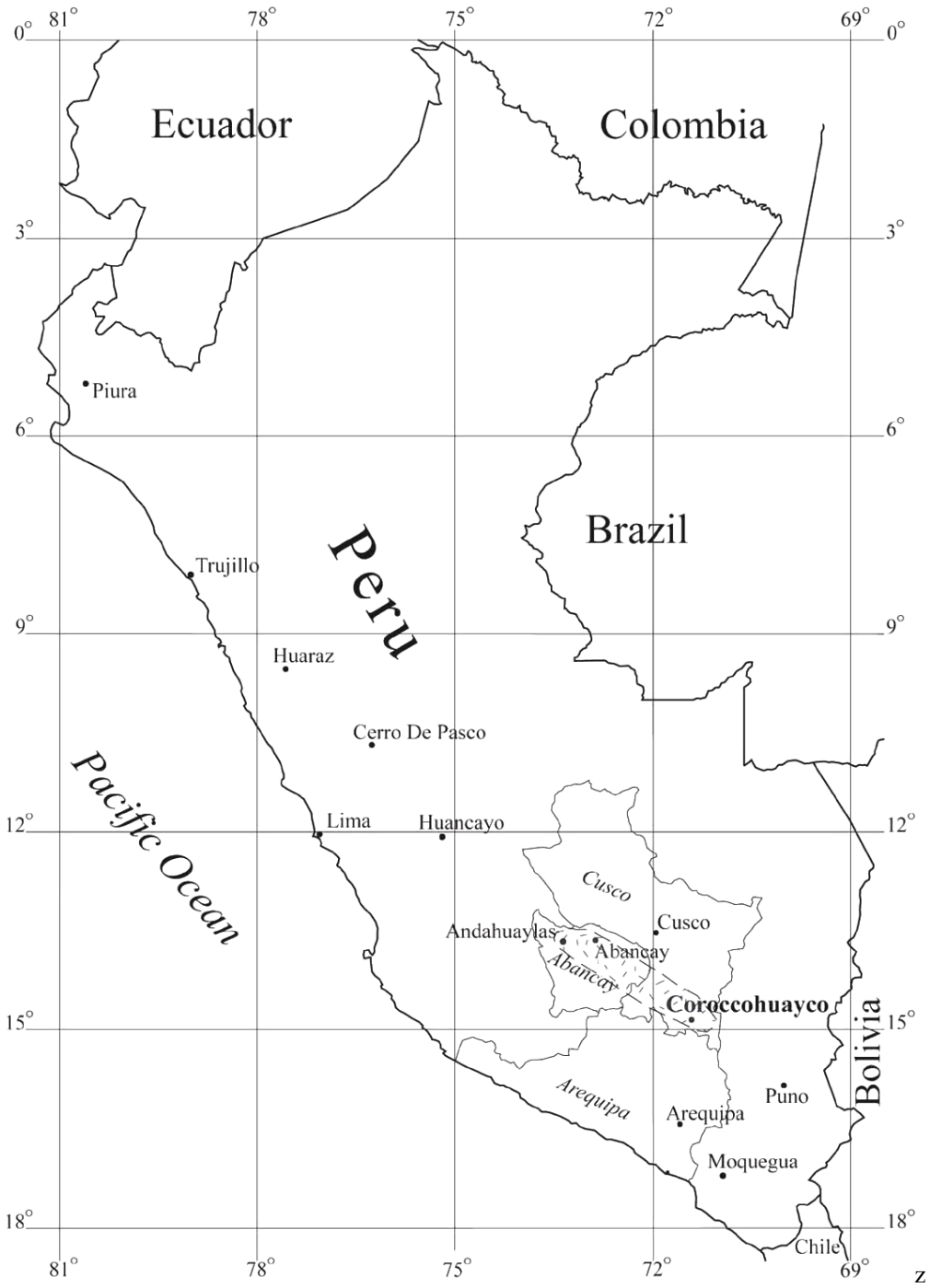

Figure 1. Location map of Coroccohuayco (in the Tintaya district) in southern Peru. The stippled area shows the location of the Andahuaylas-Yauri copper Belt (Noble et al., 1984).

in the southeastern-most part of the Andahuaylas-Yauri copper belt, an elongated belt of copper (±Au, Ag)-porphyry and skarn deposits related to the Eocene-Oligocene Andahuaylas-Yauri Batholith, and include other deposits of similar age and metallogeneis such as at the Las Bambas district and Katanga (Noble et al., 1984; Perelló et al., 2003). The general geology of the Tintaya mine and region has been presented by Saez (1996), Zweng et al. (1997), Fierro et al. (1997), Parra S. (2002), Espirilla R. (2004), and of Coroccohuayco by Maher (1999). This paper presents copper isotopic data from Coroccohuayco and the Tintaya mine.

Mineralization in the Tintaya district is generally hosted by exoskarn alteration in the Cretaceous Ferrobamba Formation. The temperature of sulfide precipitation was approximately 325º C and mineralization is locally related to magnetite replacement of earlier calc-silicates (Maher, 1999). The intrusive igneous rocks in the district are generally weakly to unmineralized, although local exceptions occur at Coroccohuayco (Maher, 1999) and Antapaccay (Jones et al., 2000). The bulk of mineable resource from skarns in the district is hosted by garnet- and magnetite-dominant alteration. Locally molybdenite is important in endoskarn-altered monzonitic dike rocks.

Copper mineralization is chalcopyrite-bornite-dominant, with lesser hypogene chalcocite in some deposits (e.g., Coroccohuayco, Antapaccay). In the Tintaya mine and Ccatun Pucara, supergene processes have produced economically significant oxide reserves which are presently being exploited. Mineralization in several of the skarn systems consists of chalcopyrite dominant mineralization in proximal garnet exoskarn and bornite-chalcopyrite-dominant mineralization in more distal garnet-dominant mineralization (Maher, 1999). However, due to multiple hydrothermal fluid pulses the mineralization and alteration zones may locally overprint and obscure paragenetic relationships and original skarn mineralogical zonation (Maher, 1999; Parra S., 2002; Espirilla R., 2004).

The skarn deposit at Coroccohuayco is a geologically well-characterized deposit (Maher, 1999). Samples of copper minerals for isotopic analyses were taken from the northern part of the deposit where calc-silicate zonation is well defined. The disseminated mineralization consists of chalcopyrite ± bornite as grains interstitial to earlier formed calc-silicates. Locally magnetite ± Cu-sulfides replace garnet. Strongly sheeted quartz-chalcopyrite ± bornite veins related to a post-skarn mineralizing intrusive occur in the deeper portions of the northern part of the deposit. Copper minerals from Coroccohuayco analyzed in this study come from both the disseminated skarn mineralization and the sheeted quartz-sulfide vein mineralization.

The skarn systems in the Tintaya district make an ideal location for studying the variation of copper isotopes in ore deposits because:

1) country rock (limestone of the Ferrobamba Formation) contains insignificant Cu so mixing of isotopically distinct reservoirs of Cu during deposition is an unlikely process,

2) skarn systems generally show clearer mineralogical evidence for distinct, multiple alteration / mineralization events than porphyry systems so these can be taken into account, and

3) zonation in calc-silicate mineralogy can often provide the direction to hydrothermal fluid sources (Johnson and Norton, 1985; Meinert, 1993), giving important information on fluid pathways and temperature trends in the system, particularly for disseminated mineralization in skarn.

Analytical Procedure

Chalcopyrite and bornite samples analyzed in this investigation were hand picked from samples of intrusive and calc-silicate altered rocks under a binocular microscope. This separation procedure insured excellent geologic control of the samples. The procedure for sample preparation, method of analysis, and effects of significant matrix on our analyses have been presented by Larson et al. (2003). In summary, samples were dissolved in a 1:1 solution of distilled concentrated nitric and hydrochloric acids. Samples were then dried and re-dissolved to 2 percent HNO_3 solutions that were diluted to 100 ppb for isotopic analysis. Sulfur is qualitatively removed during sample dissolution and evaporation. Samples were analyzed on a Finnigan Neptune® multicollector ICP-MS at Washington State University, and were corrected for machine mass fractionation by correcting to bracketing standard solutions of NIST SRM 976 copper standard. Albarède et al. (2004) have indicated the standard-sample bracketing technique can be used for correcting for machine fractionation where samples and standards have similar matrix and target element concentrations. Other investigators (Rouxel et al., 2004) have found that chromatographic purification is not necessary for obtaining reproducible and meaningful copper isotopic results in the analysis of Cu ± Fe sulfides. Elements beside Cu in our analytical solutions are generally <5ppb, with the exception of Fe. However, samples doped with Fe at concentrations higher than in the natural samples give analytically indistinguishable results from un-doped samples (see also Rouxel et al., 2004; Graham et al., 2004). Our samples are diluted to 100 (±10) ppb Cu,

the approximate Cu concentration in the standard solution. This concentration gives an approximate ^{63}Cu signal of 3V on the Neptune®.

Results are reported as per mil variation ($\delta^{65}Cu$) relative to NIST SRM 976 (copper isotope standard). Other workers (Graham et al., 2004) present their data as $\varepsilon^{65}Cu$, the difference between δ and ε being a factor of 10 greater for $\varepsilon^{65}Cu$. Analytical precision has been found to be ± 0.08 per mil $\delta^{65}Cu$ (2σ) using internal standards (Larson et al., 2003; Maher et al., 2003).

Cu Isotope Results

Table 1 presents results of copper isotope analyses for 56 samples from the northern part of Coroccohuayco and samples from the Tintaya mine. Many of these samples were analyzed multiple times and through multiple mineral dissolutions. The data from both deposits indicate a range of copper isotope values from -1.29 to 2.98 per mil $\delta^{65}Cu$ in hypogene chalcopyrite. This range is larger than that reported by Graham et al. (2004), who measured a range in values of -0.27 to 1.34 $\delta^{65}Cu$ from their laser-ablation analysis of 166 grains from 11 samples of copper mineralization in the Grasberg deposit, Irian Jaya.

Samples from disseminated mineralization and vein-controlled mineralization show generally similar ranges in values, although the average values are slightly different (Table 1). Two general trends can be observed in the data. First, vein-controlled mineralization on average tends to be isotopically lighter than disseminated mineralization. This feature of the disseminated mineralization at Tintaya is similar to that observed by Graham et al. (2004) from skarn mineralization peripheral to porphyry-hosted mineralization in Grasberg. Second, in general the mineralization hosted by igneous rocks (disseminated or vein-controlled) tends to have lower $\delta^{65}Cu$ values than the mineralization disseminated in calc-silicate alteration (exoskarn) or in veins distal to igneous rocks.

Coroccohuayco

A cross section from mine Section 1400 (Fig. 2) in the northern half of Coroccohuayco shows samples plotted in their geologic context. The skarn zonation for this section (Maher 1999; unpublished data, 2005) indicates that exoskarn-forming fluids were structurally controlled by permeability variations in the limestone protolith of the

Table 1. Cu isotope data from Coroccohuayco and the Tintaya mine, Perú, reported as $\delta^{65}Cu_{NIST\ SRM\ 976}$. Includes data previously reported in Larson et al. (2003).

sample	mineral	δ^{65}Cu (‰)	Geologic context
Coroccohuayco			
400 16.0 78.1A	cpy[1]	0.38	qtz-cpy-born-mo-garnet vein cutting weakly propylitized and albitized diorite
400 16.0 78.1B	born	0.43	as above
900 14.8 388.7a	cpy	0.00	magn-px skarn with patchy veined cpy-born
900 14.8 388.7b	born	-0.46	as above
900 15.2 401.9	cpy	-0.06	qtz-cpy vein in massive magnetite replacing green garn
900 16.2A 185.65	cpy	-0.41	kspar-qtz-cal-cpy vein in diorite
1300 16.1 208.65	cc	-0.04	chalcocite interst to green-tan garn
1300 16.1 252.65	cpy	-1.03	cpy vein in gray marble
1400 13.7 300.12	cpy	0.10	retrograde altered tan garnet with interst cpy
1400 13.7 300.6	cpy	0.24	retrograde altered tan garnet with dissem cpy
1400 14.5 244.45A	cpy	0.52	tan garn-px skarn with interst cpy-born
1400 14.5 244.45B	born	0.12	as above
1400 14.5 246.1	cpy	0.65	honey brown garnet with px and interst cpy
1400 14.5 313.3	cpy	0.16	magn replacing garn with dissem cpy
1400 14.5 340.5	cpy	-1.29	qtz-anh-cpy vein in bio hornfels (Mara Fm)
1400 15.3 326.15	cpy	0.47	green garn with local magn replacement and dissem cpy
1400 15.8 163.4	cpy	0.31	honey brown garn with interst and vein cpy
1400 15.8 191.25	born	0.40	green-brown granular garn with interst born ±cpy
1400 15.8 246.86	cpy	0.05	massive brown garn with interst cpy
1400 15.8 248.6	cpy	0.56	granular tan-brown garn with interst cpy
1400 15.8 306.4	cpy	-0.16	cpy veins cutting qtz-mo veins in Monz M
1400 16.1 147.35	cpy	0.07	white px with magn and cpy in stringers and dissem
1400 16.1 241.6A	cpy	0.45	magn replacing red-brown garn with interst cpy-born
1400 16.1 241.6B	born	0.10	as above
1400 17.7 322.6A	cpy	0.67	granular green garn with interst cpy-born
1400 17.7 322.6B	born	0.27	as above
1400 17.7 352.7	cpy	0.15	amph altered px with garn and cpy veinlets
1400 18.9 301.95	cpy	0.07	hairline kspar-cpy veinlets in Monz M
1400 18.9 331.75	cpy	-0.24	cpy interstitial to green garnet with weak retrograde hematite alterationm
1400 18.9 334.8A	cpy	1.16	breccia in px with “fragments” of cpy and born
1400 18.9 334.8B	born	0.86	as above
1400 18.9 350	born	0.41	sheeted qtz-born veins in Monz M
1400 18.9 356.9	cpy	-0.22	sheeted qtz-cpy-mo veins in Monz M
1400 18.9 357.2	cpy	-0.21	qtz-cpy-mo veins cutting Monz M
1400 18.9 365.85	cpy	-0.54	albititzed Monz M with sheeted qtz-cpy-mo veins
1400 18.9 370	cpy	-0.33	strongly sheeted qtz-cpy veins in Monz M
1400 18.9 376.5A	cpy	-0.03	magn altered tan garnet with cpy-born veins
1400 18.9 376.5B	born	-0.40	as above
1400 18.9 378.85	cpy	0.02	silicified green garn with dissem and stringer cpy-magn
1400 18.9 382.6	cpy	0.62	brown garn with interst magn-cpy and qtz-cpy-magn veins
1400 18.9 386.4a	cpy	0.66	sheeted qtz-cpy-born veins in brown garn
1400 18.9 386.4b	born	0.31	as above
1400 18.9 387.8	cpy	0.23	granular massive brown garn with magn alteration and qtz-cpy-cal veins
1400 18.9 387.9	cpy	0.32	silicified brown garn with dissem and vein cpy

Table 1. cont.

1400 20.9 49.7	cpy	-0.31	mafic clot in diorite with dissem cpy
1400 20.9 324.7	cpy	-0.15	stringer cpy veins in Monz F
1400 21.7 119.95	cpy	0.52	px-biotite skarn with dissem cpy
1400 21.7 183.5	cpy	-0.63	px-garn skarn near Monz F with veinlet cpy
1400 21.7 416.95	cpy	0.27	honey brown garn with dissem cpy
1400 21.7 425.8	cpy	0.32	epidote-plagioclase endoskarn in Monz F with dissem cpy
Tintaya Mine			
Tajo	cpy	-0.05	green garn with interst cpy
T6237E-4	cpy	2.98	white px with interst cpy
T1900N-9 21.45	cpy	0.06	coarse amphibole skarn with interst cpy
T1975N-4 111.35	cpy	0.21	massive pyrrhotite-cpy ± py replacement of igneous rock
Tajo-MS1	born	0.11	massive born-cpy replacement
Tajo-MS2	cpy	0.54	as above
T440N255E	cpy	-0.20	sheeted cpy-py veins cutting px
T448N268E	cpy	0.07	sheeted cpy veins in silicified skarn
T982N042E	cpy	0.01	monz PM1a with cpy veins
T990N080E	cpy	-0.43	green garn with sheeted cpy vein
TT008-214	cpy	0.19	cpy-chlorite vein in monzonite
Chab-E-Mar	cpy	1.87	dark gray marble with cpy-qtz vein
Chab-Este	cpy	-0.83	green garnet with vein cpy-py and dissem cpy; from vein
Chab-Esteb	cpy	-0.84	as above, from dissem
CHE-039-424	cpy	-0.41	cpy-qtz vein in strongly kspar altered monzonite
Chab-Sur-Cp-Ma	cpy	0.19	massive magnetite with dissem cpy

sample type	number	mean (‰)	range (‰)
veins	32	-0.09	-1.29 to 1.87
disseminated	30	0.37	-0.84 to 2.98
cpy-born pairs	8	0.38 (difference)	0.3 to 0.46

[1]Abbreviations: cpy = chalcopyrite, born = bornite, cc = chalcocite, py = pyrite, mo = molybdenite, qtz = quartz, magn = magnetite, px = pyroxene, garn = garnet, kspar = potassium feldspar, cal = calcite, dissem = disseminated, interst = interstitial.

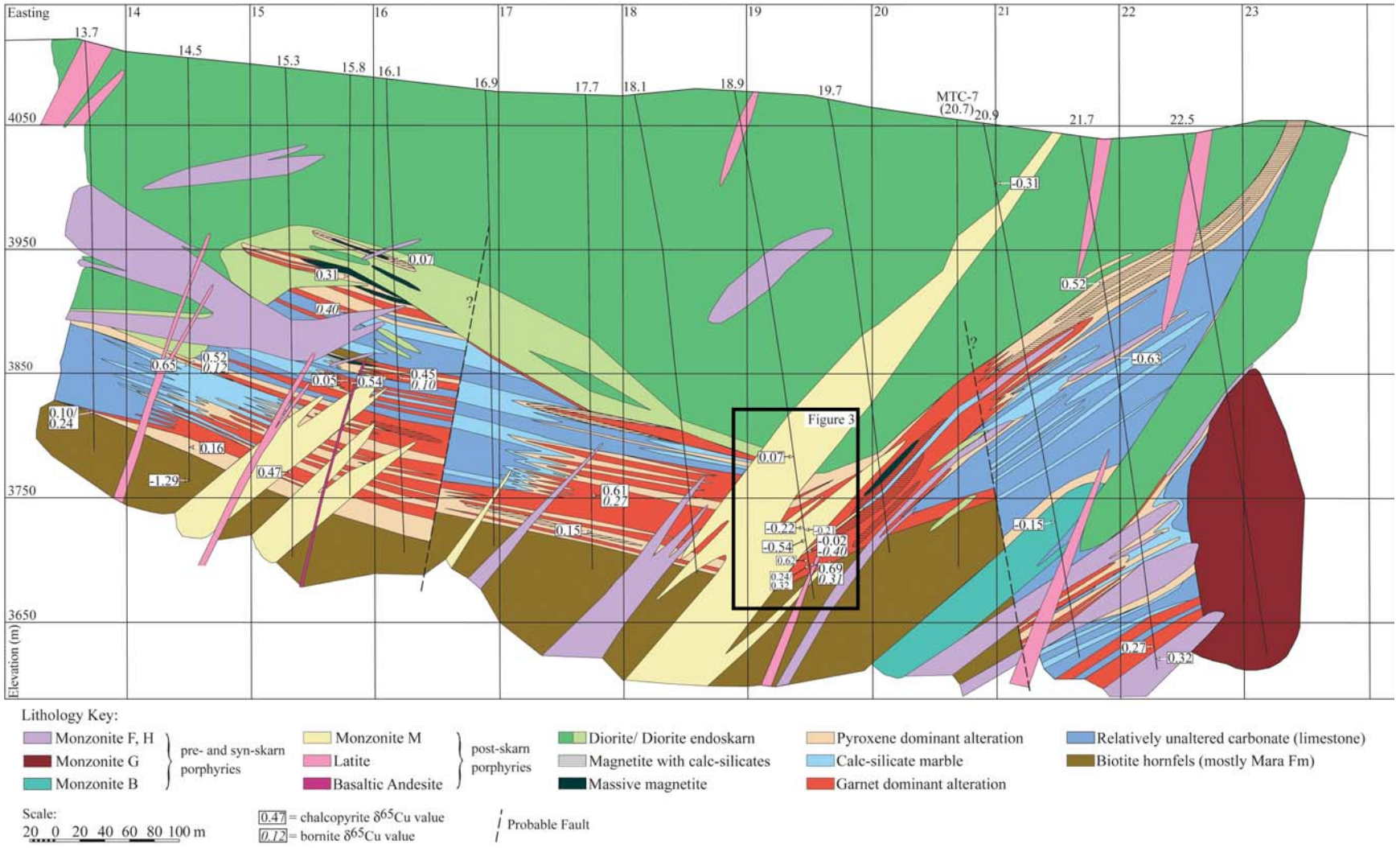

Figure 2. Geology of mine section 1400 at Coroccohuayco, Peru. Numbers above surface represent diamond drill hole locations. Cu isotope values for selected samples are plotted next to drill hole traces. Geology from Maher (1999; unpublished data, 2005).

Ferrobamba Formation. These fluids flowed up the limbs of a minor syncline and altered the limestone to garnet-dominant alteration, grading into pyroxene skarn or calc-silicate marble distal from the fluid sources. As the temperatures decreased locally, Cu-Fe sulfides (dominantly chalcopyrite and bornite) were precipitated interstitial to the calc-silicates, and in places were accompanied by magnetite replacement of calc-silicates. Homogenization temperatures of primary fluid inclusions in quartz precipitated interstitial to garnet indicate that the temperature of disseminated mineralization in exoskarn was approximately 300-325 ºC, similar to that of mineralization in quartz-sulfide veins hosted by igneous rocks (Maher, 1999).

Copper isotope ratios from the interstitial mineralization in exoskarn at Coroccohuayco are generally isotopically heavy. However, samples closer to fluid sources (generally of lower Cu-grade due to lower remnant interstitial porosity: Maher, 1999) tend to be isotopically lighter. Locally this is expressed by as much as a 0.5 per mil difference over 2m vertical separation in the same package of skarn alteration (e.g., samples 1400 15.8 246.86, 0.05‰, and 1400 15.8 248.6, 0.56‰). The difference in the style of mineralization between these two samples is due to the non-calc-silicate material ("porosity") interstitial to garnet that can be replaced by sulfides. The sample higher up (246.86) is of lower grade (approx. 4% chalcopyrite) due to lower remnant porosity, and the higher-grade sample (about 8% chalcopyrite) at 248.6 has much higher remnant porosity. Higher-grade disseminated mineralization along this mine section in general tends to be isotopically heavier relative to lower-grade disseminated mineralization.

Very strongly sheeted quartz-sulfide veins occur in monzonite dikes at easting 19 in mine section 1400 at a depth of 350m. These veins consist of quartz-chalcopyrite ± bornite ± molybdenite and quartz-bornite (Maher, 1999). Locally the ore grade in this veined rock is >10 percent Cu. Samples were analyzed over the vertical extent of this mineralization and are shown in Figure 3. Here copper isotope ratios are zoned, with δ^{65}Cu values increasing vertically up and down from the lowest value of -0.54 per mil at a depth of 365.85m. In this zone, as in other places, isotopic values change significantly over 10's of meters.

Tintaya Mine

The samples taken from the Tintaya mine are from disseminated, massive and vein-controlled mineralization. Tintaya is a complex ore deposit, with various alteration and mineralization events (Zweng et al.,

1997; Parra S., 2002; Espirilla R., 2004). Tintaya also shows the largest range in copper isotope values (Fig. 4) in hypogene mineralization yet discovered for a single deposit to date (-0.84 to 2.98‰), and this is likely a result of the complexity of the mineralization process. These samples come from early disseminated skarn-hosted mineralization and late vein-controlled mineralization that cuts the earlier skarn. Disseminated mineralization tends to be > 0.0 per mil and reaches 2.98 per mil in distal skarn alteration/mineralization. The vein-controlled proximal samples have isotopically light values (to -0.83‰) and the more distal vein samples have isotopically heavier values (up to 1.87‰). A sample of massive garnet skarn with disseminated chalcopyrite and cross-cutting chalcopyrite-pyrite ± molybdenite veins (Chab-Este) yields analytically identical values (-0.83‰) for both styles of mineralization.

Discussion

The trends in copper isotope ratios in both Coroccohuayco and the Tintaya mine show similarities. In both cases the proximal samples (as determined from skarn alteration zonation and proximity to possible sources of ore-forming fluids) tend to be isotopically lighter (lower $\delta^{65}Cu$) and the more distal samples of disseminated mineralization tend to be isotopically heavier. Graham et al. (2004) observed that skarn samples on average were isotopically heavier than igneous-hosted samples from the Grasberg district, Irian Jaya. However, since their samples probably represent products from different mineralizing events and likely chemically diverse fluids (representing at least propylitic, prograde skarn, retrograde skarn/QSP, and massive carbonate replacement) their data are paragenetically heterogeneous and contexturally difficult to compare to ours without additional geologic and isotopic information.

Most disseminated chalcopyrite mineralization at Tintaya and Coroccohuayco lies in the range between 0.0 and 0.6 per mil. The lowest values observed at Coroccohuayco are from thin veins outside of the main skarn alteration in samples 1300 16.1 252.6 and 1400 14.5 340.5 (-1.03 and -1.29, respectively). These samples are from chalcopyrite ± pyrite veins in limestone and biotite hornfels, respectively. Other low values are related to thin sulfide ± quartz veins hosted by monzonite (Fig. 3), generally >2mm in width (samples 1400 18.9 356.9, 357.2, 365.85, 370). At Tintaya, the lowest isotopic values are related to paragenetically late vein-hosted mineralization in the southern part of the deposit (Fig. 4). Geologic mapping by mine geologists and structural evaluation by Espirilla R. (2004) have identified an overprinting mineralization event related to a later intrusive phase which generally cuts

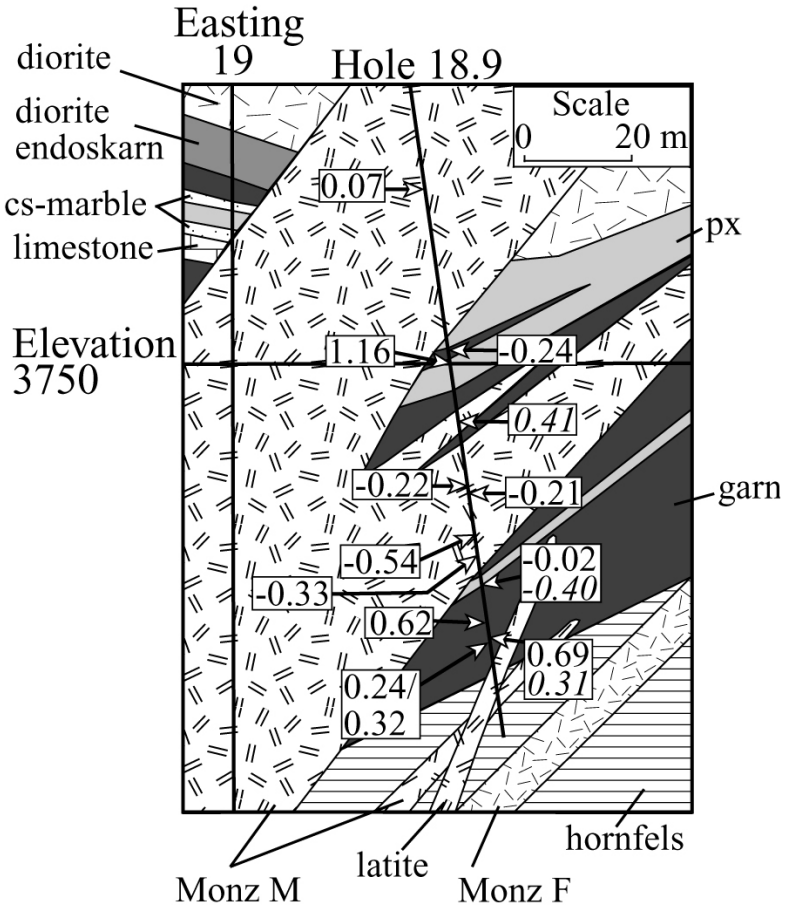

Figure 3. Inset from Figure 2 showing copper isotope analyses in the highly quartz-veined and mineralized monzonite and skarn from drill hole 18.9 on mine section 1400 at Coroccohuayco. Bornite analyses in italics. Monz F and Monz Z are syn- and post-skarn porphyries.

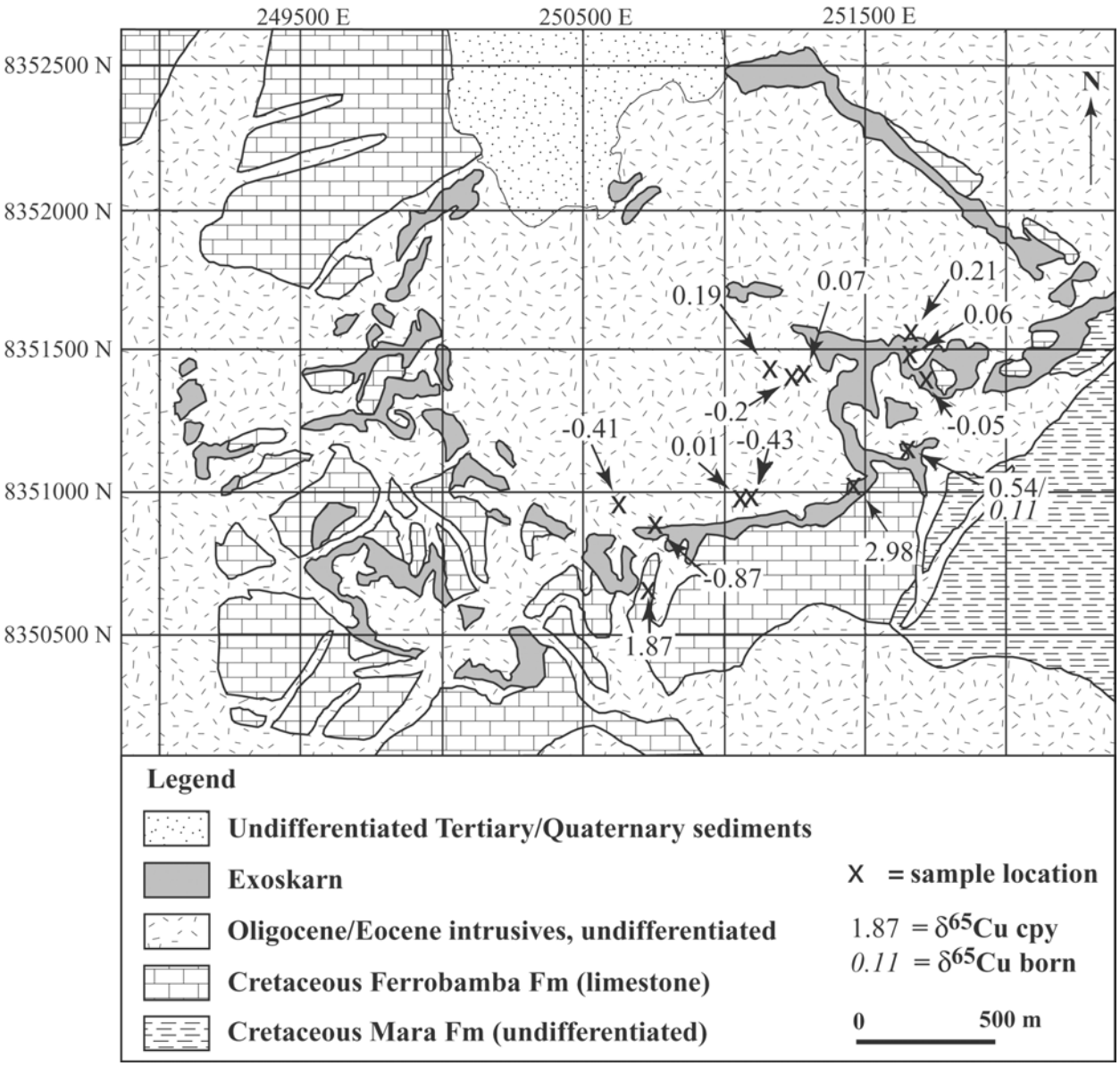

Figure 4. Generalized geologic map of the Tintaya mine taken from elevation 3950 showing locations of samples analyzed in this study. Adapted from Espirilla R. (2004).

skarn and brought important copper and magnetite mineralization, similar to that observed locally in Coroccohuayco by Maher (1999). In both deposits, the highest δ^{65}Cu value comes from disseminated mineralization in skarn, although Tintaya also has some veins of higher values.

Possible causes of variations in copper isotope ratios

These findings suggest that a systematic variation in copper isotope ratios was produced during the genesis of both deposits. The variations in copper isotope ratios could be produced from several factors such as heterogeneous source fluids, fluid temperature variation, fluid mixing, intensive parameters in the hydrothermal fluids, Cu-remobilization and overprinting (Rouxel et al., 2004; Graham et al., 2004) and copper fractionation between different complexing species in solution (Maréchal and Albarède, 2002). In this study the hydrothermal systems precipitated Cu at high temperatures (>250º C) and it is unlikely that the mineralized zones had much of a temperature variation (<25º C drop) over distances of 50m. This is different from Cu-mineralization in sea-floor hydrothermal systems (Rouxel et al., 2004) where temperature changes of up to 250º C occur over a few meters, but still the δ^{65}Cu range of recently precipitated chalcopyrite is small. Thus, direct temperature-controlled equilibrium fractionation is unlikely to be a significant fractionation mechanism of copper isotopes in these skarn samples. Since the important country rocks in the Tintaya district are clean limestones, mixing between two reservoirs of isotopically distinct Cu at the site of mineralization, such as between igneous-derived magmatic Cu (dominant in these systems) and some other sedimentary Cu reservoir, is probably of low significance.

At Coroccohuayco the calc-silicate assemblage is early andraditic garnet > diopsidic pyroxene, with later and lower-temperature replacement of calc-silicates by magnetite-sulfide ±Fe-rich pyroxene (Maher, unpublished data, 2005). This indicates that slight changes in oxidation of the hydrothermal fluids likely occurred between the early high-T calc-silicate alteration and the lower-temperature mineralization. However, these changes were not sufficient to oxidize or reduce copper so changes in the oxidation state of copper as a fractionation mechanism was unimportant in hypogene mineralization at Coroccohuayco and Tintaya. For systematic trends such as at Easting 19 on section 1400 at Coroccohuayco (Fig. 3) it is especially unlikely that redox of the fluid changed significantly over the distance of the strong isotopic zonation (50 m vertically). This mineralization is mainly hosted by monzonite, with local overprinting of earlier skarn alteration. The percent bornite in the veins increases with distance vertically

up and down from sample 1400 18.9 386.85, the isotopically lightest sample in this zone, suggesting that the fluid was chemically evolving with distance/time. The variations indicate that early/proximal (and lower grade) chalcopyrite ± bornite mineralization is isotopically lighter than the massive mineralization.

Effects of remobilization

To determine if variations of Cu-isotope values were produced by hydrothermal remobilization, we looked for some indicator of mineralization overprinting or leaching in our samples. Apart from often equivocal ore textures, a characteristic fractionation between two co-precipitated copper minerals could be used to define whether these minerals represent an equilibrium state, or disequilibrium where one phase is paragenetically distinct from the other even though they occur together. Remobilization of copper with subsequent re-deposition may produce isotopic disequilibrium between minerals that might otherwise be texturally interpreted as co-precipitated (such as bornite and chalcopyrite, or chalcocite and bornite).

We have analyzed nine samples of chalcopyrite-bornite pairs from Coroccohuayco and Tintaya with samples from other deposits to explore for possible equilibrium fractionation between co-precipitated chalcopyrite and bornite. Table 2 shows analyses from several ore deposits where bornite and chalcopyrite occur together. Of this number, 15 samples were chosen based on geologic context to be the best representatives of co-precipitated bornite-chalcopyrite. Twelve of the fifteen sample pairs have a consistent δ^{65}Cu fractionation of 0.38 per mil (±0.04‰, 1σ). The common 0.38 per mil fractionation suggests that the fractionation mechanism for these 12 samples was similar. The other pairs that do not show the 0.38 per mil fractionation are from samples where bornite is paragenetically different from chalcopyrite.

Chalcopyrite and bornite have similar structural relationships in their Cu-S bond type. A proxy of bond length can be used for vibrational frequency since the Cu-S bond type is similar for these minerals but their bond length differs (M. Gaspar, pers. comm., 2002). The Cu-S bond is longer and therefore weaker in bornite than the Cu-S bond in chalcopyrite. There should therefore exist a mass fractionation effect between these two minerals based on the differences in vibrational frequencies of these Cu-S bonds (O'Neil, 1986). It appears that under the conditions of precipitation at Coroccohuayco and Tintaya (as well as in other deposits) bornite appears to have a lower overall vibrational frequency for copper than does chalcopyrite. This implies that bornite preferentially

Table 2. Analyses of chalcopyrite-bornite mineral pairs from Coroccohuayco, the Tintaya mine and other deposits. Includes data from Larson et al. (2003).

Coroccohuayco, Tintaya Perú					
veins	cpy[1] (‰)	born (‰)	difference (‰)	expected co-precipitation	Geologic Context
900 14.8 388.7a,b	0.00	-0.46	0.46	yes	magn-px skarn with patchy veined cpy-born
1400 18.9 376.5A,B	-0.03	-0.40	0.37	yes	magn altered tan garnet with cpy-born veins
1400 18.9 386.4a,b	0.66	0.31	0.35	yes	sheeted qtz-cpy-born veins in brown garn
400 16.0 78.1A,B	0.38	0.43	(-0.05)[2]	yes	distal qtz-born-cpy-mo-garn vein cutting diorite, Coroccohuayco, Perú
disseminated					
1400 14.5 244.45A,B	0.52	0.12	0.4	yes	tan garn-px skarn with interst cpy-born
1400 16.1 241.6A,B	0.45	0.10	0.35	yes	magn replacing red-brown garn with interst cpy-born
1400 17.7 322.6A,B	0.67	0.27	0.4	yes	granular green garn with interst cpy-born
1400 18.9 334.8A,B	1.16	0.86	0.3	yes	breccia in px with “fragments” of cpy and born
Tajo-MS1,2	0.54	0.11	0.43	yes	massive born-cpy replacement
		mean	0.38		
Other Ore Deposits					
AR-17a,b	0.18	-0.04	0.22	no	massive sulfide from the Superior mine, AZ, USA
Ar-14 a,b	0.19	-0.01	0.2	no	as above
Troy-1A,B	0.23	0.3	-0.07	yes	disseminated cpy-born in skarn, Troy, ID, USA
Troy-4A,B	0.34	0.19	0.15	yes	as above
Beav-1,2	1.38	1	0.38	yes	monzonite hosted qtz-kspar-cpy-born±mo veins Beaver Harrison Mine, UT, USA
BEAV-4A,B	0.8	0.4	0.4	yes	as above
BEAV-5a,b	1.22	0.9	0.32	yes	as above
SLAKE-1 A,B	0.22	-0.14	0.36	yes	sediment hosted dissem copper from Spar Lake, MT, USA

[1]Abbreviations as in Table 1.
[2]Not computed in mean.

incorporates ^{63}Cu from the fluid relative to chalcopyrite, producing a chalcopyrite-bornite fractionation. This mechanism itself may not be sufficient to cause the total 0.38 per mil difference observed in chalcopyrite-bornite samples, but could produce observable fractionation.

It is presently unclear why the other 3 samples that likely co-precipitated have different, and even reversed fractionation. Since the 0.38 per mil $\delta^{65}Cu$ fractionation is not observed in all chalcopyrite-bornite pairs where co-precipitation was interpreted, the equilibrium fractionation based on vibrational frequencies may only produce a part of the total fractionation, with the total fractionation between the pairs produced by a combination of fractionation mechanisms. In addition, samples in which the chalcopyrite-bornite pairs do not have this 0.38 per mil difference may reflect isotopic disequilibrium or equilibrium fractionation at temperatures or chemical conditions different from the consistent fractionation population. Samples where bornite is clearly later than chalcopyrite do not seem to show this fractionation and the $\delta^{65}Cu$ difference between pairs tends to be smaller (Table 2).

Seven of the twelve consistent mineral pairs come from different areas of Coroccohuayco (Fig. 2) and are from disseminated as well as vein-controlled mineralization. The chalcopyrite from these samples range from 0.00 to 0.67 per mil and the alteration mineralogy indicates a variety in proximal and distal ore deposition environments. These data do not represent a post-crystallization isotopic equilibration because of the sampling scale utilized in this study. The fractionation of copper isotopes observed in these mineral pairs was produced during high-temperature ore deposition and could be used as a test of equilibrium fractionation. The samples at Coroccohuayco where strong isotopic zonation occurs in drill hole 1400 18.9 (Fig. 3) contain two analyzed chalcopyrite and bornite pairs within the isotopic zonation that exhibit the ≈ 0.4 per mil fractionation. The Cu isotope fractionation observed in this sequence is probably due to some other process than simple equilibrium fractionation due to temperature changes, copper remobilization, or by mineralization overprinting.

Copper isotope evolution in fluids at Coroccohuayco and Tintaya

From the zonation of copper isotope ratios observed in Coroccohuayco and Tintaya and considering the ore-forming conditions in these deposits, the most likely explanation for the variations observed is that isotopic evolution of the fluid reservoir occurred with time and extent of copper precipitation. The empirical evidence suggests preferential removal of one isotope over another from the fluid reservoir during mineralization.

In both of these ore systems copper is precipitated from a magma-derived fluid, and any copper contributed by wall rocks (limestone) at the site of deposition is insignificant. Pulses of mineralizing fluids (including the original skarn-forming fluids) commence precipitation of Cu-bearing phases in veins and disseminated in the calc-silicate alteration due to physicochemical aspects of the systems (pH, fO_2, temperature, etc.). The ore-forming fluid with a specific isotopic value begins to precipitate copper when intensive fluid conditions and/or temperatures are favorable for copper sulfide saturation. The actual initiation of mineralization likely relates to thermodynamic constraints over the copper complexes present in the fluid. Empirically, the early/proximal mineralization preferentially removes ^{63}Cu from the reservoir. As precipitation of Cu proceeds, the residual ore fluid evolves in its bulk Cu-isotope signature towards isotopically heavier copper ratios. When mineralization is massive, its copper isotope ratio should more closely reflect the bulk Cu-isotope ratio of the ore-forming fluid at that point in its evolution. During late/distal mineralization the Cu-isotope ratio of the "spent" fluids has evolved to an isotopically heavier character, producing the corresponding isotopically heavy copper mineralization.

At Coroccohuayco and Tintaya it appears that chalcopyrite preferentially incorporates ^{63}Cu during precipitation from a chalcopyrite-saturated fluid. If more than one copper complex is present in significant concentrations in the fluid, and depending on the chloride complex with the lowest stability constant (Wood and Samson, 1998) and the conditions of precipitation, the early, proximal chalcopyrite at Coroccohuayco may preferentially form from a Cu-complex that is relatively enriched in ^{63}Cu. This implies that when chalcopyrite first precipitates there are certain important ^{65}Cu-enriched copper complexes in the hydrothermal fluid which are not liberating copper at that point. The complexes that are giving up copper to chalcopyrite at this stage of precipitation are presumably enriched in ^{63}Cu. When bornite is co-precipitating, chalcopyrite will incorporate the heavier isotope preferentially, as there is competition for copper from a competing co-precipitating Cu-phase. In their study of isotopic fractionation of Cu and Zn on exchange resin, Maréchal and Albarède (2002) indicate that fractionation of Cu^{2+} may occur among different polynuclear copper chloride complexes in solution. It is presently unknown whether polynuclear copper chloride complexes exist in high temperature fluids and under what conditions mass fractionation between these or other copper complexes could be significant. However, due to the limited possibilities of other factors controlling fractionation in the Tintaya district, the role of Cu-fractionation between complexes should not be ignored.

Our data suggests that in a general sense ^{63}Cu is preferentially incorporated in early/proximal mineralization and ^{65}Cu tends to be concentrated in the hydrothermal fluid during precipitation. Leaching and precipitation experiments (Young and Ruiz, 2003; Ehrlich et al., 2004) indicate that at low temperatures isotopically heavy Cu is preferentially leached and isotopically lighter copper is preferentially precipitated. We see similar trends in the mineralization at Coroccohuayco and Tintaya even though these hydrothermal samples were precipitated at higher temperatures than the conditions under which these experiments were run. However, in both of these experiments, reduction or oxidation of the copper in solution occurred, a process not important in the samples we studied.

Possible complexation of copper in high temperature fluids

Many experimental studies have sought to identify and evaluate the role of different copper complexing ligands in ore forming systems. Copper chloride complexes are the most important complexes for Cu (and other base metals) in high-temperature, saline hydrothermal systems (Crerar and Barnes, 1976; Var'yash and Rekharski, 1981; Var'yash, 1992; Xiao et al., 1998; Fulton et al., 2000; Archibald et al., 2002; Liu et al., 2002). Under certain chemical conditions hydrosulfide complexes can also be important (Mountain and Seward, 2003). Recent experimental investigations involving X-ray absorption and spectrophotometry at high temperatures (Fulton et al., 2000, and Liu et al., 2002, respectively) have shown that $CuCl_2^-$, $CuCl_3^{-2}$ and $CuCl_4^{-3}$ are the most important Cu(I) complexes at high temperatures and higher chloride molalities.

Fluid inclusion studies at Coroccohuayco (Maher, 1999) indicate that the deposition of copper sulfides likely occurred between 250 to 350º C from high-salinity fluids (average 43 wt % NaCl eq). Calculations of predominance of different Cu-complexes using thermodynamic data from Liu et al. (2002) indicate that for the temperatures and salinities of interest at Coroccohuayco there are two chloride complexes which would be important in the hydrothermal fluid, $CuCl_2^-$ and $CuCl_4^{-3}$ (Fig. 5). The temperature dependence of the stability of these complexes is very different: $CuCl_2^-$ increases in predominance with decreasing temperature, and $CuCl_4^{-3}$ rapidly decreases in predominance from 350 to 325º C. Since precipitation of Cu into a sulfide phase depends on the instability of the complexes and the stability of the solid phase, the precipitation of the earliest and highest temperature Cu-phases is related to temperature or other chemically induced instability in the complexes. The

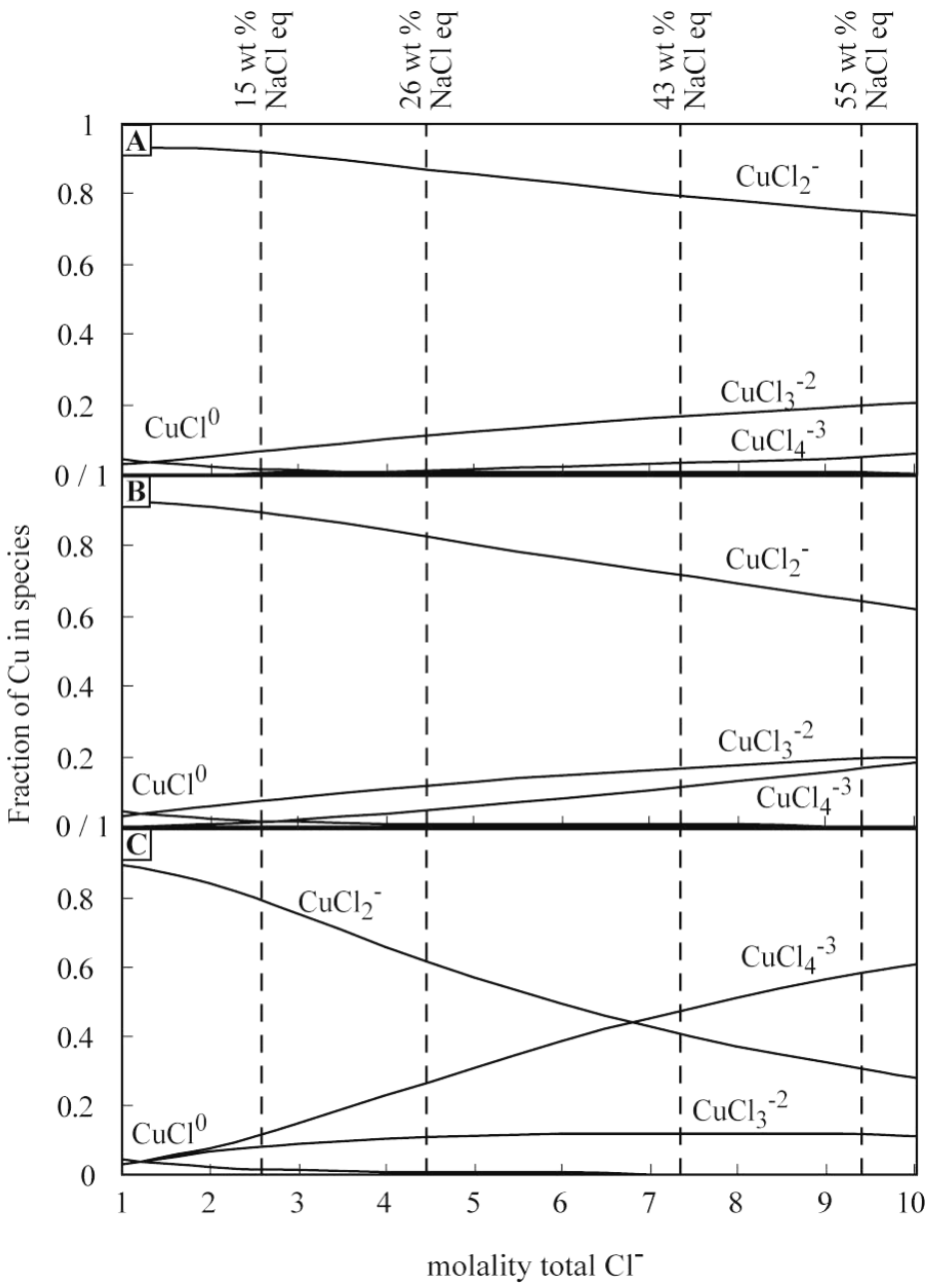

Figure 5. Speciation of copper in chloride complexes for 300°, 325°, and 350° C (A, B, C above respectively) for various chloride concentrations using data from Liu et al. (2002). Shown for reference are salinities in wt % NaCl eq. Coroccohuayco quartz fluid inclusions related to mineralization show an average of 43 wt % NaCl eq.

temperature-related instability of the $CuCl_4^{-3}$ complex with decreasing temperature (Fig. 5) could be an effective mechanism for precipitating the first Cu from solution, when other chemical aspects of the system are relatively unchanged over the interval of 350 to 325º C. If copper as Cu(I) is fractionated between different chloride complexes at high temperatures as postulated at low temperature for Cu(II) by Maréchal and Albarède (2002), this mechanism could provide an explanation for the differences observed in the copper isotope ratios between early, slightly higher temperature mineralization verses more distal mineralization.

Significant fractionation of Fe has been predicted by Schauble et al. (2001) between different complexes in solution due to ligand-bond strength, oxidation state, and coordination number of Fe in the complex. These investigators calculated that tetrahedral Fe complexes should preferentially concentrate isotopically heavy Fe relative to their octahedral counterparts. Differences in the ligand coordination geometry of $CuCl_4^{-3}$ and $CuCl_2^{-}$ (and related vibrational bond frequency) may provide the basis for a mass fractionation between these complexes. Liu et al. (2002) found that higher coordination chlorocomplexes of Cu were characterized by a likely tetrahedral coordination. Fulton et al. (2000) interpreted $CuCl_2^{-}$ in up to 2m NaCl as being linear in geometry, due to the lack of water in the first hydration shell of this complex. It is unknown whether this geometry would persist at higher NaCl concentrations. Schauble et al. (2001) suggested that strongly bonding ligands will preferentially incorporate the heavier isotopes of Fe, and that bond strengths are generally greater for complexes with lower coordination numbers. It is possible that a similar isotopic behavior exists for copper complexes, and in that light, the tetrahedral ligand field should preferentially form around ^{63}Cu since the coordination number of $CuCl_4^{-3}$ is greater than for $CuCl_2^{-}$. If the tetrahedral ligand field is weaker, it should be thermodynamically less stable than the linear ligand field at decreasing temperature and lead to decreasing complex stability with falling temperature. Therefore, subsequent chalcopyrite precipitation would commence initially from the tetrahedral complex.

The implications of Figure 5 are significant in terms of copper fractionation in other hypogene ore deposits and the importance of chloride concentration over the fractionation of copper isotopes. A study by Larson et al. (2003) of hypogene native copper precipitated from lower-salinity fluids indicated near district-scale uniformity in $\delta^{65}Cu$. The study by Rouxel et al. (2004) of mid-ocean hot-spring copper mineralization showed that active Cu mineralization comprised a relatively narrow range in $\delta^{65}Cu$ (-0.3 to 0.8‰) even over large temperature gradients. An unpublished Cu-isotopic study of chalcopyrite mineralization from the Crown Jewel Au-skarn system, Washington, USA (M. Gaspar, personal communication, 2002) indicates a very narrow range (-0.4 to +0.3‰) in

δ^{65}Cu values of chalcopyrite over most of the deposit. These systems are characterized by relatively low salinities in the hydrothermal fluids and tend to have restricted δ^{65}Cu ranges (relative to Coroccohuayco and Tintaya). The skarn minerals in the Ertsberg district, Irian Jaya, commonly have salinities >38 weight percent NaCl equivalent (Meinert et al., 1997), and so mineralization should be expected to have a greater range in δ^{65}Cu. Preliminary copper isotope analyses at Bingham Canyon, USA, on potassic-altered porphyry- and skarn-hosted mineralization show a range in δ^{65}Cu in chalcopyrite of -0.37 to 0.95 per mil (Maher, unpublished data, 2005). These empirical data suggest that lower-salinity hypogene Cu-mineralization may be more restricted in the range of δ^{65}Cu values, with lesser fractionation occurring because of there being only one predominant Cu-complex present in the mineralizing fluid. In the case of chloride complexes, this may be due to the stability of $CuCl_2^-$ at all temperatures for the salinities of interest in these systems (Fig. 5). The other important implication from these observations is that only hydrothermal systems with temperatures of precipitation >325º C and salinities approximately greater than 6.9 molal chloride (40 wt % NaCl eq.) will likely show significant hypogene Cu-isotope variations.

Other hydrothermal systems where chloride is not the dominant copper complex (e.g., hydrosulfide, Mountain and Seward, 2003) could show similar isotopic fractionation controls to Cu-complex relationships as the previous examples if more than one complex is important during the history of precipitation of Cu. Chemical controls over what mineral phase is precipitated (e.g., bornite preferred over chalcopyrite or chalcocite preferred over bornite) may also influence the Cu-isotopic evolution of the hydrothermal fluid. More experimental work and other Cu-isotope analyses with complete geologic contexts are required to further define these possible relationships.

There probably also exists an equilibrium fractionation between the hydrothermal fluid and copper mineral(s) precipitating out of the fluid. The magnitude of this equilibrium fractionation is presently unknown, but theoretically it is not expected to be large at high temperatures due to the small mass differences between ^{63}Cu and ^{65}Cu. In terms of disseminated mineralization in skarns, the textural and thermodynamic evidence (Johnson and Norton, 1985) suggests that mineralization intimately associated with skarn minerals can be derived from the same pulse of hydrothermal fluid that formed the calc-silicate alteration. During mineralization the concentration of copper in the fluid reservoir should decrease continuously. The mineralizing process can then be considered a Rayleigh fractionation of copper from the fluid. However, during massive precipitation the fluid copper concentration decreases rapidly to very small values, so a step-wise fluid-mineral equilibrium fractionation may not occur as fast as the actual precipitation process. Thus, the latest/most distal/lowest temperature mineralization would

have an isotopic value similar to that of the last remaining Cu-complex(es) in the fluid after the majority of mineralization has occurred. Isotopically heavy Cu-mineralization at Coroccohuayco and Tintaya may represent this residual copper. Whether this is due to a pure Rayleigh-type fractionation related to preferential incorporation of the lighter isotope during precipitation of chalcopyrite or is related to preferential isotope retention by a specific complex is difficult to assess.

Exploration Potential of Copper Isotopes

Due to the variability of copper isotope ratios in high-temperature hydrothermal systems important controls on Cu fractionation can also be related to controls on mineralization. Certain minerals tend to define narrow ranges in isotopic composition (e.g., cpy, bornite). Other minerals tend to be uniformly isotopically heavier, such as copper carbonates, sulfates and sulfides formed from supergene processes (Shields et al., 1965; Maréchal et al., 1999; Larson et al., 2003; Rouxel et al., 2004). Other minerals, such as chalcocite, can be either isotopically heavy or light, depending on the process of formation. All of these features reflect the dominant conditions of mineral formation and the isotopic fractionation mechanisms must be different in these environments.

For example, copper carbonates formed from supergene processes are higher in ^{65}Cu relative to the supergene minerals forming at the water table (such as native copper, cuprite, or secondary sulfides). This implies that the oxidation process removes ^{65}Cu which is rapidly bound up in the carbonate/sulfate phases, and preferentially removes ^{63}Cu (possibly in hydroxide complexes as Cu^{+1}) and carries it to the water table. Once there it is either reduced and precipitated (e.g., native copper) or simply precipitated as a sulfide phase (e.g., chalcocite/covellite). Variations observed in supergene mineralization are expected to be much larger than in hypogene mineralization simply due to the fact that many more chemical processes, lower temperatures, and repetitive dissolution/precipitation can occur due to changes in hydrologic aspects of the supergene zones. In addition, more copper complexes are stable in these environments relative to high temperature systems (Wood and Samson, 1998), and each complex may preferentially incorporate copper of different masses leading to highly varying isotope ratios observed in supergene zones.

Although much more detailed work needs to be done from a variety of deposits, some generalizations can be made about the aspects of copper isotopes in hydrothermal systems. For example, distal features, both in veins

and in disseminated mineralization unaffected by supergene/oxidation processes, tend to be isotopically heavier than proximal mineralization in high-salinity hydrothermal systems. As such, copper isotope ratios could be used as a zonation guide in terms of defining locations of more massive Cu-mineralization, and the direction to the center of the system, or source of the mineralizing fluid. Similarly, knowledge of Cu-grade zonation assisted by copper isotope zonation, in concert with other structural and alteration zonation characteristics, can assist modelers in more confidently ascribing ore values to less-drilled parts of individual deposits. Since copper isotopes directly relate to the ore-forming process, these can be less equivocal than other methods (such as light stable isotopes or alteration patterns). The usefulness of this approach to systems such as volcanic hosted massive sulfide systems is likely to be less useful, due to the probable long-term Cu isotopic evolution of the black smoker fluids (Rouxel et al., 2004).

Other more pragmatic uses of copper isotope ratios could be to simply differentiate supergene verses hypogene sulfide mineralization. Many porphyry ore deposits (e.g., Rosario, Chile, Chavez, 1994; Superior, Arizona, USA, Paul and Manske, 1999) contain disseminated chalcocite mantling earlier pyrite. This chalcocite may have formed from late, copper-rich high-sulfide fluids (e.g., Rosario Vein) which preferentially replaced pyrite, or from supergene enrichment where copper replaces unoxidized disseminated pyrite (e.g., Escondida, Chile, Padilla G. et al, 2001). Texturally it is difficult to differentiate these styles of mineralization but the copper isotope ratios would be different, due to the differing modes of genesis for each. More work is necessary to test this hypothesis but several deposits would be amenable to this type of investigation using laser sampling similar to the study by Graham et al. (2004). We expect that as routine analysis of copper isotope ratios becomes more common, further light will be shed on their use in exploration and for constraining ore forming processes.

Conclusions

The copper isotope fractionations observed in Coroccohuayco and the Tintaya mine indicate that important copper fractionation in mineralization can occur in high temperature hydrothermal ore deposits. These fractionations can be explained in terms of fractionation produced from preferential incorporation of one isotope (^{63}Cu) in the early/proximal mineralization and with the fluid isotopic composition evolving with precipitation of copper sulfides (Fig. 6). Should different Cu-complexes preferentially incorporate one isotope over another (Schauble et al., 2001; Maréchal and Albarède, 2002) under hydrothermal conditions then the stability of the individual complexes (e.g.,

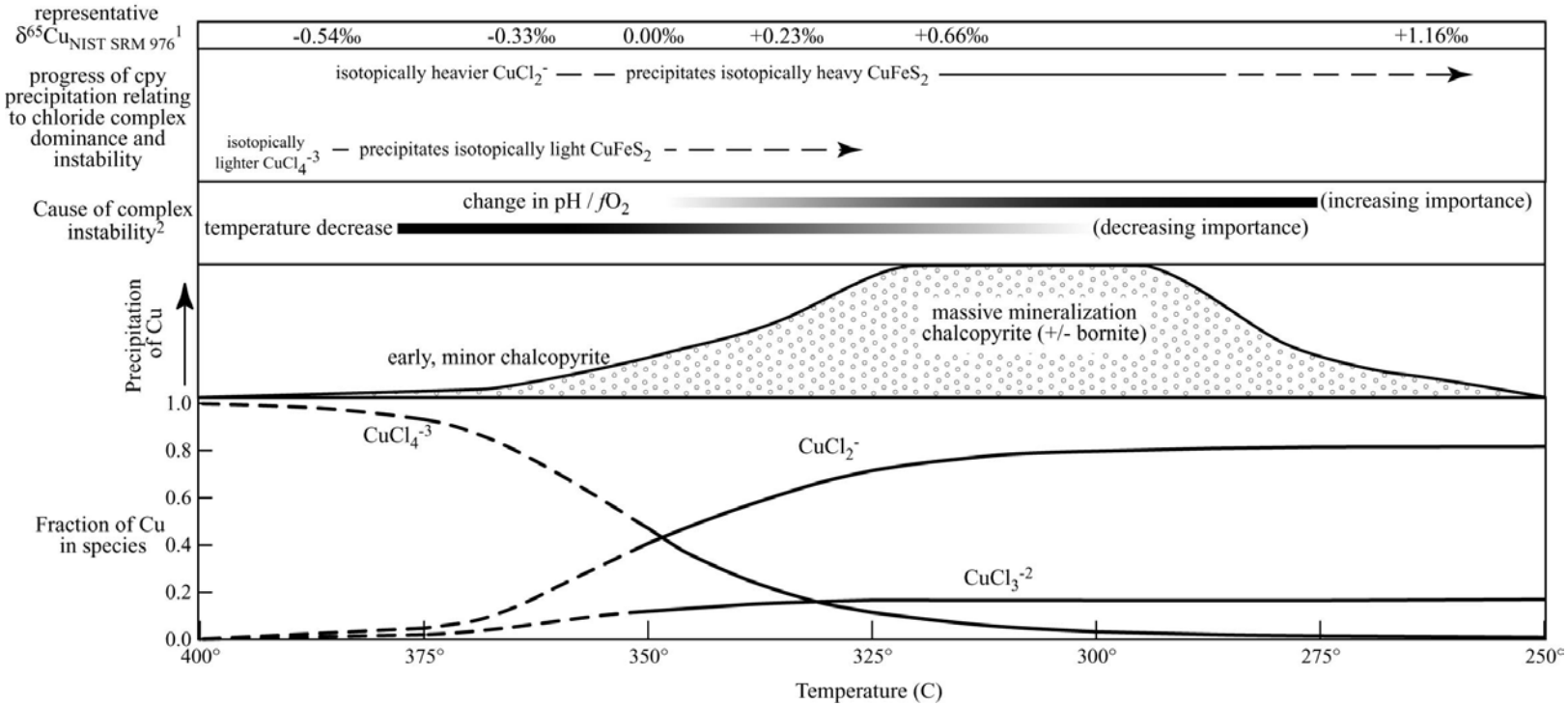

Figure 6. Diagram of the relationship of Cu-chloride complexes, chalcopyrite (cpy) precipitation mechanisms, and resulting $\delta^{65}Cu_{NIST\ SRM\ 976}$ values from Coroccohuayco, Perú. Chloride complex predominance (bottom) plotted from log K values taken from Liu et al. (2002) at 7.36m Cl^- (43 wt % NaCl eq). Dashed curves are extrapolated from log K data up to 350° C and should be considered estimates only.

[1]Based on values from mineralization below 300m depth in drill hole 1400 18.9 (see Table 1).

[2]The causes of complex instability and mineral precipitation are varied, and in addition to mechanisms shown may be related to boiling, fluid mixing, etc.

their stability constants) will also determine, to a certain extent, the isotopic composition of the resulting mineralization. The actual mechanism of fractionation may result from isotopic fractionation among different complexes, and also a possible fractionation between the fluid and any precipitating mineral phase. Instability of one chloride/ligand complex over another at specific points of mineralization (Fig. 6) would lead to isotopic variation between copper minerals produced from the same fluid. Thus, copper fractionation by this mechanism would be indirectly related to the physicochemical properties (pressure, temperature, composition) of the fluid at any spatial or temporal point of the system. In our study, high chloride content of the mineralizing hydrothermal fluid and high temperature of primary Cu-precipitation were probably important in the fractionation of copper, due to isotope fractionation between differing Cu-complexes, their thermodynamic stabilities, and their relationship to copper mineralization. Equilibrium fractionation between co-precipitated copper phases likely plays a role in producing isotopic variability in mineralization and can be used for evaluating the effects of copper remobilization and/or overprinting in ore deposits, although more work on the temperature and compositional dependence of this fractionation mechanism needs to be pursued.

The exploration potential for copper isotope analysis is significant in terms of use as an exploration guide since copper isotope ratios can be zoned across a deposit. These variations are produced by geologic processes, and, therefore, can be utilized as directional indicators for fluid transport, and more importantly, metal deposition. Copper isotope ratios probably show their greatest variation in hydrothermal systems, and thus are most useful in terms of defining isotope zonation, where copper transport was characterized by fluids containing more than one important copper complex. The resulting mineralization would depend on the causes of instability of any Cu-complex present in the fluid, and so the isotopic character of the mineralization will reflect the isotopic signature of the unstable copper-complex at the time of precipitation. Massive mineralization likely reflects the overall fluid copper isotope composition from all of the complexes contributing copper (bulk fluid copper ratio). Should this be confirmed by experimental studies, then copper isotopes will help in explaining copper precipitation mechanisms as well as defining the chemical conditions of copper transport.

Acknowledgements

The first author wishes to thank the Society of Economic Geologists Foundation, Inc., for partially funding copper isotope analyses through a Hugh E. McKinstry Grant. Appreciation is expressed to BHP Tintaya, S.A. (now

BHP Billiton Tintaya, S.A.), for the collection of samples from Coroccohuayco and Tintaya, and to Mike Anglin and Jeff Brooks for facilitating the geologic investigation of Coroccohuayco.

References

Albarède, F., Telouk, P., Blichert-Toft, J., Boyet, M., Agranier, A., and Nelson, B., 2004, Precise and accurate isotopic measurements using multiple-collector ICPMS: Geochimica et Cosmochimica Acta, v. 68, p. 2725-2744.

Archibald, S.M., Migdisov, A.A., and William-Jones, A.E., 2002, An experimental study of the stability of copper chloride complexes in water vapor at elevated temperatures and pressures: Geochimica et Cosmochimica Acta, v. 66, p. 1611-1619.

Chavez, W.X., 1994, Geologic setting and mineralogy of the Cu-Ag-(As) Rosario vein system, Collahuasi District, Chile: SEG Newsletter, v. 19, p. 6-11.

Crerar, D.A. and Barnes, H.L., 1976, Ore solution chemistry V. Solubilities of chalcopyrite and chalcocite assemblages in hydrothermal solution at 200º and 350º C: Economic Geology, v. 71, p. 772-794.

Ehrlich, S., Butler, I., Halicz, L., Rickard, D., Oldroyd, A., and Matthews, A., 2004, Experimental study of the copper isotope fractionation between aqueous Cu (II) and covellite, CuS: Chemical Geology, v. 209, p. 259-269.

Espirilla R., C.R. 2004, Controles estructurales sobre emplazamiento de intrusivos, y mineralización en Tintaya, Perú:Unpulished Titulo Profesional de Ingeniería Geológica, Universidad Naciónal San Agustin, Arequipa, Perú, 68 p.

Fierro R., J., Zweng, P.L., Gamarra R., H., and Garate LL., G., 1997, Chabuca Este Cu-(Au,Ag) skarn deposit at Tintaya, Peru: Socieded Geologica del Peru, Vol. Esp. 1, p 37-39.

Fulton, J.L., Hoffmann, M.M., and Darab, J.G., 2000, An X-ray adsorption fine structure study of copper(I) chloride coordination structure in water up to 325 ºC: Chemical Physics Letter, v. 330, p. 300-308.

Graham, S., Pearson, N., Jackson, S., Griffin, W., and O'Reilly, S.Y., 2004, Tracing Cu and Fe from source to porphyry: in situ determination of Cu and Fe isotope ratios in sulfides from the Grasberg Cu-Au deposit: Chemical Geology, v. 207, p. 147-169.

Johnson, J.W. and Norton, D., 1985, Theoretical prediction of hydrothermal conditions and chemical equilibria during skarn formation in porphyry copper systems: Economic Geology, v. 80, p. 1797-1823.

Jones, B., Fierro, J., and Lenzi, G., 2000, Antapaccay project - geology: Seminario Internacional "Yacimientos tipo Pórfido de Cu-Au", Lima 2000, Facultad de Ingeniería Geológica, Minera y Metalúrgia, Promoción de Geólogos 2000 Abstracts, v. II, 1 p.

Larson, P.B., Maher, K., Ramos, F.C., Chang, Z., Gaspar, M., and Meinert, L.D., 2003, Copper isotope ratios in magmatic and hydrothermal ore-forming environments: Chemical Geology, v. 201, p. 337-350.

Liu, W., Brugger, J., McPhail, D.C., and Spiccia, L., 2002, A spectrophotometric study of aqueous copper(I)-chloride complexes in LiCl solutions between 100 ºC and 250 ºC: Geochimica et Cosmochimica Acta, vol. 66, p. 3615-3633.

Maher, K.C., 1999, Geology of the Cu-skarn at Coroccohuayco, Peru: Unpublished MS thesis, Washington State University, Pullman, WA, USA. 133 p.

Maher, K.C., Ramos, F.C., and Larson, P.B., 2003, Copper isotope characteristics of the Cu (+Au, Ag) skarn at Coroccohuayco, Peru: Geological Society of America, Annual Meeting, paper 211-4.

Maréchal, C. N., Telouk, P., and Albarède, F., 1999, Precise analysis of copper and zinc isotopic compositions by plasma-source mass spectrometry: Chemical Geology, v. 156, p. 251-273.

Maréchal, C. and Albarède, F., 2002, Ion-exchange fractionation of copper and zinc isotopes: Geochimica et Cosmochimica Acta, v. 66, p. 1499-1509.

Meinert, L.D., 1993, Skarns and skarn deposits: Geoscience Canada, v. 19, p. 145-162.

Meinert , L.D., Hefton, K.K., Mayes, D., and Tasiran, I., 1997, Geology, zonation, and fluid evolution of the Big Gossan Cu-Au deposit, Ertsberg district, Irian Jaya: Economic Geology, v. 92, p. 509-534.

Mountain, B.W. and Seward, T.M., 2003, Hydrosulfide/sulfide complexes of copper (I): Experimental confirmation of the stoichiometry and stability of $Cu(HS)_2^-$ to elevated temperatures: Geochimica et Cosmochimica Acta, v. 67, p. 3005-3014.

Noble, D.C., McKee, E.H., Eyzaguirre, V.R., and Marocco, R., 1984, Age and regional tectonic and metallogenic implication of igneous activity and mineralization in the Andahuaylas-Yauri Belt of southern Peru: Economic Geology, v. 79, p. 172-176.

O'Neil, J.R., 1986, Theoretical and experimental aspects of isotopic fractionation, *In* Valley, J.W., Taylor-H.P.,Jr., and O'Neil, J.R., eds., Stable isotopes in high temperature geological processes: Reviews in Mineralogy, v. 16. p. 1-40.

Padilla G., R.A., Titley, S.R., and Pimentel B., F., 2001, Geology of the Escondida porphyry copper deposit, Antofagasta Region, Chile: Economic Geology, v. 96, p. 307-324.

Parra S., R., 2003, Alteración, mineralización y geoquímica dentro del yacimiento tipo skarn Cu (Au,Ag,Mo) de Tintaya :Unpulished Titulo Profesional de Ingeniería Geológica. Universidad Naciónal San Antonio Abad, Cusco, Perú, 220 p.

Paul, A.H. and Manske, S.L., 1999, Discovery of the Magma porphyry system, Superior, Arizona: *In:* Century of the Pacific Rim, "the past as prologue to the future"; Geological Society of America, Cordilleran Section, 95th annual meeting; Centennial meeting 1899-1999; Abstracts with Programs-Geological Society of America. vol. 31, p. 6.

Perelló, J., Carlotto, V., Fuster, N., and Muhr, R., 2003, Porphyry-style alteration and mineralization of the middle Eocene to early Oligocene Andahuaylas-Yauri Belt, Cuzco region, Peru: Economic Geology, v. 98, p. 1575-1605.

Rouxel, O., Fouquet, Y., and Ludden, J.N., 2004, Copper isotope systematics of the Lucky Strike, Rainbow, and Logatchev sea-floor hydrothermal fields on the Mid-Atlantic Ridge: Economic Geology, v. 99, p. 585-600.

Saez, J., 1996, Skarn and ore parageneses in the Cu (-Fe) Tintaya deposit, southern Peru: Unpublished Ph.D. dissertation, Ruprecht-Karls Universitat, Heidelberg, 205 p.

Schauble, E.A., Rossman, G.R., and Taylor, H.P., Jr., 2001, Theoretical estimates of equilibrium Fe-isotope fractionations from vibrational spectroscopy: Geochimica et Cosmochimica Acta, v. 65, p. 2487-2497.

Shields, W.R., Goldich, S.S., Garner, E.L., and Murphy, T.J., 1965, Natural variations in the abundance ratio and the atomic weight of copper: Journal of Geophysical Research, v. 70, p. 479-491.

Urey, H.C., 1947, The thermodynamic properties of isotopic substances: Journal of the Chemical Society, v. 1, p. 562-582.

Var'yash, L.N., 1992, Cu(I) complexing in NaCl solution at 300 and 350 ºC: Geochemistry International, v. 29, p 84-92.

Var'yash, L.N. and Rekharski, V.I., 1981, Behavior of Cu(I) in chloride solutions: Geochemistry International, v. 18, p 61-67.

Wood, S.A. and Samson, I.M., 1998, Solubility of ore minerals and complexation of ore metals in hydrothermal solutions, *In* J. Richards and P. Larson, eds., Techniques in Hydrothermal Ore Deposits: Reviews in Economic Geology, v. 10, p. 33-80.

Xiao, Z., Gammons, C.H., and Williams-Jones, 1998, Experimental study of copper(I) chloride complexing in hydrothermal solutions at 40 to 300 ºC and saturated water vapor pressure: Geochimica et Cosmochimica Acta, vol. 62, p. 2949-2964.

Young, S. and Ruiz, J., 2003, Inorganic controls of copper isotope fractionation in supergene environment: Geophysical Research Abstracts, 5: 02045.

Zhu, X.K., O'Nions, R.K., Guo, Y., Belshaw, N.S., and Rickard, D., 2000, Determination of natural Cu-isotope variation by plasma-source mass spectrometry: implication for use as geochemical tracers: Chemical Geology, v. 163, p. 139-149.

Zweng, P.L., Yagua P., J., Fierro R., J., Gamarra R., H., Jordan G., L., Brooks, J., Yurko, E., and Mulhollen, R., 1997, The Cu - (Au,Ag) skarn

Appendix 5

Data from Hydrothermal Chalcopyrite Synthesis Experiments

This Appendix contains X-ray diffraction data for samples presented in Section VI, a Table listing the experimental conditions and qualitative results, and illustrations of the experimental tubes.

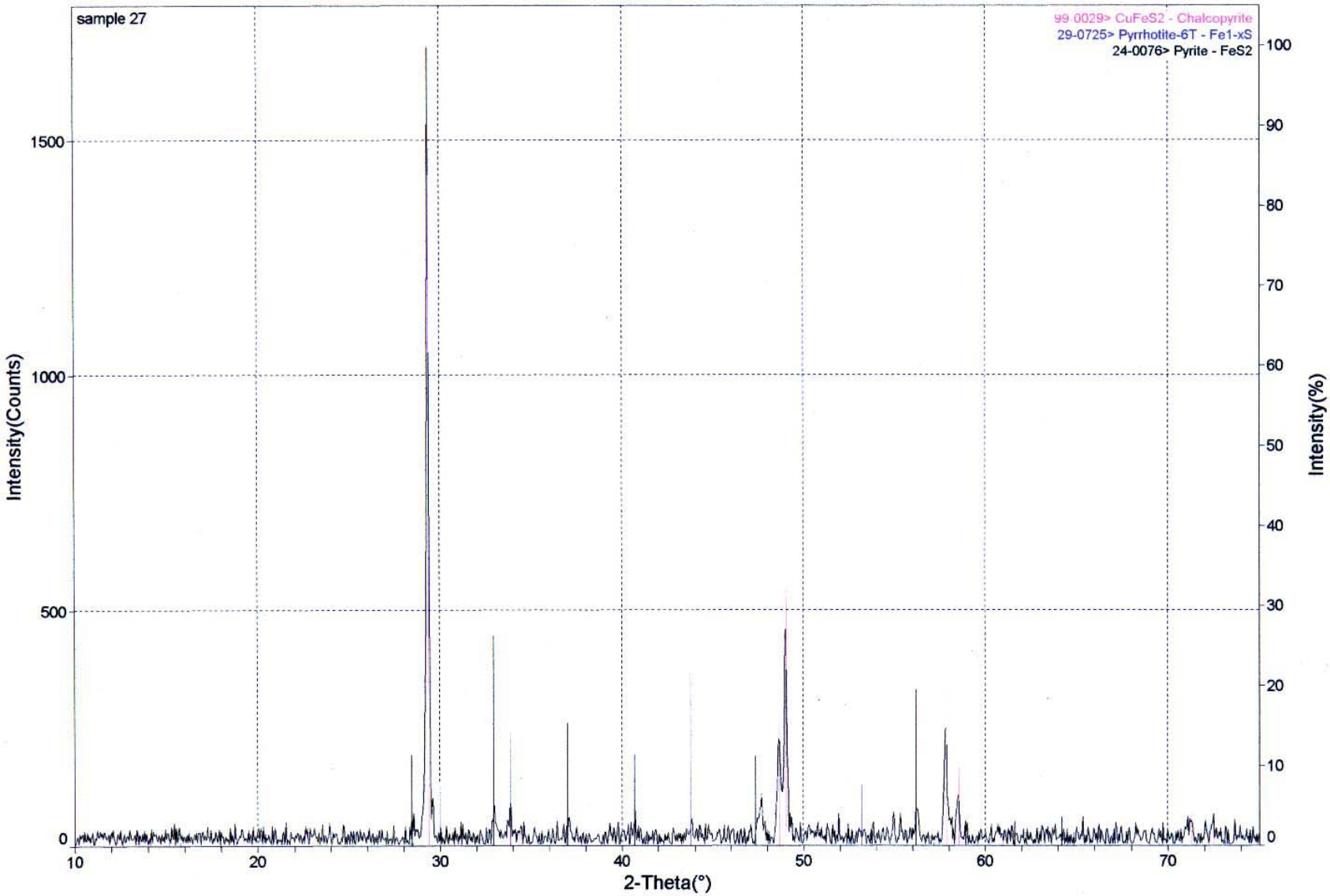

X-ray diffraction pattern for sample 27.

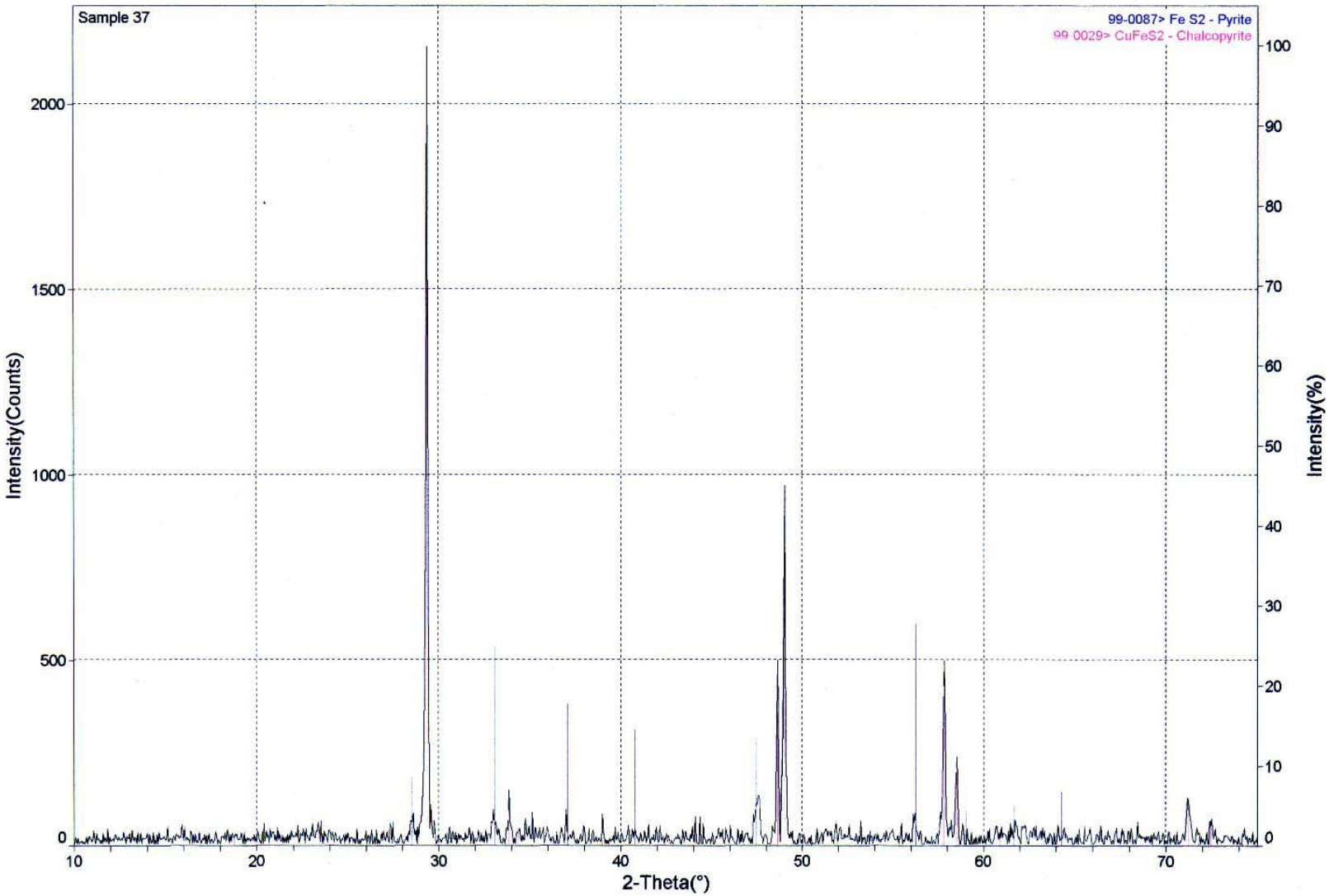

X-ray diffraction pattern for sample 37

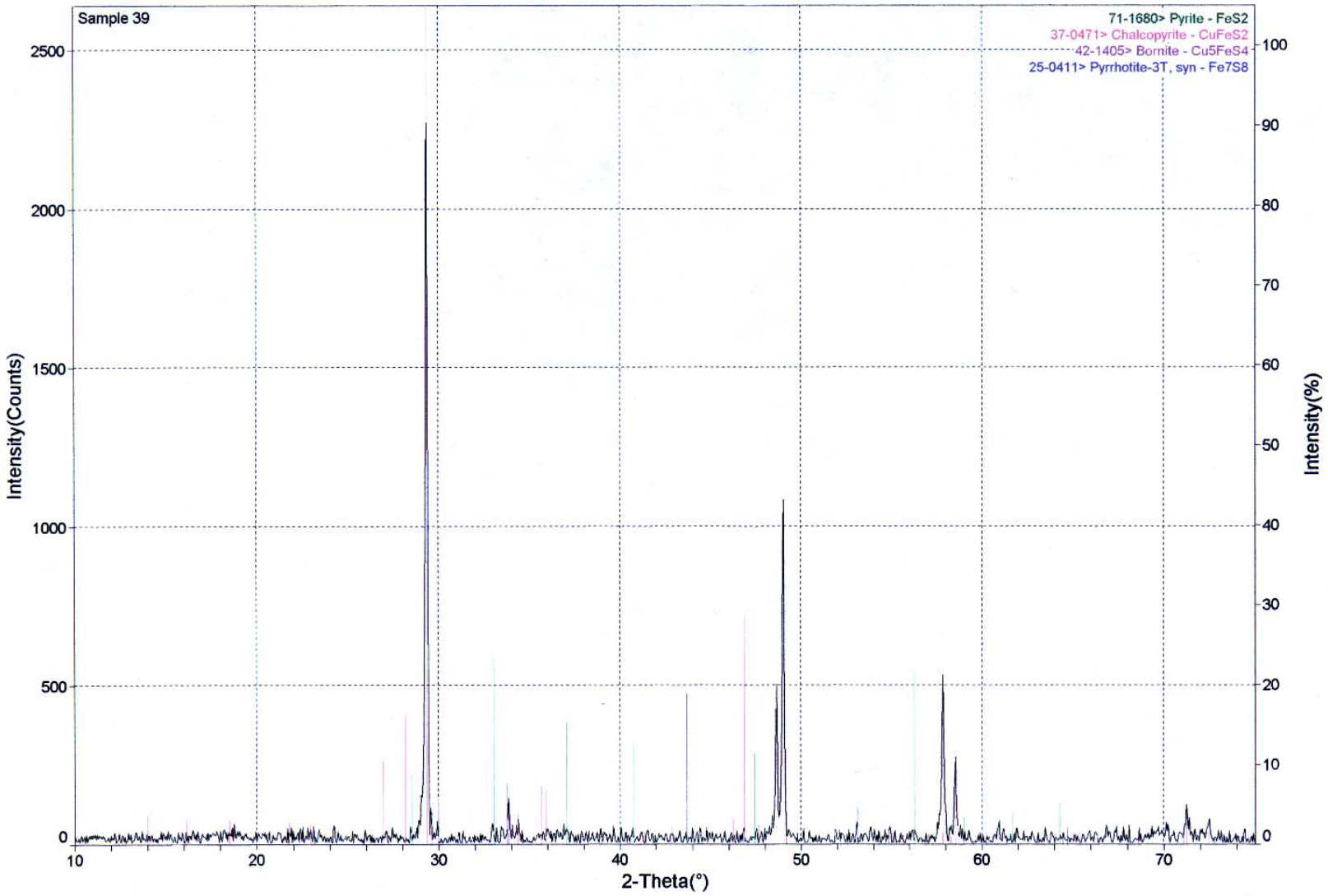

X-ray diffraction pattern for sample 39

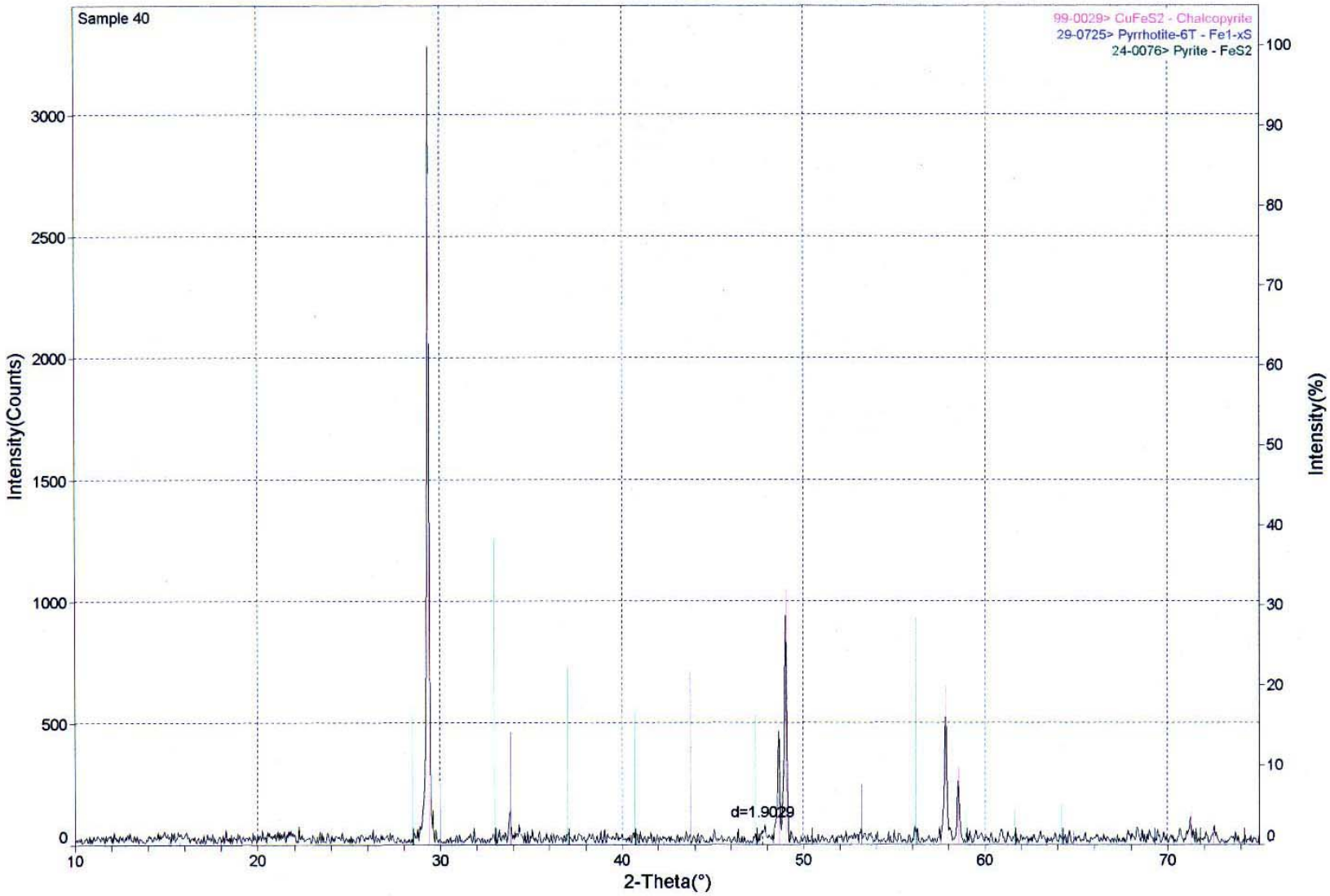

X-ray diffraction pattern for sample 40

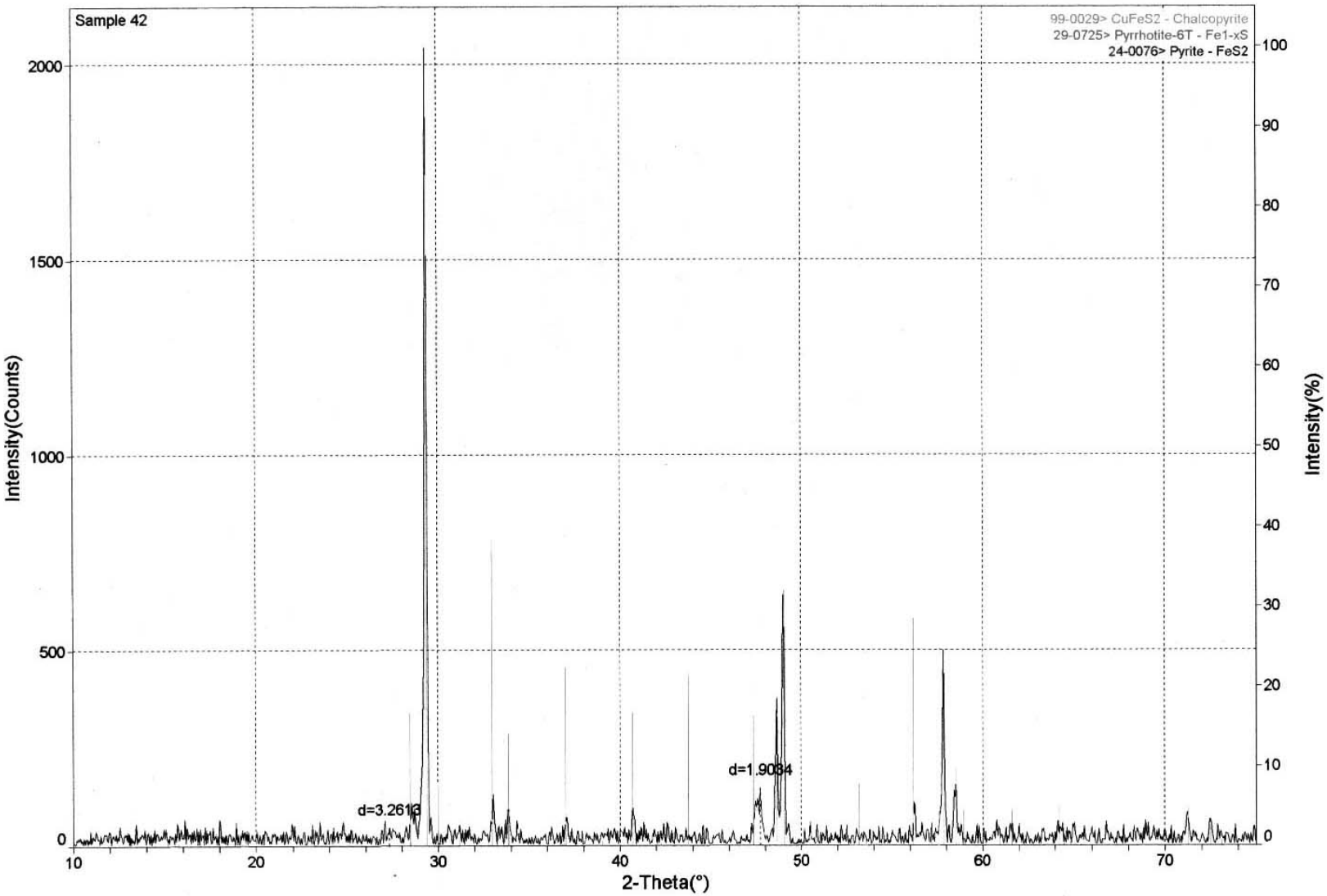

X-ray diffraction pattern for sample 42

Appendix 5 cont.

Concentrations of selected elements in chromatographically purified chalcopyrite synthesis fluids

sample	27 Cu(2)	39 Cu(2)	42 Cu(2)	27 chrom	42 chrom	27 Cu Chrom[1]	39 Cu Chrom[1]	42 Cu Chrom[1]
element (ppb)								
Na	4	79.8	50.1	2.1	10.9	-	-	-
Mg	0.1	0.48	0.05	0.3	1.3	-	-	-
Al	<0	0.5	<0	0.3	1.3	-	-	-
Ca	3	9.6	1.3	3.2	11.8	-	-	-
Fe	1.16	1.6	<0	1.9	15.2	-	-	-
Cu	64.2	26.3[2]	70.9	71.5	82.6[3]	62	24	68
Zn	0.3	0.4	<0	0.27	3.0	-	-	-

[1]Only Cu determined (by MC-ICPMS from ^{65}Cu intensities relative to ^{65}Cu intensities of standard solution (100ppb Cu)).
[2]Was 24ppb when determined by MC-ICPMS.
[3]Was 77ppb when determined by MC-ICPMS.

Appendix 5 Cont.

Sulfide synthesis composition and results

sample	form of Cu	form of Fe	NaCl	HCl	Total nutrient (g)	Temperature (ºC)	Result
1	Cu wire	Fe wire	1m	0.01m	1.5	225	cpy-py-cov (late) with undrained yellow liquid
2	Cu wire	Fe wire	2m	0.01m	1.5	225	as above
3	Cu wire	Fe wire	3m	0.01m	1.5	225	py-cpy-po-cc with minor yellowish undrained liquid
4	Cu wire	Fe wire	1m	0.1m	1.5	225	py-cpy-cc-cov; undrained
5	Cu wire	Fe wire	2m	0.1m	1.5	225	py-po-cpy-cov; undrained
6	Cu wire	Fe wire	3m	0.1m	1.5	225	cpy-po-cov-cc-born; drained (polished section made)
7	Cu wire	Fe wire	1m	0.01m	0.75	225	cc-cpy; drained
8	Cu wire	Fe wire	1m	0.1m	0.75	225	not drained; silica on surface of tube
9	Cu wire	Fe wire	3m	0.01m	0.75	225	not drained; cc-cpy
10	Cu wire	Fe wire	3m	0.1m	0.75	225	drained; silica on surface of tube
11	Cu wire	Fe wire	5m	0.01m	0.75	225	not drained; silica on surface of tube
12	Cu wire	Fe wire	5m	0.1m	0.75	225	as above
13	CuCl	$FeCl_2$+4H_2O	4.08m (Cl^-)	0.01m	0.5	225	well developed cov crystals; drained; green-yellow liquid
14	CuCl	$FeCl_2$+4H_2O	4.08m (Cl^-)	0.1m	0.5	225	as above
15	Cu wire	$FeCl_2$+4H_2O	3m	0.01m	0.5	225	cov-cc; drained, green-blue liquid
16	Cu wire	$FeCl_2$+4H_2O	5m	0.01m	0.5	225	cov-cc; not drained, green-blue liquid
17	Cu wire	$FeCl_2$+4H_2O	3m	0.1m	0.5	225	cov-py-cc; drained; green-blue liquid
18	Cu wire	$FeCl_2$+4H_2O	5m	0.1m	0.5	225	as above
19	CuCl	Fe wire	5m (Cl-)	0.1m	0.5	225	cpy-py-hematite; drained
20	Cu wire	Fe wire	5m (Cl-)	0.1m	0.5	225	cpy±py; not drained
21	CuCl	$FeCl_2$+4H_2O	3m (Cl-)	0.1m	0.5	225	py-cov; drained
22	CuCl	$FeCl_2$+4H_2O	3m (Cl-)	0.1m	0.5	225	py-cov-hematite; drained
23	Cu wire	$FeCl_2$+4H_2O	3m (Cl-)	0.1m	0.5	225	cpy-hematite; not drained
24	Cu wire	$FeCl_2$+4H_2O	3m (Cl-)	0.1m	0.5	225	cpy-py-po(?); not drained
25	Cu wire	Fe wire	1m	0.1m	0.3	225	cpy; drained; XRD scan
26	Cu wire	Fe wire	3m	0.1m	0.3	225	cpy-py; drained; XRD scan
27	Cu wire	Fe wire	5m	0.1m	0.3	225	cpy-po(?)-py; drained
28	Cu wire	Fe wire	1m	0.1m	0.3	225	cpy-py-po; drained
29	Cu wire	Fe wire	3m	0.1m	0.3	225	cpy-py-po(±cov?); not drained
30	Cu wire	Fe wire	3m	0.1m	0.3	300	cpy-py; drained
31	Cu wire	Fe wire	1m	0.1m	0.3	300	burst (bolts not tight enough - 40ft-lbs)
32	Cu wire	Fe wire	1m	0.1m	0.3	300	burst
33	Cu wire	Fe wire	3m	0.1m	0.3	300	burst
34	Cu wire	Fe wire	3m	0.1m	0.3	300	burst

Appendix 5 Cont.

Sulfide synthesis composition and results cont.

sample	form of Cu	form of Fe	NaCl	HCl	Total nutrient (g)	Temperature (ºC)	Result
35	Cu wire	Fe wire	5m	0.1m	0.3	300	cpy-py-po; drained (surprise survivor) - XRD scan
36	Cu wire	Fe wire	5m	0.1m	0.3	300	burst
37	Cu wire	Fe wire	3m	0.1m	0.3	300	cpy-py; drained; XRD scan
38	Cu wire	Fe wire	3m	0.1m	0.3	300	cpy-py-po-born; drained; XRD scan
39	Cu wire	Fe wire	4.9m	0.1m	0.3	300	cpy; drained; XRD scan
40	Cu wire	Fe wire	4.9m	0.1m	0.3	300	cpy-po; drained; XRD scan
41	Cu wire	Fe wire	7.4m	0.1m	0.3	300	cpy-py; undrained
42	Cu wire	Fe wire	7.4m	0.1m	0.3	300	cpy, drained; XRD scan

Abbreviations: cpy = chalcopyrite, born = bornite, cov = covellite, cc = chalcocite, py = pyrite, po = pyrrhotite

Appendix 5 cont.

An example of sealed experimental tubes prior to high-temperature sulfide synthesis loaded with fluid and elemental nutrient, separated by silica wool at the constriction. Width of tubes is 1cm.

Appendix 5 cont.

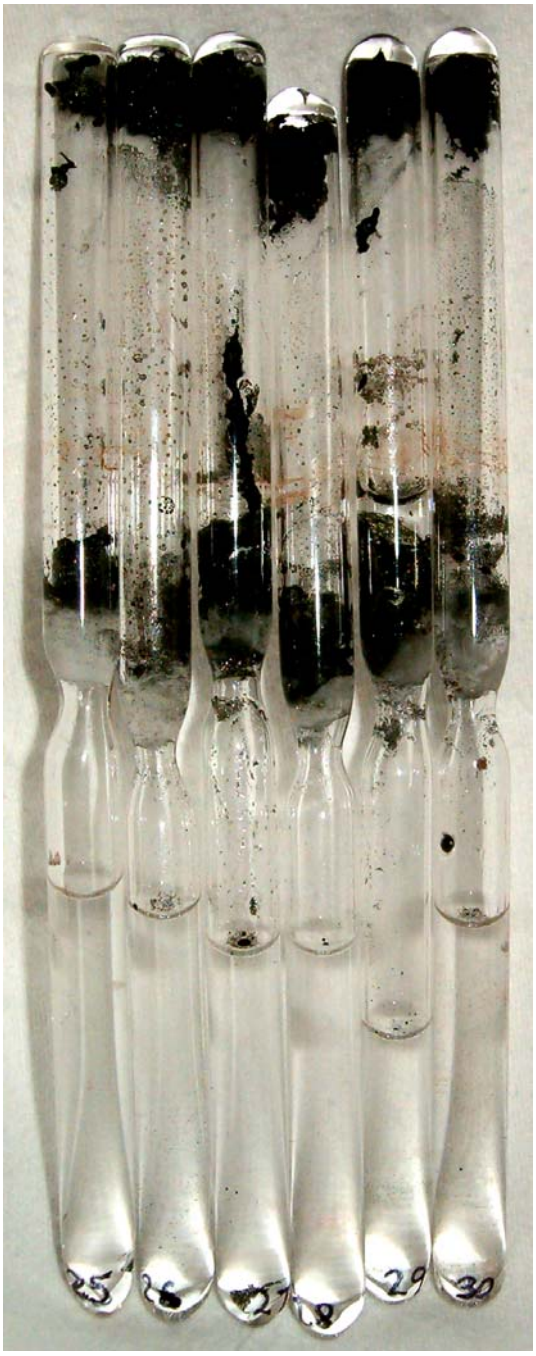

An example of experimental tubes after synthesis at 225° C. Sulfide has precipitated at top and at the middle silica wool. Width of tubes is 1cm. Note, experiment 29 did not drain completely.

Appendix 5 cont.

An example of experimental sulfide synthesis samples after the experimental run. Width of tubes is 1cm.